Hydration and Ion Pairing of Aqueous Phosphate Solutions as Observed by Dielectric Spectroscopy

Dissertation
zur Erlangung des
Doktorgrades der Naturwissenschaften
(Dr. rer. nat.)
der Naturwissenschaftlichen Fakultät IV
Chemie und Pharmazie
der Universität Regensburg

vorgelegt von
Andreas Eiberweiser
aus Kaimling

Regensburg 2013

Promotionsgesuch eingereicht am:	15.03.2013
Tag des Kolloquiums:	12.04.2013
Die Arbeit wurde angeleitet von:	Apl. Prof. Dr. R. Buchner
Prüfungsausschuss:	Apl. Prof. Dr. R. Buchner Prof. Dr. W. Kunz Prof. em. Dr. H. Brunner Prof. Dr. A. Pfitzner (Vorsitzender)

meinen Eltern
und
Geschwistern

Eine jede wissenschaftliche Betrachtungsweise hat zur Vorraussetzung die Einführung einer gewissen Ordnung in der Fülle des zu betrachtenden Stoffes.

Max Planck

Contents

Vorwort

Diese Doktorarbeit entstand in der Zeit von Mai 2010 bis März 2013 am Institut für Physikalische und Theoretische Chemie der naturwissenschaftlichen Fakultät IV – Chemie und Pharmazie – der Universität Regensburg.

An erster Stelle darf ich mich bei Herrn Apl. Prof. Dr. Richard Buchner für die Aufnahme in seine Gruppe und die Erteilung des Themas bedanken. Sein Interesse am Fortschritt der Arbeit, sowie die stete Bereitschaft zum fachlichen Gespräch waren für den erfolgreichen Abschluss meiner Dissertation von entscheidender Bedeutung.
Auch möchte ich mich für die Gewährung großer wissenschaftlicher Freiheiten bedanken, die ich mehr als einmal genutzt habe. Bedenkt man, dass er mich wiederholt auf den Pfad dieser Arbeit zurückführen musste, scheint es doch verwunderlich, dass mir und nicht ihm graue Haare gewachsen sind.
Vielen Dank für die zahlreichen Dienstbesprechungen!

Weiterhin gilt mein Dank dem Leiter des Lehrstuhls, Herrn Prof. Dr. Werner Kunz für die großzügige zur Verfügung Stellung von Laboratorien und Verbrauchsmaterial. Auch wurde durch Ihm ein Teil dieser Arbeit finanziert: vielen Dank dafür!

Der Deutschen Forschungsgemeinschaft (DFG) sei für die Bereitstellung der Mittel zur Durchführung des Projektes Bu 1153/11-1 gedankt. Ohne die mit diesem Projekt verbundenen Stelle wäre die vorliegende Arbeit nicht möglich gewesen.

Für die stets freundliche Atmosphäre und kollegiale Hilfsbereitschaft möchte ich mich bei allen Mitgliedern des AK Mikrowellen bedanken. Herr Dr. Hafiz M.A. Rahman, Frau Dr. Saadia Shaukat, Herr Dr. Alexander Stoppa und Herr M.Sc. Thomas Sonnleitner haben mich in die Bedienung der Geräte und die generelle Arbeitsweise eingeführt. In besonderer Weise möchte ich mich an dieser Stelle bei Thomas Sonnleitner bedanken: ich hatte stets das Gefühl einen in wissenschaftlichen und menschlichen Fragen gleichgesinnten Kollegen zu haben. Auch möchte ich meinem ersten Bachelor-Studenten, und mittlerweile Kollegen, Herrn B.Sc. Andreas Nazet alles Gute für die Zukunft wünschen, sowie meine Hoffnung zum Ausdruck bringen, dass wir auch in Zukunft noch zusammenarbeiten. Allen Gästen und temporären Mitgliedern des AK Mikrowellen,

- Herr M.Sc. Waheed Gul Khan
- Herr B.Sc. Julian Rieder

- Herr M.Sc. Phillip Kahl
- Herr M.Sc. Bernd Mühldorf
- Herr M.Sc. Alexander Wankmüller
- Herr M.Sc. Hiroyuki Doi
- Frau Dr. Kamila Mazur
- Frau M.Sc. Gözde Keskin
- Herr M.Sc. Nicolás Moreno Gómez
- Frau M.Sc. Vikoriya A. Nikitina
- Herr M.Sc. Filipe da Silva Lima

danke ich für die angenehme Zusammenarbeit.

Herrn Prof. Dr. Glenn Hefter danke ich für die zahlreichen Diskussionen über Teile des in Kapitels 4 präsentierten Materials. Herrn B.Sc. Andreas Nazet für die Durchführung von Leitfähigkeitsmessungen und Korrekturlesen des vorliegenden Textes. Für das Letztere bin ich ebenfalls Herrn M.Sc. Thomas Sonnleitner zu Dank verpflichtet.

Allen Mitgliedern und Kollegen des Lehrstuhls möchte ich meinen tiefen Dank für die außeruniversitären Aktivitäten ausdrücken. Ich habe mich in dieser Gemeinschaft stets wohl gefühlt, und so war es mir auch möglich die Herausforderung der mittäglichen Kaffeerunde zu meistern. Frau Dr. Evi Müller und Frau Dr. Agnes Harrar danke ich für die herzliche Aufnahme in die morgendliche Runde zu Beginn meiner Doktorarbeit. Allen Mitgliedern der Mittagsrunde (Michl, Vroni, Julien, Auriane, Eva, Olli und Tobi) herzlichen Dank für die angenehmen, nicht-fachlichen Gespräche.

Ein besonderer Dank gilt meiner ganzen Familie, die immer mit Interesse und Hilfsbereitschaft meinen Werdegang verfolgt hat.

Allen Mitarbeitern der Werkstätten möchte ich für die schnelle und gewissenhafte Erledigung der Aufträge meinen Dank aussprechen und meine besondere Hochachtung zum Ausdruck bringen.

Zuletzt und in besonderer Weise möchte ich mich bei Susanne bedanken: unsere Gespräche habe ich immer sehr genossen, und sehr viel Gutes das mir in den letzten Jahren widerfahren ist, habe ich dir zu verdanken. Du machst aus mir einen besseren Menschen, und wirst dies hoffentlich auch noch lange tun!

Constants and symbols

Constants

Elementary charge	e_o	$= 1.60217739 \cdot 10^{-19}\,\mathrm{C}$
Permittivity of free space	ε_o	$= 8.854187816 \cdot 10^{-12}\,\mathrm{C^2(Jm)^{-1}}$
Avogadro's constant	N_A	$= 6.0221367 \cdot 10^{23}\,\mathrm{mol^{-1}}$
Speed of light	c	$= 2.99792458 \cdot 10^{8}\,\mathrm{m\,s^{-1}}$
Boltzmann's constant	k_B	$= 1.380658 \cdot 10^{-23}\,\mathrm{J\,K^{-1}}$
Permeability of free space	μ_0	$= 4\pi \cdot 10^{-7}\,\mathrm{(Js)^2(C^2m)^{-1}}$
Planck's constant	h	$= 6.6260755 \cdot 10^{-34}\,\mathrm{Js}$

Symbols

$\vec{P}$	polarization ($\mathrm{C\,m^{-2}}$)	$\vec{M}$	macroscopic dipole moment ($\mathrm{C\,m^{-2}}$)
ω	angular frequency ($\mathrm{s^{-1}}$)	ν	frequency (Hz)
$\vec{E}$	electric field strength ($\mathrm{V\,m^{-1}}$)	$\hat{\varepsilon}$	complex permittivity
ε'	real part of $\hat{\varepsilon}$	ε''	imaginary part of $\hat{\varepsilon}$
ε	$\lim_{\nu\to 0}(\varepsilon')$	ε_∞	$\lim_{\nu\to\infty}(\varepsilon')$
χ	electric susceptibility	μ	dipole moment ($\mathrm{C\,m}$)
τ	relaxation time (s)	T	temperature (K)
t	time (s)	$\hat{\gamma}$	complex propagation coefficient
α_a	absorption coefficient ($\mathrm{Np\ m^{-1}}$)	β	phase constant ($\mathrm{m^{-1}}$)
$\hat{k}$	complex wave number	$\hat{n}$	complex refractive index
c	molarity ($\mathrm{mol\ dm^{-3}}$)	η	viscosity ($\mathrm{Pa\,s}$)
κ	conductivity ($\mathrm{S\ m^{-1}}$)	ρ	density ($\mathrm{kg\,m^{-3}}$)

Acronyms

ib	irrotational bound	CC	Cole-Cole
CD	Cole-Davidson	CIP	contact ion-pair
D	Debye	DHO	damped harmonic oscillator
DMA	*N*,*N*-dimethylacetamide	DR(S)	dielectric relaxation (spectroscopy)
FIR	far-infrared	HN	Havriliak-Negami
IFM	interferometer	IR	infrared
MD	molecular dynamics	NMR	nuclear magnetic resonance
OKE	optical Kerr effect	QM	quantum mechanics
PC	propylene carbonate	SED	Stokes-Einstein-Debye
SIP	solvent separated ion-pair	2SIP	double solvent separated ion-pair
VNA	vector network analyzer	vdW	van der Waals
IC	ion cloud	IP	ion pair
PRT	platinum resistance thermometer	QENS	quasi-elastic neutron scattering
TCF	time-correlation function		

Introduction

General aspects

Many compounds contain various types of phosphate groups that play fundamental roles in life processes and in the environment. Much organic phosphate is present in biopolymer form: as phosphopolysaccharides, phospholipids, phosphoproteins or nucleic acids.[1] Such compounds are essential for life, because they stabilize cells and enable them to reproduce. Organic phosphate esters are involved in many biochemical reaction sequences: as energy carriers, coenzymes and intermediates. To build up their phosphate ester levels, animals and plants usually absorb phosphorous in the form of inorganic phosphates $H_xPO_4^{(3-x)-}$, $x = 0$, 1 or 2.[2] In organisms, inorganic phosphates are found in blood, urine and tissue fluids, where the $H_2PO_4^-$ / HPO_4^{2-} system acts as the key buffer.[3] The most important biochemical role of inorganic phosphates on the other hand is in the formation of bone material, mostly in the form of apatite.[4] Thus, phosphates play critical roles in metabolism, both as solid material and in solution. To ensure that commercial crops have a sufficient supply of inorganic phosphates for growth, phosphate fertilizers are used throughout the world which makes inorganic phosphate production the fourth largest by tonnage globally.[5] Other important applications of inorganic phosphates include food additives, detergents, rust proofing and metal cleaning but there are many more.[2]

The phosphate groups present in biological systems and also most inorganic phosphate used for technical applications are present in aqueous solution. There, the specific solute-solute and solute-solvent interactions, especially in comparison with the solvent-solvent interactions are in the focus of scientific research. But also the (possible) effect on water structure is of importance,[6] especially as water nowadays is seen as an active player in biological processes, rather than being a mere solvent.[7,8] Thus the changing properties, especially dynamics, of water molecules that are not in close proximity of the solute are of interest. Nevertheless, most attention is on solute-solvent and solute-solute interactions.

Regarding proteins, there is an ongoing debate whether the influence of an added solute on protein stability is mediated through changes in the solvent structure or is based on direct solute-protein interactions. Recent experiments and computer simulations found that direct solute-solute interactions maybe more important for protein-electrolyte interactions,[9–12] however for aqueous systems containing amphiphilic molecules and proteins, the situation is under discussion.[13–15]

The matter of a recent DFG project (BU1153/11-1) in our group were the major hydration sites of proteins: hydrophilic anionic residues, but also hydrophobic parts. A previous PhD

project[16] was dealing with carboxylate, sulfate and sulfonate as anionic residues and was mainly focusing on the interplay of hydrophilic and hydrophobic hydration. This work continues this project, focusing on hydration and ion-pairing in inorganic phosphate ions, as a further hydrophilic group present in many biomolecules.

Recently, weak ion association in aqueous media has attracted increasing attention.[17,18] Fueled by Collin's "rule of matching water affinities", which states that ions of comparable hydration properties preferably associate,[19] it is claimed on the basis of theoretical considerations and computer simulations that Na^+ is slightly stronger binding to biologically relevant anionic moieties, like carboxylate or phosphate, than K^+ and that this small difference in binding constants is decisive for the different physiological properties of both cations.[10,20]

Experimental quantification of weak ion association, though, is not a trivial task and even such well established techniques as conductometry or potentiometry yield only a rough estimate for the overall association constant if $K_A^\circ \lesssim 10$.[21,22] Common spectroscopic techniques, like NMR or vibrational spectroscopy, are generally not useful at all as they are sensitive only to contact ion pairs (CIPs).[23] In contrast, dielectric relaxation spectroscopy (DRS) has the unique ability to detect and quantify also solvent shared (SIP) and solvent-separated (2SIP) ion pairs.[24] DRS probes the response of the sample to a time-dependent electric field in terms of its complex permittivity spectrum, $\hat{\varepsilon}(\nu) = \varepsilon'(\nu) - \mathrm{i}\varepsilon''(\nu)$, where $\varepsilon'(\nu)$ is the relative permittivity and $\varepsilon''(\nu)$ the associated dielectric loss at frequency ν.[25,26] This method is sensitive to all processes leading to fluctuations of the macroscopic dipole moment of the sample, like, *e.g.*, the reorientation of ion pairs possessing a permanent dipole moment, μ_{IP}.[18]

A weak mode in the $\sim 0.5-1$ GHz region of the dielectric spectrum of weakly associating 1:1 electrolytes was found in previous DRS studies.[27–29] This mode also appeared for sodium formate and acetate,[30] as well as sodium sulfate and sulfonate.[16] Most interesting is the striking similarity of this low-frequency mode in all those investigated solutions, regarding the concentration dependent amplitude. This rises the important question, if this mode is due to a process different from ion-pair relaxation.

Aims of this study

The overall aim of the present study is to quantify hydration and ion-pairing in aqueous phosphate solutions at 25 °C. The adopted approach is a three step analysis, mirrored in the three experimental chapters of this study.

The first experimental chapter (Chapter 3) deals with aqueous NaCl solutions at $c \leq 2.112\,\mathrm{mol\,L^{-1}}$. This substance is a model salt for, at best, weakly associated electrolytes. The study of the dielectric properties of NaCl(aq), and comparison with a previous study by Buchner *et al.*,[31] sheds some light on the aforementioned low-frequency process observed in a number of 1:1 electrolytes. Different relaxation mechanisms, like ion-cloud relaxation,[32] might be (at least partly) responsible for this process.

Chapter 4 is focusing on hydration of aqueous potassium phosphate solutions KH_2PO_4(aq), K_2HPO_4(aq) and K_3PO_4(aq) up to 1.332, 3.987 and 3.012 mol L^{-1}, respectively. This yields detailed insight into the changes in hydration upon increasing charge of the phosphate anion and the effect on ion-pairing. Despite the importance of inorganic phosphate ions, surprisingly little is known about their hydration properties.[33–37] The current work provides further insight into this important topic, presents information on the solute effect on water dynamics and reveals the degree of solute-solute interactions.

The third experimental chapter (Chapter 5) presents the DRS studies of NaH_2PO_4(aq), Na_2HPO_4(aq), $(NH_4)H_2PO_4$(aq) and $(NH_4)_2HPO_4$(aq) for concentrations c up to 4.794, 0.6184, 2.459 and 3.173 mol L^{-1}. The studied cations, Na^+ and $NH_4{}^+$, were chosen due to the importance of ammonium salts as fertilizers and the potentially important difference of Na^+ and K^+ for biological processes.[10,20] The results on hydration and ion-pairing are presented and compared with those for the respective potassium salts.

Eventually the results of this work are summarized regarding ion specific effects on hydration and ion-pairing in aqueous phosphate solutions, as well as general implications for dielectric spectroscopy of aqueous electrolyte solutions.

Chapter 1

Theoretical Background

1.1 Polarization

1.1.1 Static polarization

Relative permittivity ε is one of the central quantities to describe materials, especially those intended for application in electronic devices. It describes how an external electric field $\vec{E}$ interacts with a dielectric medium, but can also be described as the effect of the dielectric medium on the electric field within the material (Section 1.4). The main impact of a low intensity electric field on a molecular liquid is the establishment of an effective charge separation (Figure 1.1). This phenomenon is known as polarization $\vec{P}$, which is defined as the macroscopic dipole moment per unit volume:

$$\vec{P} = \frac{\vec{M}}{V} \tag{1.1}$$

where $\vec{M}$ is the macroscopic dipole moment in the volume V.
In a linear, homogeneous and isotropic dielectric material $\vec{P}$ depends in a linear manner on the electric field[38]

$$\vec{P} = \varepsilon_0 \chi \vec{E} \tag{1.2}$$

where ε_0 is the permittivity of free space and χ is the electric susceptibility

$$\chi = \varepsilon - 1 \tag{1.3}$$

Figure 1.1 depicts the effect of an electric field $\vec{E}$ on a dipolar molecular liquid: the dipole molecules partially align according to the external field and additional charge separation in the molecules due to polarizability, α_k, is induced. The latter process is symbolized in Figure 1.1b through a more intense color gradient within the generic molecules, however, it is emphasized that the charge separation takes place along the external electric field (actually the local field $\vec{E}_{\text{loc}}$ at the postition of the molecule) and **not** along the direction of the existing permanent dipole moment.

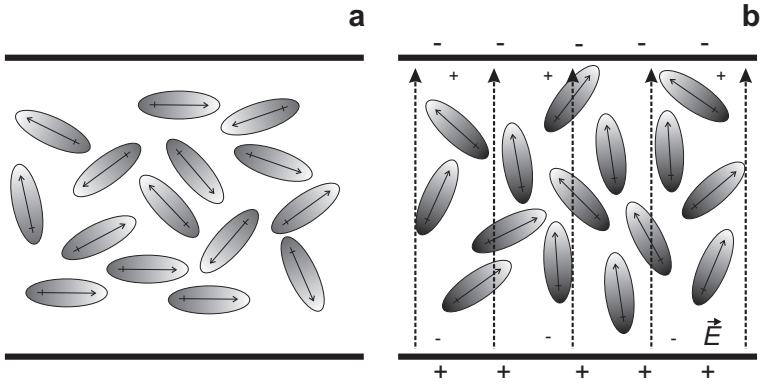

Figure 1.1: Liquid consisting of dipolar molecules within a capacitor: (a) without and (b) after charging of the capacitor. Broken arrows indicate the external electric field $\vec{E}$, the darker part of the dipolar molecules corresponds to the negative, the lighter part to the positive end of the dipoles. Charges outside of the capacitor represent the charge of the capacitor plates, smaller charges within the liquid but near the plates symbolize the effective charge separation.

Polarization (Eq. 1.1) can thus be divided into two microscopic contributions,

$$\vec{P} = \vec{P}_\alpha + \vec{P}_\mu \tag{1.4}$$

the induced polarization

$$\vec{P}_\alpha = \sum_k \rho_k \vec{\mu}_{k,\mathrm{ind}} = \sum_k \rho_k \alpha_k (\vec{E}_{\mathrm{loc}})_k \tag{1.5}$$

and the dipolar (orientational) polarization

$$\vec{P}_\mu = \sum_k \rho_k \langle \vec{\mu}_k \rangle \tag{1.6}$$

where $\vec{\mu}_k$ and $\vec{\mu}_{k,\mathrm{ind}}$ are the permanent and induced dipole moments, respectively, α_k is the molecular polarizability and ρ_k the number density of particles k. $(\vec{E}_{\mathrm{loc}})_k$ is the local field acting at the position of the particles k (see Chapter 1.5.1).
The induced polarization (Eq. 1.5) refers to the generation of an electrical dipole, $\vec{\mu}_{k,\mathrm{ind}}$, due to the displacement of electrons or atoms by the local field, $(\vec{E}_{\mathrm{loc}})_k$. The proportionality factor between $(\vec{E}_{\mathrm{loc}})_k$ and $\vec{P}_\alpha$, the molecular polarizability α_k, is generally expressed as a polarizability volume, $\alpha'_k = \alpha_k/(4\pi\varepsilon_0)$ of magnitude $10^{-30}\,\mathrm{m}^3$ ($=\text{Å}^3$).[39] It is in fact a sum of two contributions: atomic polarization, $\alpha_{k,\mathrm{n}}$, and electronic polarization $\alpha_{k,\mathrm{e}}$.

$$\alpha_k = \alpha_{k,\mathrm{n}} + \alpha_{k,\mathrm{e}} \tag{1.7}$$

with $\alpha_{k,\mathrm{n}} \approx 0.1\alpha_{k,\mathrm{e}}$.[39]
The orientational polarization (Eq. 1.6) originates from the partial alignment of permanent molecular dipoles, $\vec{\mu}_k$, along the applied external field against thermal motion.

Thus, the macroscopic dipole moment $\vec{M}$ from Eq. 1.1 can be expressed as

$$\vec{M} = \sum_k (\vec{\mu}_{k,\mathrm{ind}} + \langle\vec{\mu}_k\rangle) \tag{1.8}$$

Orientational polarization in liquids does not occur instantaneously, in contrast to $\vec{P}_\alpha$, but takes pico- to nanoseconds for full establishment. This corresponds to an approximate frequency scale of 1 MHz to 10 THz.
Due to the different time scales of $\vec{P}_\mu$ and $\vec{P}_\alpha$, both effects are generally well separated and can be regarded as linearly independent.[40] Thus the induced polarization can be incorporated into the infinite frequency permittivity, ε_∞. This enables a division of the macroscopic definition of $\vec{P}$ (Eq. 1.2) into two contributions:

$$\vec{P}_\mu = \varepsilon_0(\varepsilon - \varepsilon_\infty)\vec{E} \tag{1.9}$$

$$\vec{P}_\alpha = \varepsilon_0(\varepsilon_\infty - 1)\vec{E} \tag{1.10}$$

1.1.2 Response functions of the orientational polarization

Figure 1.2 illustrates a time domain experiment monitoring the time evolution of the polarization $\vec{P}(t)$, when the static electric field $\vec{E}$ is switched off at time $t = 0$. The instantaneous drop in $\vec{P}$ due to the disappearance of $\vec{P}_\alpha$, is followed by a monotonic decay, which can be related to $\vec{P}_\mu$ alone. This decay of the orientational polarization can be expressed as,

$$\vec{P}_\mu(t) = \vec{P}_\mu(0) \cdot F_P(t) \tag{1.11}$$

where $F_P(t)$ is the step response function (time autocorrelation function) defined by

$$F_P(t) = \frac{\langle\vec{P}_\mu(0) \cdot \vec{P}_\mu(t)\rangle}{\langle\vec{P}_\mu(0) \cdot \vec{P}_\mu(0)\rangle} \tag{1.12}$$

with limiting values $F_P(0) = 1$ and $F_P(\infty) = 0$.
Frequency domain experiments are in fact of greater practical importance than time domain experiments. The employed harmonically oscillating electric fields are conveniently expressed in complex notation as

$$\hat{\vec{E}} = \vec{E}_0 \exp(\mathrm{i}\omega t) \tag{1.13}$$

where $\omega = 2\pi\nu$ is the angular frequency of a wave of frequency ν. Now also polarization, $\hat{\vec{P}}$, and permittivity, $\hat{\varepsilon}$, are expressed as complex values. Experiments in both, the frequency and the time domain, are able to provide a wealth of information on the structure and dynamics of the investigated liquid. For the conversion of time domain experiments into

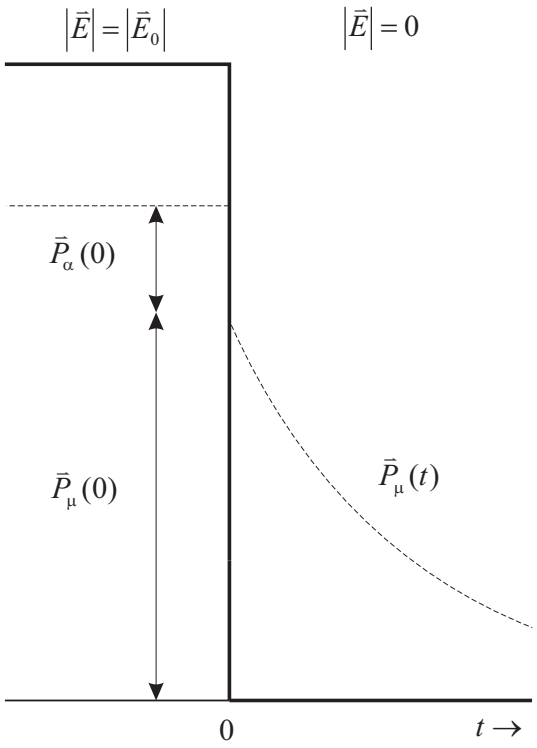

Figure 1.2: Time evolution of polarization, $\vec{P}(t)$, after the static electric field of strength $|\vec{E}| = |\vec{E}_0|$ has been switched off at time $t = 0$.[41] Bold line denotes modulus of electric field, $|\vec{E}|$, dotted line polarization.

frequency domain, Laplace transformation is applied. First, the negative time-derivative of the normalized step response function

$$f_P(t') = -\frac{\partial F_P(t-t')}{\partial(t-t')} \quad \text{normalized with} \quad \int_0^\infty f_P(t')\mathrm{d}t' = 1 \tag{1.14}$$

is formed, and then Laplace transformed to yield the relaxation function

$$\tilde{F}_p(\omega) = \int_0^\infty \exp(-\mathrm{i}\omega t') f_P(t')\mathrm{d}t' = \mathcal{L}_{\mathrm{i}\omega}[f_P(t')] \tag{1.15}$$

The frequency dependent time evolution of $\hat{\vec{P}}(\omega, t)$ is thus given by

$$\hat{\vec{P}}_\mu(\omega, t) = \varepsilon_0(\varepsilon - \varepsilon_\infty)\tilde{F}_p(\omega)\hat{\vec{E}} \tag{1.16}$$

1.2 Spectra of complex permittivity

Usually not the orientational polarization $\hat{\vec{P}}_\mu(\omega, t)$, but the closely related complex relative permittivity, $\hat{\varepsilon}(\omega)$, is investigated. $\hat{\varepsilon}(\omega)$ can be determined from the effect of dielectric media on electromagnetic waves as described in Section 1.4.
The complex permittivity, $\hat{\varepsilon}(\omega)$, can be calculated via[26]

$$\hat{\varepsilon}(\omega) = \varepsilon'(\omega) - \mathrm{i}\varepsilon''(\omega) = \varepsilon_\infty + (\varepsilon - \varepsilon_\infty) \cdot \mathcal{L}_{\mathrm{i}\omega}[f_P(t')] = \varepsilon_\infty + (\varepsilon - \varepsilon_\infty) \cdot \tilde{F}_p(\omega) \qquad (1.17)$$

The real part of $\hat{\varepsilon}(\omega)$ is the permittivity spectrum and describes the polarization of the system. The imaginary part, ε'', called dielectric loss, is a measure for the energy dissipation in the system.[41]
Figure 1.3 shows a generic dielectric spectrum. In principle all processes that are contributing to the polarization show up in the frequency dependent dielectric spectrum. With increasing frequency ν, less processes are able to follow the rapidly changing electric field and will thus cease to contribute to $\hat{\varepsilon}$. At low frequencies the main contribution to $\hat{\varepsilon}$ stems from the rotational motion of dipolar molecules. Depending on the size, shape and degree of binding to the surrounding molecules, the rotating molecules will not be able to follow the electric field with increasing frequency anymore: a dispersion of the relative permittivity $\varepsilon'(\omega)$ is observed. Simultaneously energy is dissipated in the system, which is evident in a maximum of the dielectric loss $\varepsilon''(\omega)$.

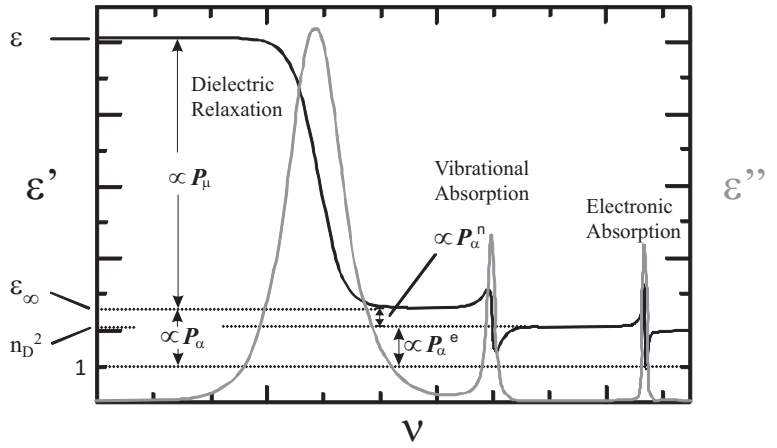

Figure 1.3: Generic dielectric spectrum containing one relaxation process, one IR active vibration and one UV-VIS absorption.

Additionally to full molecular rotation, dielectric dispersion can occur due to librations at THz and far infrared frequencies. Those represent partial or hindered reorientations of molecular dipoles.[41] The origin of these restricted rotations lies in the interactions (e.g. hydrogen bonding) with other molecules.
As in condensed phase the reorienting dipoles are coupling with the surrounding medium, relaxations manifest themselves as rather broad bands. The high frequency limit of the

permittivity ε_∞ is reached when orientational polarization no longer contributes to the total polarization.

The value of $\hat{\vec{P}}_\alpha$ is rather constant in the microwave frequency range although its frequency dependence at infrared frequencies yields information about the intramolecular dynamics of the system.[42] The dispersion steps related to $\vec{P}_\alpha$ are resonance processes governed by quantum mechanics, in contrast to the relaxation processes related to $\vec{P}_\mu$. Atomic polarization vanishes at infrared frequencies (intramolecular vibrations) and electronic polarization in the ultraviolet range. The absorbtion peaks are in most cases more narrow compared to those at microwave frequencies.[43]

For heterogeneous systems dielectric processes in the MHz frequency range can arise additionally from polarization at the interfaces of the system (interfacial polarization).[26,44,45]

1.3 Empirical description of dielectric relaxation

Several empirical and semi-empirical equations have been developed to describe dielectric relaxation phenomena. Ideally each molecular species of a sample shows up as a separate relaxation process, thus the dielectric spectra of most real systems are composed of several processes. Assuming that each relaxation process can be treated as linearly independent, the relaxation function $\tilde{F}_p(\omega)$ can be described by a superposition of n single relaxation processes j:

$$(\varepsilon - \varepsilon_\infty \tilde{F}_p(\omega) = \sum_{j=1}^{n} S_j F_j(\omega) \tag{1.18}$$

The dielectric spectrum can then generally be described as

$$\hat{\varepsilon}(\nu) = \varepsilon_\infty + \sum_{j=1}^{n} S_j F_j(\omega) \tag{1.19}$$

The relaxation modes j can be modeled by modifications of the Havriliak-Negami equation (HN, Eq. 1.20) with relaxation time τ_j and shape parameters α_j ($0 \leq \alpha_j < 1$) and β_j ($0 < \beta_j \leq 1$). Simplified versions of the Havriliak-Negami equation are the Cole-Davidson (CD, $\alpha_j = 0$, Eq. 1.21), Cole-Cole (CC, $\beta_j = 1$, Eq. 1.22) and Debye equations (D, $\alpha_j = 0$, $\beta_j = 1$).[25,26]

$$\text{HN}: \qquad F_j(\omega) = \frac{1}{(1 + (\mathrm{i}\omega\tau_j)^{1-\alpha})^\beta} \tag{1.20}$$

$$\text{CD}: \qquad F_j(\omega) = \frac{1}{(1 + \mathrm{i}\omega\tau_j)^\beta} \tag{1.21}$$

$$\text{CC}: \qquad F_j(\omega) = \frac{1}{1 + (\mathrm{i}\omega\tau_j)^{1-\alpha}} \tag{1.22}$$

$$\text{D}: \qquad F_j(\omega) = \frac{1}{1 + \mathrm{i}\omega\tau_j} \tag{1.23}$$

1.4 Effect of a dielectric medium on electric fields

As already stated in Section 1.1 external electric fields influence a dielectric medium as expressed in the generated polarization, $\hat{\vec{P}}$. Inversely, the dielectric medium also has an influence on the electric field, which can be utilized to probe the dielectric properties of the medium.

The electric field strength of a plane electromagnetic wave is conveniently expressed in complex notation as given in Eq. 1.13, which is sufficient to express the propagation in free space. However, if the wave is traveling through a medium characterized through dielectric

constant $\hat{\varepsilon}$, permeability $\hat{\mu}$ and conductivity $\hat{\kappa}$, the electric field $\hat{\vec{E}}(t,z)$ after traveling a distance z in the medium is expressed as

$$\hat{\vec{E}} = \vec{E}_0 \exp(\mathrm{i}\omega t) \exp(-\hat{\gamma} z) \tag{1.24}$$

The influence of the medium is thereby summarized in the complex propagation coefficient $\hat{\gamma}$ given by

$$\hat{\gamma} = \sqrt{\hat{\mu}\mu_0 \left(-\mathrm{i}\omega\hat{\kappa} + \hat{\varepsilon}\varepsilon_0\omega^2\right)} \tag{1.25}$$

where μ_0 and ε_0 are the permeability and permittivity of free space. The complex relative permittivity, $\hat{\varepsilon}$, was already introduced in Eq. 1.17 as $\hat{\varepsilon}(\omega) = \varepsilon'(\omega) - \mathrm{i}\varepsilon''(\omega)$. The complex relative permeability, $\hat{\mu}(\omega)$ and the complex conductivity, $\hat{\kappa}(\omega)$ are expressed analogously as

$$\hat{\mu}(\omega) = \mu'(\omega) - \mathrm{i}\mu''(\omega) \tag{1.26}$$

$$\hat{\kappa}(\omega) = \kappa'(\omega) - \mathrm{i}\kappa''(\omega) \tag{1.27}$$

For nonmagnetic materials (applies to all studied solutions of this work) $\hat{\mu} = 1$, which leads to a simplified version of Eq. 1.25

$$\hat{\gamma} = \frac{\omega}{c_0}\left[\frac{\hat{\kappa}}{\mathrm{i}\omega\varepsilon_0} + \hat{\varepsilon}\right]^{1/2} = \frac{\omega}{c_0}\sqrt{\hat{\eta}(\omega)} = \hat{k} \tag{1.28}$$

Here, the speed of light in vacuum, c_0, was introduced via the equivalency $c_0 = 1/(\mu_0\varepsilon_0)^{1/2}$. The complex wavenumber, $\hat{k}$, is intimately related to $\hat{\gamma}$ via Eq. 1.28. Generally, $\hat{k}$ contains all effects of the medium, whereas $\hat{\gamma}$ also includes boundary conditions from the used transmission line type. For coaxial lines $\hat{\gamma}$ and $\hat{k}$ can be interchanged.[46] However, for waveguides differences between both quantities exist due to the imposed boundary conditions (Chapter 2.2.1).

The relation between the complex wavenumber and the generalized permittivity, $\hat{\eta}(\omega)$ is given by

$$\hat{k} = k_0\left[\hat{\varepsilon}(\omega) + \frac{\hat{\kappa}(\omega)}{\mathrm{i}\omega\varepsilon_0}\right]^{1/2} = k_0\sqrt{\hat{\eta}(\omega)} \tag{1.29}$$

where k_0 is the propagation constant of free space, $k_0 = \omega\sqrt{\varepsilon_0\mu_0} = 2\pi/\lambda_0$ with the wavelength of a monochromatic wave in vacuum, λ_0[42]. The generalized permittivity $\hat{\eta}(\omega)$ is related to the actually interesting complex permittivity via

$$\varepsilon'(\omega) = \eta'(\omega) + \frac{\kappa''(\omega)}{\varepsilon_0\omega} \tag{1.30}$$

$$\varepsilon''(\omega) = \eta''(\omega) - \frac{\kappa'(\omega)}{\varepsilon_0\omega} \tag{1.31}$$

The main implementation of Eqs. 1.30 is, that for conducting samples the experimentally accessible quantities are the real and imaginary part of $\hat{\eta}(\omega)$. Thus an independent mea-

surement of dielectric properties and conductivity is not possible. A pragmatic way to split the two contributions is to use the limits of $\hat{\kappa}(\omega)$:

$$\lim_{\nu\to 0}\kappa' = \kappa \Rightarrow \varepsilon''(\omega) = \eta''(\omega) - \frac{\kappa}{\omega\varepsilon_0} \tag{1.32}$$

$$\lim_{\nu\to 0}\kappa'' = 0 \Rightarrow \varepsilon'(\omega) = \eta'(\omega) \tag{1.33}$$

By using this approach, $\hat{\varepsilon}$ contains all time dependent processes (rotational, translational and vibrational) that contribute to the polarization. This treatment is problematic, as the generally accepted theory of Debye and Falkenhagen[47] predicts a dispersion, i.e. frequency dependence of the conductivity due to ion-cloud relaxation. As a consequence, a potential dispersion of $\hat{\kappa}$ should show up in $\hat{\varepsilon}$ and lead to misinterpretations. This problem is actually the topic of Chapter 3 of this work.
The relationship between $\hat{\eta}$ and the complex refractive index $\hat{n}$ is given by

$$\hat{n}(\omega) = n'(\omega) - \mathrm{i}n''(\omega) = \sqrt{\hat{\eta}(\omega)} \tag{1.34}$$

where $n'(\omega)$ is the refractive index and $n''(\omega)$ the absorption index. Squaring and separation into real and imaginary parts yields the equation set

$$\eta'(\omega) = n'(\omega)^2 - n''(\omega)^2 \tag{1.35}$$

$$\eta''(\omega) = 2n'(\omega)n''(\omega) \tag{1.36}$$

Elimination of $n''(\omega)$ yields

$$4n'(\omega)^4 - 4n'(\omega)^2\varepsilon'(\omega) - \varepsilon''(\omega)^2 = 0 \tag{1.37}$$

which is quadratic in $n'(\omega)^2$. The (positive) solution of this equation eventually gives the relation between $\hat{n}$ and $\hat{\eta}$:

$$n'(\omega) = \sqrt{\frac{1}{2}\sqrt{\eta'(\omega)^2 + \eta''(\omega)^2} + \eta'(\omega)} \tag{1.38}$$

$$n''(\omega) = \sqrt{\frac{1}{2}\sqrt{\eta'(\omega)^2 + \eta''(\omega)^2} - \eta'(\omega)} \tag{1.39}$$

Insertion of Eqs. 1.34 & 1.28 into Eq. 1.24 yields

$$\vec{E} = \vec{E}_0\exp[\mathrm{i}(\omega t - \beta z)]\exp[-\alpha_\mathrm{a} z] = \vec{E}_0\exp[\mathrm{i}\omega t]\exp[-(\alpha_\mathrm{a} + \mathrm{i}\beta)z] \tag{1.40}$$

with the absorption coefficient $\alpha_\mathrm{a} = \omega n''(\omega)/c_0$ and the phase constant $\beta = \omega n'(\omega)/c_0$. The measurement of the latter two quantities, forms the basis for the determination of $\hat{\eta}(\omega)$. The correlation between those quantities is revealed by comparison of Eq. 1.24, 1.28 and 1.40

$$\hat{\gamma} = \alpha_\mathrm{a} + \mathrm{i}\beta = \mathrm{i}\hat{k} \tag{1.41}$$

1.5 Microscopic models of dielectric relaxation

Spectra of complex permittivity can be described by a mathematical model as shown in Section 1.3. This description, however, yields only macroscopic properties that need to be linked to microscopic properties to retrieve valuable information on structure and dynamics of the system.

1.5.1 Onsager equation

The response of a single dipole, which is embedded in a dielectric continuum, on an electrical field is described by the Onsager model.[26,48] This model describes the continuum by its macroscopic properties and neglects specific interactions as well as the anisotropy of the surrounding field.
Based on this approach, Onsager deduced following relation for the interpretation of dielectric properties

$$\varepsilon_0(\varepsilon-1)\vec{E} = \vec{E}_\mathrm{h} \cdot \sum_j \frac{\rho_j}{1-\alpha_j f_j}\left(\alpha_j + \frac{1}{3k_\mathrm{B}T}\cdot\frac{\mu_j^2}{1-\alpha_j f_j}\right) \tag{1.42}$$

where ρ_j is the dipole density, α_j the polarizability, f_j the reaction field factor and μ_j the dipole moment of species j.
$\vec{E}_\mathrm{h}$ represents the local electric field in the cavity

$$\vec{E}_\mathrm{h} = \frac{3\varepsilon}{2\varepsilon+1}\vec{E} \tag{1.43}$$

assuming the molecule is within a spherical cavity of the dielectric material characterized by its static permittivity ε.
Inserting the expression for the local field into Eq. 1.42 yields the general form of the Onsager equation which relates the macroscopic static permittivity with the microscopic properties (polarizability and dipole moment) of a mixture of dipoles j.

$$\frac{(\varepsilon-1)(2\varepsilon+1)\varepsilon_0}{3\varepsilon} = \sum_j \frac{\rho_j}{1-\alpha_j f_j}\left(\alpha_j + \frac{1}{3k_\mathrm{B}T}\cdot\frac{\mu_j^2}{1-\alpha_j f_j}\right) \tag{1.44}$$

This equation can be simplified to

$$\frac{(\varepsilon-\varepsilon_\infty)(2\varepsilon+\varepsilon_\infty)}{\varepsilon(\varepsilon_\infty+2)^2} = \frac{\rho\mu^2}{9\varepsilon_0 k_\mathrm{B}T} \tag{1.45}$$

if a liquid with just one dipolar species exhibiting only one dielectric dispersion step is under investigation.

1.5.2 Kirkwood-Fröhlich equation

The Onsager equation was derived under the assumption of completely uncorrelated dipoles. However, in reality the orientation of dipolar molecules shows some sort of correlation with the neighboring molecules. Those specific interactions can be introduced with the help of statistical mechanics and result in the Kirkwood-Fröhlich equation[49,50]

$$\frac{(\varepsilon - \varepsilon_\infty)(2\varepsilon + \varepsilon_\infty)}{\varepsilon(\varepsilon_\infty + 2)^2} = \frac{\rho\mu^2}{9\varepsilon_0 k_\mathrm{B} T} \cdot g_\mathrm{K} \tag{1.46}$$

where g_K is the Kirkwood factor, which is a measure for the interactions among the particles. Preferential parallel orientation of neighboring molecules is expressed by $g_\mathrm{K} > 1$, whereas $g_\mathrm{K} < 1$ indicates an antiparallel correlation. The value $g_\mathrm{K} = 1$ is observed for statistical (i.e., fully random) alignment.

1.5.3 Cavell equation

The Kirkwood-Fröhlich equation is still limited as just one dipolar species, showing a single relaxation step is considered. The Cavell equation[51] is a more general expression describing systems with more than one dispersion step due to different dipolar species. It can be written as

$$\frac{\varepsilon + A_j(1-\varepsilon)}{\varepsilon} \cdot S_j = \frac{N_\mathrm{A} c_j}{3 k_\mathrm{B} T \varepsilon_0} \cdot \mu_{\mathrm{eff},j}^2 \tag{1.47}$$

Each amplitude, S_j, of relaxation step j of a combination of relaxations (Eq. 1.19) is connected to the molar concentration c_j, of the species j and its effective dipole moment μ_eff. A_j is the shape factor of species j. For spherical particles $A_j = 1/3$, and for ellipsoids with half-axes $a_j > b_j > c_j$ it can be calculated by[26,43]

$$A_j = \frac{a_j b_j c_j}{2} \int_0^\infty \frac{\mathrm{d}s}{(s + a_j^2)^{3/2}(s + b_j^2)^{1/2}(s + c_j^2)^{1/2}} \tag{1.48}$$

For prolate ellipsoids ($b_j = c_j$) Scholte[52] derived a simplified expression

$$A_j = -\frac{1}{p_j^2 - 1} + \frac{p_j}{(p_j^2 - 1)^{3/2}} \ln\left(p_j + \sqrt{p_j^2 - 1}\right) \quad \text{with} \quad p_j = \frac{a_j}{b_j} \tag{1.49}$$

The value of $\mu_{\mathrm{eff},j}$ is related to μ_j, the dipole moment of an isolated gas phase species via

$$\mu_{\mathrm{eff},j} = \sqrt{g_j}\mu_{\mathrm{ap},j} = \sqrt{g_j}\frac{\mu_j}{(1 - f_j\alpha_j)} \tag{1.50}$$

where $\mu_{\mathrm{ap},j}$ accounts for the apparent dipole moment of the species j in absence of orientational correlations, which are included via the empirical factor g_j. The values of g_j are interpreted as for the Kirkwood factor g_K (Eq. 1.46). Cavity- and reaction-field-effects are included in $\mu_{\mathrm{ap},j}$ and are introduced by dividing μ_j by $(1 - f_j\alpha_j)$, where α_j is the

polarizability of the species j and f_j the corresponding reaction field factor, which can be calculated for a spherical cavity of radius a_j via[26]

$$f_j = \frac{1}{4\pi\varepsilon_0 a_j^3} \cdot \frac{2\varepsilon - 2}{2\varepsilon + 1} \tag{1.51}$$

For ellipsoidal particles with half-axes $a_j > b_j > c_j$ the reaction field factor can be calculated from the geometry of the particle:[26,53]

$$f_j = \frac{3}{4\pi\varepsilon_0 a_j b_j c_j} \cdot \frac{A_j(1 - A_j)(\varepsilon - 1)}{\varepsilon + (1 - \varepsilon)A_j} \tag{1.52}$$

1.5.4 Debye model of rotational diffusion

For the relation of the relaxation time with (geometric) microscopic properties of the relaxing species, Debye considered a system of spherical inelastic dipoles which do not interact with each other. Within this system, frequent uncorrelated collisions among the particles cause rotational motion of the dipoles. This picture is known as diffusion of dipolar orientation.[54]

Yet, in this model inertia effects and dipole-dipole interactions are neglected. Furthermore, it is assumed that the laws of hydrodynamics, describing the rotation of a macroscopic particle in a liquid, can be applied to microscopic particles as well. Thus, this theory is limited to non-associated systems for particles that are large in comparison to the surrounding ones. Within these limitations and by describing the inner field with a Lorentz field, Debye obtained the dipole correlation function,

$$\gamma(t) = \exp\left(-\frac{t}{\tau_{\mathrm{rot}}}\right) \tag{1.53}$$

where the relaxation time, τ_{rot}, can be obtained from the friction factor, ζ,

$$\tau_{\mathrm{rot}} = \frac{\zeta}{2k_{\mathrm{B}}T} \tag{1.54}$$

Under the assumption of a hydrodynamically controlled rotation of the sphere in a viscous media, the Stokes-Einstein-Debye equation

$$\tau_{\mathrm{rot}} = \frac{3V_{\mathrm{m}}\eta'}{k_{\mathrm{B}}T} \tag{1.55}$$

is obtained, where V_{m} represents the volume of the sphere and η' the (microscopic) dynamic viscosity of the environment of the sphere. This treatment is problematic, as the relation between microscopic viscosity, η', and the actually measured macroscopic viscosity, η is not clear.

Thus, Dote *et al.*[55] derived a more general relationship by introducing the effective volume of rotation, V_{eff}

$$\tau' = \frac{3V_{\text{eff}}\eta}{k_{\text{B}}T} + \tau^0_{\text{rot}} \tag{1.56}$$

The empirical axis intercept, τ^0_{rot}, is occasionally interpreted as the correlation time of the freely rotating particle. For the derivation of microscopic relaxation times, τ' in this work, only the first term of Eq. 1.56 was considered. V_{eff} is introduced to account for differences between macroscopic and microscopic viscosity by the introduction of a hydrodynamic friction factor, C, as well as for deviations from spherical shape, characterized by the shape factor f:

$$V_{\text{eff}} = fCV_{\text{m}} \tag{1.57}$$

where V_{m} is the molecular volume of the particle. C has limiting values of $C_{\text{stick}} = 1$ for *stick* and $C_{\text{slip}} = 1 - f^{-2/3}$ for *slip* boundary conditions. The hydrodynamic friction parameter hints at the strength of interaction between the rotating particle and the surrounding molecules.

Calculation of the shape parameter f is possible when the geometry of the particle is known,[56,57]

$$f = \frac{\frac{2}{3}[1-(\alpha^\perp)^4]}{\frac{[2-(\alpha^\perp)^2](\alpha^\perp)^2}{[1-(\alpha^\perp)^2]^{1/2}} \ln\left[\frac{1+[1-(\alpha^\perp)^2]^{1/2}}{\alpha^\perp}\right] - (\alpha^\perp)^2} \tag{1.58}$$

where $\alpha^\perp$ represents the ratio between the volume of the particle and the volume swept out as the particle rotates about an axis perpendicular to the symmetry axis. For a prolate spheroid with major axis a and minor axis b, $\alpha^\perp = b/a$.[57]

1.5.5 Microscopic and macroscopic relaxation time

The experimentally accessible dielectric relaxation time, τ, is a collective property[26] and has to be converted to a corresponding microscopic quantity, the rotational correlation time, τ'. Powles suggested an expression which is valid for a single Debye relaxation[58]

$$\tau = \frac{3\varepsilon}{2\varepsilon + \varepsilon_\infty} \cdot \tau' \tag{1.59}$$

Glarum[59] confirmed and extended the work by Powles to account for two-Debye relaxations

$$\tau_1 = \frac{3\varepsilon}{2\varepsilon + \varepsilon_1}\tau_1' \tag{1.60}$$

$$\tau_2 = \frac{2\varepsilon + \varepsilon_1}{2\varepsilon + \varepsilon_\infty}\tau_2' \tag{1.61}$$

where $\tau_1 > \tau_2$, and for a single Cole-Cole relaxation

$$\tau_0 = \left(\frac{3\varepsilon}{2\varepsilon + \varepsilon_\infty}\right)^{1/(1-\alpha)} \tau_0' \tag{1.62}$$

Usually, the macroscopic and microscopic relaxation times do not differ greatly,[59] especially in the case of ion-pairs, for which Eq. 1.60 is normally used. Therefore, in this work it was mostly refrained from converting the macroscopic into microscopic relaxation times for comparison with Eq. 1.56.
Madden and Kivelson[60] extended the approach by Powles and Glarum to additionally account for dipole-dipole correlations

$$\tau = \frac{3\varepsilon}{2\varepsilon + \varepsilon_\infty} \cdot \frac{g_\mathrm{K}}{\dot{g}} \cdot \tau_\mathrm{rot} \tag{1.63}$$

where g_K is the Kirkwood correlation factor and $\dot{g}$ the dynamic correlation factor. For the limit $g_\mathrm{K}/\dot{g} = 1$ eq. 1.63 reduces to the Powles-Glarum equation (eq. 1.59).

1.6 Dielectric Relaxation of Neat Water

1.6.1 Current Knowledge from Experiment

The dielectric properties of water have been studied extensively,[31,42,61,62] however, still open questions on the physical origin of some of the observed relaxation modes remain. The so far most detailed description was given by Hunger,[42] which will be shortly summarized in the following.
A detailed analysis of data covering a frequency range ~ 0.1 GHz to 25 THz yielded a best fit model consisting of two Debye processes at the low frequency end (20 GHz and 300 GHz), and three damped harmonic oscillators (DHOs) at $\sim$5 THz, $\sim$12 THz and $\sim$ 21 THz at higher frequencies.
The high frequency DHOs are well characterized and correspond to a hydrogen-bond stretching vibration at $\sim$5 THz and two librations at $\sim$12 THz and $\sim$ 21 THz.[62,63]
For DR measurements restricted to the frequency range $0.2 \leq \nu/\mathrm{GHz} \leq 89$ at best the two Debye type relaxations are observable. The dominating relaxation at $\sim$18 GHz is easily detectable and attributed to the cooperative hydrogen-bond dynamics in liquid water.[62]
The next section presents a recent model of water relaxation derived by MD simulations, which gives more insight into this relaxation. The origin of the fast water process at $\sim$300 GHz is still not resolved. A good overview of the existing interpretations is given by Hunger.[42] For this work, the common assignment to weakly or even non-hydrogen-bonded water molecules is adopted.

1.6.2 Implications from MD on Water Rotation

Laage *et al.* introduced a molecular model, that does not describe water rotation through rotational or Debye diffusion (Section 1.5.4), but through a large angle jump reorientation.[64,65]

Basis of this model is the time-correlation function (TCF) of the molecular reorientation[66]

$$C_n(t) = \langle P_n[\mathbf{u}(0) \cdot \mathbf{u}(t)] \rangle \tag{1.64}$$

where P_n is the nth-rank Legendre polynomial and $\mathbf{u}$ a vector attached to the water molecule like the dipole moment. Different experimental techniques detect different order TCFs: DRS and IR spectroscopy detect first order TCFs, whereas nuclear magnetic resonance (NMR), optical Kerr-effect spectroscopy (OKE), femtosecond infrared spectroscopy (fs-IRS) and quasi-elastic neutron scattering (QENS) detect the second order TCF. The ratio of the associated relaxation times, τ_1/τ_2 should be 3, if water relaxes through rotational diffusion. MD simulations, however gave a numerical ratio of 2.0,[65] which clearly indicates that water relaxation does not proceed through rotational diffusion.

The orientation TCF $C_2(t)$ as detected by MD shows a bimodal decay: fast ($<$200 fs) partial reorientation, followed by slower (picosecond) full reorientation.[65] The fast part is attributed to librations, which occur in the DRS spectrum at $\sim$12 THz and $\sim$ 21 THz. The longer time decay of $C_2(t)$ is attributed to large-amplitude angular jumps due to a switch of H-bond acceptors of a water molecule, and provides a molecular picture for the observed dominating relaxation at $\sim$18 GHz in DR spectra.

Considering a rotating OH moiety, first, the initial H-bond is elongated, with the simultaneous approach of a new water oxygen acceptor from the second shell. When the two oxygen acceptors are equidistant with regard to the rotating water oxygen, a transition state is reached, where the rotating water forms a symmetric bifurcated hydrogen bond with the old and new oxygen acceptors. Then, hydrogen bond acceptor switch is executed via a sudden large-amplitude angular jump.[66]

The angular jump of a water molecule is accompanied by frame reorientation, which means that the surrounding water molecules have to rearrange to allow for the substituting water molecule to reach the rotating water from the second shell. After a successful jump, the surrounding water molecules have to rearrange again, to reach the energetically most favorable topology. As jump and frame contributions occur on different timescales, they can be treated as independent and be combined in an extended jump model (EJM),[66] resulting in the overall reorientation time

$$\frac{1}{\tau_n^{\mathrm{EJM}}} = \frac{1}{\tau_n^{\mathrm{jump}}} + \frac{1}{\tau_n^{\mathrm{frame}}} \tag{1.65}$$

with $\tau_2^{\mathrm{EJM}} = 2.2\,\mathrm{ps}$, $\tau_2^{\mathrm{jump}} = 3.6\,\mathrm{ps}$ and $\tau_n^{\mathrm{frame}} = 5.6\,\mathrm{ps}$.[65] Interestingly, the Debye process at $\sim$300 GHz observed in experimental spectra, does not show up in the simulations.[42]

1.7 Ion Association

Electrolyte solutions are generally described within the Debye-Hückel theory, stating that each ion is surrounded by a symmetrical ion-cloud[67]. This theory, however, is just valid at the infinite-dilution limit. It neglects, among others, ion-ion interactions beyond mere screened Coulomb interactions, which can result in more or less pronounced ion association. Ion pairing equilibria

$$\underset{\text{solvated free ions}}{\mathrm{M}^{x+}(\mathrm{aq}) + \mathrm{X}^{y-}(\mathrm{aq})} \overset{K_\mathrm{A}}{\rightleftharpoons} \underset{\text{solvated ion pair}}{\mathrm{MX}^{(x-y)}(\mathrm{aq})}$$

are of general scientific interest.[21] However, in aqueous solution ions are generally strongly solvated and associate via a three-step process[68,69] in which the free hydrated ions initially combine with their (inner) hydration sheaths essentially intact to form a double solvent-separated ion pair (2SIP). This is followed by successive losses of water molecules to form a solvent-shared(SIP) and then a contact (CIP) ion pair (Figure 1.4).

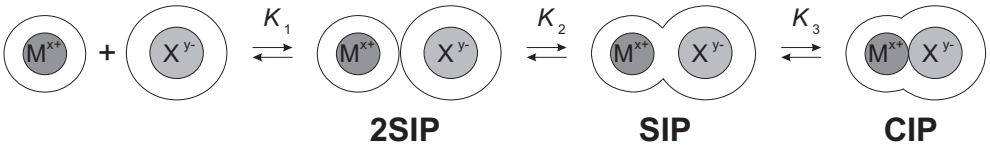

Figure 1.4: Scheme of stepwise ion association according to Eigen and Tamm.[68,69]

DRS is especially well suited to study ion-pairing equilibria, as its sensitivity (i.e. the detected amplitude S) is proportional to μ_{eff}^2 (Eq. 1.47). Thus, this technique has been successfully used to quantify multi-step association equilibria in aqueous and non-aqueous solutions.[18,70] As the dipole moment of ion-pairs increases with increasing number of intervening solvent molecules, the sensitivity of DRS towards the different types of ion-pairs decreases as 2SIP $>$ SIP $>$ CIP.

For the determination of ion-pair dipole moments a suitable geometric model is necessary. In this work, the procedure as described by Barthel *et al.*,[53] for the determination of gas phase dipole moments, μ_{IP} was adopted (Figure 1.5). Here a distinction between symmetric and asymmetric electrolytes has to be made.

For symmetric electrolytes, calculation of μ_{IP} starts from the dipole moment given by the distance h of cation and anion of charge $z \cdot e_0$,

$$\mu_0 = z \cdot e_0 \cdot h \tag{1.66}$$

Anion and cation of the ion pair create an electric field E_{dipole}, which forces the intervening n water molecules and the ions themselves (if they possess a permanent dipole moment

μ_+ or μ_-) to align in an antiparallel fashion to μ_0. Additionally, E_{dipole} induces a dipole moment in the ions due to the polarizability given by[71]

$$\mu_{\text{ind}} = \frac{h^4 e_0(|z_-|\alpha_+ + z_+\alpha_-) + 2h\alpha_+\alpha_- e_0(|z_-| + z_+)}{h^6 - 4\alpha_+\alpha_-} \tag{1.67}$$

The final gas phase dipole moment of symmetrical electrolytes thus is calculated as

$$\mu_{\text{IP}} = \mu_0 - \mu_+ - \mu_- - \mu_{\text{ind}} - n\mu_{\text{H}_2\text{O}} \tag{1.68}$$

For the calculation of the effective dipole moment, $\mu_{\text{eff,IP}}$, the field factor f_{IP} is calculated via Eq. 1.52 and the ion-pair polarizability, α_{IP}, is given by the sum of the ion polarizabilities and intervening water molecules. As ion-pairs are considered to be uncorrelated, $g_j = 1$ and thus $\mu_{\text{ap,IP}} = \mu_{\text{eff,IP}}$.

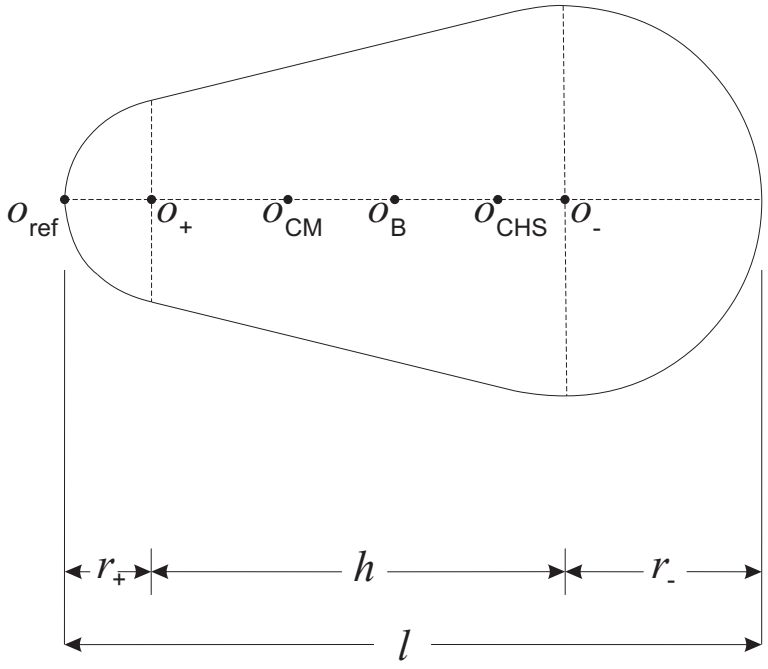

Figure 1.5: Scheme of a spherocone, with an cation of radius r_+ at position o_+, and an anion of radius r_- at o_-. h denotes the cone length and l the length of the ion pair. The position of the center of mass, o_{CM}, the center of hydrodynamic stress, o_{CHS} and the pivot, o_{B} are also indicated.[53]

For asymmetric electrolytes the calculation of μ_{eff} differs in the calculation of μ_0. The decisive value is the pivot, o_B, of the dipole molecule, which is situated on the symmetry axis of the spherocone, defined by the position of the cation, o_+, and the anion, o_-.

$$\mu_0 = e_0|z_+(o_+ - o_B) + z_-(o_- - o_B)| \tag{1.69}$$

The two extreme values of o_B are given by the center of mass, o_{CM}, and the center of hydrodynamic stress, o_{CHS}. For o_{CM} it is assumed, that the dipole rotation is only controlled

by its moment of inertia with no hydrodynamic interaction with the surrounding solvent molecules

$$o_{\mathrm{CM}} = \frac{\sum_i m_i o_i}{\sum_i m_i} \tag{1.70}$$

The center of hydrodynamic stress boundary conditions imply that the frictional force on the dipole dominates the rotational motion and thus governs the position of the pivot. Unfortunately, there is no simple relationship for the calculation of o_{CHS}, however, Barthel *et al.* gave an approximation for the used spherocone model,[53] based on an approach by Dote and Kivelson[57]

$$o_{\mathrm{ref}} - o_{\mathrm{CHS}} = l \cdot \left(0.608 - 0.0917 \frac{r_+}{r_-} - 0.0186 \left(\frac{r_+}{r_-} \right)^2 \right) \tag{1.71}$$

where $o_{\mathrm{ref}} = 0$ is a reference point, l is the length of the spherocone and r_+ and r_- are the radii of the cation and anion, respectively.
DRS experiments revealed, that all strong electrolytes are ion-paired to some extent,[18] with the degree of ion-pairing depending on the ion charges and the permittivity.
The ion pair dispersion amplitude S_{IP} can be converted to ion-pair concentrations c_{IP} via Eq. 1.47 and subsequently used to calculate the ratio

$$K_{\mathrm{A}} = \frac{c_{\mathrm{IP}}}{c_+ c_-} \tag{1.72}$$

where c_+ and c_- are the concentrations of free cations and anions respectively.
For multi-step association equilibria as shown in Figure 1.4 the overall association constant is usually calculated as $K_{\mathrm{A}} = K_1 + K_1 K_2 + K_1 K_2 K_3$ with

$$K_1 = \frac{c_{\mathrm{2SIP}}}{c_+ c_-} \quad \text{and} \quad K_2 = \frac{c_{\mathrm{SIP}}}{c_{\mathrm{2SIP}}} \quad \text{and} \quad K_3 = \frac{c_{\mathrm{CIP}}}{c_{\mathrm{SIP}}} \tag{1.73}$$

The multi-step equilibria of this work are treated in a different way. For each detected type of ion pair an association constant according to Eq. 1.72 was calculated. For the overall association constant the same equation was used, where $c_{\mathrm{IP}} = c_{\mathrm{2SIP}} + c_{\mathrm{SIP}} + c_{\mathrm{CIP}}$.
Extrapolation to infinite dilution yields the standard state association constant $K_{\mathrm{A}}^{\circ} = \lim_{c \to 0} K_{\mathrm{A}}(c)$ which can be compared to corresponding values deduced by other techniques. In this work this was done by fitting the obtained $K_{\mathrm{A}}(c)$ values to a Guggenheim-type equation[24]

$$\log K_{\mathrm{A}} = \log K_{\mathrm{A}}^0 - \frac{2 \mid z_+ z_- \mid A_{\mathrm{DH}} \sqrt{I}}{1 + A_{\mathrm{K}} \sqrt{I}} + B_{\mathrm{K}} I + C_{\mathrm{K}} I^{3/2} \tag{1.74}$$

where I ($= c$ for 1:1 electrolytes) is the nominal ionic strength; $A_{\mathrm{DH}} = 0.5115\,(\mathrm{L/mol})^{1/2}$ is the Debye-Hückel constant for activity coefficients in water at 25 °C, z_+ and z_- are the formal charges of the ions, and A_{K} B_{K} and C_{K} are adjustable parameters[72]. For 1:1 electrolytes A_{K} was fixed at 1.00 $\mathrm{M}^{-1/2}$.[73]

Chapter 2

Experimental

2.1 Materials and sample preparation

All salts used for the present work were purchased from commercial suppliers in the highest, or due to the price close to the highest, available purity grade. Prior to sample preparation, salts (with the exception of NaH_2PO_4) were dried at elevated temperatures under reduced pressure ($p \leq 2 \cdot 10^{-6}$ bar) applying P_2O_5 (Siccapent, Merck) as a desiccant and then stored in a glove box under dry nitrogen. Table 2.1 provides details on the purchased salts and the drying conditions.

Table 2.1: Name, Purity Grade, Supplier and Drying Details (Drying Temperature T and Time t) of the Purchased Compounds Used For This Work.

compound	purity grade	supplier	T / K	t /h
NaCl	$\geq 99.5\%$	Merck	473	48
KH_2PO_4	$\geq 99\%$	Sigma Aldrich	383	120
$K_2HPO_4 \cdot 3H_2O$	$\geq 99\%$	Sigma Aldrich	383	120
K_3PO_4	$\geq 98\%$	Sigma Aldrich	323	24
NaH_2PO_4	$\geq 99.99\%$, anhydrous	Merck	used as received	
$(NH_4)H_2PO_4$	$\geq 99.5\%$	Fluka	333	24
$Na_2HPO_4 \cdot 2H_2O$	$\geq 99.5\%$	Merck	373	96
$(NH_4)_2HPO_4$	$\geq 99\%$	Fluka	333	48

Preparation of aqueous solutions was done gravimetrically on an analytical balance without buoyancy correction using degassed Millipore MILLI-Q water with a specific resistance of $\geq 18\,\mathrm{M\Omega\,cm}$.

2.2 Measurement of dielectric properties

Dielectric spectroscopy covers a frequency range from megahertz to terahertz, corresponding to wavelengths of several hundred meters to a few millimeters. The handling of electromagnetic waves in this frequency region is technically demanding and requires a combination of instruments. For the probed frequency range of this work, $0.2 \leq \nu/\mathrm{GHz} \leq 89$, coaxial line and waveguide setups were used. Table 2.2 summarizes the used setups with their respective frequency range.

Table 2.2: Overview of the Used Instrumental Setups with Transmission Line, Cell Type and Covered Frequency Range.

setup name	transmission line type	cell type	frequency range / GHz
VNA	coaxial cable	reflectance	0.2 - 50
X-Band	waveguide	transmission	8 - 12
Ku-Band	waveguide	transmission	12 - 18
A-Band	waveguide	transmission	27 - 40
E-Band	waveguide	transmission	60 - 89

2.2.1 Interferometer measurements

For frequencies $> 50\,\mathrm{GHz}$, problems with probe head construction pose restrictions for the use of coaxial line setups employing a Vector Network Analyzer (VNA) as described in Chapter 2.2.2. Therefore, waveguide setups are used for this frequency region. Central part of the present setup in Regensburg is a high precision receiver (Micro-Tel 1295). This instrument is able to detect the signal amplitude, thus rendering determination of absorption coefficients, α_a, possible. However, no information on the phase coefficient, β, is obtained. Alternatively, the wavelength of the electromagnetic wave in the sample, $\lambda_\mathrm{M} = 2\pi/\beta$, may be determined. The setup is thus operated as an interferometer of the Mach-Zender type[74], which additionally allows the determination of the medium wavelength, λ_M. Both parameters, α_a and λ_M, are then used to calculate the generalized complex permittivity from the relationship:

$$\hat{\gamma}^2 = \left(\alpha_\mathrm{a} + \mathrm{i}\frac{2\pi}{\lambda_\mathrm{M}}\right)^2 = k_\mathrm{c}^2 - \hat{k}^2 \tag{2.1}$$

The additional parameter $k_\mathrm{c} = \pi/a$ as compared to Eq. 1.28, is the limiting wavenumber and stems from the requirements of wave propagation in a rectangular waveguide of dimensions a and b with $a > b$. Real and imaginary part of $\hat{\eta}(\nu)$ are obtained by insertion of Eq. 1.29 into Eq. 2.1 and separation into real and imaginary parts:

$$\eta'(\nu) = \left[\left(\frac{k_c}{2\pi}\right)^2 + \left(\frac{1}{\lambda_{\mathrm{M}}(\nu)}\right)^2 - \left(\frac{\alpha_{\mathrm{a}}(\nu)}{2\pi}\right)^2\right]\left(\frac{c_0}{\nu}\right)^2 \tag{2.2}$$

$$\eta''(\nu) = \frac{\alpha_{\mathrm{a}}(\nu)}{\pi\lambda_{\mathrm{M}}(\nu)}\left(\frac{c_0}{\nu}\right)^2 \tag{2.3}$$

Instrumentation[75] Figure 2.1 shows the principle E-band setup as used in Regensburg. Individual frequencies (60, 66, 72 and 89 GHz) are generated by phase locked Gunn oscillators (**PLO**). The control unit **PLO-D** allows for selection of one oscillator and the setting of the waveguide switches. The signal is then split into a reference path and the measuring path by a directional coupler **2a**. Along the measuring path a precision phase shifter **4** and E/H tuner **5a** are arranged. Eventually it leads to the sample cell **C**, which is composed of a piece of wave guide filled with the sample liquid. The sample cell is separated from the preceding waveguide by a $\sim$0.1 mm thick mica window. Immersed in the sample cell is a gold plated ceramic probe **P**, which can be varied in its relative position as it is connected to a piece of flexible waveguide **6b**. After passing the sample cell, the signal of the measurement path is recombined with the reference signal at coupler **2b** and the relative amplitude, A, is measured as a function of optical path length z_0 after mixing and down conversion.

Measurement principle[42,75] Before a measurement, the signal amplitude, A, is maximized ($= A_{\max}$) with the probe completely descended (position $z_0 = 0$). Then the probe is moved to position z_0', where the amplitude has decreased to $\sim (A_{\max} + 10)\mathrm{dB}/2$ and full destructive interference is set with the help of the attenuators and the phase shifter. The probe is now moved back to the starting position and a measurement with total path length $2 \times z_0'$ is started.
Assuming harmonically oscillating fields, the time-dependent electric field propagating through the reference beam is given by

$$\hat{E}_1(t) = E_0 \exp(\mathrm{i}\omega t) \tag{2.4}$$

Assuming z_0 is the absolute optical path length of the transmission cell and x the relative distance from the interference minimum, $x = z_0 - z_0'$, the electromagnetic wave of the sample beam can be expressed as

$$\hat{E}_2(t, x) = E_0 \exp(-\alpha_{\mathrm{a}} x) \exp\left[\mathrm{i}(\omega t + \pi - \beta x)\right] \tag{2.5}$$

The term π of the second exponential term results from the condition of fully destructive interference, which requires a phase shift of $\Delta\varphi$ of the interfering waves:

$$\Delta\varphi = (2n+1)\pi \quad \text{with } n \in \mathbb{Z} \tag{2.6}$$

At the receiver, the superposition of the fields propagating through the sample and reference beam,

$$\hat{E}(t, x) = \hat{E}_1(t) + \hat{E}_2(t, x) = \hat{E}_0 \exp(\mathrm{i}\omega t)\left[1 + \exp(-\alpha_{\mathrm{a}} x)\exp(\mathrm{i}(\pi - \beta x))\right] \tag{2.7}$$

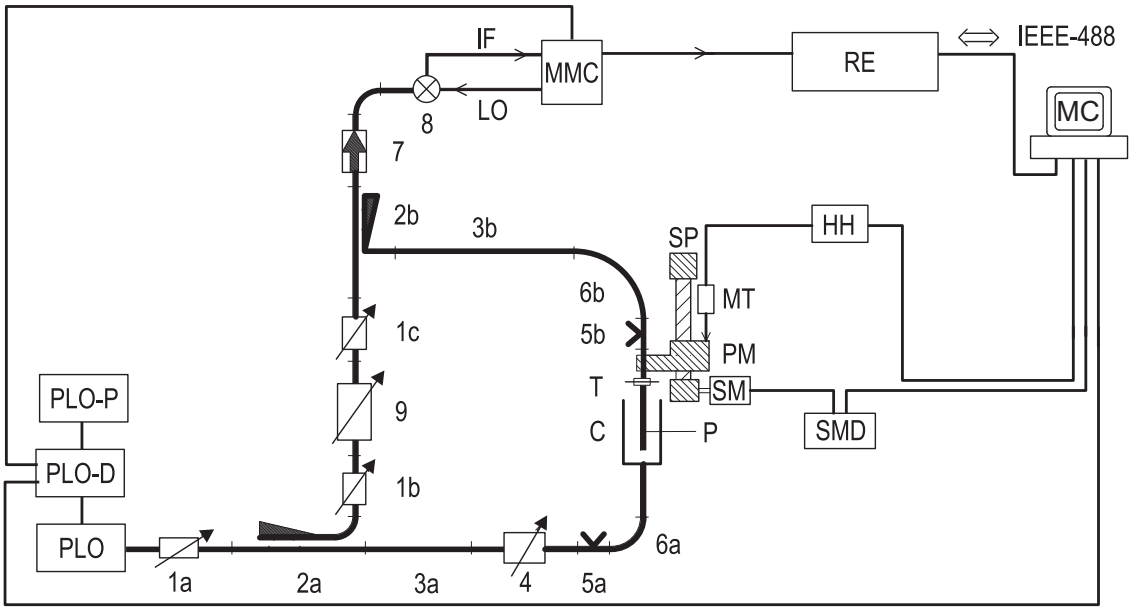

Figure 2.1: Block diagram of the E-band equipment:[75] **1a**, **b**, **c** represent variable attenuators; **2a**, **b** directional couplers; **3a**, **b** waveguide sections; **4** precision phase shifter; **5a**, **b** E/H tuners; **6a**, **b** flexible waveguides; **7** isolator; **8** harmonic mixer; **9** variable precision attenuator; **C** cell, **HH** bidirectional counter; **MC** microcomputer; **MMC** millimeter-wave to microwave converter; **MT** digital length gauge; **P** probe; **PLO** phase locked oscillators; **PLO-D** PLO-control unit; **PLO-P** PLO-power supply; **PM** probe mount; **RE** precision receiver; **SM** stepping motor; **SMD** stepping motor control unit; **SP** spindle and spindle mount; **T** tapered transmission; double lines represent waveguides, thick lines semi-rigid microwave cables and normal lines symbolize data transfer connections (analog or digital).

is detected. The magnitude of the detected signal, P, which is the experimentally accessible quantity, is defined by the squared amplitude of the electric field,

$$P = \hat{E} \cdot \hat{E}^* = E_0^2 \cdot I(x) \tag{2.8}$$

where $I(x)$ is the interference function,

$$\begin{aligned} I(x) &= [1 + \exp(-\alpha_\mathrm{a} x)\exp(\mathrm{i}(\pi - \beta x))] \cdot [1 + \exp(-\alpha_\mathrm{a} x)\exp(\mathrm{i}(\pi - \beta x))] && (2.9)\\ &= 1 + \exp(-2\alpha_\mathrm{a} x) + \exp(-\alpha_\mathrm{a} x) \cdot 2\cos(-\pi + \beta x) && (2.10) \end{aligned}$$

The quantity actually measured by the experiment is the relative attenuation of the signal on a logarithmic scale, $A(x)$, eq. 2.11.

$$A(x) = 10 \lg \frac{P(x)}{P_\mathrm{ref}} \tag{2.11}$$

P_ref is usually not known and consequently the measured attenuation is normalized by A_0 corresponding to $P_0 = E_0^2$:

$$\begin{aligned} A_{\mathrm{rel}}(x) &= A(x) - A_0 \\ &= 10\lg\frac{P(x)}{P_{\mathrm{ref}}} - 10\lg\frac{P_0}{P_{\mathrm{ref}}} \\ &= 10\lg\frac{P(x)}{P_0} \\ &= 10\lg\frac{E_0^2\cdot I(x)}{E_0^2} \end{aligned} \tag{2.12}$$

The actually determined power attenuation coefficient, α_{dB}, is measured in dB/m and thus needs conversion to the natural units by multiplication with the conversion factor

$$p = \left(20\lg e\cdot\frac{dB}{Np}\right)^{-1} \tag{2.13}$$

A fit of the recorded interference data $A(z_0 - z_0')$ by the expression[75]

$$\begin{aligned} A(z_0 - z_0') = A_0 + 10\lg\{&1 + \exp\left[-2p\alpha_{\mathrm{dB}}(z_0 - z_0')\right] \\ &- 2\cos\left(\frac{2\pi}{\lambda_M}(z_0 - z_0')\right)\cdot\exp\left[-2\alpha_{\mathrm{dB}}(z_0 - z_0')\right]\Big\} \end{aligned} \tag{2.14}$$

yields α_{dB} and the wavelength of the radiation within the sample, λ_{M}. Insertion of $\alpha_{\mathrm{a}} = p\alpha_{\mathrm{dB}}$ and $\beta = 2\pi/\lambda_{\mathrm{M}}$ into Eqs. 2.2 & 2.3 yields the complex permittivity data.

2.2.2 Vector network analysis

During recent years the application of vector network analyzers (VNAs) for the measurement of dielectric data has attracted growing interest. This is due to the increased frequency range but mainly due to the user friendly measuring principle: for liquid samples a dielectric probe connected to the VNA has simply to be immersed into the sample.
An arbitrary electrical network is analyzed by determining the reflection and transmission of electrical signals, yielding the scattering parameter matrix, $\hat{S}$, which is defined as follows:

$$\begin{pmatrix}\hat{b}_1\\ \hat{b}_2\end{pmatrix} = \begin{pmatrix}\hat{S}_{11} & \hat{S}_{12}\\ \hat{S}_{21} & \hat{S}_{22}\end{pmatrix}\begin{pmatrix}\hat{a}_1\\ \hat{a}_2\end{pmatrix} \tag{2.15}$$

where $\hat{a}_j$ and $\hat{b}_j$ correspond to the incident and reflected power waves at port j, respectively. The scattering parameter $\hat{S}_{11}$ is equal to the relative complex reflection coefficient $\hat{\Gamma}_{\mathrm{a}}$, which can be further related to complex permittivity data.

For one-port reflection measurements on an electrical network, consisting of an impedance step from $\hat{Z}_1$ to $\hat{Z}_2$, the relative complex reflection coefficient is related to the normalized aperture admittance, $\hat{Y} = \hat{Z}_2/\hat{Z}_1$:

$$\hat{\Gamma}_\mathrm{a} = \frac{1-\hat{Y}}{1+\hat{Y}}. \tag{2.16}$$

As just one port of the instrument is used, the instrument has to be calibrated, to correct for errors in directivity, $\hat{e}_\mathrm{d}$, frequency response, $\hat{e}_\mathrm{r}$ and source match, $\hat{e}_\mathrm{s}$[76]. The actual relative complex reflection coefficient $\hat{\Gamma}_\mathrm{a}$ is then related to the one measured by the instrument, $\hat{\Gamma}$, via

$$\hat{\Gamma}_\mathrm{a} = \frac{\hat{\Gamma} - \hat{e}_\mathrm{d}}{\hat{e}_\mathrm{s}\left(\hat{\Gamma} - \hat{e}_\mathrm{d}\right) + \hat{e}_\mathrm{r}} \tag{2.17}$$

For the determination of $\hat{e}_\mathrm{d}$, $\hat{e}_\mathrm{d}$ and $\hat{e}_\mathrm{d}$, at least three references have to be measured.

Open-ended coaxial probe

An Agilent E8364B VNA in combination with a dielectric probe kit (85070E) was used to probe the frequency range $0.2 \leq \nu/\mathrm{GHz} \leq 50$. Additionally, a electronic calibration module (Agilent N4693B) was used to correct for calibration accuracy degradation between calibration and measurement. Those are caused by changes in the environment with thermal changes in the length of external and internal cables being the major effect[77].
Two distinct dielectric probes covered the frequency range $0.2 \leq \nu/\mathrm{GHz} \leq 20$ (high temperature probe) and $1 \leq \nu/\mathrm{GHz} \leq 50$ (performance probe). Both were mounted in thermostated cells as described by Schrödle[78]. Thereby the sample is poured into the sample holder, with the open-ended coaxial probe being at the bottom, rather than immersing the dielectric probe into the liquid.
The temperature was controlled to (25 ± 0.02)°C with a Huber CC505 thermostat and measured with a platinum resistance thermometer (PRT, PT-100) in combination with a Agilent 34970A datalogger.
A simplified coaxial aperture opening model[76,79,80] was used to calculate the complex dielectric properties $\hat{\eta}_\mathrm{m}$ from the normalized aperture admittance of the probe head, $\hat{Y}$, by numerical solution of eq. 2.18,

$$\hat{Y} = \frac{\mathrm{i}\hat{k}_\mathrm{m}^2}{\pi \hat{k}_\mathrm{c} \ln(D/d)} \left[\mathrm{i}\left(I_1 - \frac{\hat{k}_\mathrm{m}^2 I_3}{2} + \frac{\hat{k}_\mathrm{m}^4 I_5}{24} - \frac{\hat{k}_\mathrm{m}^6 I_7}{720} + \ldots \right) + \left(I_2 \hat{k}_\mathrm{m} - \frac{\hat{k}_\mathrm{m}^3 I_4}{6} + \frac{\hat{k}_\mathrm{m}^5 I_6}{120} - \ldots \right) \right] \tag{2.18}$$

where $\hat{k}_\mathrm{c} = \omega\sqrt{\hat{\eta}_\mathrm{c}\varepsilon_0\mu_0}$ is the propagation constant within the dielectric material of the coaxial probe head and $\hat{k}_\mathrm{m} = \omega\sqrt{\hat{\eta}_\mathrm{m}\varepsilon_0\mu_0}$ the propagation constant of the sample. For an accurate calculation, the first 28 probe constants, I_i, initially calculated from a theoretical approach[80] and further optimized via measurement of reference liquds[76], are used by the Agilent 85070C software package. The constants d and D are the radii of the inner and outer conductor of the coaxial line, respectively.

Calibration according to eq. 2.17 of the VNA with respect to the probe-sample interface was performed using three calibration substances with well known dielectric properties: air (open), purified mercury (short) and pure water (load). For investigations on aqueous solutions of NaCl, KH_2PO_4 and K_2HPO_4 the calibration was performed using the dielectric properties of water as reported by Schrödle[78]. Due to slight deviations of those from the literature values on the static permittivity of water[81], the data set of Schrödle ($0.2 \leq \nu/\mathrm{GHz} \leq 89$; $0.2 \leq \theta/\ ^\circ\mathrm{C} \leq 65.0$) was refitted yielding the parameters summarized in Table 2.3.

Table 2.3: Water Relaxation Parameters, ε_j and τ_j as Obtained by Refitting Data Given by Schrödle[78] and Fixing Static Permittivity, ε_1, at the Literature Value.

T / K	ε_1	τ_1 / ps	ε_2	τ_2 / ps	$\varepsilon_3 = \varepsilon_\infty$	$10^3\,\chi^2_\mathrm{r}$
273.35	87.773	17.2	6.31	0.645	4.04	189.1
278.15	85.868	14.7	6.28	0.509	3.96	105.3
283.15	83.929	12.6	6.24	0.449	3.86	104.5
288.15	82.033	10.9	6.04	0.343	3.68	58.3
293.15	80.179	9.44	5.92	0.299	3.55	65.2
298.15	78.368	8.35	5.95	0.278	3.52	55.6
303.15	76.598	7.39	5.62	0.212	3.29	89.2
308.15	74.867	6.59	5.63	0.212	3.20	123.1
313.15	73.176	5.99	5.58	0.196	3.02	81.7
318.15	71.523	5.33	5.41	0.165	2.78	88.1
323.15	69.907	4.82	5.36	0.157	2.68	64.2
328.15	68.328	4.42	5.50	0.189	2.84	145.0
333.15	66.784	4.03	5.33	0.139	2.60	101.8
338.15	65.276	3.70	5.26	0.128	2.58	108.8

With increasing electrolyte concentration the dielectric properties of the sample progressively deviate from the properties of neat water. For cases of strong deviation generally a secondary calibration of $\hat{\varepsilon}(\nu)$ is applied. As systematic deviations are likely to be due to the model for the aperture impedance (eq. 2.18), a complex Padé approximation[82] is usually applied to correct raw permittivity spectra, $\hat{\varepsilon}_\mathrm{m}$ after subtraction of contributions due to Ohmic loss:

$$\hat{\varepsilon}_\mathrm{m}^\mathrm{corr} = P_{n/m}\left[\hat{\varepsilon}_\mathrm{m}\right] = \frac{\hat{A}_0 + \hat{A}_1\hat{\varepsilon}_\mathrm{m} + ... + \hat{A}_n(\hat{\varepsilon}_\mathrm{m})^n}{1 + \hat{B}_1\hat{\varepsilon}_\mathrm{m} + ... + \hat{B}_m(\hat{\varepsilon}_\mathrm{m})^m} \tag{2.19}$$

The approximation constants, $\hat{A}_n(\omega)$ and $\hat{B}_m(\omega)$ can be obtained by a complex linear fit algorithm[61] by measuring a set of reference substances with known dielectric properties that should be close to the investigated system.
To test the necessity of Padé calibration for the studied aqueous electrolyte solutions, VNA spectra of NaCl(aq) at $0.1004 \leq c\,/\,\mathrm{mol\,L^{-1}} \leq 1.926$ have been measured and corrected with propylene carbonate (PC, Sigma-Aldrich, 99.7%)[83–85] and N,N-dimethylacetamide

(DMA, Fluka, >99.8%)[83,85] as secondary standards. Figure 2.2 shows the measured and corrected spectra for the lowest and highest NaCl concentration. At low concentrations the two sets of spectra are virtually identical and only minor deviations (mainly for $\varepsilon''(\nu)$) occur at the highest c. It was thus refrained of applying complex Padé calibration for the aqueous electrolyte concentrations of this work.

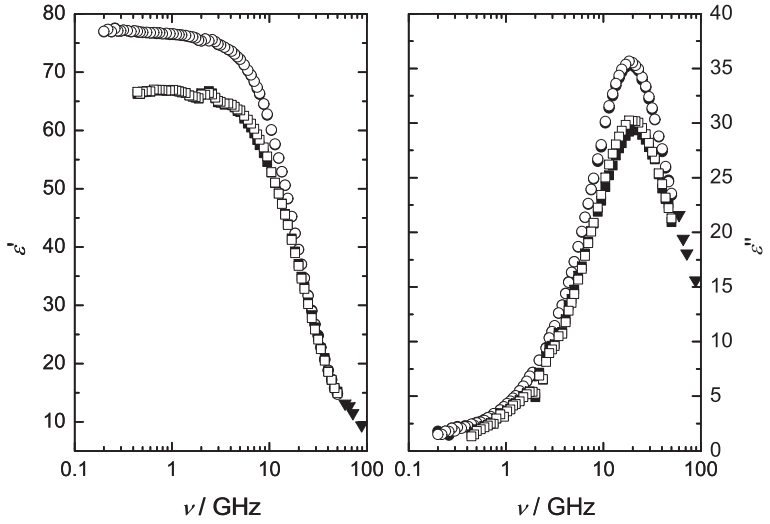

Figure 2.2: Permittivity (a) and dielectric loss (b) spectra of NaCl at concentrations $c\,/\,(\mathrm{mol\,L^{-1}}) = 0.1004$ (circles) and 1.926 (squares). Filled symbols correspond to raw data, open symbols show data corrected with a complex Padé calibration (Eq. 2.19) using PC and DMA as secondary calibration standards.

Wave guide transmission cells

Waveguide transmission-cells analogous to the E-band setup presented in Section 2.2.1 are available for X-, Ku-, and A-band and are connected to the VNA. As this instrument is able to detect amplitude and phase simultaneously, a simple transmission experiment is sufficient for the determination of complex permittivity data. All tested frequencies are probed as a function of optical path length z simultaneously, thus significantly reducing the measurement time.

A personal computer was used to control the stepper motor, the VNA and a precision gauge for the determination of the optical path length through the sample, thus enabling automation of the measurement.

The quantity of interest is the complex scattering parameter, $\hat{S}_{12}$ (Eq. 2.15), whose amplitude and phase are recorded as a function of optical path length. Linear regression of both parameters yields the absorbtion coefficient α_{dB} and medium wavelength λ_{M}, respectively, which are used to calculate complex permittivity data via Eqs. 2.2 and 2.3.

Temperature of the A-band transmission cell was controlled to (25 $\pm$0.02)°C by a Huber CC505 thermostat, whereas X- and Ku-band cells were hooked to a Julabo FP 50 thermostat enabling temperature control to (25 $\pm$ 0.03)°C. Temperature was determined

with a Agilent 34970A datalogger, by measuring the resistance of a platinum resistance thermometer (PRT, PT-100) in 4-wire configuration.
A-band measurements were mainly performed for electrolyte solutions with specific conductivities $\kappa > 6\,\mathrm{S\,m^{-1}}$, as for those often systematic deviations in the complex permittivity data obtained by the high temperature and performance probe occurred. Then the performance probe measurements were replaced by the A-band data. X- and Ku-band measurements were only performed for the NaCl solutions to provide further hints on the necessity of Padé calibration.

2.2.3 Data processing

Prior to analysis of the combined total permittivity spectra, they were corrected for dc conductivity to yield $\hat{\varepsilon}(\nu)$ (Eqs. 1.32 & 1.33) using experimental conductivity, κ, values. Due to imperfections of the probe-head geometries[86] and of the short-circuit calibrations with mercury, conductivity corrections for the VNA cells, κ_{VNA}, were slightly adjusted ($\Delta\kappa/\kappa \leq 0.035$) to get smooth $\varepsilon''(\nu)$ curves, provided the corresponding combined $\varepsilon'(\nu)$ spectrum, which is not affected by conductivity correction, was smooth and the subsequent simultaneous fit of $\varepsilon'(\nu)$ and $\varepsilon''(\nu)$ did not yield systematic deviations for $\varepsilon'(\nu)$. Spectra were then cut-off at a concentration (conductivity) dependent minimum frequency, ν_{min}, where for $\nu < \nu_{\mathrm{min}}$ the experimental noise in $\eta''(\nu)$ exceeded the magnitude of $\varepsilon''(\nu)$.
For formal description, the so obtained spectra were fitted by a sum of n relaxation models as described in Section 1.3. Generally all reasonable combinations of band-shape functions were tested for $1 \leq n \leq 5$ by simultaneously fitting $\varepsilon'(\nu)$ and $\varepsilon''(\nu)$ with a home-built software package (MWFIT) utilizing a non-linear fitting routine based on the Gauss-Marquardt algorithm. The quality of the fit was assessed by the reduced error function[87]

$$\chi^2_{\mathrm{r}} = \frac{1}{2N - m - 1}\left[\sum_{k=1}^{N} \delta\varepsilon'(\nu_k)^2 + \sum_{k=1}^{N} \delta\varepsilon''(\nu_k)^2\right] \tag{2.20}$$

depending on the number of adjustable parameters, m, the number N of data triples $(\nu_k, \varepsilon'_k, \varepsilon''_k)$ and the sum over the squared residuals of permittivity, $\delta\varepsilon'(\nu_k)$, and dielectric loss, $\delta\varepsilon''(\nu_k)$.
The successful formal description of the experimental spectra does not automatically imply, that the used relaxation model is physically meaningful. Thus, besides finding a model with lowest χ^2_{r}, additional criteria are used for identifying the most probable relaxation model. Those include, but are not restricted to:

- The number of relaxation processes should be reasonably small.
- Obtained relaxation times and amplitudes should not be negative.
- No change in the relaxation model over a concentration series, except for specific physical reasons.

Note, that the determined best model can depend on the measured frequency range as well as on the precision and the "density" of the data. The latter denotes the number density of data points over the frequency range, and should be uniform to avoid an overvaluation of a certain frequency region.
Additionally, the spectra were analyzed by the procedure of Zasetzky[88]. This linear least squares minimization with constraints[89] directly yields the probability $p(\tau)$ of finding a Debye-type relaxation of relaxation time τ for the tested spectrum. As this procedure needs no assumptions on the number of relaxation processes, it can be seen as an unbiased way to determine the actual number of modes present.

2.3 Auxiliary measurements

2.3.1 Density

Densities, necessary for conversion of molality into molarity, were determined with a vibrating tube densimeter (DMA5000M, Anton Paar, Austria) according to the method of Kratky *et al.*[90]. This method is based on measuring the eigenfrequency of a U-shaped borosilicate glass tube containing the liquid. Depending on the density of the liquid, the period τ of the vibration is altered. Density is calculated as

$$\rho = A \times \frac{\tau}{\tau_0} \times f_1 - B \times f_2 \tag{2.21}$$

with A and B as calibration constants, τ_0 the period of a reference oscillator and the additional correction terms f_1 and f_2 compensate for temperature, viscosity and nonlinearity. Temperature compensation is needed, as calibration of the instrument is done with water and air at 20 °C. The stated uncertainty of the instrument is $\pm 5 \cdot 10^{-6}$ g mL^{-1}, but is higher at temperatures different than 20 °C and viscosities markedly different from pure water.

2.3.2 Viscosity

Viscosities for some, but not all, aqueous salt solutions were determined using a rolling-ball viscometer (AMVn, Anton Paar). The sample is filled in a glass capillary, equipped with a steel ball, which is then allowed to roll a fixed distance at a given angle. The rolling time of the steel ball corresponds to the dynamic viscosity of the fluid according to

$$\eta = K \times (\rho_{\mathrm{sb}} - \rho_{\mathrm{sample}}) \times t \tag{2.22}$$

Thereby K denotes a temperature and angle dependent calibration constant, ρ_{sb} the density of the used steel ball, ρ_{sample} the density of the fluid and t the rolling time of the steel ball. For the present work two distinct glass capillaries, with inner diameter of 1.6 mm were used. The first one was an already calibrated capillary, that could be used as received. For the second capillary, temperature and angle dependent calibration constants, K, needed to be determined with degassed MILLI-Q water, first. The determined K values were

Table 2.4: Angle Dependant Calibration Constants K, as Determined for Capillary SN 17547949. Stated Uncertainties Result From Standard Deviations of Corresponding Rolling Times.

angle / °	K / $m^2\,s^{-2}$
20	$4.054{\cdot}10^{-3} \pm 5{\cdot}10^{-6}$
30	$5.940{\cdot}10^{-3} \pm 4{\cdot}10^{-6}$
40	$7.646{\cdot}10^{-3} \pm 3{\cdot}10^{-6}$
50	$9.114{\cdot}10^{-3} \pm 4{\cdot}10^{-6}$
60	$1.0298{\cdot}10^{-2} \pm 2{\cdot}10^{-6}$
70	$1.1190{\cdot}10^{-2} \pm 4{\cdot}10^{-6}$
80	$1.2357{\cdot}10^{-2} \pm 3{\cdot}10^{-6}$

additionally verified at selected temperatures and angles with a suitable viscosity standard oil (CANNON, Certified Viscosity Reference Standard S3, Lot Number 11201). Table 2.4 contains the determined calibration constants.

2.3.3 Conductivity

Specific electrical conductivities, κ, were determined at (25±0.01) °C (temperature stability ≤ 0.005 °C) with a computer controlled setup[91]. A set of five two-elecrode capillary cells with cell constants $C = (25 \text{ - } 360)\,cm^{-1}$) was calibrated with KCl(aq)[92]. The cell resistance, R, was determined in the frequency range $100 \leq \nu/Hz \leq 10000$ and extrapolated to infinite frequency, R_∞, using the empirical function

$$R(\nu) = R_\infty + A/\nu^a \tag{2.23}$$

A is specific to the cell and the exponent a shows values of $0.5 < a < 1$. Data acquisition, temperature control and extrapolation of R_∞ values was done automatically by a home-built software package. The measurement was repeated at least 40 times in a row and the extrapolated R_∞ averaged. Specific conductivity of the sample is calculated as C/R_∞. The achieved repeatability is < 0.05 % but note that, because of various possible error sources, the relative overall uncertainty of κ is probably only ≤ 0.5%.

2.3.4 Quantum mechanical calculations

Semiempirical quantum mechanical calculations have been performed for inorganic phosphate anions utilizing MOPAC2009[93] with the PM6 Hamiltonian[94]. The eigenvector-following (EF) routine was used for the optimization of ion geometry. To obtain condensed phase dipole moments, solvent effects were accounted for by the COSMO technique[95], using 78 as the relative static permittivity, ε, of pure water at 25°C. Van der Waals radii, $r_{v.d.W}$, were determined with WINMOSTAR[96] using the MOPAC optimized geometry of the ions.

Chapter 3

Ion Cloud Relaxation in NaCl(aq)

The material presented in this chapter forms the basis of the paper:

Andreas Eiberweiser and Richard Buchner *"Ion-pair or ion-cloud relaxation? On the origin of small-amplitude low-frequency relaxations of weakly associating aqueous electrolytes."* *J. Mol. Liq.* **2012**, *176*, 52-59.

3.1 Introduction

Recent DRS studies of aqueous solutions of weakly associating 1:1 electrolytes,[27–29] including sodium carboxylate solutions,[30] detected a weak mode in the $\sim 0.5 - 1\,\mathrm{GHz}$ region of the dielectric spectrum, that is in a region typical for ion-pair relaxation. However, until recently the amplitude (relaxation strength) of this spectral feature was just at the detection limit and accordingly quantitative analysis rarely attempted.[28] This situation was changed by recent improvements of the DRS instrumentation in Regensburg, now allowing for samples of static permittivity $\varepsilon(= \lim_{\nu \to 0} \varepsilon'(\nu)) \approx 80$ and dc conductivity $\kappa \lesssim 1\,\mathrm{S\,m^{-1}}$ the resolution of modes with amplitudes $S \gtrsim 0.2$. Thus, at least semi-quantitative investigation of weak ion pairing appears to be feasible now, provided the low-frequency relaxation can be unequivocally assigned to ion-pair reorientation.
With ion-cloud relaxation, however, there is a process which should show up in the same spectral region as ion-pair relaxation.[97] This effect, predicted by Debye and Falkenhagen,[47] arises from the field-induced fluctuations of the diffuse ion cloud surrounding each charged particle in solution. For charged colloids,[98] including poly-electrolytes[99] and charged micelles,[100] ion-cloud relaxation is indeed a major contribution to $\hat{\varepsilon}(\nu)$. For electrolyte solutions this effect was thought to be small and thus elusive to detection[101] but according to recent calculations[32] this should not necessarily be the case. Obviously, the possible overlap of ion-cloud and ion-pair relaxation has implications on the investigation of weak ion association with DRS. In order to resolve the true nature of the small-amplitude low-frequency mode of aqueous 1:1 electrolytes, a detailed study of aqueous sodium chloride solutions as a model system for strong electrolytes was conducted. Additionally, dielectric spectra of aqueous 1:1 electrolytes previously recorded in our laboratory were re-evaluated.

3.2 Data treatment and description of spectra

In total, 35 samples in the concentration range $0.05 \leq c/\mathrm{mol\,L^{-1}} \leq 2.11$ have been studied at 25 °C, whereby special attention was given to concentrations $\leq 0.5\,\mathrm{mol\,L^{-1}}$ (24 samples). For formal description, the obtained spectra were fitted via Eq. 1.19 by a sum of n independent relaxations j. Each mode was modeled by a Havriliak-Negami equation of amplitude (relaxation strength) $S_j = \varepsilon_j - \varepsilon_{j+1}$, relaxation time τ_j and shape parameters $0 \leq \alpha_j < 1$ and $0 < \beta_j \leq 1$, or its simplified variants, the Cole-Davidson (CD, $\alpha_j = 0$), the Cole-Cole (CC, $\beta_j = 1$) or Debye (D, $\alpha_j = 0$ & $\beta_j = 1$) equations.[25,26]

All reasonable combinations of band-shape functions were tested for $1 \leq n \leq 4$ by simultaneously fitting $\varepsilon'(\nu)$ and $\varepsilon''(\nu)$. Additionally, the spectra were analyzed by the procedure of Zasetzky.[88] With both approaches the overall best fitting model for the spectra of samples with $c < 1\,\mathrm{mol\,L^{-1}}$ was found to be the superposition of a low-frequency Debye process, with relaxation time τ_1 and amplitude $S_1 = \varepsilon_1 - \varepsilon_2$, centered at ∼0.8 GHz, and a Cole-Cole mode peaking at ∼20 GHz with parameters τ_2, $S_2 = \varepsilon_2 - \varepsilon_\infty$ and α_2 (the D+CC model). For higher concentrations the low-frequency mode could not be resolved anymore and here spectra are best described by a single Cole-Cole equation. Table 3.1 lists the obtained fit parameters for all samples and Figure 3.1 shows experimental spectra and fits for selected concentrations. Amplitudes S_j ($j = 1, 2$) are plotted in Figure 3.2. Note that for $c < 1\,\mathrm{mol\,L^{-1}}$ the static permittivity of the sample, $\varepsilon = \lim_{\nu \to 0} \varepsilon'(\nu)$, is given by ε_1, whereas for higher concentrations $\varepsilon = \varepsilon_2$.

From its relaxation time and amplitude it is straightforward to assign the CC mode at ∼20 GHz to the cooperative relaxation of (bulk) water that is — at least at low c — essentially unaffected by the dissolved NaCl.[62] The small-amplitude low-frequency D mode at ∼0.8 GHz is specific to the solute (see Section 3.3). Note that for the present spectra restricted to $\nu \leq 89$ GHz the fast water mode at ∼500 GHz could not be resolved.[62] However, its presence is indicated by values of $\varepsilon_\infty(c) \approx 5 - 6$, which significantly exceed the infinite-frequency permittivity of pure water, $\varepsilon_\infty(0) = 3.48$, obtained from $\hat{\varepsilon}(\nu)$ extending to the far-infrared region.[78] This has to be considered in the analysis of the water amplitude (see Section 3.4).

NaCl has been the subject of a previous DRS study restricted to $\nu \leq 20$ GHz.[31] In contrast to the present data, which are best fitted by the D+CC model, a single Cole-Cole equation is sufficient to model the spectra of the previous study. There are two reasons for the different fit models. First, mainly thanks to the ECal module and improvements in cell construction, experimental noise and instrument drift are reduced by a factor of 3-5 for the present instrument compared to the previously used setup. Thus, it is easier now to detect small amplitude modes. Second, the present frequency range is much larger and now almost entirely covers the bulk-water relaxation. This is essential for reliably separating a small excess contribution, like the (τ_1, S_1) mode, from a dominating relaxation, especially if the latter is broadened. Thus, possible indications for a solute mode in the spectra of Buchner *et al.*[31] were subsumed in the parameters of their CC fit. Indications for that are for $c \lesssim 1\,\mathrm{mol\ L^{-1}}$ static permittivities that are in between the present values for ε_1 and ε_2 (Figure 3.3a) and Cole-Cole parameters that are somewhat larger than the present α_2

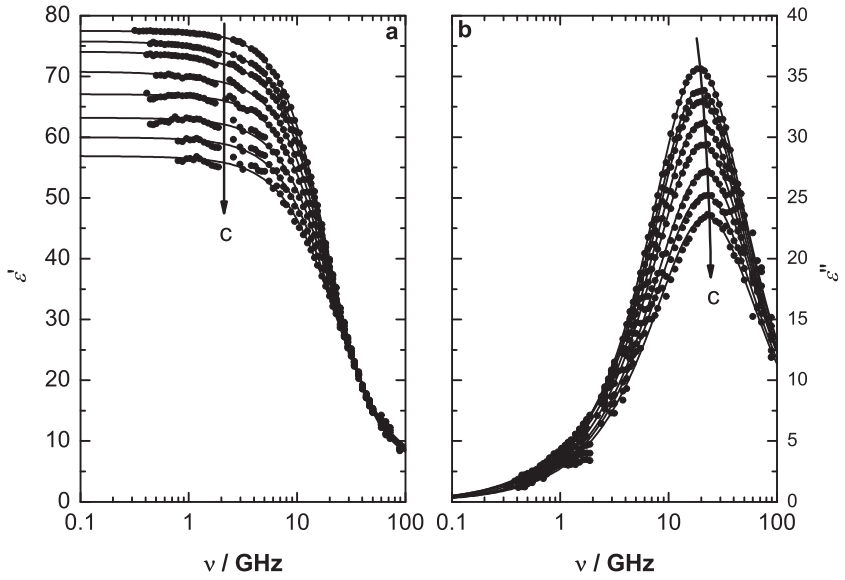

Figure 3.1: Spectra of relative permittivity, $\varepsilon'(\nu)$ (a), and dielectric loss $\varepsilon''(\nu)$ (b), for NaCl(aq) at 25 °C and concentrations c / (mol L^{-1}) = 0.0503, 0.2492, 0.3966, 0.6912, 0.9815, 1.365, 1.741 and 2.112 (top to bottom). Symbols show typical experimental data; lines represent the D+CC fit.

(Figure 3.3b). The systematically lower bulk-water relaxation times of Ref. 31 (Figure 3.4) are mainly a consequence of lacking high-frequency data.

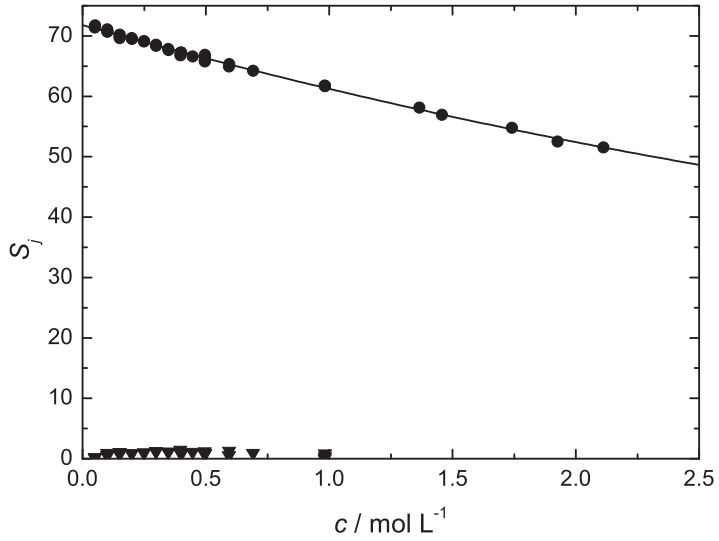

Figure 3.2: Concentration dependent amplitudes of the D+CC fit of spectra of NaCl(aq) at 25 °C. The relaxations are attributed to bulk water (●) and ion pair + ion cloud relaxation (▼). Lines represent empirical fits of the experimental values.

Table 3.1: Parameters of a D+CC Fit For the Observed DR Spectra of Aqueous Solutions of NaCl at 25 °C: Conductivity, κ, Limiting Permittivities, ε_j ($j = 1, 2$) & ε_∞, Relaxation Times, τ_j, and CC Broadness Parameter, α_2, Together With the Value of the Reduced Error Function, χ^2_{r}.[a,b]

c / mol L^{-1}	κ / S m^{-1}	ε_1	τ_1 / ps	ε_2	τ_2 / ps	α_2	ε_∞	χ^2_{r}
0[c]		78.37			8.32		3.48	0.05
0.0498	0.540	77.46	203	77.24	8.31	0	5.83	0.03
0.0503	0.545	77.48	273	77.33	8.30	0.004	5.56	0.07
0.0995	1.025	77.26	283	76.73	8.27	0.006	5.66	0.03
0.1004	1.037	77.39	382	76.48	8.31	0.001	5.80	0.06
0.1008	1.050	77.16	200	76.57	8.24	0.002	5.80	0.02
0.1496	1.500	76.69	187	75.68	8.26	0.002	5.77	0.05
0.1501	1.498	76.68	232	75.94	8.29	0.005	5.75	0.04
0.1504	1.492	76.51	280	75.47	8.19	0	5.83	0.05
0.1989	1.965	76.14	193	75.32	8.21	0.006	5.67	0.04
0.1997	1.962	76.21	185	75.32	8.25	0.006	5.82	0.05
0.2486	2.400	75.73	222	74.73	8.20	0.010	5.59	0.07
0.2592	2.389	75.76	195	74.78	8.14	0.012	5.67	0.08
0.2980	2.820	75.32	200	74.09	8.15	0.009	5.55	0.03
0.2981	2.832	75.24	181	74.11	8.10	0.012	5.74	0.07
0.3475	3.255	74.55	171	73.47	8.10	0.012	5.65	0.05
0.3481	3.245	74.71	177	73.57	8.18	0.011	5.91	0.07
0.3966	3.660	74.05	167	72.58	8.10	0.007	5.80	0.06
0.3970	3.703	74.00	176	72.98	8.07	0.015	5.75	0.09
0.3997	3.710	73.41	198	72.67	7.95	0.015	5.39	0.07
0.4463	4.054	73.69	186	72.59	8.10	0.018	5.97	0.14
0.4953	4.455	72.27	188	71.49	7.90	0.016	5.46	0.10
0.4954	4.508	72.94	203	72.06	8.01	0.020	5.21	0.06
0.4954	4.484	72.66	190	71.90	7.94	0.020	5.31	0.08
0.4960	4.460	73.10	195	71.90	8.07	0.019	6.13	0.12
0.5931	5.250	71.02	227	70.49	7.93	0.019	5.55	0.15
0.5949	5.235	72.04	206	70.76	8.00	0.020	5.31	0.06
0.6912	6.026	70.76	202	69.84	7.96	0.020	5.61	0.08
0.9815	8.098	67.07			7.80	0.033	5.31	0.10
0.9823	8.211	67.18	200F	66.84	7.68	0.035	5.11	0.13
0.9833	8.180	67.87	220F	67.03	7.77	0.031	5.35	0.12
1.365	10.79			63.21	7.41	0.046	5.05	0.22
1.457	11.29			62.40	7.56	0.041	5.45	0.19
1.741	13.08			60.00	7.34	0.053	5.18	0.24
1.926	13.96			58.19	7.37	0.049	5.69	0.28
2.112	15.14			56.91	7.13	0.061	5.37	0.37

[a] Units: c in mol L^{-1}, τ_j in ps, κ_{VNA} in S m^{-1}; [b] Parameter values followed by the letter F were not adjusted in the fitting procedure. [c] Values for pure water are according to Schrödle.[78]

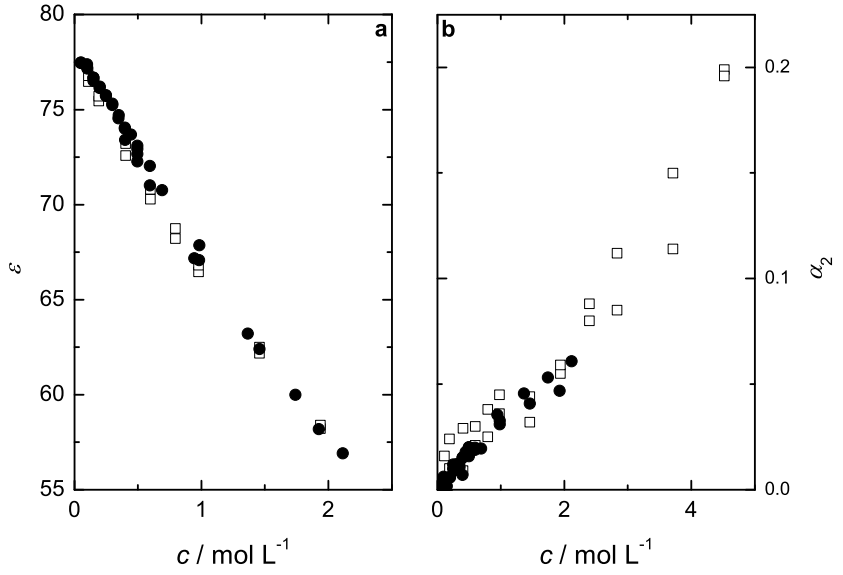

Figure 3.3: Static permittivities, ε, (a) and Cole-Cole broadness parameters, α_2 (b), of NaCl(aq) for the current study (●) and from Buchner *et al.*[31] (□).

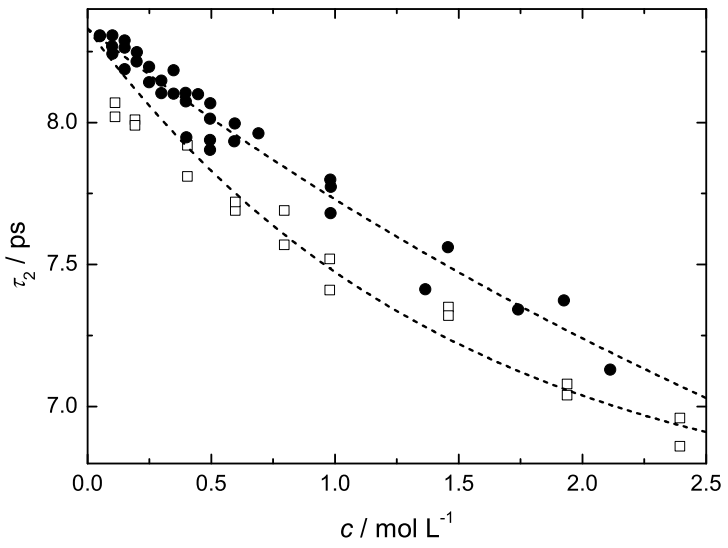

Figure 3.4: Concentration dependence of the bulk water relaxation time, τ_2, as obtained in this study (●) and by Buchner *et al.* (□)[31] (lines as a guide to the eye).

3.3 Discussion of low frequency relaxation

With values $S_1 \lesssim 1$ (Figure 3.5) the amplitudes of the reported low-frequency relaxations were clearly at the nominal detection limit of the previously used instrumentation[28,102,103] and even with the improved apparatus,[29,30] the data scatter considerably (Figure 3.5 & Table 3.1). Although the limited frequency coverage of Buchner *et al.*, $0.2 \leq \nu/\mathrm{GHz} \leq 20$, provides a straightforward explanation why no solute mode was then detected for NaCl(aq), it is necessary to ask whether the present low-frequency relaxation is not an artefact associated with the measurement system. Indeed, the necessity to calibrate the reflection probe heads of the VNA, combined with the known imperfections of the mathematical model used for their description,[86] is a challenging point, as one may rightly argue that inappropriate calibration standards combined with the need to adjust the conductivity correction of the VNA probe heads lead to a spurious low-frequency signal that could be misinterpreted as a relaxation process.

However, if the used calibration standards, air, mercury and water, were a problem, then the suspicious low-frequency mode should also show up for other samples, including well characterized molecular solvents. To test this hypothesis, deuterium oxide and propylene carbonate (PC), which have similar dielectric properties as water and thus should not require Padé correction with secondary standards,[82] were measured in the same way as the NaCl(aq) samples. For both liquids, the relaxation models given in the literature (D for D_2O[104] and CD+D for propylene carbonate[84]) were used to fit their spectra, yielding static permittivities and relaxation times in good agreement with the literature. More importantly, neither for deuterium oxide nor for propylene carbonate indications for a spurious low-frequency relaxation could be found.

The other likely scenario is that conductivity correction for the probe heads leads to the emergence of a non-existent mode. Conductivity correction is most prominent in the low frequency region and indeed influences the amplitude of the resolved low-frequency process crucially. Though $\varepsilon'(\nu)$ is not affected by the conductivity correction, real and imaginary part of $\hat{\varepsilon}(\nu)$ are fitted simultaneously. Thus, improper conductivity correction leads to a systematic deviation of the experimental $\varepsilon'(\nu)$ from the fit curve. Therefore, the conductivity-correction procedure is such that the experimental κ value is taken as the starting point and conductivity correction is altered until systematic deviations exceeding experimental repeatability are eliminated for both $\varepsilon'(\nu)$ and $\varepsilon''(\nu)$ and best fit (minimum in χ^2) is achieved. If systematic deviations between fit and experimental data cannot be removed with reasonably small (here $< 3.5\,\%$) conductivity corrections for the VNA probe heads this suggest that the chosen fit model is inappropriate. Thus, the adopted correction procedure is reasonably unbiased regarding the possible existence of a low-frequency mode.

A further possibility for the observed low-frequency relaxation might be electrode polarization, as this is an unavoidable contribution to the dielectric spectra of ion-conducting systems.[25] However, for dilute solutions electrode polarization shows up at much lower frequencies than studied here. Spectral features of electrode polarization do shift to higher frequencies with increasing conductivity and its magnitude increases with conductivity. Thus, a possible contribution of electrode polarization should become more and more prominent the higher c. However, for the present NaCl(aq) solutions, as well as for all other 1:1

electrolytes where a comparable low-frequency mode was observed so far,[27–30,102,103] the amplitude of the solute relaxation decreases for $c \gtrsim 0.5\,\mathrm{mol\,L^{-1}}$ and vanishes at high concentrations. Thus, electrode polarization can almost certainly be ruled out as the origin of the here observed low-frequency relaxation. The question now is, what else is the possible origin of this mode and in the following two possible options for a solute-specific relaxation in electrolyte solutions, namely ion-pair rotation and ion-cloud relaxation, will be discussed.

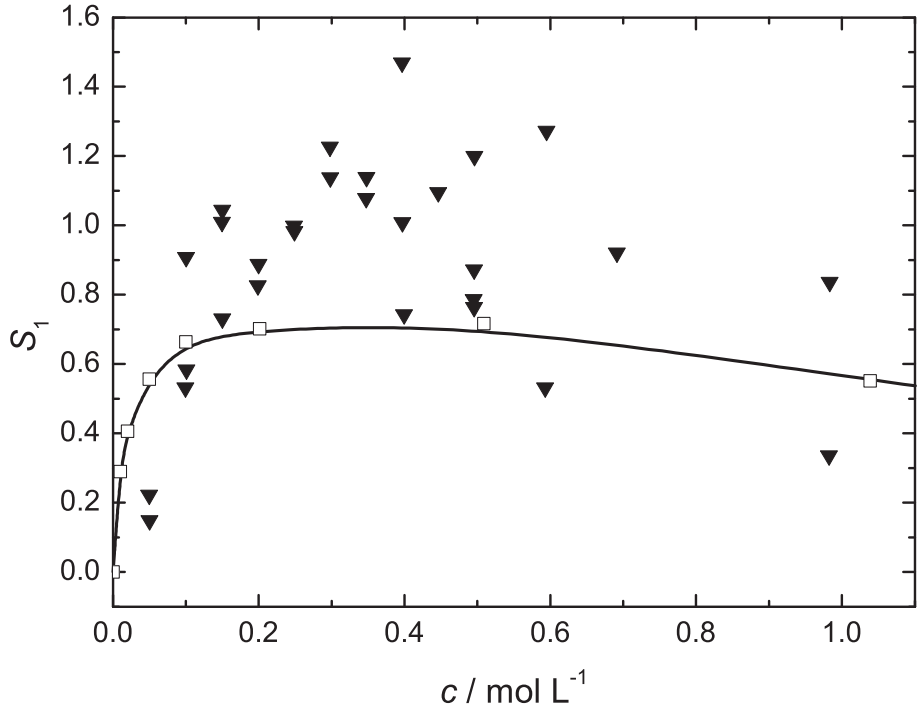

Figure 3.5: Experimental amplitudes of the low-frequency mode, S_1 (▼), and values reported by Yamaguchi et al. (□)[32,105] (line as a guide to the eye).

3.3.1 Ion-pair Relaxation

Ion-pair relaxation can be assumed to occur through small-angle rotational diffusion of the ion pair's dipole vector in a medium of viscosity η and should thus follow the Stokes-Einstein-Debye equation (Eq. 1.56).[57] The single-particle rotational correlation time used in the SED equation, τ'_{IP}, is linked to the experimental dielectric relaxation time, τ_{IP}, through Eq. 1.60.[59] Thus from the geometric data of reasonable ion-pair models an estimate of their relaxation time is possible.

Following Barthel et al.,[53] it was assumed for the present calculations of V_{m} and $f_\perp$ that the ion-pair can be approximated by a spherocone of variable cone length l to account for the number of solvent layers (CIP: 0; SIP: 1; 2SIP: 2) separating the ions in the pair. The water molecule was assumed to be spherical with radius 144 pm[106] and the ion radii of Marcus[107] were used for Na^+ (97 pm) and Cl^- (180 pm). For η the value of pure water

($\eta = 0.8903\,\mathrm{mPa{\cdot}s}$[108]) was inserted, so that for the species CIP, SIP and 2SIP theoretical infinite-dilution limits of their ion-pair relaxation times, τ_{IP}, were obtained with Eqs. 1.56 and 1.60.

Table 3.2: Relaxation Times, τ, of Different Ion Pair Species, Estimated via Eqs. 1.56 and 1.60 Assuming Stick or Slip Boundary Conditions, Together With Their Effective Dipole Moments, μ_{eff}, and Associated Standard-State Association Constants, K_{A}°.[a]

	τ_{stick}	τ_{slip}	μ_{eff}	K_{A}°
CIP	29.7	3.6	10.9	32 ± 8
SIP	64.9	20.3	24.6	4.4 ± 0.8
2SIP	122	55.0	36.7	2.1 ± 0.3

[a]Units: τ in ps, μ_{eff} in Debye (1D = $3.3356 \times 10^{-30} C \cdot m$), K_{A}° in $\mathrm{L\,mol^{-1}}$.

Table 3.2 lists the estimated CIP, SIP and 2SIP relaxation times for stick and slip boundary conditions. As can be seen, only the 2SIP result for stick boundary conditions is in fair agreement with the experimental average, $\tau_1 \approx 210\,\mathrm{ps}$ (Figure 3.6). However, it should be kept in mind that the SED equation, Eq. 1.56, allows only a rough estimate of τ'_{IP} (and thus τ_{IP}) because in general V_{m} and especially $f_{\perp}$ can only be approximated and C is generally not known. Even more problematic, for the above calculations ion pairs were assumed to be not solvated. However, it is unlikely that on IP formation $\mathrm{Na}^+_{\mathrm{aq}}$ completely looses its complete hydration shell **except** for the intervening water molecules in SIP and 2SIP. Thus, at least for ion pairs involving strongly solvated ions, like $\mathrm{Na}^+_{\mathrm{aq}}$, larger τ_{IP} values have to be expected (but cannot be reasonably predicted) than those assigned to CIP, SIP and 2SIP in Table 3.2.

Relaxation times are obviously only a rough guide for the identification of the ion-pair species behind an observed solute relaxation. Generally more straightforward, even for multi-step ion association, is a comparison of K_{A}° values estimated from the amplitude(s) of the solute relaxation(s) with standard-state association constants determined by standard techniques,[18,24] *provided the latter are reasonably well known.* In the following, this approach is applied to NaCl(aq).

Assuming, as for the evaluation of τ_{IP}, that a mode j resolved in the formal fit is due to the relaxation of a single species (here either CIP, SIP or 2SIP), its amplitude, S_j, can be related to the concentration, c_j, of that species via Eq. 1.47. Following Barthel *et al.*[53] and using polarizabilities of $1.44\,\mathrm{Å}^3$ for water,[109] $0.258\,\mathrm{Å}^3$ for Na^+ and $3.40\,\mathrm{Å}^3$ for Cl^-,[107] the bare ion-pair dipole moments, μ_{IP}, of Table 3.2 were calculated for CIP, SIP and 2SIP models of NaCl, and from that corresponding ion-pair concentrations, c_{IP}, obtained by evaluating S_1 with the help of Eq. 1.47. For each of the three ion pair models, CIP, SIP and 2SIP, K_{A} values, Eq. 1.72, were calculated and the associated standard-state association constants, K_{A}°, obtained by fitting the data via Eq. 1.74.[72] The thus obtained

values for K_A°, which differ significantly for CIP, SIP and 2SIP, are also summarized in Table 3.2.

Identification of the predominating ion-pair species for NaCl(aq) and validation of the corresponding $K_A(I)$ values would then proceed through comparison of the DRS values of K_A° for the model ion pairs CIP, SIP and 2SIP (Table 3.2) with standard-state association constants from other methods. Unfortunately, the data basis for such a comparison is very limited. To the best of our knowledge, only the values of $K_A^\circ = 0.82\,\mathrm{L\,mol^{-1}}$,[110] and $2.83\,\mathrm{L\,mol^{-1}}$,[111] were published. Both were obtained with dilute-solution conductometry, a method that is intrinsically species-unspecific and yields only a rough estimate for $K_A^\circ < 10\,\mathrm{L\,mol^{-1}}$.[21] Nevertheless, these data are most compatible with 2SIP and thus seem to confirm the inference from τ_1. This result is somewhat surprising as Cl^- is known to be only weakly hydrated, *i.e.* the residence time of a H_2O molecule in the hydration shell of Cl^- is comparable to the bulk-water residence time.[112] Thus, it seems more plausible that SIPs should be immediately formed on encounter of Na^+_{aq} and Cl^-_{aq} but not 2SIPs.

Interestingly, some computer simulations suggest that formation of CIPs should always be dominant over SIPs in aqueous NaCl,[12,17,113] although ion association is generally low ($K_A < 1\,\mathrm{L\,mol^{-1}}$). On the other hand, the HNC-based theory of Yamaguchi *et al.* predicts that at low c the small amount of ion pairs formed in this electrolyte is dominated by SIPs but CIPs become the major IP species above $1\,\mathrm{mol\,L^{-1}}$.[32,105] Different again, Mancinelli *et al.* conclude that computer simulations compatible with their neutron scattering data indicate only SIPs over the entire concentration range.[114]

Obviously, reliable reference data for K_A° of NaCl(aq) are lacking and the information from computer simulations regarding the dominant IP species is, at least for $c < 1\,\mathrm{mol\,L^{-1}}$, somewhat contradicting. Nevertheless, CIPs can be almost certainly excluded to be responsible for the low-frequency relaxation detected for NaCl(aq) because the associated DRS value for the association constant, $K_A^\circ(\mathrm{CIP}) \approx 32\,\mathrm{L\,mol^{-1}}$ is far too large and the corresponding relaxation time, $\tau_{\mathrm{CIP}} \approx 4 - 30\,\mathrm{ps}$, too small. Despite reasonable DRS values for $K_A^\circ(\mathrm{2SIP})$ and τ_{2SIP}, 2SIPs are also unlikely because this species is neither compatible with computer simulations nor with general knowledge on Cl^- hydration.

There are some arguments in favour of SIPs as the relaxing species behind the present low-frequency relaxation. In particular, the calculations of Yamaguchi *et al.*[32,105] and the simulations of Mancinelli *et al.*[114] strongly hint at the predominance of SIPs over other IP species at $c \lesssim 1\,\mathrm{mol\,L^{-1}}$. Also, the relaxation time of hydrated SIPs should be similar to the τ_{2SIP} values listed for the "naked" 2SIPs in Table 3.2. However, summarizing all evidence, it is very unlikely that the association constant of NaCl(aq) exceeds $1\,\mathrm{L\,mol^{-1}}$. Thus, it is also unlikely that SIP reorientation is the only reason for the observed low-frequency solute relaxation.

Note that according to Yamaguchi *et al.* a significant amount of contact ion pairs should be present at $c > 1\,\mathrm{mol\,L^{-1}}$,[32,105] for which there is no indication in the present dielectric spectra. This situation is similar to aqueous RbF solutions where HNC calculations indicated a significant amount of direct cation-anion contacts but DRS also could not detect CIPs.[29] Of course, CIP relaxation might be buried under the dominating water mode since τ_{CIP} should be small (Table 3.2). However, the more likely reason why CIPs are not observed with DRS at high NaCl concentrations is ion-pair redissociation: due to the small average distance

between ions at $c > 1\,\mathrm{mol\,L^{-1}}$, and thus strong ion-ion interactions, the lifetime of individual CIPs apparently drops below their rotational correlation time, preventing thus their detection by DRS. This appears to be a rather general phenomenon,[18,29,30] and suggests that concentrated electrolyte solutions behave like a "solvent-lubricated" ionic liquid.[115] Although interactions in ionic liquids are dominated by direct anion-cation contacts, no long-lived ion pairs were found.[116]

3.3.2 Ion-cloud relaxation

Ion-cloud relaxation, that is the rearrangement in a fluctuating electric field of the diffuse ion cloud surrounding any charged entity immersed in an electrolyte solution, is a major component in the dielectric spectra of colloidal solutions,[98–100] and responsible for electrode polarization.[25] As it is well known from Debye-Hückel theory,[67] any ion in solution is surrounded by its ion-cloud and ion-cloud relaxation was accordingly predicted by Debye and Falkenhagen in 1928.[47] So far, unequivocal experimental verification of this Debye-Falkenhagen effect is lacking for conventional electrolytes as its magnitude is small and reasonable predictions for its relaxation strength (or the corresponding conductivity change) were missing.[101] However, the predicted ion-cloud relaxation times,

$$\tau_{\mathrm{ic}}(c) = \frac{\varepsilon\varepsilon_0}{c\Lambda_\infty} \tag{3.1}$$

where Λ_∞ is the molar conductivity at infinite dilution,[117] correspond to loss-peak frequencies in the 0.1-1 GHz region and are thus compatible with the present low-frequency relaxation.

Recently, Yamaguchi *et al.* proposed a new HNC-based theory for the frequency dependence of conductivity/ion-cloud relaxation in electrolyte solutions.[32,118] For aqueous NaCl solutions they predicted a relaxation in the 0.1-1 GHz region (Figure 3.6), jointly arising from ion-cloud relaxation and SIP reorientation (which their theory cannot discriminate). For the amplitude, S_{ic}, of this composite mode they found rapid initial rise until a flat maximum of $S_{\mathrm{ic}} \approx 0.7$ is reached at $c \approx 0.5\,\mathrm{mol\,L^{-1}}$, then S_{ic} slowly decays again (Figure 3.5).[32,105] Both, magnitude and concentration dependence of $S_{\mathrm{ic}}(c)$, are very similar to the relaxation strengths of the low-frequency solute modes observed for aqueous 1:1 electrolytes,[27–30,102,103] including the present NaCl(aq). It is thus worthwhile to scrutinize the experimental data for evidence in favor of ion-cloud relaxation.

An important feature of τ_{ic} predicted by Eq. 3.1 is its pronounced decrease with increasing c (Figure 3.6). For NaCl(aq) τ_{ic} drops from 400 ps at $c \approx 0.14\,\mathrm{mol\,L^{-1}}$ to 200 ps at $\sim 0.27\,\mathrm{mol\,L^{-1}}$ to 100 ps at $\sim 0.5\,\mathrm{mol\,L^{-1}}$ (Fig. 3.6). The solute relaxation times predicted by Yamaguchi *et al.*[32,105] exhibit a similar drop with 400, 200, and 100 ps marks already reached at approximately 0.08, 0.15, and $0.34\,\mathrm{mol\,L^{-1}}$ (Figure 3.6). These predictions appear to contrast experimental data, as for NaCl(aq) the solute relaxation time, τ_1, is independent of c, with an average value of $\sim$210 ps (Table 3.1 & Figure 3.6), albeit with a few values exceeding 250 ps at $c < 0.2\,\mathrm{mol\,L^{-1}}$. Corresponding τ_1 data for RbF[29] are also roughly constant, whereas those for LiCl[103] and NaOFm & NaOAc[30] are too noisy to infer a reasonable trend. The solute relaxation times for CsCl,[27] NaBr, NaI, $NaNO_3$,

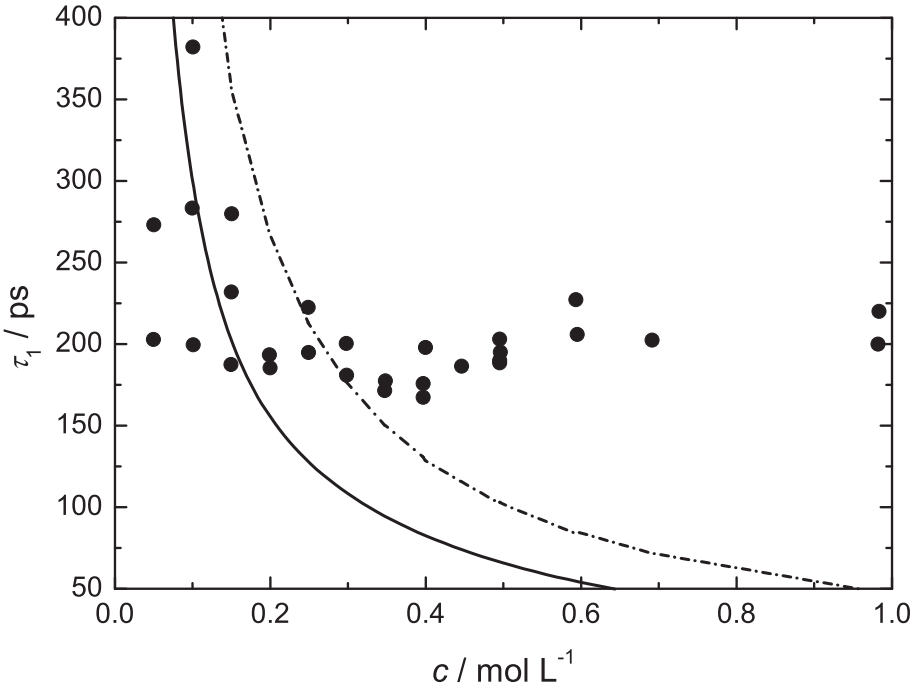

Figure 3.6: Relaxation times, τ_1 (●), for the low-frequency solute relaxation in NaCl(aq) as a function of concentration, c, at 25 °C. The broken line represents an estimate of the ion-cloud relaxation time with Eq. 3.1; the solid line is a fit of the values reported by Yamaguchi et al.[32,105]

$NaClO_4$ & NaSCN,[28] as well as for $NaBPh_4$[102] do decrease with increasing c but the large values predicted by Eq. 3.1) for $c < 0.2\,\mathrm{mol\,L^{-1}}$ are never reached and the concentration dependence of τ_1 was reasonably well explained with fast ion-pair kinetics (note that the latter feature is also implicit to the theory of Yamaguchi *et al.*[32,118]).

It has to be noted, however, that for $c < 0.2\,\mathrm{mol\,L^{-1}}$, the uncertainty in τ_1 is very large and possibly masking the decrease predicted by Eq. 3.1 and the calculations of Yamaguchi *et al.*[32]] This does not only apply to the present NaCl(aq) data (Figure 3.6) but to all aqueous 1:1 electrolytes with solute relaxation studied so far,[27–30,102,103] so that for $c \lesssim 0.2\,\mathrm{mol\,L^{-1}}$ the experimental solute relaxation times cannot be used as an argument against ion-cloud relaxation. On the other hand, the expected solute relaxation times at higher concentrations are rather reliable. From the observation that $\tau_1 \approx 200\,\mathrm{ps}$ for $c \geq 0.5\,\mathrm{mol\,L^{-1}}$ we may thus infer that ion-cloud relaxation is not the only process contributing to the low-frequency solute mode and it is reasonable to assume that this additional contribution is ion-pair reorientation, possibly from SIPs. Similar considerations apply to the other aqueous 1:1 electrolytes.[27–30,102,103]

Figure 3.5 compares the combined amplitudes of ion-cloud and SIP relaxation predicted by Yamaguchi *et al.*[32,105] with the present values, S_1, for the solute mode of NaCl(aq). As expected, the experimental data scatter considerably. Nevertheless, they show the same trend as the theoretical predictions, namely a rapid initial rise, followed by a flat maximum around 0.3–0.7 $\mathrm{mol\,L^{-1}}$ and then a gradual decrease. Also the magnitudes of

the predicted and the measured S_1 values are rather similar, albeit with somewhat larger experimental data at intermediate concentrations. This surprisingly good agreement is strong indication that the theory of Yamaguchi grasps the essential features of the experimentally observed solute relaxation.[32,118] At the same token this indicates that the small-amplitude low-frequency mode resolved for the present spectra, as well as for other aqueous 1:1 electrolytes[27–30,102,103] is not an experimental artefact.

The slightly larger experimental amplitudes at intermediate concentrations and, more importantly, the rather constant solute relaxation time, $\tau_1 \approx 210\,\mathrm{ps}$ suggest that for $c \gtrsim 0.4\,\mathrm{mol\,L^{-1}}$ SIP reorientation predominates ion-cloud relaxation. Unfortunately, neither the theoretical approach of Yamaguchi *et al.*[32,118] nor the present experiments are able to distinguish between "proper" ion-cloud relaxation, the kinetics of ion-pair formation and decay, and the reorientation of SIPs. Since both, ion-cloud relaxation and ion-pair kinetics, involve translational motions of cations and anions relative to each other, their formal distinction is probably rather futile. Thus, we have some evidence for weak ion association in dilute to moderately concentrated aqueous NaCl solutions, most likely through the formation of solvent-shared ion pairs. However, we cannot reliably determine ion-pair concentrations and hence the corresponding association constant, K_A°, by DRS. Since ion-cloud relaxation is a general phenomenon of electrolyte solutions, we have to keep in mind that a "conservative" evaluation of solute amplitudes, *i.e.* under the assumption that the latter are only due to ion pairs, will yield somewhat too large K_A°. Due to the small amplitude of ion-cloud relaxation this is no problem for moderately associating electrolytes.[18] However, for weakly associating electrolytes DRS will only provide an upper limit for K_A°.

In view of the recent discussion on physiological effects of weak ion binding[10,17,20] this is regrettable as here other techniques potentially sensitive to ion pairs, like conductometry, ultrasonic spectroscopy (US) or optical Kerr-effect spectroscopy (OKE) are also problematic. Ultrasonic spectroscopy, the only technique besides DRS able to discriminate different types of ion pairs, so far was not able to detect ion pairs in general and SIPs in particular for NaCl(aq). To the best of our knowledge, all US studies on NaCl(aq)[119,120] found little or no excess absorption due to the solute, suggesting that within the uncertainty of these experiments ion-pair formation is negligible. Of course, these rather old results do not completely rule out ion pairing in NaCl(aq) but only indicate that it is very weak. Since we may assume that the sensitivity of US instrumentation was considerably improved over the last 40 years, a new US study into ion-pair equilibria in NaCl(aq) might be worthwhile. Due to its sensitivity to polarizability fluctuations, OKE spectroscopy should be well suited to study ion-cloud relaxation. Unfortunately, the recent OKE study on NaCl(aq) is of little aid to verify our results.[121] The problem is that currently OKE spectroscopy needs rather high concentrations, typically ≥ 1 mol $\mathrm{L^{-1}}$. Additionally, the predicted ion-cloud relaxation times are too long to be in the reach of present OKE instrumentation.

3.4 Water relaxation

Due to the wider frequency range of the present spectra and the separation of a solute-related low-frequency relaxation for $c \leq 1\,\mathrm{mol\,L^{-1}}$, the characteristic parameters for the

water relaxation, S_2, τ_2 (Figure 3.4), and α_2 (Figure 3.3b), differ somewhat from those of Buchner *et al.*[31] The deviations for the latter two parameters were discussed already in Section 3.2.
A more detailed consideration is necessary for S_2, as from this quantity the amount of DRS detected water, $c_{\mathrm{w}}^{\mathrm{app}}$, and thus the number

$$Z_{\mathrm{ib}}(c) = \frac{c_{\mathrm{w}} - c_{\mathrm{w}}^{\mathrm{app}}}{c} \tag{3.2}$$

of irrotationally bound (ib) water molecules per equivalent of salt is determined by comparing $c_{\mathrm{w}}^{\mathrm{app}}$ with the analytical water concentration, c_{w}. Since $Z_{\mathrm{ib}}(\mathrm{NaCl}) = Z_{\mathrm{ib}}(\mathrm{Na^+}) + Z_{\mathrm{ib}}(\mathrm{Cl^-})$ (strictly valid only for $c \to 0$) and $Z_{\mathrm{ib}}(\mathrm{Cl^-}) = 0$,[18,24] the value for $Z_{\mathrm{ib}}(\mathrm{NaCl}) = Z_{\mathrm{ib}}(\mathrm{Na^+})$ is a cornerstone for splitting the Z_{ib} of sodium salts accessible from experiment into ionic contributions.

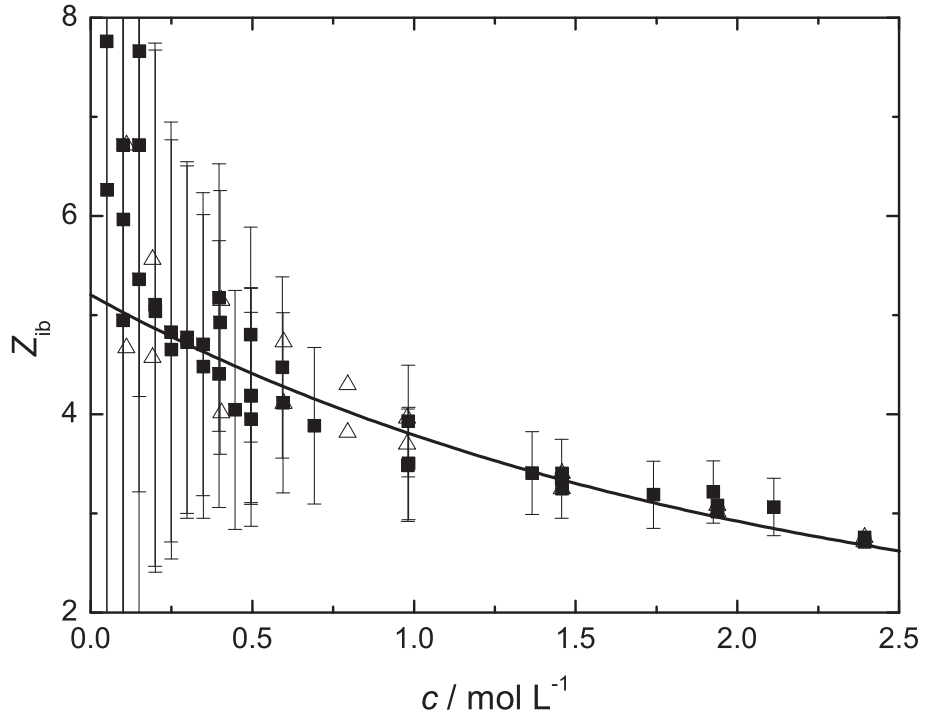

Figure 3.7: Effective hydration numbers, Z_{ib}, of NaCl(aq) for this study (■) and from Buchner *et al.* (△).[31] The solid line corresponds to a joint fit of both data sets with Eq. 3.8, using error-weighted Z_{ib} (see text). Error bars of the experimental values were estimated from the standard deviation, σ_{fit}, of the polynomial $\varepsilon_2(c) = 78.368 + a_1 \cdot c + a_2 \cdot c^{3/2} + a_3 \cdot c^2$.

To calculate $c_{\mathrm{w}}^{\mathrm{app}}$ the fast water process is added to the detected bulk water amplitude S_2 to yield S_{b} via

$$S_{\mathrm{b}} = \varepsilon_2 - \varepsilon_\infty \tag{3.3}$$

where $\varepsilon_\infty = 3.48$ is the infinite-frequency permittivity of pure water, also including the fast water process.[78] The water amplitude S_{b} now has to be further corrected for kinetic

depolarization, $\Delta_{\mathrm{kd}}\varepsilon$ which is due to the torque exerted by the electric field of migrating ions on the solvent dipole vectors.[122–124] This is given as

$$\Delta_{\mathrm{kd}}\varepsilon = \xi\kappa(c) \tag{3.4}$$

where

$$\xi = p \times \frac{\varepsilon(0) - \varepsilon_\infty}{\varepsilon(0)} \times \frac{\tau(0)}{\varepsilon_0} \tag{3.5}$$

In Eq. 3.5, $\tau(0)$ is the relaxation time of the dominant dispersion step in pure water, $\varepsilon(0)$ its static permittivity and $\varepsilon_\infty(0)$ the infinite frequency permittivity of pure water. The hydrodynamic parameter p, which characterizes the translational motion of the ions has limiting values of $p = 1$ for *stick* boundary conditions and $p = 0$ for negligible kinetic depolarization. *Slip* boundary conditions with $p = 2/3$ are generally used for electrolyte solutions.[27,30,31,125] The total water amplitude (i.e. the equilibrium amplitude of the overall solvent relaxation process) is thus given as

$$S_{\mathrm{b}}^{\mathrm{eq}}(c) = S_{\mathrm{b}}(c) + \Delta_{\mathrm{kd}}\varepsilon \tag{3.6}$$

For the calculation of DRS detected water concentration, $c_{\mathrm{w}}^{\mathrm{app}}$, it is now convenient to use a pure water normalized version of Eq. 1.47:

$$c_{\mathrm{w}}^{\mathrm{app}} = c_{\mathrm{w}}(0) \times \frac{\varepsilon(0)}{\varepsilon(c)} \times \frac{2\varepsilon(c)+1}{2\varepsilon(0)+1} \times \frac{S_{\mathrm{b}}^{\mathrm{eq}}(c)}{S(0)} \tag{3.7}$$

where $c_{\mathrm{w}}(0) = 55.34\,\mathrm{mol\,L^{-1}}$ is the concentration of pure water at 25 °C and $S(0) = 74.888$ its total amplitude.[126] Effective hydration numbers, Z_{ib}, were then calculated via Eq. 3.2. In Figure 3.7 the corresponding effective NaCl hydration numbers of this study are compared with the results of Buchner *et al.* (only the common concentration range, $c < 2.5\,\mathrm{mol\,L^{-1}}$, is shown).[31] Overall, the agreement of both data sets is very good so that they were combined for a parametrization of $Z_{\mathrm{ib}}(c)$ with the empirical equation

$$Z_{\mathrm{ib}}(\mathrm{Na^+},\, c) = A + B\exp\left(-\frac{c}{C}\right) \tag{3.8}$$

yielding $A = 1.5 \pm 0.3$, $B = 3.7 \pm 0.2$, & $C = (2.1 \pm 0.3)\,\mathrm{mol\,L^{-1}}$ in a least-squares fit weighted by the reciprocal uncertainty of Z_{ib}. In this fit, data at $c < 0.2\,\mathrm{mol\,L^{-1}}$ were omitted as they appeared to be systematically biased to too large values. In the light of recent computer simulations,[127,128] which do not find a retarding effect of $\mathrm{Na^+}$ on the dynamics of its second hydration shell, this appears to be justified.
From the parameters of Eq. 3.8 an effective hydration number of $Z_{\mathrm{ib}}^0(\mathrm{Na^+}) = 5.2 \pm 0.5$ is obtained for $\mathrm{Na^+_{aq}}$ at infinite dilution. This value is somewhat larger than the previous DRS result,[18,31] but in excellent agreement with coordination numbers $n(\mathrm{Na^+})$ recently obtained by neutron diffraction, $n(\mathrm{Na^+}) = 5.3$,[114] and different QM/MD simulations, $n(\mathrm{Na^+}) = (5.2 \pm 0.6)$[128] and $n(\mathrm{Na^+}) = (5.6 \pm 0.3)$.[129] The decrease of $Z_{\mathrm{ib}}(\mathrm{Na^+},\, c)$ with increasing c is attributed to solvation-shell overlap.[18,24]

3.5 Conclusion

The present DRS study of NaCl(aq) provides firm evidence that the low-frequency, small-amplitude relaxation observed for weakly associating aqueous 1:1 electrolytes[27–30,102,103] is not an experimental artefact but related to the solute. Separation of this mode in the numerical analysis of the complex permittivity spectra, which is not unproblematic even with the improved instrumentation used in this work, affects the parameters describing the cooperative relaxation of bulk water in the solutions, namely its relaxation time, τ_2 (Figure 3.4), and the width parameter, α_2 (Figure 3.3b). However, the "static" permittivity of water in the NaCl(aq) solutions, ε_2, and hence the water amplitude, $S_\mathrm{b}(c)$ remains rather unaffected. Hence the effective hydration numbers, $Z_\mathrm{ib}(c)$, agree well with previously published data.[31] An improved estimate for the effective hydration number of Na^+ is given, yielding an infinite-dilution value of $Z^0_\mathrm{ib}(Na^+) = 5.2 \pm 0.5$.
Evaluation of relaxation time, τ_1 (Figure 3.6), and amplitude, S_1 (Figure 3.5), of the resolved low-frequency solute mode indicates that this is a composite of ion-cloud and ion-pair relaxation, with solvent-shared ion pairs as the most probable species in case of NaCl(aq). This is in line with the theoretical study of Yamaguchi *et al.*,[32,105,118] which largely stimulated the reinvestigation of NaCl(aq). Unfortunately, at present neither theory nor experiment are able to disentangle both effects. Since ion-cloud relaxation is small but ubiquitous for electrolyte solutions, DRS is thus only able to give an upper bound for the standard-state association constant, K°_A, of weakly associating electrolytes. On the other hand, as ion association in NaCl(aq) is expected to be very small, the observed IP + IC amplitude S_1 may also serve as an upper limit for IC contribution in the DR spectra of 1:1 electrolytes. Of course, this does not give any quantitative information on the contribution of IC relaxation, however, it allows the qualitative assessment and thus an estimate for the reliability of determined association constants.

Chapter 4

Potassium Phosphates

Most of the material presented in this chapter forms the basis of a manuscript, in preparation for the Journal of Physical Chemistry B:

Andreas Eiberweiser and Richard Buchner
Institut für Physikalische und Theoretische Chemie, Universität Regensburg, D-93040 Regensburg, Germany.

Glenn Hefter
Chemistry Department, Murdoch University, Murdoch, W.A. 6150, Australia.

4.1 Introduction

Plants only contain 0.2% of phosphorous by weight.[130] Nevertheless, phosphorous is an essential element for and often acts as an limiting factor for plant growth. Therefore it is essential to ensure that commercial crops have enough supply of bio-available phosphorous, which is why phosphate fertilizers are used throughout the world. Despite their overwhelming biological importance, rather little seems to be known about the hydration of the simple inorganic phosphate ions $H_xPO_4^{(3-x)-}$, $x = 0$, 1 or 2. The strong hydration of the orthophosphate anion (PO_4^{3-}) seems to be well established or at least widely assumed,[33,34,131–133] but literature information on the hydration of $H_2PO_4^-$ and HPO_4^{2-} is scarce and inconclusive.[33–35,37,134] Also, probably due to the rich chemistry of aqueous phosphate solutions,[2,135] there is no consensus on the speciation in those systems. This seems to be especially the case in the question of ion pairing and phosphate dimerization. Most studies focus on either anion dimerization or ion pairing and neglect the other process. Due to the potential high importance of even small differences in ion pairing for biological processes,[10,20] this situation is highly unsatisfactory.
With its unique ability to differentiate different types of ion pairs, DRS is the ideal technique to resolve the still open question on whether aqueous potassium phosphate solutions show ion pairing or not. Also, further insight into the hydration of the different phosphate species can be gained by a DRS study. Accordingly a detailed broadband (0.2 - 89 GHz) dielectric relaxation study of aqueous solutions of K_3PO_4, K_2HPO_4, and KH_2PO_4 at 25 °C, with solute concentrations $c \geq 0.05$ mol L^{-1} up to the saturation limit was performed.

4.2 Experimental Details and Description of Spectra

DR spectra have been measured at 25 °C, over the frequency range $0.2 \leq \nu/GHz \leq 89$. For frequencies < 50 GHz the VNA with its two corresponding probe heads was used. The general cleaning procedure (removing the sample, washing twice with water and acetone and then drying with dry N_2) of the VNA probeheads was sufficient for KH_2PO_4(aq) and K_2HPO_4(aq). For K_3PO_4(aq), however, repetition of the described cleaning procedure for up to 5 times was necessary before re-calibration, to avoid electrode polarization errors, which probably arose from the adsorption of PO_4^{3-} on the probe-head surface. Sample pH was determined (to ± 0.01) at room temperature with a Consort C835 pH-meter, equiped with a Bioblock combination glass electrode, containing a silver chloride reference electrode. The electrode was calibrated with standard buffer solutions of pH = 4.00, 7.00 and 10.0 before measurement. The measured pH values (Table 4.1) indicated that a maximum of 5% of $H_2PO_4^-$(aq) and HPO_4^{2-}(aq) were hydrolyzed in solutions of KH_2PO_4 and K_2HPO_4 respectively at all salt concentrations. Hydrolysis was thus neglected for those salts. The phosphate ion PO_4^{3-}, however, shows considerable hydrolysis, especially at high dilutions. The measured pH values of the K_3PO_4(aq) samples were therefore used to calculate the actual speciation via the appropriate mass balance equations (see Section 4.3.2).

Figure 4.1 shows typical experimental dielectric spectra for KH_2PO_4(aq) together with the corresponding fits. Concentration dependent amplitudes of the resolved relaxations are shown in Figure 4.2. Analogous pairs of figures are given for K_2HPO_4(aq) (Figures 4.3 & 4.4) and K_3PO_4 (Figures 4.5 & 4.6). The fit parameters for all three salts are summarized in Tables 4.2, 4.3 & 4.4. The DR spectra of all of the present solutions were best described by a sum of n Debye equations. For KH_2PO_4(aq) a four-Debye (4D) model was satisfactory at all concentrations, whereas for K_2HPO_4(aq) a 3D model yielded the best fits. A 3D model was also satisfactory for K_3PO_4(aq) at low concentrations but at $c \geq 2.6\,\mathrm{mol\,L^{-1}}$ only two Debye-type relaxations could be resolved. A striking feature of the three sets of spectra is the increase of the static permittivity, ε_1. This occurs over the entire concentration range for KH_2PO_4(aq), while solutions of the other two salts show an initial increase in ε_1 with increasing c at low concentrations, followed by a decrease. This hints at the formation of ion pairs, as discussed in detail below.

The dominant mode in all spectra, centered around ~18 GHz, can be attributed unequivocally to bulk water relaxation. Pure water shows two relaxations in the DR spectrum at 25 °C.[78] The main one, with a relaxation time of $\tau_{\mathrm{bulk}} = 8.32$ ps, is attributed to the cooperative dynamics of the hydrogen-bond network.[31] A second, low amplitude mode centered at ~600 GHz is generally assigned to the small fraction of water molecules that are thought to be less hydrogen-bonded than bulk water.[62] This mode is sometimes,[102,136] but not always,[29] detected in the DR spectra of electrolyte solutions restricted to the same frequency range ($\nu \leq 89$ GHz) as the present study. For the present salts this fast water process was only resolved for KH_2PO_4(aq), but its presence can be implied in K_2HPO_4(aq) and K_3PO_4(aq) solutions by the strong increase in ε_∞ with increasing c. Apart from the two water modes, solutions of all three phosphate salts showed two additional lower-frequency relaxation modes at ~8 GHz and ~1.6 GHz (only at $c < 2.6\,\mathrm{mol\,L^{-1}}$ for K_3PO_4(aq)). The observed amplitudes of both these modes increase steadily with c and both modes are

Table 4.1: Concentrations, c, and pH Values of All Studied Potassium Phosphate Salt Solutions.[a]

KH_2PO_4		K_2HPO_4		K_3PO_4	
c	pH	c	pH	c	pH
0.0501	4.6	0.0298	9.1	0.0250	11.69
0.0999	4.4	0.0498	9.0	0.0500	12.04
0.1492	4.4	0.1500	9.1	0.0749	12.17
0.1980	4.4	0.1989	9.1	0.1015	12.19
0.2965	4.3	0.2504	9.1	0.1497	12.37
0.3933	4.3	0.2975	9.1	0.1988	12.50
0.4900	4.3	0.3943	9.2	0.2489	12.49
0.5842	4.2	0.4904	9.1	0.3016	12.41
0.6791	4.2	0.5893	9.2	0.3476	12.63
0.7721	4.2	0.6830	9.2	0.3985	12.64
0.8649	4.1	0.7771	9.2	0.5920	12.77
0.9564	4.1	0.8667	9.2	0.7826	12.66
1.0480	4.1	0.9643	9.1	0.9730	12.96
1.1369	4.1	1.4150	9.3	0.9738	12.74
1.2057	4.1	1.8480	9.4	1.4291	13.23
1.3319	4.0	2.6442	9.6	1.8623	13.41
		3.3495	9.7	2.2681	13.65
		3.9872	9.8	2.6507	13.76
				3.0119	13.93

[a] Units: c in $\mathrm{mol\,L^{-1}}$.

thought to be composites. The slowest process at ∼1.6 GHz, corresponding to an average relaxation time $\tau \approx 100\,\mathrm{ps}$, can be assigned to ion-pair reorientation with a small contribution from ion-cloud relaxation (the Debye-Falkenhagen effect).[137] The mode centered at ∼8 GHz ($\tau \approx 20\,\mathrm{ps}$) also consists of two contributions: the rotational diffusion of the dipolar anion (K^+ has no permanent dipole moment) and the presence of 'slow' water, i.e. water molecules with dynamics significantly slowed relative to those of bulk water. Both processes were required to account for the observed amplitudes $S_2(c)$.

Table 4.2: Concentration Dependence of the Dielectric Relaxation Parameters of a Four-Debye Fit of Aqueous Solutions of KH_2PO_4 at 25 °C: Concentration, c, Limiting Permittivities, ε_j ($j = 1 - 4$) & ε_∞, Relaxation Times, τ_j, VNA Conductivities, κ_{VNA}, and the Value of the Reduced Error Function, χ^2_{r}.[a,b]

c	ε_1	τ_1	ε_2	τ_2	ε_3	τ_3	ε_4	τ_4	ε_∞	κ_{VNA}	χ^2_{r}
0.0501	78.76	236	77.97	23F	77.07	8.40	6.51	1.0F	4.56	0.445	0.0287
0.0999	79.06	156	77.82	23F	75.29	8.37	6.96	1.02	4.47	0.837	0.0292
0.1492	79.48	153	77.75	23F	73.73	8.36	7.53	1.76	5.04	1.196	0.0509
0.1980	79.78	121	77.49	23.3	72.90	8.22	6.68	0.57	3.44	1.537	0.0481
0.2965	80.47	112	77.25	22.4	70.01	8.11	6.91	1.0F	4.68	2.175	0.0553
0.3933	80.85	102	76.90	24.5	69.51	8.14	6.90	1.29	4.49	2.737	0.0667
0.4900	81.19	84.7	76.01	22.9	67.52	8.12	7.18	1.0F	4.22	3.296	0.0658
0.5842	81.83	91.2	76.10	22.9	64.93	7.93	7.06	1.28	5.00	3.787	0.1124
0.6791	82.24	89.0	75.69	22.9	63.12	7.89	7.23	0.72	3.83	4.265	0.1129
0.7721	82.63	85.7	75.01	21.9	60.77	7.79	7.48	1.04	4.47	4.715	0.1254
0.8649	83.31	87.4	74.80	22.6	59.21	7.68	7.10	1.0F	5.56	5.136	0.1378
0.9564	83.69	87.6	74.33	22.6	57.80	7.61	7.13	0.70	4.19	5.551	0.1123
1.048	84.12	88.6	73.97	22.5	56.02	7.58	7.68	1.04	4.58	5.913	0.1228
1.137	84.43	88.6	73.32	21.3	52.64	7.27	7.46	0.98	4.97	6.262	0.1779
1.206	84.80	91.4	73.14	21.5	51.92	7.31	7.90	1.0F	4.25	6.518	0.2068
1.332	85.30	92.5	72.42	21.5	50.00	7.18	7.79	0.98	4.68	6.969	0.3450

[a] Units: c in $\mathrm{mol\,L^{-1}}$, τ_j in ps, κ_{VNA} in $\mathrm{S\,m^{-1}}$; [b] Parameter values followed by the letter F were not adjusted in the fitting procedure.

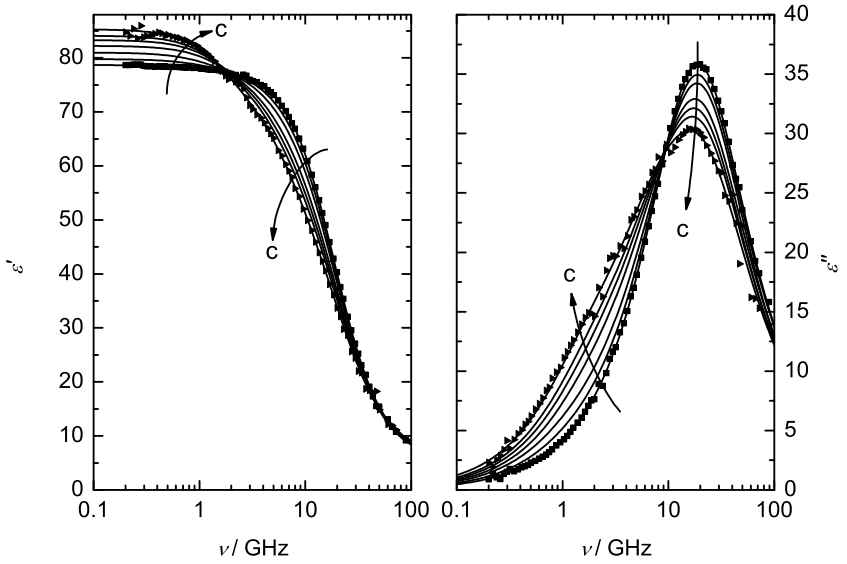

Figure 4.1: Spectra of relative permittivity, $\varepsilon'(\nu)$, and dielectric loss, $\varepsilon''(\nu)$, for KH_2PO_4(aq) at 25 °C and concentrations $c\,/\,(\text{mol L}^{-1})$ = 0.0501, 0.198, 0.393, 0.679, 0.865, 1.05 and 1.33. Symbols show typical experimental data; lines represent the D+D+D+D fit.

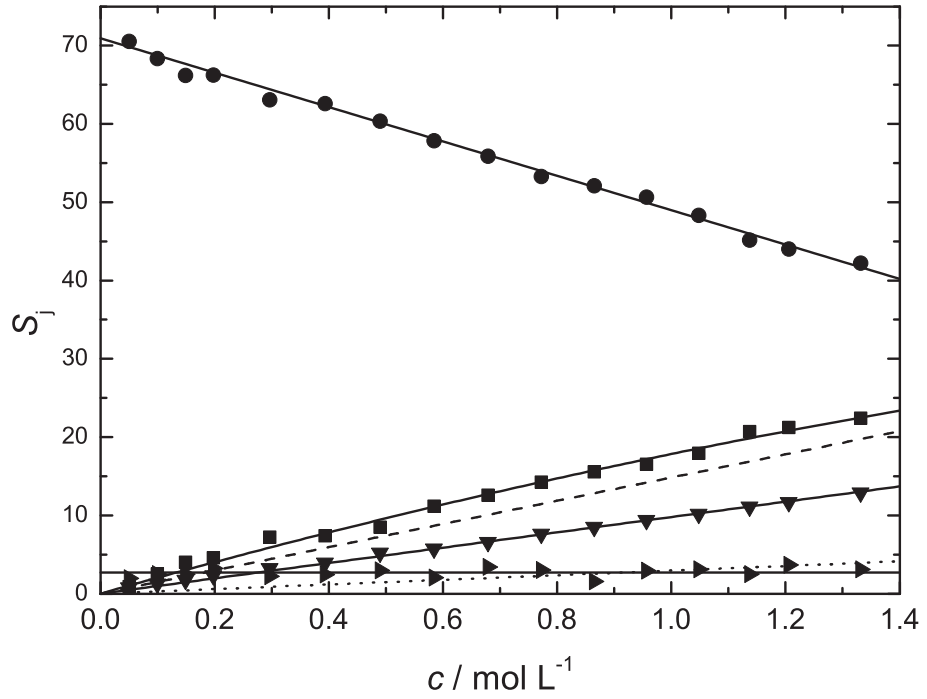

Figure 4.2: Amplitudes of the four Debye relaxation modes for KH_2PO_4(aq) as a function of solute concentration at 25 °C : bulk water (●), slow water + anion (■), IP + IC relaxation (▼) and fast water (►). Lines are visual guides only. Broken lines represent a deconvolution of S_2 into slow water (dashed line) and HPO_4^{2-} rotation (dotted line).

Table 4.3: Concentration Dependence of the Dielectric Relaxation Parameters of a Three-Debye Fit of Aqueous Solutions of K_2HPO_4 at 25 °C: Concentration, c, Limiting Permittivities, ε_j ($j = 1 - 3$) & ε_∞, Relaxation Times, τ_j, VNA Conductivities, κ_{VNA}, and the Value of the Reduced Error Function, χ^2_{r}.[a,b]

c	ε_1	τ_1	ε_2	τ_2	ε_3	τ_3	ε_∞	κ_{VNA}	χ^2_{r}
0.0298	79.23	447	77.55	21F	76.20	8.28	6.39	0.591	0.2371
0.0498	79.42	326	77.31	21F	75.24	8.20	6.20	0.929	0.0324
0.1500	79.25	171	76.33	21F	70.90	7.99	6.31	2.429	0.0940
0.1989	79.04	162	75.95	21F	69.12	7.88	6.39	3.095	0.1424
0.2504	78.77	144	75.52	21F	68.18	7.94	6.79	3.756	0.1570
0.2975	78.46	140	75.34	21F	66.19	7.80	6.74	4.333	0.2279
0.3943	77.58	116	74.68	21F	63.46	7.70	7.04	5.457	0.2450
0.4904	77.05	104	74.04	21F	60.85	7.40	6.36	6.495	0.1467
0.5893	76.39	113	73.50	21F	58.02	7.25	6.40	7.466	0.1883
0.6830	75.96	97.2	72.68	21F	57.56	7.29	6.87	8.373	0.2057
0.7771	75.30	93.8	72.05	21F	55.61	7.24	7.16	9.220	0.2899
0.8667	74.50	89.2	71.80	22.5	54.80	7.24	7.30	9.963	0.3028
0.9643	73.82	106	71.27	21F	49.87	6.77	6.59	10.72	0.3953
1.4150	70.95	79.8	66.88	21F	45.09	6.79	7.56	13.62	0.3720
1.8480	68.63	99.4	63.57	21.2	38.40	6.31	7.99	15.53	0.4791
2.6442	64.74	129	56.21	21.4	29.04	5.55	8.82	16.93	0.5631
3.3495	61.31	156	49.69	21.6	22.97	4.53	9.04	16.36	0.4955
3.9872	57.97	187	44.22	22.7	19.84	3.86	9.32	14.52	0.4378

[a] Units: c in $\mathrm{mol\,L^{-1}}$, τ_j in ps, κ_{VNA} in $\mathrm{S\,m^{-1}}$; [b] Parameter values followed by the letter F were not adjusted in the fitting procedure.

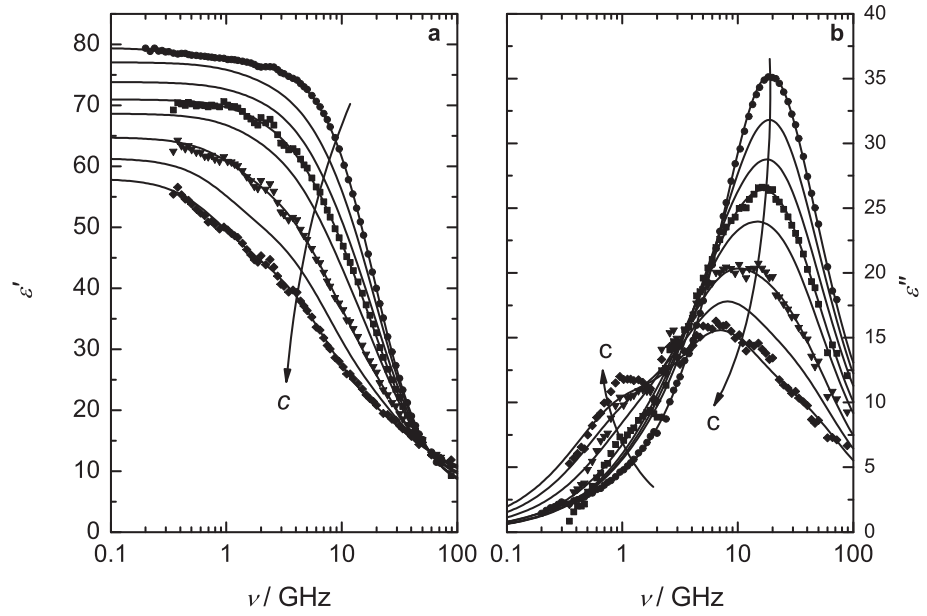

Figure 4.3: Relative permittivity (a) and dielectric loss (b) spectra for K_2HPO_4(aq) at 25 °C and concentrations c / (mol L^{-1}) = 0.0498, 0.4904, 0.9643, 1.415, 1.848, 2.644, 3.349 and 3.987. Symbols represent typical experimental data; lines represent the D+D+D fit.

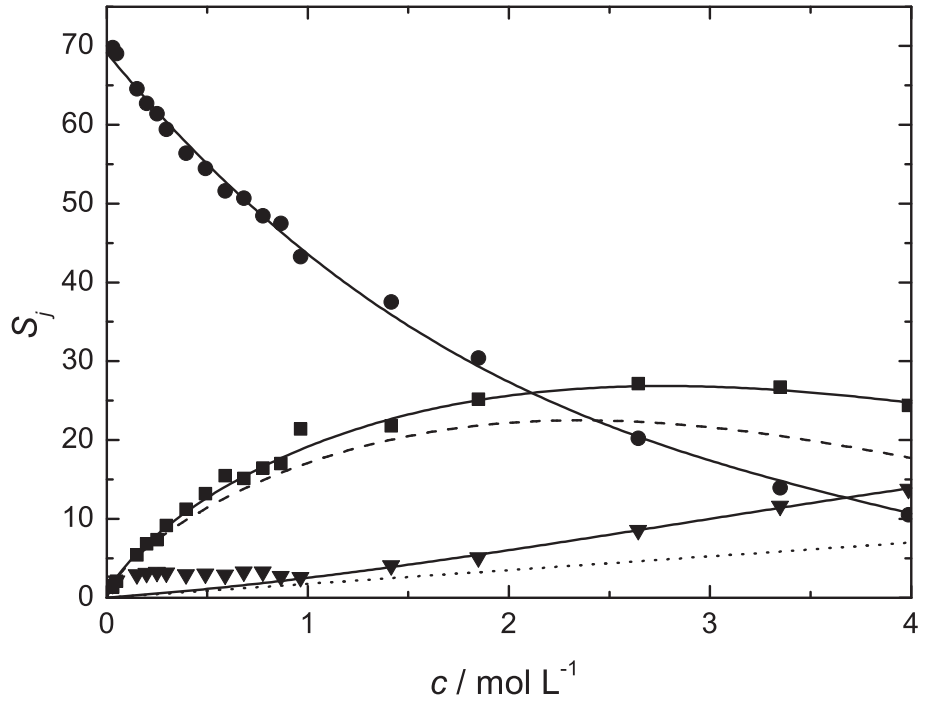

Figure 4.4: Amplitudes of the three Debye relaxation modes for K_2HPO_4(aq) as a function of solute concentration at 25 °C : bulk water (●), slow water + anion (■) and ion pairs (▼). Lines are visual guides only. Broken lines represent a deconvolution of S_2 into slow water (dashed line) and HPO_4^{2-} rotation (dotted line) contributions.

Table 4.4: Concentration Dependence of the Dielectric Relaxation Parameters of a Three-Debye Fit of Aqueous Solutions of K_3PO_4 at 25 °C: Concentration, c, Limiting Permittivities, ε_j ($j = 1-3$) & ε_∞, Relaxation Times, τ_j, VNA Conductivities, κ_{VNA}, and the Value of the Reduced Error Function, χ^2_{r}.[a,b]

c	ε_1	τ_1	ε_2	τ_2	ε_3	τ_3	ε_∞	κ_{VNA}	χ^2_{r}
0.0250	79.71	246	77.67	16.5F	77.21	8.30	5.79	0.817	0.0326
0.0500	80.04	181	76.65	16.5F	75.63	8.22	5.82	1.470	0.0551
0.0749	80.67	164	76.25	16.5F	74.49	8.21	6.11	2.022	0.0882
0.0999	80.63	178	75.56	18.1	71.50	8.03	6.49	2.545	0.1387
0.1497	80.46	135	74.93	15.9	67.62	7.78	5.87	3.522	0.0765
0.1988	80.57	140	74.72	16.0F	64.26	7.67	6.17	4.424	0.0728
0.2489	79.54	127	73.79	17.1	63.75	7.60	6.16	5.294	0.1018
0.2985	78.82	148	73.32	17.8	60.68	7.29	6.11	6.144	0.1109
0.3476	78.40	130	73.13	18.3	61.11	7.48	6.51	6.906	0.1319
0.3985	78.25	155	72.99	16.8	56.21	7.23	6.71	7.650	0.1465
0.5920	75.36	195	71.11	17.9	52.30	7.05	7.09	10.32	0.1677
0.7826	72.16	196	69.05	16.7	47.59	6.9F	7.78	12.61	0.1954
0.9730	70.17	251	67.10	15.8	41.27	6.5F	8.04	14.55	0.2977
0.9727	69.77	192	66.41	16.6	41.06	6.05	6.96	14.63	0.1924
1.4291	63.45	342	61.96	15.5	31.94	5.69	8.40	17.77	0.2277
1.8623	59.35	323	57.48	15.4	25.36	5.0F	9.23	18.93	0.2232
2.2681	54.27	333	53.72	16.0	21.00	4.12	9.14	18.85	0.2179
2.6507	50.48	–	50.48	17.3	19.29	3.88	9.64	17.93	0.1857
3.0119	47.48		47.48	18.8	17.82	3.56	10.09	16.03	0.1700

[a] Units: c in $\mathrm{mol\,L^{-1}}$, τ_j in ps, κ_{VNA} in $\mathrm{S\,m^{-1}}$; [b] Parameter values followed by the letter F were not adjusted in the fitting procedure.

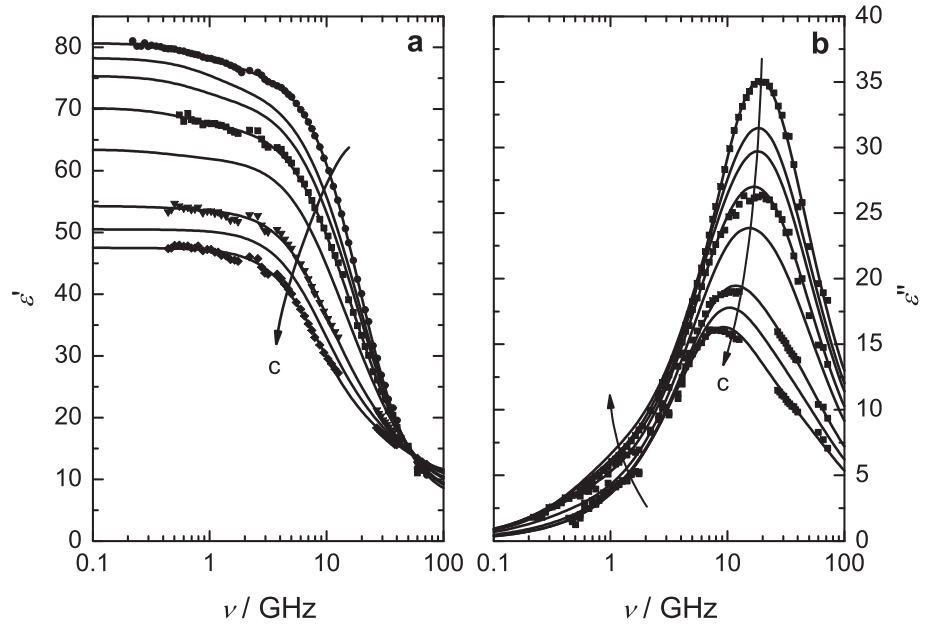

Figure 4.5: Spectra of relative permittivity (a) and dielectric loss (b) for K_3PO_4(aq) at 25 °C and concentrations $c\,/\,(\mathrm{mol\ L^{-1}}) = 0.0749$, 0.399, 0.592, 0.973, 1.43, 2.27, 2.66 and 3.01 (top to bottom). Symbols show typical experimental data.

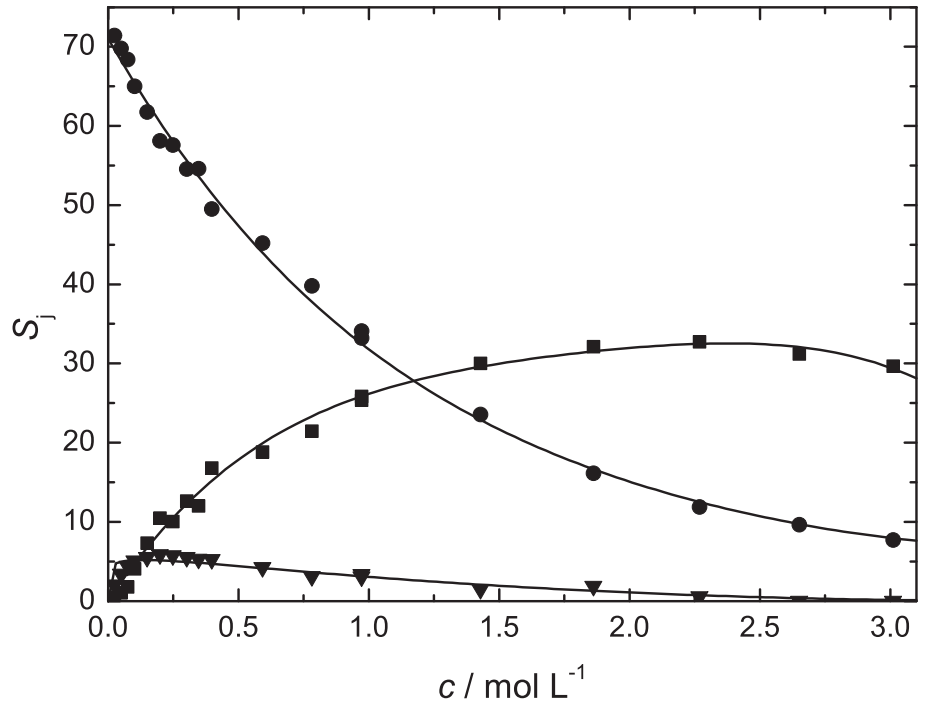

Figure 4.6: Concentration dependent amplitudes of the three Debye type relaxation modes as found in K_3PO_4(aq) at 25 °C . The relaxations are attributed to bulk water (●), slow water + anion (■) and ion pairs (▼). Lines represent empirical fits of the experimental values.

4.3 Hydration

For aqueous solutions, the hydration of a solute is one of its most important parameters. The interaction between water molecules and the solute not only determines its solubility, but also largely governs its reactivity as well as determining the physical characteristics of the solution. Despite the importance of the level of hydration of solutes, there is no general agreement about how it should be quantified. This is commonly done by determining the hydration number of the solute. However, as is well known, different techniques monitor different properties of solutions and therefore produce hydration numbers that differ markedly from each other.[6,107,138,139] DRS is particularly sensitive to hydration effects and has been able to provide a coherent picture of ionic hydration. DRS can differentiate, on the basis of their dynamic characteristics, two distinct types of hydration, which are quantified by two effective hydration numbers, Z_{ib} and Z_{slow}.[18,102] The former is the number of irrotationaly bound (ib) water molecules per unit of solute. The characterization as ib water stems from the fact, that such water molecules effectively disappear from the dielectric spectrum, as they are frozen on the DRS timescale and thus are no longer able to rotate in the external electric field.
The slow-water effective hydration numbers, Z_{slow}, for the present solutions were determined as follows. The composite, intermediate-frequency mode was split into its slow water and anion rotation contributions by deriving the free anion concentration, c_-, from the ion pairing results (see sec. 4.4): $c_- = c - c_{\mathrm{IP}}$, where c_{IP} is the total concentration of ion pairs in solution. The values of c_- were then translated into a relaxation amplitude, S_-, via Eq. 1.47.
The effective anion dipole moments have been calculated with MOPAC2009, giving values of 5.9 D for $H_2PO_4^-$ and 4.4 D for HPO_4^{2-}, whereby the anion was placed in a dielectric continuum with $\varepsilon = 78$. The symmetric PO_4^{3-} does not have a permanent dipole moment.[93,96] The slow water amplitude, S_{sw}, was obtained from the observed composite amplitude S_2 as: $S_{\mathrm{sw}} = S_2 - S_-$ and subsequently converted to the DRS detected slow water concentration, c_{sw}, with the help of Eq. 3.7.[126] Values of Z_{slow} were calculated as:

$$Z_{\mathrm{slow}} = \frac{c_{\mathrm{sw}}}{c} \tag{4.1}$$

The level of ib water was calculated as described in Section 3.4, with the difference that the total water amplitude, S_{w}, also contains a slow water amplitude:

$$S_{\mathrm{w}} = S_{\mathrm{b}} + S_{\mathrm{sw}} \tag{4.2}$$

Note, that as the fast water mode at $\sim 500\,\mathrm{GHz}$[62] is not resolved, the present ε_∞ are too large (see Tables 4.2–4.3–4.4). Thus, for the evaluation of the relaxation strength of bulk water, $S_b = \varepsilon_3 - \varepsilon_\infty$ the infinite frequency permittivity of pure water, $\varepsilon_\infty(0) = 3.48$, obtained from $\hat{\varepsilon}(\nu)$ extending to the far-infrared region,[78] was used. Kinetic depolarization, $\Delta\varepsilon_{\mathrm{kd}}$, was treated as described in Section 3.4. The final value for the total water amplitude

$$S_{\mathrm{w}}^{\mathrm{eq}} = S_{\mathrm{w}} + S_{\mathrm{sw}} + \Delta\varepsilon_{\mathrm{kd}} \tag{4.3}$$

was converted to the total DR resolved water concentration, $c_{\mathrm{H_2O,DRS}}$, via Eq. 3.7.

4.3.1 KH_2PO_4 & K_2HPO_4

As KH_2PO_4(aq) and K_2HPO_4(aq) show negligible hydrolysis ($< 5\%$) at all studied concentrations, Z_{ib} and Z_{slow} can be evaluated as outlined above. Figure 4.7 shows the resulting concentration-dependent effective hydration numbers for the two salts. $Z_{\mathrm{ib}}(KH_2PO_4)$ reaches physically meaningless negative values at concentrations $c \leq 0.5\,\mathrm{mol\,L^{-1}}$. This behavior most likely tracks back to the potassium ion, as previous DRS studies on KCl(aq) and KOH(aq) gave negative values for Z_{ib},[27,140] similar to $Z_{\mathrm{ib}}(KH_2PO_4)$. A possible explanation is, that *sub-slip* boundary conditions for the calculation of the kinetic depolarization of K^+(aq) should be applied, similar to Cs^+(aq).[141] $Z_{\mathrm{ib}}(K_2HPO_4)$ shows systematic increasing values for $c \leq 0.3\,\mathrm{mol\,L^{-1}}$. A linear fit yields an infinite dilution limit of $Z^\circ_{\mathrm{ib}}(K_2HPO_4) = Z^\circ_{\mathrm{ib}}({HPO_4}^{2-}) = 4.4 \pm 0.6$. Values of Z_{slow} were fitted with a simple exponential Eq. 3.8, where $A = 10.5 \pm 0.8$, $B = 10.2 \pm 1.8$ and $C = 0.3 \pm 0.1$ for KH_2PO_4(aq) and $A = 4.2 \pm 0.9$, $B = 24.6 \pm 1.0$ and $C = 0.9 \pm 0.1$ for K_2HPO_4(aq).

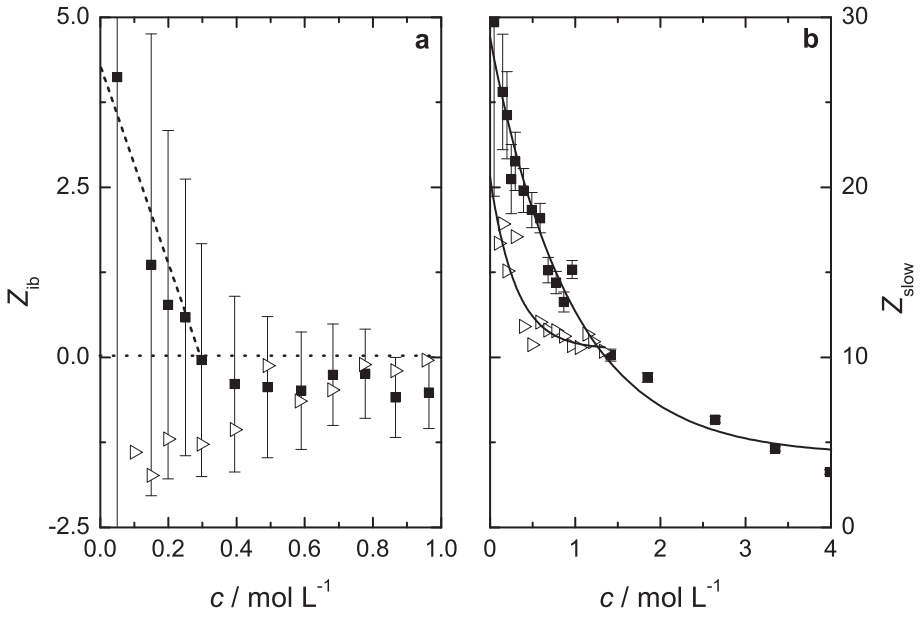

Figure 4.7: (a) Number of ib (Z_{ib}) and (b) number of slow water molecules (Z_{slow}) per unit of solute for KH_2PO_4(aq) (▷) and K_2HPO_4(aq) (■). Solid and broken lines lines correspond to empirical fits. Error bars, $\Delta Z_{\mathrm{ib}}(K_2HPO_4) = \Delta Z_{\mathrm{slow}}(K_2HPO_4)$, were estimated from the standard deviation, σ_{fit}, of the fit of the combined water related amplitudes, $S^{\mathrm{eq}}_{\mathrm{w}}$, according to $S^{\mathrm{eq}}_{\mathrm{w}} = 75.69 + a_1 \cdot c + a_2 \cdot c^{3/2} + a_3 \cdot c^2$.

At infinite dilution ionic additivity would be expected to apply and so values for the phosphate anions were obtained by subtracting the estimated values for K^+(aq)[27,29] from the calculated values for the whole salt.

$$Z^\circ_{\mathrm{slow}}({H_nPO_4}^{(3-n)-}) = Z^\circ_{\mathrm{slow}}(K_{3-n}H_nPO_4) - (3-n)Z^\circ_{\mathrm{slow}}(K^+) \tag{4.4}$$

A comparison of DRS studies on RbF(aq)[29] and KF(aq)[142] shows that $Z^\circ_{\mathrm{slow}}(K^+) \approx 9$; however $Z^\circ_{\mathrm{ib}}(K^+) = 0$.[27] The additivity of Z°_{ib} values, i.e. the meaningful existence of Z°_{ib}(ion)

values, is well established.[18] Too few systems have been studied to prove the additivity of Z°_{slow} values,[30,102,143] but it is reasonable to infer they are. Table 4.6 lists the obtained Z°_{ib} and Z°_{slow} values for $H_2PO_4^-$ and HPO_4^{2-} together with the total effective hydration number $Z^{\circ}_{\text{total}} = Z^{\circ}_{\text{ib}} + Z^{\circ}_{\text{slow}}$. At finite solute concentrations $Z_{\text{ib}}(c)$ values also seem to maintain additivity to a reasonable degree, although some anomalies are known.[103] Additivity of $Z_{\text{slow}}(c)$ is less well established, and indeed departures might well be expected as c increases due to increasing solvation shell overlap. Application of Eq. 4.4 to finite concentrations yields a non-monotonic concentration dependence of Z_{slow} for both phosphate anions. This shows that for finite concentrations Z_{slow} values of ions are not necessarily additive.

4.3.2 K_3PO_4

Evaluation of the effective hydration numbers for K_3PO_4(aq) is not straightforward, as the phosphate ion undergoes considerable hydrolysis. The observed amplitude $S_2(K_3PO_4(aq))$ thus contains contributions from slow water (due to the presence of both, HPO_4^{2-} and PO_4^{3-}) and the rotational diffusion of HPO_4^{2-}. The speciation of each K_3PO_4(aq) sample was calculated from the measured pH via the appropriate mass balance equations: only the formation of HPO_4^{2-} was found to be important, assuming a dissociation constant of $pK_a(HPO_4^{2-}) = 12.32$.[144] Table 4.5 lists the analytical K_3PO_4 concentration, the measured pH value, and the calculated concentrations of HPO_4^{2-}(aq) and PO_4^{3-}(aq) for each sample. The contribution to $S_2(K_3PO_4(aq))$ arising from the presence of HPO_4^{2-} was determined by an interpolation of $S_2(K_2HPO_4(aq))$ to the appropriate concentration. The amplitude solely due to the presence of K_3PO_4(aq) is then obtained as:

$$S_2(K_3PO_4(aq))_{\text{true}} = S_2(K_3PO_4(aq)) - S_2(K_2HPO_4(aq)) \tag{4.5}$$

Original amplitude $S_2(K_3PO_4(aq))$ and extrapolated amplitude $S_2(K_3PO_4(aq))_{\text{true}}$ are shown in Figure 4.8.
As $\mu(PO_4^{3-}) = 0$, it follows, that $S_2(K_3PO_4(aq))_{\text{true}}$ can be attributed solely to slow water associated with PO_4^{3-}(aq) and K^+(aq). Therefore, $Z_{\text{slow}}(K_3PO_4(aq))$ was calculated from $S_2(K_3PO_4(aq))_{\text{true}}$ via Eqs. 3.7 & 4.1 (Figure 4.9a) and fitted with a simple exponential $Z_{\text{slow}} = A + B \cdot \exp(-c/C)$ where $A = 7.8 \pm 2.4$, $B = 27.2 \pm 3.8$ and $C = 0.8 \pm 0.3$. The single ion Z_{slow} due to PO_4^{3-}(aq) was then evaluated with Eq. 4.4.
Z_{ib} values were determined analogously. The concentration of ib water molecules due to HPO_4^{2-} is given by $c_{\text{ib},HPO_4^{2-}} = Z_{\text{ib}}(HPO_4^{2-}) \times c(HPO_4^{2-})$. Thus $Z_{\text{ib}}(K_3PO_4) = Z_{\text{ib}}(PO_4^{3-})$ was obtained by

$$Z_{\text{ib}}(PO_4^{3-}) = \frac{c_{\text{w}} - c_{\text{w}}^{\text{app}} - [Z_{\text{ib}}(HPO_4^{2-}) \times c(HPO_4^{2-})]}{c_{PO_4^{3-}}} \tag{4.6}$$

The resulting $Z_{\text{ib}}(c)$ and $Z_{\text{slow}}(c)$ values are displayed in Figure 4.9 and single ion values for $c \to 0$ are summarized in Table 4.6.

Table 4.5: Concentrations, c, and pH Values of the K_3PO_4(aq) Solutions. Phosphate Speciation is Calculated by Considering the First Hydrolysis Step Only.[a]

$c(K_3PO_4)$	pH	$c(PO_4^{3-})$	$c(HPO_4^{2-})$
0.02499	11.69	$4.702 \cdot 10^{-3}$	0.02029
0.04997	12.04	0.01707	0.03290
0.07493	12.17	0.03084	0.04408
0.1015	12.19	0.04290	0.05855
0.1497	12.37	0.07870	0.07095
0.1988	12.50	0.1191	0.07962
0.2489	12.49	0.1478	0.1011
0.3016	12.41	0.1655	0.1361
0.3476	12.63	0.2324	0.1152
0.3985	12.64	0.2685	0.1300
0.5920	12.77	0.4357	0.1564
0.7826	12.66	0.5351	0.2474
0.9730	12.96	0.7899	0.1831
0.9738	12.74	0.7033	0.2705
1.429	13.23	1.271	0.1582
1.862	13.41	1.721	0.1415
2.268	13.65	2.166	0.1025
2.651	13.76	2.557	0.09391
3.012	13.93	2.939	0.07298

[a]Units: c, in $\mathrm{mol\,L^{-1}}$.

4.3.3 General Features of Phosphate Hydration

The results for the total effective hydration numbers, Z°_{total} (Table 4.6) indicate that more than one hydration shell is established around HPO_4^{2-} and PO_4^{3-}, however do not provide information on how the water molecules are distributed over the solvation shells.

Table 4.6: Effective Hydration Numbers, Z°_{ib}, Z°_{slow} and Z°_{t}, for Phosphate Anions at Infinite Dilution and 25 °C.

	$H_2PO_4^-$	HPO_4^{2-}	PO_4^{3-}
Z°_{ib}	0	4.4	14.8
Z°_{slow}	11.4	10.4	7.3
Z°_{t}	11.4	14.8	22.1

The interaction of orthophosphate (PO_4^{3-}) anions with water mainly occurs via H-bonding, with a maximum of up to 12 H-bonds (assuming conventional Lewis electron arrangement). The maximum number of water molecules that can fit around the phosphate anions based

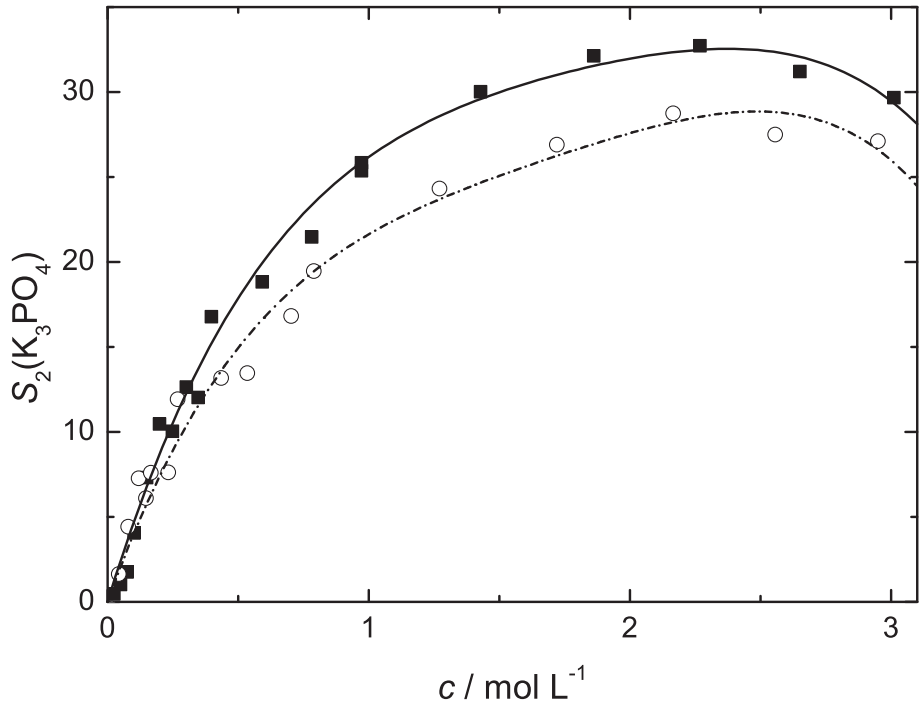

Figure 4.8: Comparison of the amplitudes $S_2(K_3PO_4(aq))$ (■) as obtained by a 3-Debye fit of the DR spectra of $K_3PO_4(aq)$ solutions and the same amplitude after subtraction of contributions due to HPO_4^{2-} and associated slow water: $S_2(K_3PO_4(aq))_{true}$ (○). Data points $S_2(K_3PO_4(aq))$ are relative to $c(K_3PO_4)$, extracted amplitudes for PO_4^{3-} are relative to the pH-dependent PO_4^{3-} concentration. Lines are visual guides only.

on geometrical considerations alone is unclear as the exact radii of the different phosphate species remain elusive.[145] The radius of the symmetrical PO_4^{3-} at 238 pm seems straightforward,[107] although it is a thermochemical value and therefore rather less well-defined than one determined from structural information. The common values of 200 pm given by Marcus[107] for $H_2PO_4^-$ **and** HPO_4^{2-} seem somewhat unrealistic, as one would expect an increasing radius with increasing negative charge. Semiempirical calculations of the maximum van der Waals radius reveal a different picture of decreasing radius with increasing charge (Table 4.7).[93,96]

Table 4.7: Radii of the Three Inorganic Phosphate Anions in pm as Given by Marcus (r_{ion})[107] and Maximum vdW Radius Calculated with Winmostar ($r_{v.d.W}$)[93,96] .

	r_{ion}	$r_{v.d.W}$
$H_2PO_4^-$	200	340
HPO_4^{2-}	200	339
PO_4^{3-}	238	309

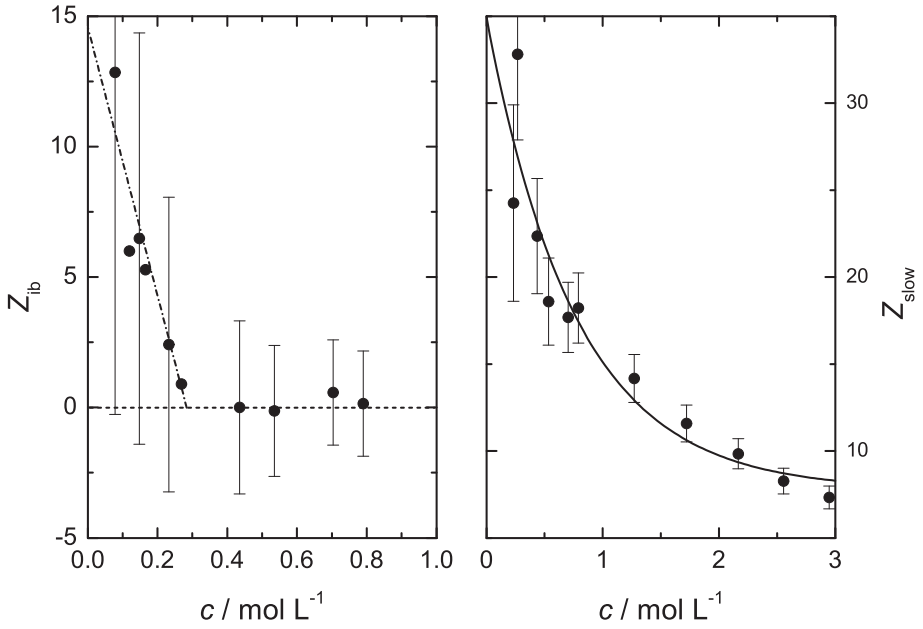

Figure 4.9: (a) Number of irrotationaly bound (Z_{ib}) and (b) number of slow water molecules (Z_{slow}) per unit of solute for K_3PO_4 (●). Solid and broken lines correspond to empirical fits. Error bars, $\Delta Z_{\mathrm{ib}}(K_2HPO_4) = \Delta Z_{\mathrm{slow}}(K_2HPO_4)$, were estimated from the standard deviation, σ_{fit}, of the fit of the combined water related amplitudes, S_{w}, according to $S_{\mathrm{w}} = 75.69 + a_1 \cdot c + a_2 \cdot c^{3/2} + a_3 \cdot c^2$.

Obviously, even though the P–O bond length is well known (and is in good agreement with the MOPAC calculation),[146–149] the definition of a reasonable radius for the orthophosphate anion is a non-trivial task. The same is true for the other two inorganic phosphate anions. As an increasing radius with increasing charge seems reasonable, even though hydrogens are stripped off in the same direction, one could speculate that the first hydration shell of PO_4^{3-} is able to accommodate more water molecules than the one of $H_2PO_4^-$ and HPO_4^{2-} which seem to be of comparable size. However, for this work a different, chemically more intuitive way is chosen. On the basis of the available sites (free electron pairs), ignoring steric and charge effects and possible bonding of water molecules to the bound protons, the maximum number of bound (and thus nearest-neighbor) water molecules is: 12 (PO_4^{3-}), 11 (HPO_4^{2-}) and 10 ($H_2PO_4^-$). If the bound protons are also taken into account, each phosphate anion is able to establish a maximum of 12 H-bonds at any given time. Therefore, the maximum number of water molecules in the first hydration shell is assumed to be 12, which forms the basis for the following discussion of the hydration pattern of the three inorganic phosphate anions. Only the infinite dilution hydration numbers, Z°_{ib} & Z°_{slow}, are taken into account, as at finite concentrations additional complications (solvation shell overlap) arise.

$H_2PO_4^-$ is able to slow down 11-12 water molecules, with no frozen water. This corresponds to the maximum number of water molecules in the first hydration shell of $H_2PO_4^-$. Those water molecules are H-bonded to the $H_2PO_4^-$ sufficiently strongly to slow down their rotational dynamics, but not so strongly as to produce ib water. This is consistent

with previous DR-results on other monovalent anions.[18,28] The higher charge density of HPO_4^{2-}, and consequently the strength of H-bonding, produces 4-5 ib water molecules in the first hydration shell. The remaining 7-8 water molecules in the first hydration shell and additional ∼3 water molecules of the second hydration shell are slowed down. Thus, HPO_4^{2-} exhibits a weak but definite second hydration shell. The higher formal charge density in PO_4^{3-} eventually is enough to produce ∼ 15 ib water molecules. Given the probable electronic and steric limitations (see above), only 12 of these ib water molecules will reside in the first hydration shell. This indicates that PO_4^{3-} must also have a well developed second hydration shell containing (on average) ∼3 ib and ∼7 slow water molecules.

The identification of slow water molecules in aqueous solutions does not mean that they have fixed characteristics. Indeed, as argued previously,[18] it is probable, that the dynamics of such molecules lie on a continuum. For example, in the present context, it is reasonable to assume slower dynamics for water molecules in the first hydration shell than in the second, but also slower dynamics around more highly charged ions. The present results indicate, that the dynamics of slow water molecules are mainly governed by the occupied solvation shell and less by the charge of the anion: the observed trend in τ_2 (see Section 4.5) shows a decrease from ∼ 23 ps (KH_2PO_4) over ∼ 21 ps (K_2HPO_4) and eventually ∼17 ps for K_3PO_4. However, it should be remembered that there will be an anion contribution (for $H_2PO_4^-$ and HPO_4^{2-}) to this effect.

The present findings on the hydration of phosphate ions are broadly consistent with recent literature data. A neutron diffraction study using isotope substitution on solutions of the three aqueous potassium phosphate salts,[33] was able to determine the hydration number for PO_4^{3-} to be 15 ± 3 which is consistent with the present $Z_{ib}(PO_4^{3-})$. A molecular dynamics study suggested that the number of water molecules in the first hydration shell is ∼ 16 for PO_4^{3-}, but ∼20 for both $H_2PO_4^-$ and HPO_4^{2-}.[34] These values are well in excess of the available h-bonding sites on the anions, and are therefore rather implausible. In contrast, a recent more sophisticated Car-Parrinello DFT MD simulation indicated that the number of water molecules in the first hydration shell decreases from 11 for PO_4^{3-}, to 10.4 for HPO_4^{2-} and 9.4 for $H_2PO_4^-$. Furthermore, while $H_2PO_4^-$ appeared to have just one hydration shell, both HPO_4^{2-} and especially PO_4^{3-} also possessed second hydration shells. Also, this study indicated an increased flexibility of, i.e. fluctuating number of water molecules in, the first hydration shell in going from PO_4^{3-} to $H_2PO_4^-$. This is in accordance with the present study, suggesting a shift from ib to slow water molecules in the first hydration shell from PO_4^{3-} to $H_2PO_4^-$. A FTIR study found that the numbers of solute affected water molecules are 11.0, 13.8 and 16.2 for $H_2PO_4^-$, HPO_4^{2-} and PO_4^{3-} respectively.[132] Those results are in good quantitative agreement with the detected total hydration number, Z_t°, except for PO_4^{3-}. Other reported hydration numbers for PO_4^{3-} are 13 (*ab initio* quantum mechanical charge field MD),[150] 12 (NMR)[131] and 12-18 (Raman+DFT).[36]

Table 4.8 lists some of the 'absolute' (single ion) thermodynamic parameters for phosphate ion hydration. These data clearly indicate that the level of hydration increases significantly from $H_2PO_4^-$ to HPO_4^{2-} to PO_4^{3-}. This trend is qualitatively reproduced in an excellent way by our proposed hydration structure, as it is well known, that the thermodynamic parameters for hydration largely reflect interactions between the ion and the first few surrounding layers of water. A simple deduction of $\Delta_{hyd}H$ and $\Delta_{hyd}S$ for frozen and slowed

Table 4.8: Hydration Enthalpies, $\Delta_{\mathrm{hyd}}H^\circ$, Entropies, $\Delta_{\mathrm{hyd}}S^\circ$, and Gibbs Energies, $\Delta_{\mathrm{hyd}}G^\circ$, for Phosphate Anions.[107] Values Correspond to the Change of the Thermodynamic Values upon Transfer of Isolated Ions from Ideal Gas Phase to Infinite Dilution in Water.

	$\Delta_{\mathrm{hyd}}H^\circ$ / J mol^{-1}	$\Delta_{\mathrm{hyd}}S^\circ$ / J mol^{-1} K^{-1}	$\Delta_{\mathrm{hyd}}G^\circ$ / J mol^{-1}
$H_2PO_4^-$	-522	-166	-473
HPO_4^{2-}	-1170[a]	-272	-1089
PO_4^{3-}	-2879	-421	-2753[b]

[a] Value has been recalculated from $\Delta_{\mathrm{hyd}}S^\circ(HPO_4^{2-})$ and $\Delta_{\mathrm{hyd}}G^\circ(HPO_4^{2-})$. [b] Value has been recalculated from $\Delta_{\mathrm{hyd}}H^\circ(PO_4^{3-})$ and $\Delta_{\mathrm{hyd}}S^\circ(PO_4^{3-})$.

down water molecules is not possible as those numbers are different for each added water molecule and of course critically depend on the charge of the anion. However it is clear, that the entropy and enthalpy of hydration depend on the solvation layer and on the type of hydration (frozen or slowed down water molecules).

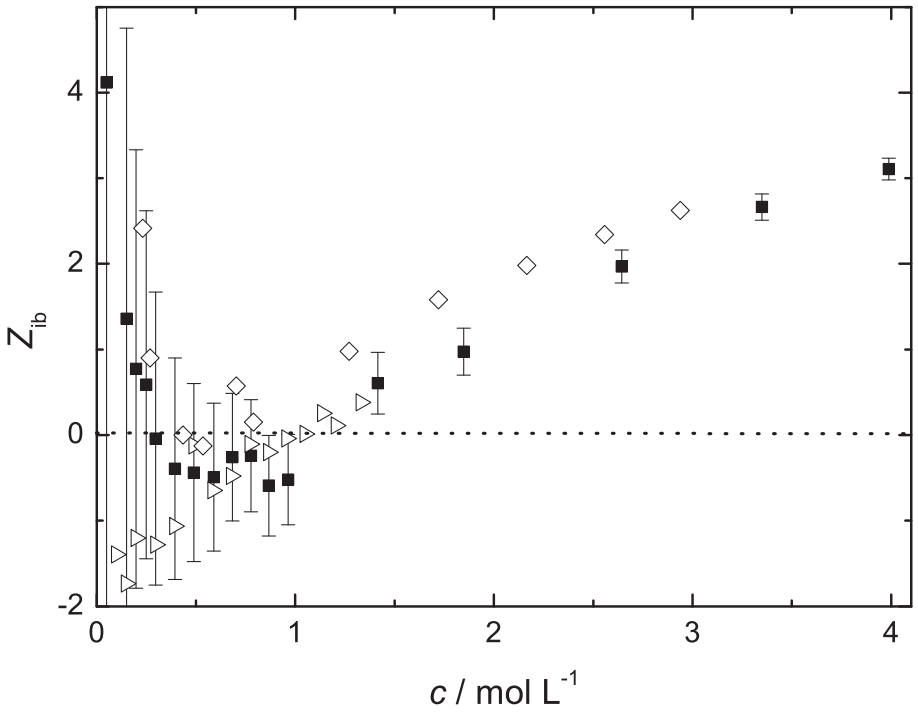

Figure 4.10: Concentration dependent Z_{ib} values of KH_2PO_4(aq) (▷), K_2HPO_4(aq) (■) and K_3PO_4(aq) (◇) for the full investigated concentration range. Error bars are only displayed for K_2HPO_4(aq) for visual clarity.

The increase in Z_{ib} with increasing c (Figure 4.10) for all three salts, is a non-common feature of simple inorganic salt solutions: those typically show a steady decrease in Z_{ib} with

concentration, which is attributed to solvation shell overlap.[27,31,103,151,152] Different from those studies, for the investigated phosphate solutions $Z_{\mathrm{ib}} = 0$ for $\sim 0.3 \leq c\,/\,\mathrm{mol L^{-1}} \leq\sim$ 1.3. Thus, at higher concentrations increasing Z_{ib} may be rationalized as water molecules that are under the influence of an increasing number of ions. Water, that has already been classified as slow, may be further slowed down and eventually disappear from the dielectric spectrum. On the other hand, the increasing Z_{ib} may also be connected to the extensive amount of ion pairing (see Section 4.4). However, recent studies on sodium carboxylate salts showed a similar trend for Z_{ib}.[16,30,143] As only marginally ion pairing was found for several of the investigated carboxylate salts, it is rather unlikely that ion association is responsible for the increasing Z_{ib}. It implies, on the other hand, that this behavior may be specific to oxyanions. Further studies on the hydration of oxyanions might thus be worthwhile.

4.4 Ion Pairing

4.4.1 General Remarks

Though ion pairing is a ubiquitous phenomenon in electrolyte solutions, quantification of the extent of weak ion pairing is a non-trivial task.[21] This problem is in part related to the different types of ion pairs that may form. Depending on the charge and degree of hydration of the ions involved, up to three distinct types of ion pairs may be detectable: double solvent-separated ion pairs (2SIPs) where the (first) hydration shells of both the anion and cation within the ion pair are essentially intact, solvent-shared ion pairs (SIPs) where both ions share one or more appropriately oriented water molecule(s) and also a more-or-less common hydration shell, and contact ion pairs (CIPs), where the cation and anion are in direct contact, while again sharing a common hydration shell.[153] The presence of solvent-separated ion pairs (2SIPs and SIPs) creates difficulties because the common techniques used to quantify ion association detect only CIPs (most spectroscopic techniques) or only the overall association (without distinction between the ion-pair types: all thermodynamic techniques and conductivity).[23] DRS is one of the few techniques that can distinguish and quantify all three ion pair types.[126] This is because the different ion-pair types differ in size (and thus relaxation time) and in their permanent dipole moment, μ. As the amplitude of a DR mode $S_j \propto \mu_j^2$, DRS has a unique sensitivity towards 2SIPs and SIPs, which are especially difficult to quantify by most other techniques.[24]

As already mentioned, the lowest frequency mode for all three sets of phosphate solutions, is a composite of ion-pair reorientation and ion-cloud relaxation (the IP + IC mode). For moderate and strong ion association ($K_{\mathrm{A}}^{\circ} \geq 10$) the ion cloud contribution is probably unimportant, because its amplitude is thought to be small.[32,137] For weakly associated salts ($K_{\mathrm{A}}^{\circ} < 10$), however, S_{IC} may be a significant proportion of the observed amplitude. Unfortunately, it is not at present possible to calculate S_{IC} theoretically, nor can it be measured separately. All that can be done in such circumstances is to derive an upper limit for the equilibrium constant.

The overall ion association constants, $K_{\mathrm{A}}(c)$, were calculated at each solute concentration via Eq. 1.72. Assuming the formation of 1:1 species only, concentrations of cations, c_+, and

anions, c_-, can be easily obtained from the analytical salt concentration, c, and the DRS detected c_{IP}. The association constants $K_A(c)$ for the three potassium phosphate salts are then calculated by:

$$K_A\left(c(\mathrm{K_{3-n}H_nPO_4})\right) = \frac{c_{\mathrm{IP}}}{(c - c_{\mathrm{IP}})((3-n)\cdot c - c_{\mathrm{IP}})} \tag{4.7}$$

The relationship between ion-pair amplitudes and concentrations is given by Eq. 1.47. Following Barthel *et al.*,[53] the bare (vacuum) ion-pair dipole moments, μ_{IP}, were calculated for CIP, SIP and 2SIP models of $KH_2PO_4{}^0$, $KHPO_4{}^-$ and $KPO_4{}^{2-}$. The effective dipole-moment, $\mu_{\mathrm{eff,IP}} = \mu_{\mathrm{IP}}/(1 - f_{\mathrm{IP}}\alpha_{\mathrm{IP}})$, accounts for the effect of induced moments on μ_{IP} through the polarizability, α_{IP}, and the corresponding reaction-field factor, f_{IP}.[51] Polarizabilities were taken to be 1.44 Å^3 for water,[154] 1.07 Å^3 for K^+, 5.79 Å^3 for $H_2PO_4{}^-$ and 5.99 Å^3 for $PO_4{}^{3-}$.[107] The polarizability of $HPO_4{}^{2-}$ (5.89 Å^3) was estimated to be in between the values for $H_2PO_4{}^-$ and $PO_4{}^{3-}$. For the charged IPs, $KHPO_4{}^-$ and $KPO_4{}^{2-}$, also the distinction between center of mass, o_{CM}, and center of hydrodynamic stress, o_{CHS} (used in this work), for the pivot of the dipole rotation had to be taken into account for the calculation of μ_{IP} (see Section 1.7).[53]
Standard-state (infinite dilution) association constants, K_{A}°, were obtained by fitting the $K_A(c)$ values via Eq. 1.74.

4.4.2 KH_2PO_4

The combined IP + IC mode of amplitude S_1 is depicted in Figure 4.11 for solutions of all three potassium phosphate salts. Also included in Figure 4.11 are the amplitudes of the low-frequency mode observed in NaCl(aq). If it is assumed that NaCl(aq) is fully dissociated, then the observed amplitude can be attributed entirely to ion-cloud relaxation. Strictly speaking this assumption can just be applied to 1:1 electrolytes (see Section 3). However, due to the lack of corresponding reference systems for 1:2 and 1:3 electrolytes, NaCl(aq) is also used as a reference for K_2HPO_4 and K_3PO_4.
On this basis it is obvious, that the possible ion-cloud relaxation contribution to S_1 is significant ($\geq 50\%$ up to $c \approx 0.2\,\mathrm{mol\,L^{-1}}$) for KH_2PO_4(aq) but somewhat lower for K_2HPO_4(aq) & K_3PO_4(aq). At higher concentrations S_1 mostly stems from ion-pair reorientation. As the determination of K_{A}° via Eq. 1.74 is sensitive to the high dilution region, only $K_A(c \geq 0.393\,\mathrm{mol\,L^{-1}})$ values were used in the fitting procedure. The results for the three possible types of ion pairs are summarized in Table 4.9. Assuming solely the formation of 2SIPs gives $K_{\mathrm{A}}^{\circ} = (2.0 \pm 0.2)\,\mathrm{L\,mol^{-1}}$, which is in qualitative agreement with the value reported by Pethybridge *et al.* $K_{\mathrm{A}}^{\circ}(KH_2PO_4{}^0) = 2.0\,\mathrm{L\,mol^{-1}}$ from high quality conductivity measurements.[155] This level of agreement is almost certainly fortuitous because of the number of assumptions involved in deriving the K_A values using both techniques. It must also be recalled, that neither K^+ nor $H_2PO_4{}^-$ are strongly hydrated, which argues against, but does not disprove, formation of 2SIPs. The value of $K_{\mathrm{A}}^{\circ}(KH_2PO_4{}^0) = (4.9 \pm 0.4)\,\mathrm{L\,mol^{-1}}$ calculated by assuming only formation of SIPs is still in reasonable agreement with the conductivity result, given that the DRS result is an upper limit because of the unknown ion-cloud contribution.

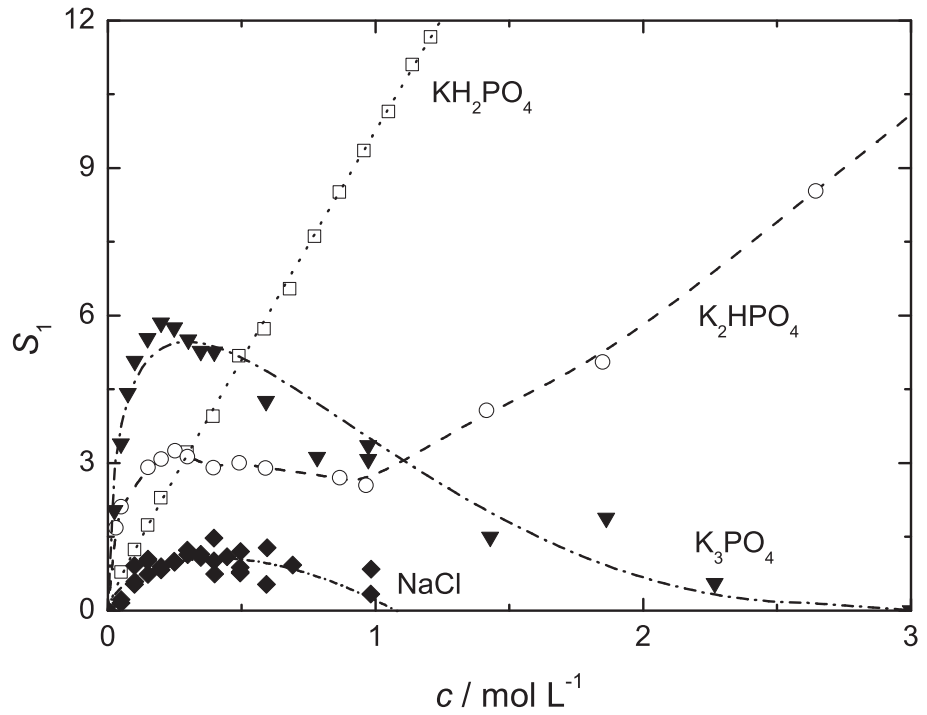

Figure 4.11: Amplitudes S_1 of the lowest-frequency DR modes in aqueous solutions of the three potassium phosphates and NaCl as function of solute concentration, c, at 25 °C . Note that $S_1(K_3PO_4(aq))$ contains contributions from $KHPO_4^-$ and KPO_4^{2-} ion pairs.

4.4.3 K_2HPO_4

The variation of $S_1(K_2HPO_4)$ with solute concentration (Figure 4.11) is strange: a strong increase until $c \approx 0.2\,\mathrm{mol\,L^{-1}}$, followed by a moderate decrease up to $c \leq 1.0\,\mathrm{mol\,L^{-1}}$ and eventually a steady increase at $c > 1.0\,\mathrm{mol\,L^{-1}}$. This surprising variation can however be accounted for by the simultaneous existence and subsequent predominance of two different types of ion pairs, according to the model of stepwise ion association by Eigen and Tamm.[68,69] Reasonable combinations of ion pairs are SIP & CIP and 2SIP & SIP. The trend of the relaxation time, τ_1, suggests, that at high concentration SIPs are the dominating species, in accordance with the result for $KH_2PO_4(aq)$. As it is reasonable to assume, that at higher concentration ion pairs with less intervening water molecules are formed, the predominating ion pair species at low concentrations must be 2SIPs, together with a contribution from ion-cloud relaxation. At $c \leq 0.964\,\mathrm{mol\,L^{-1}}$ 2SIPs are dominant (ignoring the ion-cloud contribution), whereas at $c > 1$ mol L^{-1} SIPs are assumed to be the only type of ion pair. This assumption provided a basis for splitting the two ion-pair contributions, which is described in detail below. Figure 4.12 shows the splitting of the amplitude S_1 into contributions $S(2\mathrm{SIP} + \mathrm{IC})$ and $S(\mathrm{SIP})$.

Amplitudes $S(2\mathrm{SIP} + \mathrm{IC})$ were used to calculate association constants $K_1(c)$, correspondingly $S(\mathrm{SIP})$ for the calculation of $K_2(c)$ via Eq. 4.7. Extrapolation of the $K_2(c)$ values obtained via Eq. 1.74 yielded $K_2^\circ(\mathrm{SIP\,KHPO_4^-}) = (0.26 \pm 0.05)$ L mol^{-1}, which is an upper limit due to ion-cloud contribution. Extrapolated values of $K_2(c)$ at $c <$

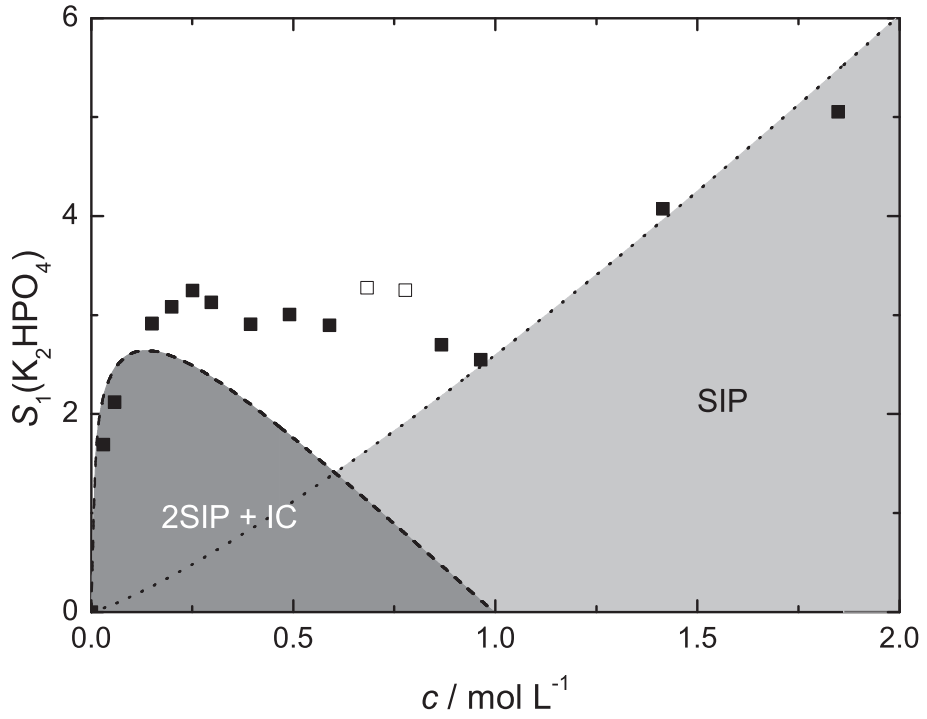

Figure 4.12: Deconvolution of the low frequency amplitude S_1 of K_2HPO_4(aq) into contributions from SIPs and 2SIP+IC. Data points (■) represent the experimental values, lines the extrapolated concentration behavior of the different ion pairs. Empty symbols (□) indicate outliers that were not considered for the splitting of S_1.

0.964 mol L^{-1} were then used to calculate c(SIP $KHPO_4^-$), which were subsequently transformed into values of S(SIP) via Eq. 1.47. Subtraction of these values from S_1, yielded $S(2\text{SIP} + \text{IC})$. As $S(2\text{SIP} + \text{IC}) \gg S_1(\text{NaCl})$ at low c (Figure 4.12), $S(2\text{SIP} + \text{IC}) \approx S(2\text{SIP})$. The amplitudes could then be converted to 2SIP concentrations and hence values of $K_1(2\text{SIP}\,KHPO_4^-)$ in a manner analogous to that described above. Extrapolation of these $K_1(c)$ values via Eq. 1.74 yielded $K_1^\circ(2\text{SIP}\,KHPO_4^-) = (18 \pm 3)$ L mol^{-1}.

The overall association constant $K_A^\circ(KHPO_4^-)$ was calculated via Eq. 4.7 and extrapolation via Eq. 1.74 yielded $K_A^\circ(KHPO_4^-) = (21 \pm 2)$ L mol^{-1}. A similar calculation of $K_A^\circ(KHPO_4^-)$ assuming the formation of SIP & CIP gave $K_A^\circ(KHPO_4^-) = 69 \pm 9$ L mol^{-1}. To our knowledge, the only available literature value, $K_A^\circ(KHPO_4^-) = 21.74$ L mol^{-1}, is again from the conductivity measurements on dilute solutions by Pethybridge *et al.*.[155] The excellent agreement with the $K_A^\circ(KHPO_4^-)$ value assuming 2SIP & SIP formation must be fortuitous to some extend, given the number of assumptions and long chain of calculations for the derivation of the DRS value. Nevertheless, it suggests that the assumption of negligible contribution of ion-cloud relaxation, the attribution of S_1 to 2SIP & SIP ion pairs and the splitting procedure of S_1 was reasonable.

4.4.4 K_3PO_4

In the case of K_3PO_4 the observed amplitude $S_1(K_3PO_4)(aq)$ first needs to be separated into contributions from $K_2HPO_4(aq)$ and $K_3PO_4(aq)$, using the respective concentrations of HPO_4^{2-} and PO_4^{3-} (Table 4.5). Note that KOH(aq), which must also be present from the hydrolysis reaction, would not be expected to make a significant contribution to the DR spectra in this region: a DRS study on aqueous KOH solutions for $c \leq 1$ molL^{-1} was performed additionally to the potassium phosphate solutions and the analysis of the obtained spectra showed no prominent ion pairing in the frequency range of the $S_1(K_3PO_4(aq))$ mode.[156] Values of $S_1(K_2HPO_4(aq))$ were interpolated empirically at $0 \leq c/\text{mol L}^{-1} \leq 0.3$ and subtracted from $S_1(K_3PO_4(aq)$. The difference was taken as the amplitude stemming only from KPO_4^{2-} ion pairs, $S(KPO_4^{2-})$ at the actual PO_4^{3-} concentrations (Figure 4.13). This procedure must be done with care because the results obtained depend on accurate pH determinations and more importantly, a precise determination and fit of the low frequency mode in K_2HPO_4.

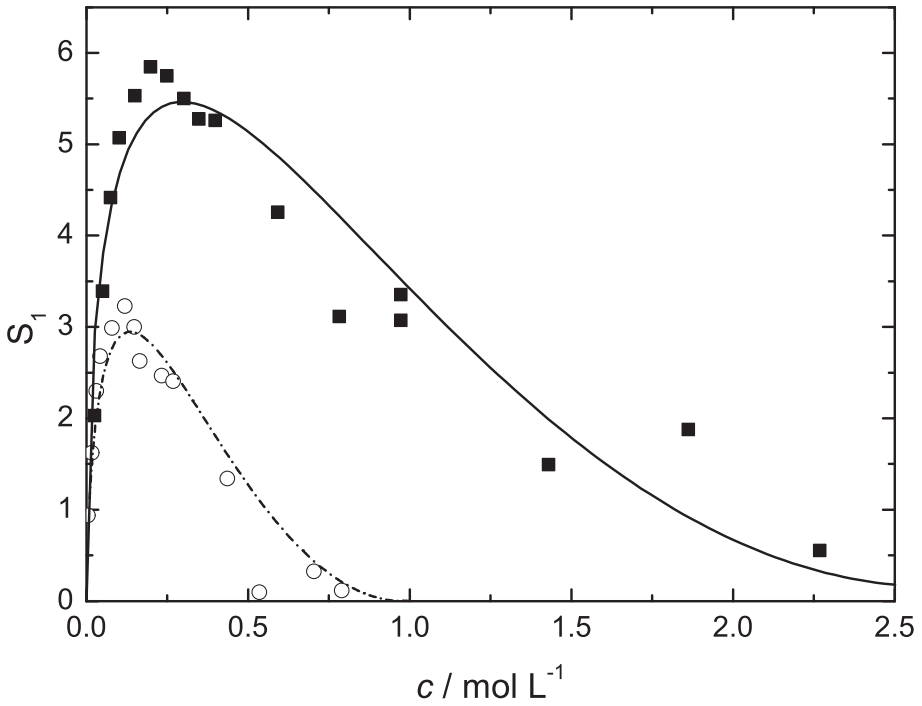

Figure 4.13: Comparison of the amplitudes $S_1(K_3PO_4(aq))$ (■) as obtained by a 3-Debye fit of the DR spectra of $K_3PO_4(aq)$ solutions and the same amplitude after substraction of contributions due to $KHPO_4^-$ ion pairs: $S(KPO_4^{2-})$(○). Data points for the neat salt are relative to $c(K_3PO_4)$, extracted amplitudes for PO_4^{3-} are relative to the pH-dependent PO_4^{3-} concentration (Table 4.5). Lines are visual guides only.

Assuming o_{CHS} boundary conditions and neglecting ion-cloud relaxation, $K_A(c)$ were calculated for different ion pair models and extrapolated to infinite dilution via Eq. 1.74 to yield $K_A^\circ(KPO_4^{2-})$ (Table 4.9). The high hydration of the orthophosphate, PO_4^{3-}, with ib water also in the second hydration shell, suggests that 2SIPs are the mainly formed ion

pair species. Also the considerably higher relaxation time, $\tau_1(c)$ as compared to KH_2PO_4 and K_2HPO_4 suggests to hypothesize that 2SIPs are the dominant ion pair type over the investigated concentration range. The corresponding standard state association constant was calculated to $K_A^\circ(KPO_4^{2-}) = 49 \pm 18\,\mathrm{L\,mol^{-1}}$. Also, Rudolph *et al.* inferred from Raman and infrared spectroscopic measurements the existence of SIPs and with further dilution the existence of 2SIPs, which are the only ion-pair species at low concentration.[36] However, no association constants are stated.

4.4.5 Features of ion association in potassium phosphates

As shown in the preceding section, the accuracy of the association constants for the various 1:1 ion-pair species derived from the DR spectra is not optimal. Nevertheless, the clear-cut presence of solute-related modes at low frequencies in the spectra for all three sets of solutions, coupled with the quantitative analysis presented above indicates that significant ion pairing occurs in solutions of all three potassium phosphate salts with overall standard state association constants (K_A° values) in the order $KH_2PO_4^0 < KHPO_4^- < KPO_4^{2-}$. The present K_A° values are in good agreement with literature results (where available) but markedly contrast with the assumptions of complete dissociation made in a number of previous publications.[33,132,157] Table 4.9 gives an overview of the standard state association constants of the detected types of ion pairs as found in aqueous potassium phosphate solutions, as well as the respective overall standard state association constant for the three salts.

Table 4.9: Estimated Ion Pair Dipole Moments, μ_{IP}, and Standard State Overall Association Constants, K_A°, for Aqueous Solutions of KH_2PO_4, K_2HPO_4 and K_3PO_4 at 25 °C.[a]

	KH_2PO_4		K_2HPO_4				K_3PO_4	
	μ_{IP}	K_A°	μ_{IP}	K_1°	K_2°	K_A°	μ_{IP}	K_A°
CIP	7.33	∞	15.8	170 ± 27	1.0 ± 0.2		24.3	687 ± 520
SIP	21.5	$\underline{5.4 \pm 0.6}$	36.8	48 ± 9	$\underline{0.26 \pm 0.05}$	$\underline{21 \pm 2}$	51.0	260 ± 123
2SIP	33.7	2.0 ± 0.2	55.5	$\underline{18 \pm 3}$	0.13 ± 0.02		75.7	$\underline{49 \pm 18}$

[a]Units: μ_{IP} in Debye ($1\,\mathrm{D} = 3.3356 \cdot 10^{-30}\mathrm{Cm}$); K_1°, K_2° and K_A° in $\mathrm{L\,mol^{-1}}$.
Preferred K_x° ($x = 1, 2$ or A) values (see text) are underlined.

Three trends in ion-pairing behavior can be distinguished: First, a shift from preferential formation of SIPs (KH_2PO_4), to simultaneous observation of SIPs and 2SIPs ($KHPO_4^-$), while the ion pair KPO_4^{2-} solely exists in the 2SIP form. Second, as already noted, K_A° increases considerably in the order $KH_2PO_4^0 < KHPO_4^- < KPO_4^{2-}$. Third, at $c > 1\,\mathrm{mol\,L^{-1}}$ the amount of formed ion pairs follows a reverse order: for KH_2PO_4 c(IP) increases linearly over the investigated concentration range, while for $KHPO_4^-$ the ion pair concentration is considerably lower at the same phosphate concentration. Most prominent is the behavior of K_3PO_4, which only shows ion-pair formation for $c(K_3PO_4) \leq 0.79\ \mathrm{mol\ L^{-1}}$.

The trend of increasing hydration of the ion pairs is mirrored by the number of irrotational bound water molecules. The increased Coulomb attraction between cation and anion in going from $H_2PO_4^-$ to PO_4^{3-} explains the increase in K_A°. Decreasing c(IP) at salt concentrations $c > 1\,\mathrm{mol\,L^{-1}}$ with increasing anion charge may be well explained with redissociation effects. With increasing ionic strength each individual ion is experiencing the electric fields of an growing number of neighbor ions. The associated screening effect makes it more and more difficult to form stable ion pairs, which rely on the specific (electrostatic) interaction of two oppositely charged ions. As a result, the absolute number of ion pairs at any given time in the solution may actually increase, however, the amount detected by DRS is decreasing, as the life time of the ion pairs gets shorter than the rotation correlation time. Thus, they are no longer able to contribute to the total polarization.
As pointed out by various authors,[157–161] dimerization of the phosphate species $H_2PO_4^-$ and HPO_4^{2-} in aqueous solution is a fact. Whereas dimerization of $H_2PO_4^-$ is present over the entire concentration range with a concentration-independent association constant,[157–160] dimerization of HPO_4^{2-} can be neglected in dilute solutions.[36,161,162] As standard state association constants and hydration numbers are generally given for infinite dilution, we should only expect an influence on those quantities in the case of KH_2PO_4. Unfortunately, the dihydrogen phosphate dimer is difficult to quantify with dielectric spectroscopy, due to the unknown effective dipole moment of the species. Ideally, by formation of two hydrogen bonds in a centrosymmetric fashion, a vanishing dipole moment is expected. As a result the anion amplitude is overestimated and the intimately connected slow water amplitude underestimated. For concentrations $c \geq 1\,\mathrm{mol\,L^{-1}}$ we find increasing Z_{ib} (Figure 4.10), that might indeed be associated to phosphate dimerization. Nevertheless, ion pairing and hydration behavior of KH_2PO_4 and K_2HPO_4 can be well explained without considering phosphate dimerization. Also, a very recent Raman study was not able to detect any features of hydrogen bonded dimeric species in dilute $H_2PO_4^-$ solutions.[163]

4.5 Solvent Dynamics

The shift of the main dispersion peak in the $\varepsilon''(\nu)$ spectra towards lower frequencies (Figures 4.14.34.5) indicates an overall slowdown of the water dynamics with increasing solute concentration for all three potassium phosphate salts. This slowdown is partially due to increasing viscosity, but also to specific solute-solvent interactions. The influence of the solute on water dynamics in aqueous solutions is a challenging task in DR because of the difficulties in separating the two water processes. The obtained relaxation times for bulk and slow water are not completely independent, and it is sometimes necessary to fix the relaxation time of one of them (mostly slow water at low solute concentrations). Due to the nature of the fit routine, fixing the slow water mode at a longer relaxation time lengthens the relaxation time for bulk water. This problem vanishes at higher concentrations ($c \gtrsim 1$ $\mathrm{mol\,L^{-1}}$), when the slow water amplitude is big enough to be resolved without ambiguity. In general, the relaxation time for the (slow water + anion mode) is extracted from the high concentration limit and fixed at this value for the lower concentrations. This is not completely bias free, but seems to produce reasonable results.[16,30,143,164] A consequence of

this procedure is that the obtained relaxation times for the slow water mode are of limited value: at best qualitative trends can be derived.
Orthophosphate anions are able to establish a maximum of 12 hydrogen bonds at any given time. As discussed in Section 4.3 the slow water molecules of $H_2PO_4^-$ fit within the first hydration shell, whereas those of HPO_4^{2-} and PO_4^{3-} also occupy the second hydration shell. It is reasonable to assume, that the retarded water molecules in the second hydration shell are slowed down to a lesser extend than those of the first hydration shell. Also, the slow water molecules that reside in the second hydration shell are not hydrogen bonded to the anion, but rather slowed down due to electrostatic interactions. We thus get the picture of marked slowdown of water molecules in the first hydration shell, less slowdown in the second hydration shell (if existent) and eventually vanishing influence of the anion on solvent in further hydration shells i.e. the bulk. We can thus conclude, that the phosphate anions are able to slow down water molecules in the first two hydration shells (with the exception of $H_2PO_4^-$), which show up in the S_2 amplitude of the respective dielectric spectra. The deduced distribution of slow water over the first two solvation layers, combined with the different slowdown in the two solvation layers thus explains the apparent speed up of slow water dynamics in the course KH_2PO_4(aq) (~ 23 ps), K_2HPO_4(aq) (~ 21 ps) and K_3PO_4(aq) (~ 17 ps).

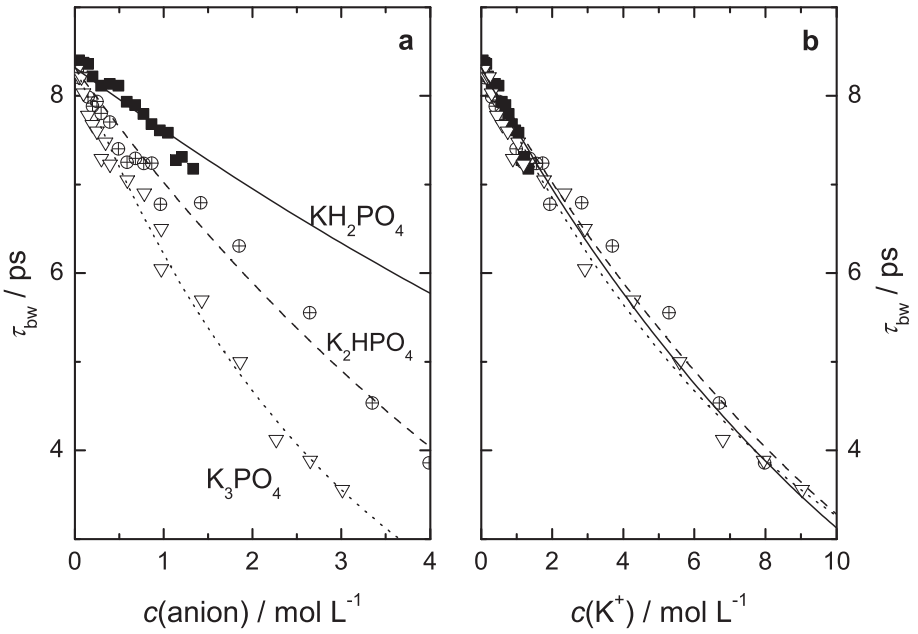

Figure 4.14: Bulk water relaxation time, τ_{bw}, as a function of (a) phosphate anion concentration and (b) potassium concentration. Symbols represent experimental values and lines are empirical fits thereof.

The bulk water relaxation time, τ_{bw}, decreases with increasing solute concentration for all three phosphate salts. Figure 4.14 shows this decrease for the three salts as a function of (a) phosphate (anion) concentration and (b) cation concentration. Whereas distinct differences exist between the former three curves (which have differing $c(K^+)$ at each c_-),

τ_{bw} shows essentially the same behavior for all three salts when plotted against $c(K^+)$, with varying c_-. This implies, that the apparent speedup of bulk water dynamics is mostly due to the cations, and largely independent of the phosphate anions. Thus it appears, at least for the potassium phosphate salts of this study, that the anions slow down water dynamics sufficiently to give rise to Z_{slow}, whereas potassium is able to slow down water molecules (as evident from $Z_{slow}(K^+)$) and at the same time speed up bulk water dynamics. The apparent contradiction of simultaneous slowdown and speedup of water dynamics due to the K^+ is not resolved at present. It might well be, that the speedup of bulk water dynamics is solely due to the increased fraction of fast water, as the bulk water mode subsumes the fast water mode. This would render the observed dependence of the bulk water dynamics on the potassium concentration a mere coincidence.
Clearly, it is desirable to gain more insight on the influence of solutes, and especially of cations and anions, on water dynamics. First, the question needs to be settled, whether for salts of simple ions, the cation is the only solute that has a decisive influence on the bulk water dynamics. A previous DRS study on a range of simple sodium salts already indicated that the impact of the studied anions (Br^-, I^-, NO_3^-, ClO_4^- and SCN^-) on water dynamics is remarkably similar,[28] though subtle differences were detectable. This is broadly consistent with **no** influence of the anions on τ_{bw}. However, recent DRS studies of Rahman on sodium alkyl carboxylates ($C_{m-1}H_{2m-1}COONa$ with m = 1, 2, 3, 4, 5) showed that the bulk water dynamics depends on the nature of the anion. Nevertheless, the studied alkyl carboxylates, with the exception of formate (m = 1) are no simple anions as they show mixed hydrophilic - hydrophobic hydration. A decisive influence of hydrophobic hydration on the detected relaxation times, can be inferred from the non-monotonic dependence of τ_{bw} on the length of the alkyl chain and the completely different behavior for sodium pentanoate (m = 5). It seems to be worthwhile to conduct combined systematic DRS studies and MD simulations regarding the dependence of τ_{bw} on cations and anions. Especially regarding the specific influence of cations on the dynamics of water molecules in their first and second hydration shell, MD simulations might be able to deliver invaluable information.

4.6 Conclusion

Phosphate anions are highly hydrated, and show systematic changes in their ability to slow or hinder the rotation of water molecules. The number of irrotationally bound water molecules per unit of salt at infinite dilution, Z°_{ib}, was found to be ∼0 ($H_2PO_4^-$), ∼4.4 (HPO_4^{2-}), and ∼14.8 (PO_4^{3-}). In addition to ib water all three potassium phosphate salts were found to slow the dynamics of an even greater number of water molecules. The number of water molecules so affected at infinite dilution per unit of solute, $Z^{\circ}_{\mathrm{slow}}$, was: ∼20 ($KH_2PO_4$), ∼29 ($K_2HPO_4$) and ∼35 ($K_3PO_4$). Assuming a value of $Z^{\circ}_{\mathrm{slow}}(K^+) \approx 9$, $Z^{\circ}_{\mathrm{slow}}$ of the anions was calculated to be ∼11 ($H_2PO_4^-$), ∼10 (HPO_4^{2-}) and ∼7 (PO_4^{3-}). Thus the total hydration numbers $Z^{\circ}_{\mathrm{t}} = Z^{\circ}_{\mathrm{ib}} + Z^{\circ}_{\mathrm{slow}}$ for the three anions are ∼11 ($H_2PO_4^-$), ∼15 (HPO_4^{2-}) and ∼22 (PO_4^{3-}). These values indicate that more than one solvation shell is present for HPO_4^{2-} and PO_4^{3-}.

Aqueous solutions of the potassium phosphate salts KH_2PO_4, K_2HPO_4 and K_3PO_4 contrary to most previous opinion are significantly ion-paired with the standard state overall association constant K°_{A} increasing in the order $KH_2PO_4^0 < KHPO_4^- < KPO_4^{2-}$. In addition the nature of the IPs formed varied systematically: SIPs for $KH_2PO_4^0$, SIPs + 2SIPs for $KHPO_4^-$ and 2SIPs for KPO_4^{2-} consistent with the level of hydration of the anions.

The effect of potassium phosphates on bulk water dynamics can be split up in anion and cation contributions. Phosphate anions are slowing down water dynamics, whereby the slow water relaxation times of the three different phosphate salts can be reasonably explained with the detected hydration pattern. Potassium cations are also able to slow down water, but at the same time are responsible for the speed up of bulk water dynamics, that apparently was not affected by phosphate anions.

Chapter 5

Sodium and Ammonium Phosphates

5.1 Introduction

Ion specific effects have attracted significant amount of interest during the last decade.[165–168] Since the first systematic investigations in this area by Hofmeister and co-workers in the late 1800s,[169–175] many macroscopic properties have been shown to depend in a specific manner on the nature of the present ions,[176] which led later on to the establishment of the so called "Hofmeister series" of cations and anions. However, an explanation for the observed ordering of ions remained elusive. Just about one decade ago, interest in specific ion effects was revitalized through a series of conferences in Regensburg (2004), Prague (2007), Munich (2008) and Oxford (2012).[166] At the first conference in Regensburg the attendees expressed the necessity to formulate the right questions regarding specific ion effects. Almost a decade later, the same people expressed the hope that the questions are formulated now and people may start to answer them.[177] Even though a significant amount of knowledge was gathered during the last decade, still many questions remain unanswered. The intention of this chapter is to gather additional data on phosphate hydration and ion pairing, when ions different from K^+ are present. A summary of (possible) ion specific effects in phosphate hydration and ion pairing will be given in the conclusion of this work. The additionally probed cations were Na^+, $NH_4{}^+$ and K^+ (Chapter 4). As already stated, the overwhelming use of inorganic phosphates is in the form of fertilizers. Without the large-scale use of fertilizers for crop production throughout the world, the earth would not be able to sustain the by now more than seven billion human beings.[178] Most important are ammonium phosphates $(NH_4)H_2PO_4$ and $(NH_4)_2HPO_4$, which are able to provide two essential nutrients for plant growth: phosphorous and nitrogen. Due to the overwhelming importance, ammonium salts were chosen to be part of this study. Sodium phosphates are presented first and were chosen due to the potential high importance of small differences in ion binding of Na^+ and K^+ for biological processes.[9,10,12]
The results on dielectric spectroscopy of sodium phosphate salts (NaH_2PO_4 & Na_2HPO_4) and ammonium phosphate salts ($(NH_4)H_2PO_4$ & $(NH_4)_2HPO_4$) are finally compared with the respective potassium salts.

5.2 Aqueous solutions of NaH_2PO_4 and Na_2HPO_4

5.2.1 Choice of fit model and assignment of relaxation modes

Aqueous solutions of NaH_2PO_4 ($c \leq 4.794\,\mathrm{mol\,L^{-1}}$) and Na_2HPO_4 ($c \leq 0.6184\,\mathrm{mol\,L^{-1}}$) have been measured up to the saturation limit at 25 °C, over the frequency range $0.2 \leq \nu/\,\mathrm{GHz} \leq 89$. Sample pH (Table 5.1) was determined to ± 0.01 at room temperature with a glass electrode, containing a silver chloride reference electrode (Metler Toledo, InLab Micro) and indicated that hydrolysis of $H_2PO_4^-$(aq) and HPO_4^{2-} was $\leq 5\%$ and could thus be neglected.

Table 5.1: Concentrations, c, and pH Values of All Studied Sodium Phosphate Salt Solutions.[a]

NaH_2PO_4				Na_2HPO_4	
c	pH	c	pH	c	pH
0.0520	4.43	0.7765	3.98	0.0498	8.71
0.0993	4.31	0.8734	3.93	0.0999	8.96
0.1484	4.28	0.9632	3.93	0.1499	8.99
0.2005	4.26	1.860	3.70	0.1996	9.02
0.2469	4.22	2.682	3.52	0.2496	8.98
0.2960	4.19	3.438	3.40	0.2992	9.01
0.3966	4.14	4.153	3.27	0.3488	9.01
0.4932	4.09	4.794	3.15	0.3989	8.99
0.5882	4.05			0.4965	8.96
0.6834	4.01			0.6184	8.91

[a] Units: c in $\mathrm{mol\,L^{-1}}$.

At $c \leq 1\,\mathrm{mol\,L^{-1}}$ the best model for NaH_2PO_4(aq) proved to be a four-Debye fit, whereas for $c > 1\,\mathrm{mol\,L^{-1}}$ a three-Debye fit yielded best results. Also, for the two lowest concentrations just three Debye-type relaxations could be resolved. Table 5.2 contains the obtained fit parameter, typical experimental spectra are given in Figure 5.1, and the amplitudes of the four resolved processes are depicted in Figure 5.2.

For Na_2HPO_4(aq) a three-Debye model was sufficient for the whole investigated concentration range. As the solubility of Na_2HPO_4 in water is too low to extract reasonable τ_{sw}, the bulk water relaxation time was fixed to obtain smooth changes for the relaxation parameter. Deviant from that, for the three lowest concentrations the slow water relaxation time was fixed at 23 ps to account for the usually observed initial drop of τ_{bw}. Table 5.3 lists the obtained fit parameter, typical spectra are shown in Figure 5.3 and Figure 5.4 shows the concentration dependence of the three detected modes.

The respective lowest frequency relaxation of both salts can be attributed to ion-pair + ion-cloud relaxation. For NaH_2PO_4(aq) an additional ion-pair mode at higher frequencies is resolved, indicating the simultaneous presence of two different types of ion pairs. Also,

both salts show two water related relaxations at $\sim 8\,\mathrm{GHz}$ and $\sim 18\,\mathrm{GHz}$. The lower frequency process is attributed to slow water, which also contains a contribution from anion relaxation. The dominating process at $\sim 18\,\mathrm{GHz}$ can be unequivocally attributed to bulk water, as all obtained fit parameters of this process smoothly converge to the ones for pure water at $c \to 0$. For both salts it was not possible to resolve a fast water mode, but the existence of it can be implied by the strong increase in ε_∞ with increasing c.
The correct disentanglement of bulk and slow water at low concentrations ($c < 1\,\mathrm{mol\,L^{-1}}$) poses a problem, as both relaxation modes are generally too close to each other as that the fitting routine could treat them independently. The traditional way to solve this consists of two steps: first a free fit (without fixing any relaxation time) is applied to the complete investigated concentration range. This yields, in general, quite scattered relaxation times for bulk and slow water at low concentrations due to the low amplitude of the slow water process. At higher concentrations (typically $c \geq 1\,\mathrm{mol\,L^{-1}}$) the relaxation strength of the slow water process is big enough to be reasonably resolved. In the second step the relaxation time of the slow water process at $c \leq 1\,\mathrm{mol\,L^{-1}}$ is fixed for the value obtained in the high concentration regime. This procedure is quite cumbersome, as in addition to the detection of the best fit model, also the slow water relaxation time has to be determined separately. The results on the bulk water dynamics of the previous chapter, however, offer a faster and more elegant way for the disentanglement of the two water processes. As was shown in Chapter 4.5, the bulk water dynamics for potassium phosphates is largely independent of the anion. Yet, so far it is not clear, if this is only true for phosphate salts (and maybe even only for potassium phosphates) or if this can be generalized for all simple salt solutions. To gain more insight into this important question, NaH_2PO_4(aq) was fitted in two different ways: first, the slow water relaxation time was held constant at 25 ps for $c < 1\,\mathrm{mol\,L^{-1}}$. In a second attempt, the bulk water relaxation time was adjusted to the value as observed in NaCl(aq) at the respective Na^+ concentrations.[137] This procedure involves the assumption, that Cl^- also has almost no effect on the bulk water relaxation time. In the light of MD simulations,[65] finding equal residence times of water around water and Cl^-, this seems reasonable though. Figure 5.5 compares the two sets of τ_{bw}. Virtually no difference in ion-pairing for the whole investigated c range and in hydration for $c > 1\,\mathrm{mol\,L^{-1}}$ was obtained for the two sets of fit-parameter. Thus Figure 5.6 compares the obtained relaxation amplitudes S_j ($j = 1 - 4$) for $c \leq 1\,\mathrm{mol\,L^{-1}}$. As the fit parameter set based on fixed τ_{bw} gave more consistent results on ion-hydration (the hydration results for both approaches are shortly discussed in Chapter 5.2.2), it was chosen as the best fit model. The parameter set based on τ_{sw} is presented in Table 5.4.
Nevertheless, both approaches have to be regarded as auxiliary constructions for the disentanglement of bulk and slow water. Thus, even though fixing τ_{bw} gave more consistent results for NaH_2PO_4(aq), both approaches should be tested for future studies (provided reliable τ_{bw} for the respective cation chloride are available). A future reliable disentanglement of bulk and slow water without major assumptions on either relaxation time is just possible when the spectra are extended by high frequency data (THz regime). This frequency region, however, is currently not available with the instrumentation in Regensburg.

Table 5.2: Concentration Dependence of the Dielectric Relaxation Parameters of a Four-Debye Fit of Aqueous Solutions of NaH_2PO_4 at 25 °C Obtained by Largely Fixing the Bulk Water Relaxation Time τ_4: Concentration, c, Limiting Permittivities, ε_j $(j = 1-4)$ & ε_∞, Relaxation Times, τ_j, VNA Conductivities, κ_{VNA}, and the Value of the Reduced Error Function, χ^2_{r}.[a,b]

c	ε_1	τ_1	ε_2	τ_2	ε_3	τ_3	ε_4	τ_4	ε_∞	κ_{VNA}	χ^2_{r}
0.05200	78.01	605	77.67		77.67	47.2	76.71	8.31	5.61	0.343	0.0658
0.09933	77.82	185	77.26		77.26	41.2	75.51	8.27	5.65	0.613	0.0948
0.1484	79.18	419	78.48	85F	77.01	23.4	74.27	8.3F	6.02	0.875	0.0651
0.2005	78.81	342	77.98	84.4	76.57	29.2	72.77	8.19F	5.73	1.116	0.0594
0.2470	79.50	472	78.15	83.2	76.04	27.7	71.75	8.15F	5.75	1.325	0.0443
0.2960	79.33	324	78.70	95.1	76.22	27.3	70.31	8.11F	5.83	1.546	0.0672
0.3966	81.28	512	79.48	87.4	75.24	21.8	67.63	8.07F	6.12	1.947	0.0470
0.4932	81.30	655	79.49	98.2	75.00	26.8	66.38	8.05F	6.22	2.294	0.0558
0.5882	81.40	514	79.74	89.8	73.95	24.4	64.21	7.96F	6.28	2.626	0.0972
0.6834	81.47	446	80.33	93.6	73.57	23.9	62.07	7.9F	6.33	2.943	0.0726
0.7765	82.39	390	80.51	91.0	72.98	23.7	59.99	7.84F	6.50	3.204	0.0950
0.8734	82.78	681	80.96	95.6	72.23	23.9	58.51	7.79F	6.61	3.465	0.0949
0.9632	83.81	485	80.93	96.4	72.26	25.8	57.55	7.76F	6.87	3.688	0.0754
1.861	83.89		83.89	121	65.21	23.0	43.20	7.4F	7.16	5.236	0.1180
2.682	83.06		83.06	129	57.73	21.6	33.00	7.0F	7.56	5.800	0.1276
3.438	82.45		82.45	174	53.74	24.7	28.02	6.75F	7.81	5.802	0.1437
4.153	77.28		77.28	189	48.28	25.0	23.27	6.5F	8.28	5.557	0.1410
4.794	70.76		70.76	207	43.94	26.1	20.18	6.2F	8.59	5.053	0.1403

[a] Units: c in $\mathrm{mol\,L^{-1}}$, τ_j in ps, κ_{VNA} in $\mathrm{S\,m^{-1}}$; [b] Parameter values followed by the letter F were not adjusted in the fitting procedure.

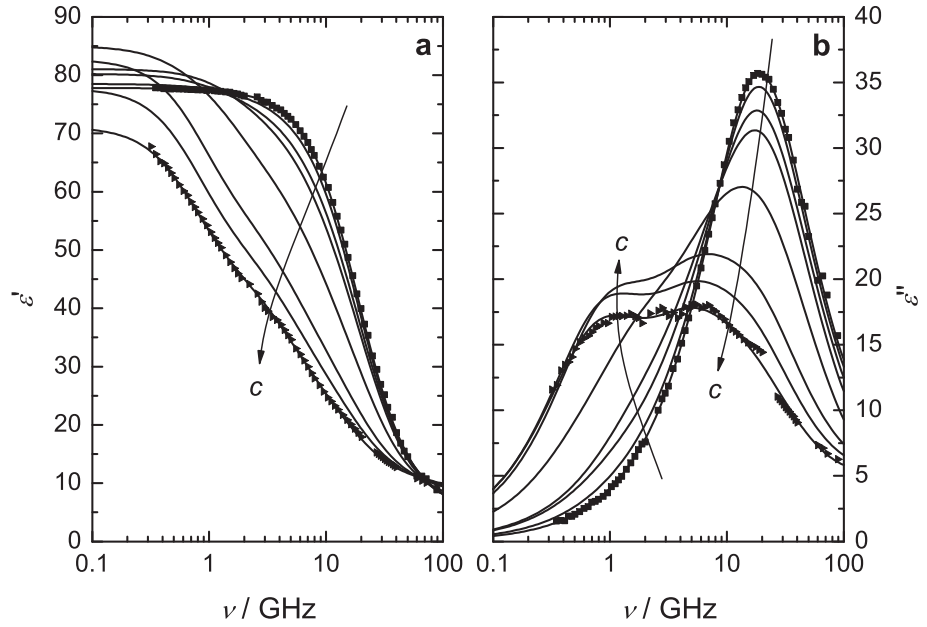

Figure 5.1: Relative permittivity (a) and dielectric loss (b) spectra for NaH_2PO_4(aq) at 25 °C and concentrations $c\,/\,(\mathrm{mol\,L^{-1}})$ = 0.05200, 0.2005, 0.4932, 0.7765, 1.8605, 3.438, 4.153 and 4.795. Symbols represent typical experimental data (mostly omitted for visual clarity), lines the D+D+D+D fit and arrows indicate increasing concentration c.

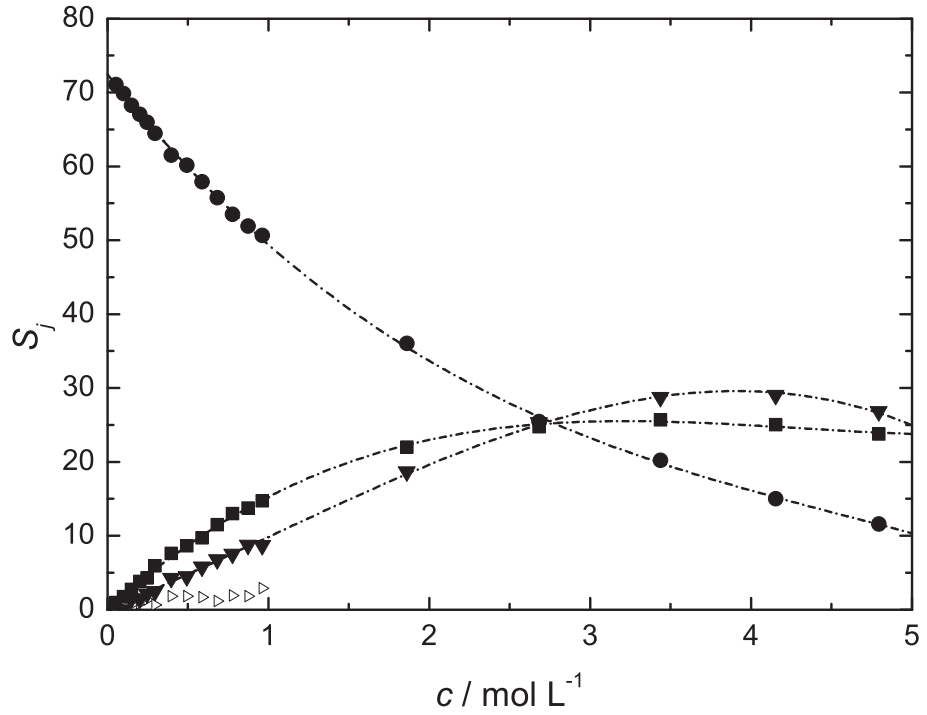

Figure 5.2: Amplitudes of the four Debye-type relaxation modes for NaH_2PO_4(aq) as a function of solute concentration at 25 °C: bulk water (S_4,●), slow water + anion (S_3,■), ion pair (S_2,▼) and ion-pair + ion-cloud relaxation (S_1,▷). Lines are visual guides only.

Table 5.3: Concentration Dependence of the Dielectric Relaxation Parameters of a Three-Debye Fit of Aqueous Solutions of Na_2HPO_4 at 25 °C: Concentration, c, Limiting Permittivities, ε_j ($j = 1 - 3$) & ε_∞, Relaxation Times, τ_j, VNA Conductivities, κ_{VNA}, and the Value of the Reduced Error Function, χ^2_{r}.[a,b]

c	ε_1	τ_1	ε_2	τ_2	ε_3	τ_3	ε_∞	κ_{VNA}	χ^2_{r}
0.0498	79.10	264	77.30	23.0F	76.30	8.28	5.85	0.715	0.0229
0.0999	79.29	202	76.42	23.0F	74.48	8.22	5.92	1.254	0.0485
0.1499	79.14	165	75.62	23.0F	72.96	8.18	6.03	1.764	0.0571
0.1996	78.91	142	74.78	21.3	70.85	8.07F	6.23	2.198	0.0647
0.2496	78.55	126	74.09	21.5	69.42	8.01F	6.29	2.600	0.0724
0.2992	78.59	120F	73.18	19.8	67.39	7.96F	6.32	2.955	0.0791
0.3488	78.17	115F	72.40	20.4	65.81	7.90F	6.44	3.280	0.0872
0.3988	78.06	111	72.04	18.9	64.26	7.86F	6.52	3.615	0.1205
0.4965	77.43	105	70.97	18.4	60.73	7.74F	6.84	4.167	0.1846
0.6184	76.56	103	69.61	19.2	57.74	7.68F	7.25	4.739	0.2239

[a] Units: c in $\mathrm{mol\,L^{-1}}$, τ_j in ps, κ_{VNA} in $\mathrm{S\,m^{-1}}$; [b] Parameter values followed by the letter F were not adjusted in the fitting procedure.

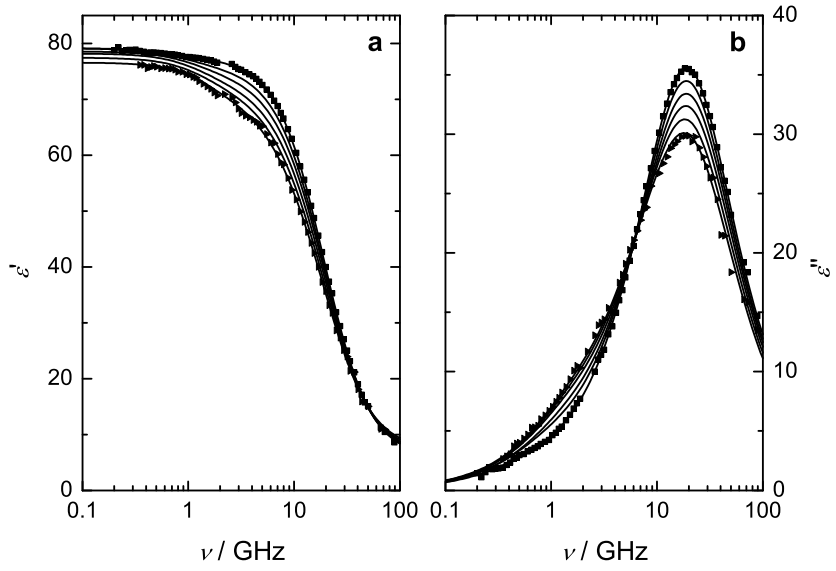

Figure 5.3: Relative permittivity (a) and dielectric loss (b) spectra for Na_2HPO_4(aq) at 25 °C and concentrations $c\,/\,(\mathrm{mol\,L^{-1}})$ = 0.04980, 0.09986, 0.1499, 0.1996, 0.2496, 0.2992, 0.3488, 0.4965 and 0.6184. Symbols represent typical experimental data (mostly omitted for visual clarity), lines the D+D+D fit and arrows indicate increasing concentration c.

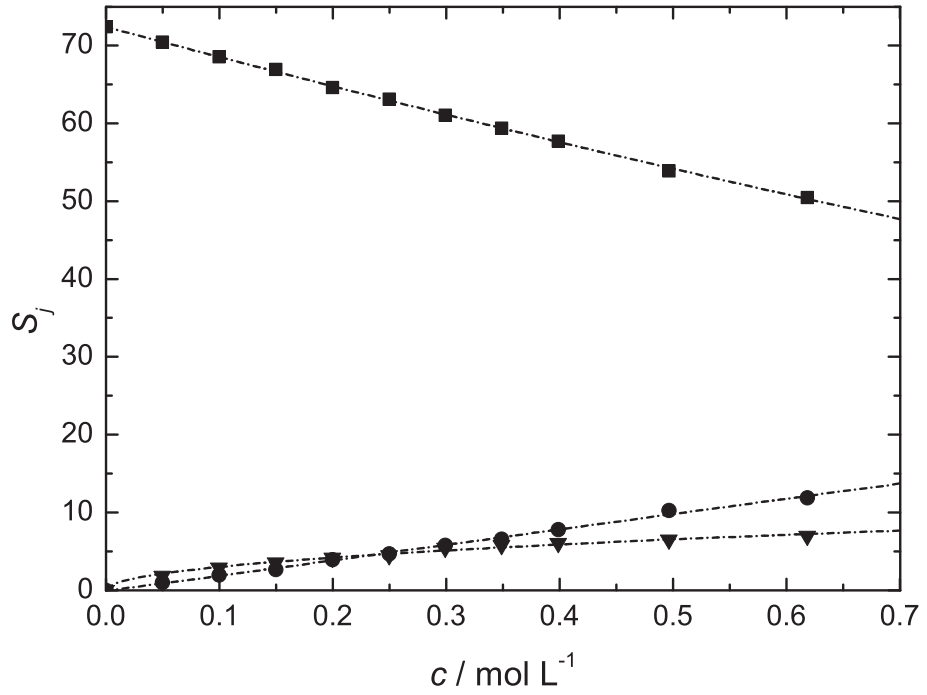

Figure 5.4: Amplitudes of the three Debye-type relaxation modes for Na_2HPO_4(aq) as a function of solute concentration at 25 °C: bulk water (S_3,■), slow water + anion (S_2,●), ion-pair + ion-cloud relaxation (S_1,▼). Lines are visual guides only.

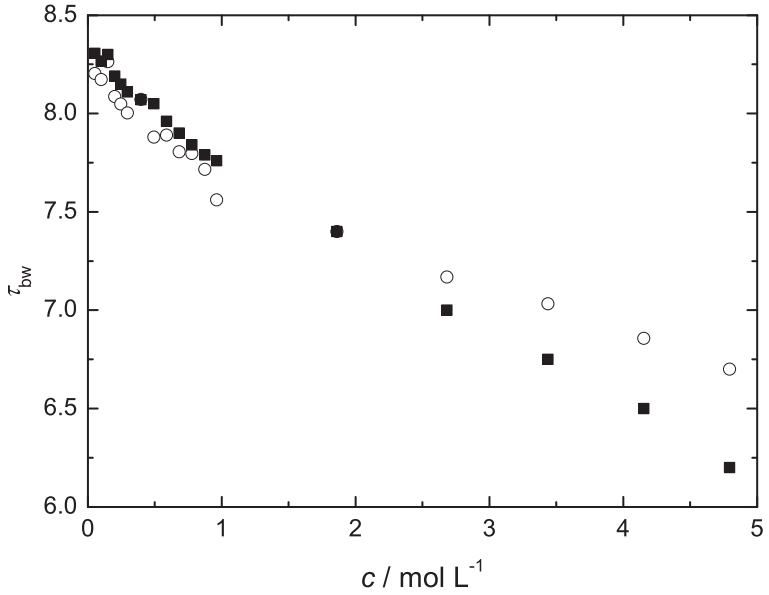

Figure 5.5: Comparison of bulk water relaxation time as observed for 4D-fits of NaH_2PO_4(aq) with fixed slow water relaxation time (○) and bulk water relaxation time fixed to the respective value as observed in NaCl(aq) (■).

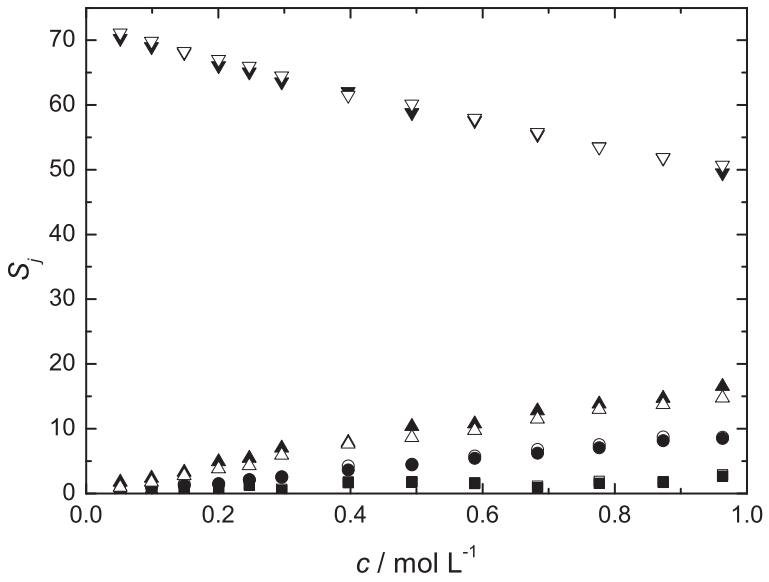

Figure 5.6: Comparison of amplitudes of the 4D fit for the two alternative fitting procedures for NaH_2PO_4(aq) using fixed slow water relaxation times (open symbols) or fixed bulk water relaxation times (filled symbols).

Table 5.4: Concentration Dependence of the Dielectric Relaxation Parameters of a Four-Debye Fit of Aqueous Solutions of NaH_2PO_4 at 25 °C Obtained by Largely Fixing the Slow Water Relaxation Time τ_3: Concentration, c, Limiting Permittivities, ε_j $(j = 1-4)$ & ε_∞, Relaxation Times, τ_j, VNA Conductivities, κ_{VNA}, and the Value of the Reduced Error Function, χ^2_{r}.[a,b]

c	ε_1	τ_1	ε_2	τ_2	ε_3	τ_3	ε_4	τ_4	ε_∞	κ_{VNA}	χ^2_{r}
0.05200	77.83		77.83	207	77.51	25.0F	75.75	8.20	5.46	0.344	0.0748
0.09933	77.79		77.79	128	76.89	25.0F	74.55	8.17	5.56	0.613	0.0936
0.1484	79.17	417	78.53	103	77.32	25.0F	74.04	8.26	5.97	0.875	0.0654
0.2005	78.81	382	78.12	97.9	76.59	25.0F	71.70	8.09	5.63	1.116	0.0577
0.2470	79.50	502	78.24	93.5	76.17	25.0F	70.76	8.05	5.65	1.325	0.0427
0.2960	79.32	359	78.85	105	76.29	25.0F	69.27	8.00	5.73	1.546	0.0653
0.3966	81.29	558	79.65	104	76.02	25.0F	68.14	8.07	6.08	1.947	0.0483
0.4932	81.37	754	79.64	107	75.22	25.0F	64.90	7.88	6.06	2.294	0.0512
0.5882	81.43	581	79.92	99.2	74.49	25.0F	63.78	7.89	6.20	2.626	0.0965
0.6834	81.48	553	80.62	107	74.40	25.0F	61.64	7.81	6.21	2.943	0.0714
0.7765	82.39	433	80.82	102	73.79	25.0F	59.98	7.80	6.43	3.204	0.0952
0.8734	82.86	805	81.15	104	73.00	25.0F	58.30	7.72	6.51	3.465	0.0945
0.9632	83.82	523	81.18	104	72.70	25.0F	56.19	7.56	6.68	3.689	0.0704
1.860	83.89		83.89	121	65.21	23.0	43.20	7.40F	7.16	5.236	0.1180
2.681	83.88		83.88	139	58.59	23.0	34.22	7.17	7.57	5.778	0.1186
3.438	82.06		82.06	170	53.63	25.1	28.84	7.03	7.98	5.811	0.1498
4.153	77.32		77.32	191	48.48	25.8	24.18	6.86	8.41	5.557	0.1402
4.794	71.03		71.03	212	44.27	27.4	21.19	6.70F	8.73	5.057	0.1431

[a] Units: c in $\mathrm{mol\,L^{-1}}$, τ_j in ps, κ_{VNA} in $\mathrm{S\,m^{-1}}$; [b] Parameter values followed by the letter F were not adjusted in the fitting procedure.

5.2.2 Ion hydration

NaH_2PO_4(aq)

Hydration in NaH_2PO_4(aq) should in principle be more straightforward than for the corresponding potassium salt: Na^+ shows only strong hydration, leading to ib water, with no slow water.[31,137] Contrary, $H_2PO_4^-$ is only able to slow water rotation at $c \leq 1\,\mathrm{mol\,L^{-1}}$, leading to the emergence of a slow water mode, but not to strongly bind water. At $c > 1\,\mathrm{mol\,L^{-1}}$ $H_2PO_4^-$ also freezes water rotation. Thus, in NaH_2PO_4(aq) at low concentrations the two effective hydration numbers, Z_{ib} and Z_{slow}, can be attributed solely to the cation and anion respectively.
From the anion + slow water relaxation with amplitude S_3 the slow water amplitude, S_{sw}, was obtained by subtraction of the free anion contribution, S_- which was calculated from the free anion concentration c_-, utilizing the anion dipole moment $\mu_- = 5.905\,\mathrm{D}$,[93,96] via Eq. 1.47. The latter was accessible from ion pairing results (see Section 5.2.3) as $c_- = c - c_{\mathrm{IP}}$. Insertion of S_{sw} into a solvent normalized Cavell equation (Eq. 3.7) gave the concentration of slow water, c_{sw}, which eventually allowed the calculation of $Z_{\mathrm{slow}}(NaH_2PO_4(aq))$ via Eq. 4.1. As Na^+ does not give rise to slow water, this number is equivalent to $Z_{\mathrm{slow}}(H_2PO_4^-)$ and depicted in Figure 5.7b. The experimental Z_{slow} values are best fitted by an empirical equation (solid line in Figure 5.7b)

$$\ln(Z_{\mathrm{slow}}) = a + bc^{1.5} \tag{5.1}$$

with $a = 2.49 \pm 0.02$ and $b = 0.20 \pm 0.01$, which gives an infinite dilution value of $Z^\circ_{\mathrm{slow}} = 12.0 \pm 0.2$ in excellent agreement with the value obtained from KH_2PO_4(aq).
As the relaxation of fast water was not resolved, it was combined with the bulk water amplitude S_3 to $S_{\mathrm{w}} = \varepsilon_3 - \varepsilon_\infty(0)$ where $\varepsilon_\infty(0) = 3.52$ is the infinite frequency permittivity of pure water (see Chapter 2). The amplitude of all DRS detected water is given by $S_{\mathrm{w}}^{\mathrm{eq}} = S_{\mathrm{w}} + S_{\mathrm{sw}} + \Delta\varepsilon_{\mathrm{kd}}$. The value of kinetic depolarization $\Delta\varepsilon_{\mathrm{kd}}$ was calculated under *slip* boundary conditions. Figure 5.7a shows Z_{ib} values which were calculated via Eq. 3.2. A linear fit for $c < 1\,\mathrm{mol\,L^{-1}}$ yielded $Z^\circ_{\mathrm{ib}} = 4.3 \pm 0.3$, in reasonable agreement with $Z^\circ_{\mathrm{ib}}(Na^+) = 5.2 \pm 0.5$. At infinite dilution the experimental results are thus in good agreement with the expected values (dotted line in Figure 5.7a), with $Z^\circ_{\mathrm{ib}}(NaH_2PO_4) \approx 4.3$ and $Z^\circ_{\mathrm{slow}}(NaH_2PO_4) \approx 12.0$. At finite concentrations, however, the detected Z_{ib} are lower than the sum of $Z_{\mathrm{ib}}(Na^+)$ from NaCl(aq)[137] and $Z_{\mathrm{ib}}(H_2PO_4^-)$ from KH_2PO_4(aq) (Section 4.3). The concentration dependence, on the other hand, parallels surprisingly well the expected trend assuming additivity of Z_{ib} values. For Z_{slow} the deviation from the expected concentration trend (as obtained for $H_2PO_4^-$ in $(NH_4)H_2PO_4$(aq), see Section 5.3.2) is positive, i.e. more water molecules are slowed down as expected. Though both observations may well be explained with experimental uncertainties, they hint at a shift from frozen to slow water for a small proportion of the frozen water molecules. As at $c \leq 1\,\mathrm{mol\,L^{-1}}$ only Na^+ is able to freeze water, the affected water molecules must be located in the hydration sphere of Na^+. The most reasonable explanation of this shift can be seen in ion-pairing: the partial charge neutralization, that goes along with ion-pair formation, results in the inability of Na^+ to maintain its entire ib hydration shell. It is interesting to note, however, that the total

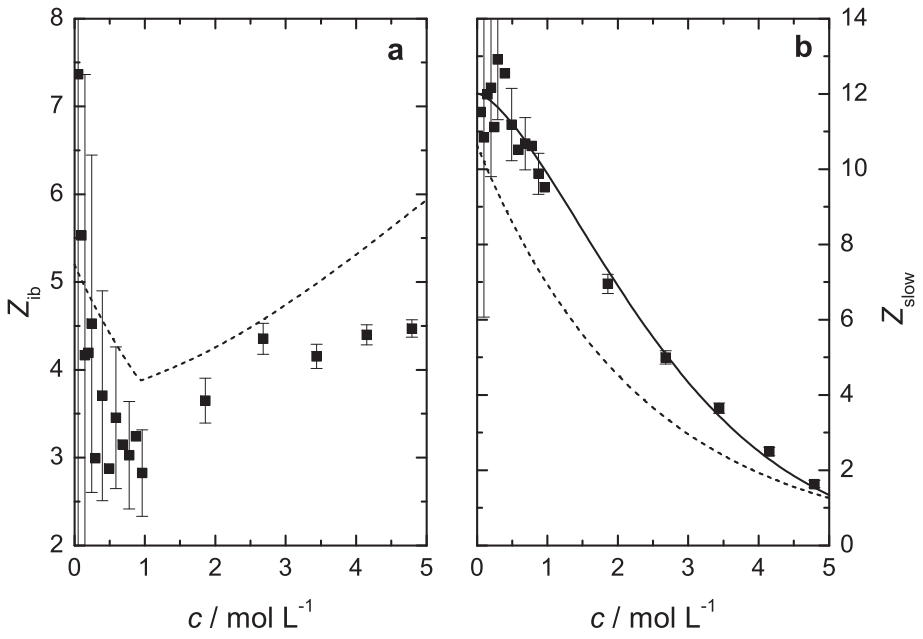

Figure 5.7: (a) Number of irrotationally bound, Z_{ib}, and (b) slow water molecules, Z_{slow}, per unit of solute. Symbols represent experimental values, broken lines expected values from (a) NaCl(aq) & KH_2PO_4(aq) and (b) $(NH_4)H_2PO_4$(aq). The solid line in (b) represents an empirical fit. Error bars, $\Delta Z_{\mathrm{ib}} = \Delta Z_{\mathrm{slow}}$ were estimated from the standard deviation, σ_{fit}, of the fit of the combined water related amplitudes, $S_{\mathrm{w}}^{\mathrm{eq}}$, according to $S_{\mathrm{w}}^{\mathrm{eq}} = 74.848 + a_1 \cdot c + a_2 \cdot c^{3/2} + a_3 \cdot c^2$.

hydration number, $Z_{\mathrm{t}} = Z_{\mathrm{ib}} + Z_{\mathrm{slow}}$ very well resembles the expected value for the whole investigated concentration range.

A comparison of the results on hydration for the two probed fitting approaches (fixed τ_{sw} and fixed τ_{bw}) is given in Figure 5.8. Only data points up to $c = 1\,\mathrm{mol\,L^{-1}}$ are presented, as for higher c both fitting alternatives virtually yield identical results for S_j, Z_{ib} and Z_{slow}. This is remarkable, as the difference in τ_{bw} is greatest at $c > 1\,\mathrm{mol\,L^{-1}}$ (Figure 5.5, but can be rationalized through the low amplitude of the bulk water process at these concentrations.

As is evident from Figure 5.8a, the differences of the two approaches manifest themselves in the solvent related amplitudes, leaving the ion-pair modes largely unaffected. The bulk water amplitude is systematically lower, and conversely the slow water + anion amplitude is systematically higher for the traditional fitting approach of fixed τ_{sw}. Consequently, the traditional approach yielded higher Z_{slow} with an infinite dilution limit of ~ 16.5, whereas $Z_{\mathrm{ib}}^{\circ} \approx 2.5$ is significantly lower than the expected value of 5.2. Apparently, fixing of τ_{sw} leads to an overestimation of Z_{slow}, which is partly, but not quantitatively, compensated by an underestimation of Z_{ib}. Quite consistent with previous results for the two effective solvation numbers are, however, the results obtained by fixing τ_{bw}. Rather robust against the chosen fitting approach seems to be the total hydration number, $Z_{\mathrm{t}} = Z_{\mathrm{ib}} + Z_{\mathrm{slow}}$, which shows deviations of +1.8 from the expected infinite dilution value for fixed τ_{sw} and -0.7 for fixed τ_{bw}.

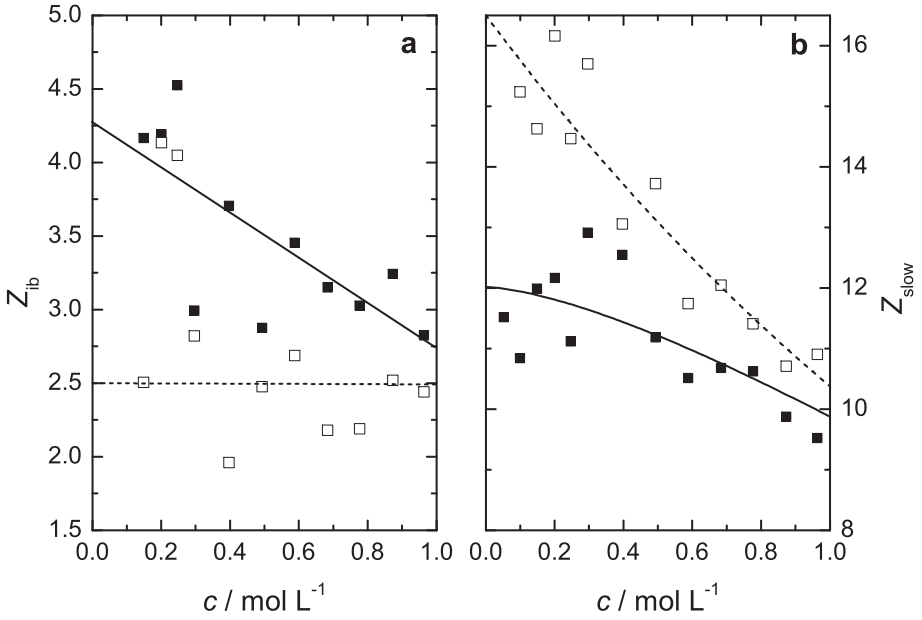

Figure 5.8: Comparison of the obtained hydration properties for the two alternative fitting procedures for NaH_2PO_4(aq) using fixed slow water relaxation times (open symbols) or fixed bulk water relaxation times (filled symbols). (a) Z_{ib} values and (b) Z_{slow} values for the two alternative approaches. Dotted lines represent empirical fits for fixed τ_{sw}, solid lines such for fixed τ_{bw}.

Na_2HPO_4(aq)

For Na_2HPO_4(aq) the disentanglement of cation and anion hydration is more complicated, as both, Na^+ and $HPO_4{}^{2-}$ are able to strongly bind water molecules. However, only for $HPO_4{}^{2-}$ slow water has been observed so far. The calculation of the effective hydration numbers follows the pattern as outlined for NaH_2PO_4(aq). For the effective dipole moment of $HPO_4{}^{2-}$ a value of 4.409 D was used.[93,96] The results for the concentration dependence of Z_{ib} and Z_{slow} are presented in Figure 5.9.

For the infinite dilution limit, strong deviations from the expected (ideal) values are observed. The number of strongly bound water molecules per unit of salt, $Z^\circ_{\mathrm{ib}}(Na_2HPO_4(aq))$ is expected to be the sum of the corresponding single ion values:

$$Z^\circ_{\mathrm{ib}}(Na_2HPO_4(aq)) = Z^\circ_{\mathrm{ib}}(HPO_4{}^{2-}) + 2 \cdot Z^\circ_{\mathrm{ib}}(Na^+) \tag{5.2}$$

The experimental value, however, is significantly lower than the expected one (about 4-5, or 30%). While this may suggest, that the additivity of Z°_{ib} is not strongly followed, it is interesting to note, that $Z^\circ_{\mathrm{ib}}(Na_2HPO_4(aq)) = 2 \cdot Z^\circ_{\mathrm{ib}}(Na^+)$. Also, the concentration dependence of $Z_{\mathrm{ib}}(Na_2HPO_4(aq)$ follows in an almost perfect way the one observed in NaCl(aq):

$$Z_{\mathrm{ib}}(Na_2HPO_4(aq)) = 2 \cdot Z_{\mathrm{ib}}(Na^+) \tag{5.3}$$

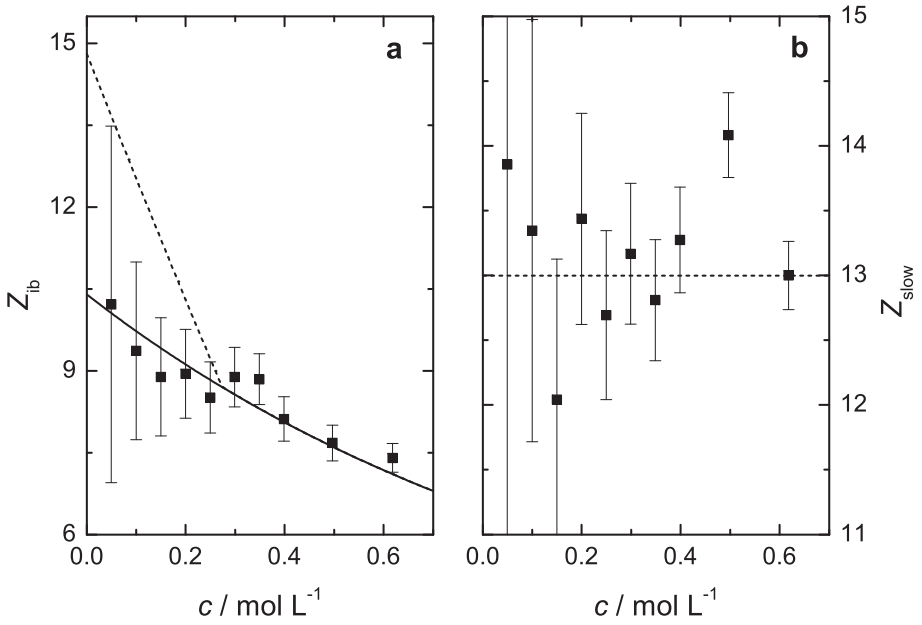

Figure 5.9: (a) Number of irrotationally bound, Z_{ib}, and (b) slow water molecules, Z_{slow}, per unit of solute. Symbols represent experimental values. Broken lines represent (a) expected values from NaCl(aq) & K_2HPO_4(aq) and (b) the average $Z_{\mathrm{slow}}(Na_2HPO_4(aq))$ for the whole investigated concentration range. Solid line in (a) represents the expected $Z_{\mathrm{ib}}(Na_2HPO_4(aq))$ value from NaCl(aq) only. Error bars, $\Delta Z_{\mathrm{ib}} = \Delta Z_{\mathrm{slow}}$ were estimated from the standard deviation, σ_{fit}, of the fit of the combined water related amplitudes, $S_{\mathrm{w}}^{\mathrm{eq}}$, according to $S_{\mathrm{w}}^{\mathrm{eq}} = 74.848 + a_1 \cdot c + a_2 \cdot c^{3/2} + a_3 \cdot c^2$.

where $c(Na^+) = 2 \cdot c(Na_2HPO_4)$. The solid line in Figure 5.9a represents the theoretical concentration dependence of $Z_{\mathrm{ib}}(Na^+)$ as obtained from NaCl(aq),[137] rather than an empirical fit of the $Z_{\mathrm{ib}}(Na_2HPO_4(aq))$ values. The dotted line in Figure 5.9a gives the expected value, if irrotational bonding due to HPO_4^{2-} is considered. The experimental Z_{ib} data suggest, that HPO_4^{2-} in Na_2HPO_4(aq) is not able to strongly bind water molecules, in marked contrast to the observations for K_2HPO_4(aq). This is corroborated by the results for the effective slow water hydration number, $Z_{\mathrm{slow}}(Na_2HPO_4(aq))$. Due to the high scattering of the data points, it is just possible to extract an average Z_{slow} value for all concentrations: $Z_{\mathrm{slow}} \approx 13$, thus also $Z^{\circ}_{\mathrm{slow}}(Na_2HPO_4(aq)) = 13$. Nevertheless, this is significantly higher than the value obtained from K_2HPO_4(aq). Considering the infinite dilution values only, it is possible to state, that the Na^+ hydration shell appears unchanged as compared to the one found in NaCl(aq), whereas the HPO_4^{2-} hydration shell is altered as compared to the one in K_2HPO_4(aq): HPO_4^{2-} is not able to irrotationaly bind water molecules, however, more water molecules are slowed in their rotational dynamics. The total hydration number $Z_{\mathrm{t}}(HPO_4^{2-})$, however, is approximately the same as found in K_2HPO_4.
However, it is quite likely that the strong resemblance of the experimental $Z_{\mathrm{ib}}(Na_2HPO_4(aq))$ to the literature values for Na^+ is a coincidence. It is reasonable to assume that both ions, Na^+ and HPO_4^{2-}, show a transition of irrotationaly bound to slow water due to ion pairing as outlined for NaH_2PO_4(aq).

5.2.3 Ion pairing

The position and amplitude of the two low frequency relaxation modes ($\tau_1 \sim 450\,\text{ps}$ & $\tau_2 \sim 80\,\text{ps}$) for NaH_2PO_4(aq) and the lowest frequency relaxation mode ($\tau_1 \sim 120\,\text{ps}$) for Na_2HPO_4(aq) suggest, that those are solute related. The position is consistent with ion-pair relaxation, but we have to keep in mind that also ion-cloud relaxation is contributing to the low frequency part of DR spectra in all electrolyte solutions (see Chapter 3). As a disentanglement of ion-pair and ion-cloud contribution is generally not possible in the moment,[32,137] the determined association constants have to be seen as an upper limit. This is most important for weakly associated electrolyte systems, as for those ion-cloud relaxation can contribute significantly to the determined amplitude (see Chapter 4.4).

NaH_2PO_4

For aqueous solutions of NaH_2PO_4 two relaxation processes can be attributed to ion-pair relaxation: one at $\tau_1 \sim 450\,\text{ps}$, the other at $\tau_2 \sim 80\,\text{ps}$. The relaxation time of the first process, τ_1, is significantly scattered over a broad range ($200 \leq \tau_1\,/\,\text{ps} \leq 700$). As this process is at the low end of the probed frequency range, it is in general difficult to extract reliable relaxation times. Due to the broad nature of the relaxation modes, the presence of a second solute related relaxation mode at the same frequency range is an additional complication. It is interesting to note, that this is the first time that two ion-pair processes can be resolved for a 1:1 electrolyte with DR. The amplitude of the lowest frequency process, S_1, shows an initial increase up to ~ 2 at about $0.5\,\text{mol}\,\text{L}^{-1}$, a value that is kept roughly constant up to $1\,\text{mol}\,\text{L}^{-1}$ (Figure 5.2). At higher concentrations it is no longer possible to resolve this process. This behavior is consistent with the low frequency process observed in NaCl(aq). Therefore, the lowest frequency process in NaH_2PO_4(aq) cannot solely be attributed to ion-pair rotation, but also contains contributions from ion-cloud relaxation. The second process shows a relaxation time, τ_2, that can smoothly be extrapolated to $\sim 80\,\text{ps}$. This indicates, that this relaxation is solely due to ion-pair rotation, and that all contributions from ion-cloud relaxation are found within the first process.
Derivation of standard state association constants, K_A°, was done in the way described for potassium phosphates (see Section 4.4). Effective dipole moments, $\mu_{\text{eff,IP}}$, of the different types of ion pairs were derived using the Barthel model,[53] with ionic radii $r(Na^+) = 102\,\text{pm}$, $r(H_2PO_4^-) = 200\,\text{pm}$, $r(H_2O) = 143\,\text{pm}$, polarizabilities of $1.44\,\text{Å}^3$ for water,[109] $0.258\,\text{Å}^3$ for Na^+ and $5.79\,\text{Å}^3$ for $H_2PO_4^-$[107] and an effective dipole moment $\mu_{\text{eff}}(H_2PO_4^-) = 5.904\,\text{D}$.[93,96] Then the $\mu_{\text{eff,IP}}$ were used to calculate ion-pair concentrations, c_{IP}, from the relaxation amplitudes S_1 and S_2 via Eq. 1.47. Association constants, K_1 for the process due to ion-pair + ion-cloud relaxation and K_2 for the process due to ion pairs only, were obtained in the usual way (Eq. 1.72) and extrapolated to infinite dilution by means of an Guggenheim-type equation (Eq. 1.74) to yield standard state association constants K_1° and K_2°. The overall standard state association constant, K_A°, is obtained by an Guggenheim-extrapolation of the overall association constant $K_A = c_{\text{IP}}/(c_{\text{anion}} \times c_{\text{cation}})$, where c_{IP} is the sum of both detected IP concentrations. Extrapolated association constants are summarized in Table 5.5 together with the rotational correlation times obtained via Eq. 1.56 and μ_{eff} for all possible types of IPs.

Table 5.5: Relaxation Times, τ, of All Possible Ion Pair Species, Estimated via Eq. (1.56) Assuming Stick or Slip Boundary Conditions, Together with Their Effective Dipole Moments, μ_{eff} as well as Standard State Association Constants for the Two Lowest Frequency Processes in NaH_2PO_4(aq), K_1° and K_2°, and the Overall Standard State Association Constant for NaH_2PO_4(aq), K_A°.

	τ_{stick}	τ_{slip}	μ_{eff}	K_1°	K_2°	K_A°
CIP	39.4	4.49	5.28	∞^b	∞^b	
SIP	80.8	23.4	19.6	7 ± 1	$\underline{5.0 \pm 0.6}$	11 ± 3^c
2SIP	145	61.6	31.9	$\underline{1.3 \pm 0.2}$	2.7 ± 0.3	

[a] Units: τ in ps; μ_{IP} in Debye ($1\,\text{D} = 3.3356 \cdot 10^{-30}\text{Cm}$); K_1°, K_2° and K_A° in L mol^{-1}. [b] Association constants ∞ denote, that $c_{\text{IP}} > c$. [c] Combined 2SIP + SIP model. Preferred K_x° values (x = 1, 2) are underlined.

A comparison of the experimental relaxation times of both processes with the calculated rotational correlation times (Eq. 1.56) reveals that SIP and 2SIP may be responsible for the second process, however, τ_1 is far higher than the calculated rotation correlation time for *slip* and *stick* boundary condition. This is mainly related to the difficulties in the separation of the two solute related processes, but also hints at a strong contribution from ion-cloud relaxation. Possible combinations of IPs are 2SIP + SIP and SIP + CIP. As Na^+ is highly solvated ($Z_{\text{ib}} \approx 5.2$), it is reasonable to attribute the first process to 2SIP + ion-cloud relaxation and the second to SIP reorientation. A contribution of CIPs can be disregarded for two reasons: first, the expected relaxation time of a CIP, $4 \leq \tau \,/\, \text{ps} \leq 40$, is much shorter than the relaxation time of the second (faster) process. Second, assignment of any of the two IP relaxations to CIPs, leads to $c_{\text{IP}} > c$, which is physically impossible. With the assumption of a combined 2SIP + SIP model, a standard state overall association constant of $K_A^\circ = 11 \pm 3\,\text{L mol}^{-1}$ was calculated, which has to be regarded as an upper limit due to the contribution of ion-cloud relaxation. This value is significantly higher than the only available literature value from dilute conductivity measurements $K_A^\circ = 1.78$.[155] This is also the case for KH_2PO_4(aq) (Chapter 4.4.2). However, the concentration dependence of τ_2 indicates, that the ion-cloud contribution is completely subsumed in the first relaxation. Thus K_2° can be regarded as an good estimate for the true SIP association constant. This value is still significantly higher than the one reported by Pethybridge *et al.*, and shows that also dilute conductivity measurements have difficulties in determining weak ion association.

Na_2HPO_4

As already mentioned above, the lowest frequency process in Na_2HPO_4 is solute related. The relaxation time τ_1 shows a steep decrease for $c \leq 0.25\,\text{mol L}^{-1}$, and gradually levels off to $\tau \sim 100\,\text{ps}$ at higher concentrations. The relaxation strength, S_1, shows a marked non-linear behavior, with a steep increase for $c \leq 0.25\,\text{mol L}^{-1}$ and decreasing slope for higher

c (Figure 5.4). The already high amplitude at the lowest concentration ($c = 0.05\,\mathrm{mol\,L^{-1}}$) indicates strong ion-pairing, and, for reasons already discussed in Chapter 4.4, allows to neglect ion-cloud relaxation for the purpose of K_A° extrapolation. A contribution to this mode from ion cloud relaxation, however, is evident from the strong decrease of τ_1.
The calculation of μ_eff of the different possible ion-pair species was done by the method described by Barthel *et al.*,[53] using $\alpha(\mathrm{HPO_4^{2-}}) = 5.79\,\mathrm{Å}^3$, $r(\mathrm{HPO_4^{2-}}) = 200\,\mathrm{pm}$ and an effective dipole moment $\mu_\mathrm{eff}(\mathrm{H_2PO_4^-}) = 4.409\,\mathrm{D}$.[93,96] As $\mathrm{Na_2HPO_4(aq)}$ is a 1:2 electrolyte, also the distinction between center of mass, o_{CM}, and center of hydrodynamic stress, o_{CHS}, for the pivot of the dipole rotation had to be taken into account for the calculation of μ_IP. The relaxation strength of the first process, S_1, was translated into ion-pair concentrations, c_IP via Eq. 1.47, using the calculated $\mu_\mathrm{eff,IP}$. Association constants, K_A were calculated in the usual way and extrapolated with the help of Eq. 1.74 to yield standard state association constants, K_A°. Table 5.6 contains the results on dipole moments and infinite dilution association constants for all possible ion pairs.

Table 5.6: Relaxation Times, τ, of All Possible Ion Pair Species, Estimated via Eq. (1.56) Assuming Stick or Slip Boundary Conditions, Together with The Effective Dipole Moments, μ_eff and Standard State Association Constants for Center of Mass (CM) and Center of Hydrodynamic Stress (CHS) Boundary Conditions.[a]

	τ_stick	τ_slip	μ_eff(CM)	K_A°(CM)	μ_eff(CHS)	K_A°(CHS)
CIP	39.4	4.49	14.0	$(4 \pm 1)\times10^3$	14.5	$(1.4 \pm 0.6)\times10^4$
SIP	80.8	23.4	32.4	54 ± 5	34.8	$\underline{42 \pm 2}$
2SIP	145	61.6	49.4	20 ± 1	53.2	16.2 ± 0.8

[a]Units: τ in ps, μ_eff in Debye ($1\mathrm{D} = 3.3356 \times 10^{-30} C \cdot m$), K_A° in $\mathrm{L\,mol^{-1}}$. Preferred K_A° value is underlined.

The experimental relaxation time τ_1 is consistent with 2SIPs and SIPs as the dominating ion-pair species. The strong decrease of τ_1 with c is due to the influence of ion-cloud relaxation on τ_1, which is further illustrated by the fact that τ_IP is viscosity dependent and should thus increase with c. Ion cloud relaxation on the other hand shows the inverse concentration dependence.[117] Taking into account the concentration dependence of the viscosity (estimates via Eq. 1.56 are generally done for infinite dilution), the SIP relaxation time of the most concentrated sample ($c = 0.618\,\mathrm{mol\,L^{-1}}$) was estimated to be in between 35 ps for *slip* and 119 ps for *stick* boundary conditions. For the 2SIP relaxation time the values are 91 ps for *slip* and 215 ps for *stick* boundary conditions. The experimental values agree very well with the rotational correlation time for SIP under near stick boundary conditions, but also with a 2SIP under near slip boundary conditions. As both ions are highly hydrated, and it seems rather unlikely that they completely loose their hydration sphere within the ion pair, it is reasonable to assume *stick* boundary conditions. This strongly hints at SIPs as the dominating type of ion pair. Also, the available literature data on ion-association in $\mathrm{Na_2HPO_4(aq)}$ is scarce. The only experimental value is from dilute

conductivity measurements, with $K_A^\circ = 47.6\,\mathrm{L\,mol^{-1}}$.[155] This is in excellent agreement with the DR results assuming solely formation of SIP under both, CM and CHS boundary conditions.

5.3 Aqueous solutions of $(NH_4)H_2PO_4$ and $(NH_4)_2HPO_4$

5.3.1 Choice of fit model and assignment of relaxation modes

Solutions of $(NH_4)H_2PO_4$ ($c \leq 2.459\,\mathrm{mol\,L^{-1}}$) and $(NH_4)_2HPO_4$ ($c \leq 3.173\,\mathrm{mol\,L^{-1}}$) in water have been measured at 25 °C up to the saturation limit, over the frequency range $0.2 \leq \nu/\,\mathrm{GHz} \leq 89$. Sample pH was determined to ± 0.01 at room temperature with a glass electrode (Metler Toledo, InLab Micro), which was calibrated with standard buffer solutions of pH = 4.01 and 7.00 before measurement. The measured pH values (Table 5.7) indicated that a maximum of 5% of $H_2PO_4^-$(aq) was hydrolyzed in solutions of $(NH_4)H_2PO_4$ at all salt concentrations. Hydrolysis was thus neglected for this salt. The hydrogen phosphate ion in $(NH_4)_2HPO_4$(aq), however, shows considerable hydrolysis. The pH values of the $(NH_4)_2HPO_4$(aq) samples were therefore used to calculate the actual speciation. Only the hydrolysis to $H_2PO_4^-$(aq) proofed to be significant at the detected pH values and was thus solely considered. Table 5.7 also lists the calculated $H_2PO_4^-$(aq) and HPO_4^{2-}(aq) concentrations assuming $pK_a = 7.21$ for $H_2PO_4^-$(aq).[144]

Both sets of spectra show a marked difference in the concentration dependence of the static permittivity, $\varepsilon = \lim_{\nu\to 0}\varepsilon' = \varepsilon_1$. $(NH_4)H_2PO_4$(aq) exhibits a steady increase in ε with increasing c, whereas the same quantity in $(NH_4)_2HPO_4$(aq) shows a steady decrease after an initial increase at low c. Qualitatively, the two ammonium salts show the same concentration behavior for ε as the corresponding potassium salts, but significant differences to the sodium salts. The static permittivity of aqueous electrolyte solutions is influenced by several factors: kinetic depolarization, a dilution effect, as the water density is reduced upon addition of solute, a hydration effect, as strongly bound water molecules are no longer able to contribute to the total polarization and a solute effect, as the solute as such or subsequently formed species (most important: ion pairs) may have permanent dipole moments and thus contribute to the macroscopic dipole moment.[18] The latter two are generally the major factors in electrolyte solutions. As ε of the ammonium salts shows a very similar concentration behavior as the respective potassium salts, it is already possible to state that the hydration and ion-pairing of ammonium phosphates is similar to the potassium phosphates.

Regarding the dielectric loss, $\varepsilon''(\nu)$, both sets of spectra show similar behavior. The maximum in $\varepsilon''(\nu)$ exhibits a clear red-shift and drop in height with increasing c. At the same time the dielectric loss curve becomes marked asymmetric, with an shoulder emerging at the low frequency end. Those observations are consistent with previous DRS investigations on aqueous electrolyte solutions,[30,164,179] and hint at ion-pair formation and the emergence of slow water.

Different from the potassium and sodium phosphates, free fits of the two ammonium phosphates yielded bulk water relaxation times that did **not** show a simple dependence on the cation concentration. Moreover, they also differed significantly from the results obtained

Table 5.7: Concentrations, c, and pH Values of Ammonium Phosphate Salt Solutions. For $(NH_4)H_2PO_4$(aq) the Measurements Were Restricted to $c < 1\,\mathrm{mol\,L^{-1}}$. For $(NH_4)_2HPO_4$(aq) also the calculated $c(H_2PO_4^-)$ and $c(HPO_4^{2-})$ are given. [a]

$(NH_4)H_2PO_4$		$(NH_4)_2HPO_4$			
c	pH	c	pH	$c(H_2PO_4^-)$	$c(HPO_4^{2-})$
0.09976	4.41	0.09905	7.56	0.03058	0.06847
0.2018	4.29	0.1976	7.50	0.06698	0.1306
0.2964	4.27	0.2962	7.45	0.1082	0.1880
0.3917	4.16	0.3914	7.43	0.1472	0.2442
0.4865	4.11	0.4886	7.41	0.1890	0.2996
0.5810	4.07	0.5813	7.39	0.2313	0.3501
0.6695	4.04	0.6719	7.39	0.2673	0.4046
0.7520	4.02	0.7647	7.38	0.3085	0.4563
0.8575	3.97	0.8558	7.37	0.3500	0.5059
0.9465	3.94	0.9468	7.36	0.3925	0.5544
		1.367	7.35	0.5739	0.7922
		1.771	7.33	0.7641	1.0073
		2.165	7.31	0.9582	1.2063
		2.512	7.31	1.1119	1.3998
		2.851	7.31	1.2623	1.5891
		3.173	7.30	1.4228	1.7504

[a] Units: c in $\mathrm{mol\,L^{-1}}$.

for NH_4Cl(aq).[164] The marked differences in the relaxation time, however, showed only up for $c \geq 0.75\,\mathrm{mol\,L^{-1}}$. At lower concentrations, the trend in τ_{bw} appears to be dependent on $c(NH_4^+)$ only. Nevertheless, it was refrained from fixing the bulk water relaxation time according to the results of NH_4Cl(aq).

Analysis with Eq. 1.19 showed that both sets of spectra are best fitted with a three-Debye model, which was confirmed independently by the relaxation time distribution analysis of Zasetsky.[88] Fit parameter of the three-Debye model for $(NH_4)H_2PO_4$(aq) are presented in Table 5.8, Figure 5.10 shows typical spectra and Figure 5.11 the concentration dependence of the relaxation amplitudes. An analogous representation of the results for the three-Debye fit of $(NH_4)_2HPO_4$(aq) is given in Table 5.9, Figure 5.12 and Figure 5.13.

The assignment of molecular species to the different relaxation modes is analogous to the respective potassium and sodium salts (see Chapters 4.2 & 5.2.1). The main relaxation peak, centered at ∼18 GHz is attributed to bulk water, i.e. water molecules that are relatively unperturbed as compared to neat water. The intermediate mode, centered at ∼8 GHz contains contributions from slow water and the anion. The lowest frequency process at ∼1.6 GHz is a composite mode as well: different to the one at ∼8 GHz though, it does not solely contain contributions from molecular species, but is a sum of ion-pair reorientation and ion-cloud relaxation. The nature of the ion pair will be discussed in Chapter 5.3.3.

Table 5.8: Concentration Dependence of the Dielectric Relaxation Parameters of a Three-Debye Fit of Aqueous Solutions of $(NH_4)H_2PO_4$ at 25 °C: Concentration, c, Limiting Permittivities, ε_j ($j = 1-3$) & ε_∞, Relaxation Times, τ_j, VNA Conductivities, κ_{VNA}, and the Value of the Reduced Error Function, χ^2_{r}.[a,b]

c	ε_1	τ_1	ε_2	τ_2	ε_3	τ_3	ε_∞	κ_{VNA}	χ^2_{r}
0.09976	79.25	144	78.27	25.0F	74.89	8.16	5.76	0.812	0.039
0.2018	79.67	125	77.65	23.0F	71.56	8.00	5.68	1.50	0.039
0.2964	80.54	99.3	77.04	18.3	67.04	7.88F	5.98	2.07	0.076
0.3917	81.38	91.1	76.72	17.0	63.11	7.77F	6.28	2.61	0.125
0.4865	81.68	95.2	76.57	19.0F	62.21	7.67	6.24	3.10	0.144
0.5810	82.73	104	76.88	19.6	60.10	7.56F	6.22	3.56	0.059
0.6695	83.28	103	76.62	19.0F	56.92	7.43	6.43	3.98	0.081
0.7520	83.53	91	75.82	19.0F	55.78	7.38	6.46	4.42	0.089
0.8575	83.98	96	75.49	18.9	53.51	7.3F	6.54	4.77	0.090
0.9465	84.74	99	75.40	18.8	51.02	7.23	6.95	5.12	0.166
1.383	86.19	99	72.82	19.1	45.72	6.95	6.87	6.63	0.093
1.798	88.37	108	71.27	19.8	41.29	6.71F	7.10	7.81	0.100
2.188	90.25	118	69.88	20.7	37.83	6.56F	7.41	8.66	0.129
2.459	90.85	126	68.68	21.6	35.75	6.46	7.74	9.13	0.143

[a] Units: c in $\mathrm{mol\,L^{-1}}$, τ_j in ps, κ in $\mathrm{S\,m^{-1}}$; [b] Parameter values followed by the letter F were not adjusted in the fitting procedure.

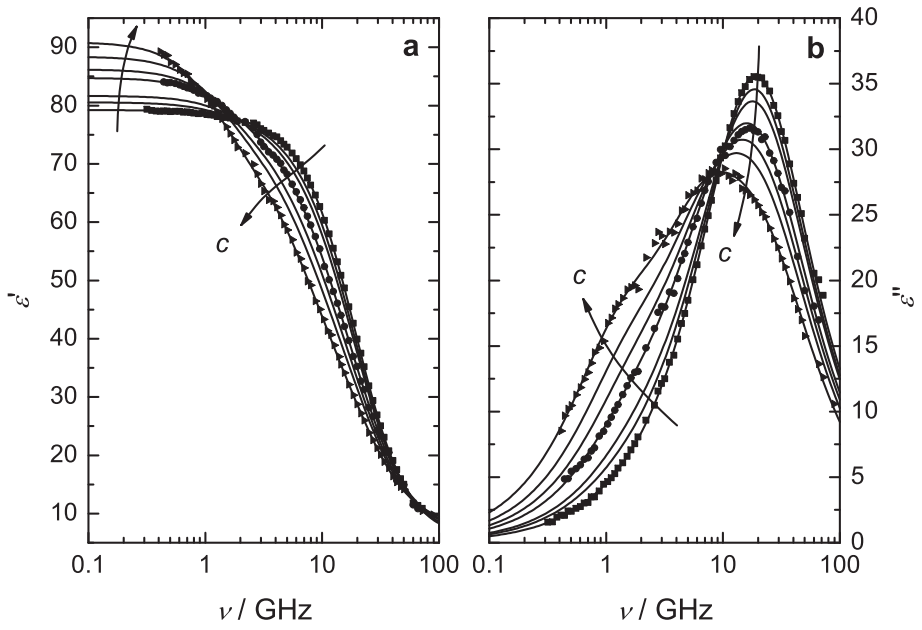

Figure 5.10: Relative permittivity (a) and dielectric loss (b) spectra for $(NH_4)H_2PO_4$(aq) at 25 °C and concentrations $c\,/\,(\mathrm{mol\,L^{-1}})$ = 0.09976, 0.2964, 0.4865, 0.9465, 1.383, 1.798 and 2.459. Symbols represent experimental data (mostly omitted for visual clarity), lines the D+D+D fit; arrows indicate increasing concentration c.

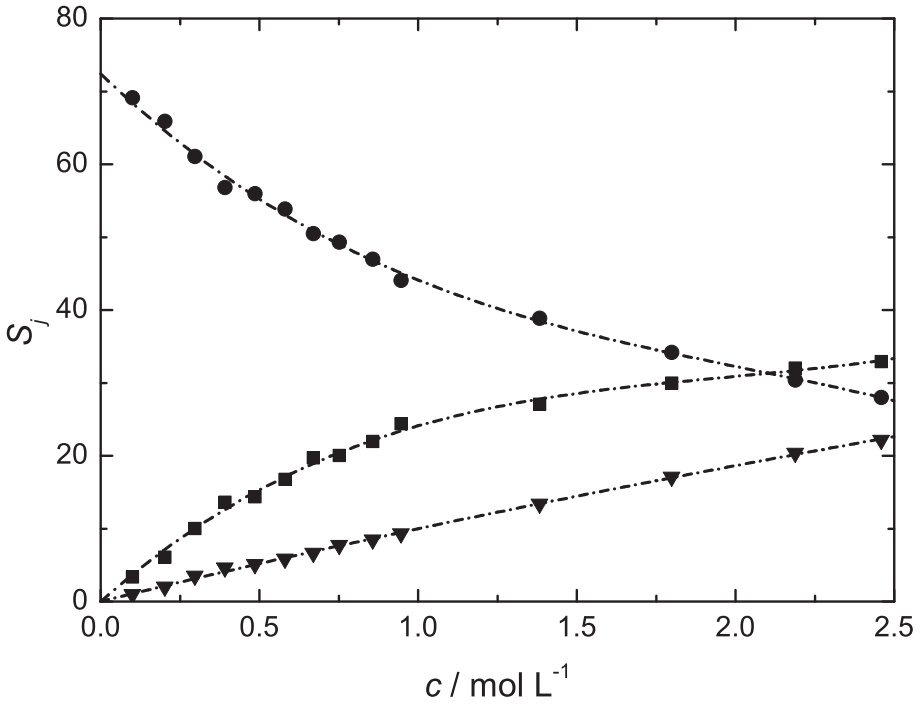

Figure 5.11: Amplitudes of the three Debye relaxation modes for $(NH_4)H_2PO_4$(aq) as a function of solute concentration at 25 °C: ion-pair + ion-cloud relaxation (S_1,▼), slow water + anion (S_2,■) and bulk water (S_3,●). Lines are visual guides only.

Table 5.9: Concentration Dependence of the Dielectric Relaxation Parameters of a Three-Debye Fit of Aqueous Solutions of $(NH_4)_2HPO_4$ at 25 °C: Concentration, c, Limiting Permittivities, ε_j ($j = 1-3$) & ε_∞, Relaxation Times, τ_j, VNA Conductivities, κ_{VNA}, and the Value of the Reduced Error Function, χ^2_{r}.[a,b]

c	ε_1	τ_1	ε_2	τ_2	ε_3	τ_3	ε_∞	κ_{VNA}	χ^2_{r}
0.09905	80.54	193	77.64	19.0F	73.26	8.06	5.89	1.41	0.028
0.1976	81.07	161	76.98	19.0F	69.15	7.85	5.91	2.45	0.065
0.2962	81.02	140	76.36	19.0F	65.66	7.71	5.85	3.32	0.045
0.3914	81.26	141	76.04	19.0F	62.88	7.60	5.91	4.07	0.081
0.4886	81.30	143	75.77	19.0F	59.17	7.35	5.95	4.78	0.108
0.5813	80.53	113	75.21	19.0F	57.48	7.32	6.29	5.42	0.071
0.6719	80.44	113	74.70	18.4	54.60	7.21	6.46	5.97	0.075
0.7647	80.99	124	75.12	19.0F	53.34	7.21	6.47	6.54	0.081
0.8558	80.52	111	74.20	18.7	51.72	7.21	6.68	7.03	0.092
0.9468	80.28	129	73.30	19.0F	49.68	7.02	6.56	7.33	0.093
1.366	78.29	131	70.81	20.6	44.01	6.81	6.91	8.96	0.099
1.771	77.56	142	68.68	21.3	39.72	6.77	7.43	10.1	0.110
2.165	76.30	144	65.73	21.2	34.57	6.40	7.67	10.8	0.094
2.512	75.03	150	62.78	21.2	29.91	5.88	7.83	11.1	0.105
2.851	73.40	152	60.09	21.8	27.49	5.64	7.98	11.2	0.124
3.173	72.17	157	57.37	22.6	25.76	5.57	8.18	11.0	0.115

[a] Units: c in $\mathrm{mol\,L^{-1}}$, τ_j in ps, κ in $\mathrm{S\,m^{-1}}$; [b] Parameter values followed by the letter F were not adjusted in the fitting procedure.

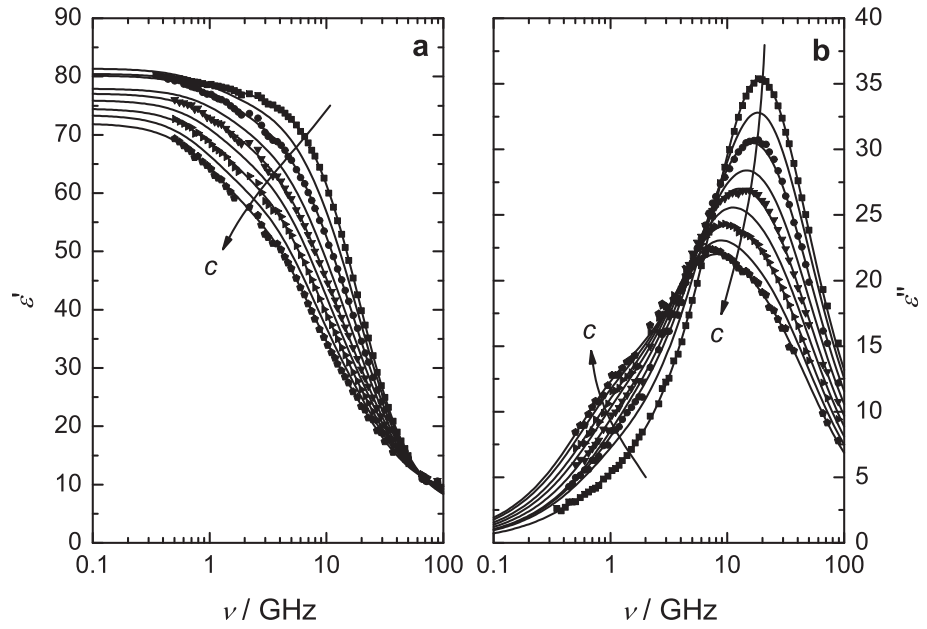

Figure 5.12: Relative permittivity (a) and dielectric loss (b) spectra for $(NH_4)_2HPO_4$(aq) at 25 °C and concentrations $c\,/\,(\mathrm{mol\,L^{-1}})$ = 0.09905, 0.4886, 0.9468, 1.366, 1.771, 2.165, 2.512, 2.851 and 3.173. Symbols represent experimental data (partly omitted for visual clarity), lines the D+D+D fit; arrows indicate increasing concentration c.

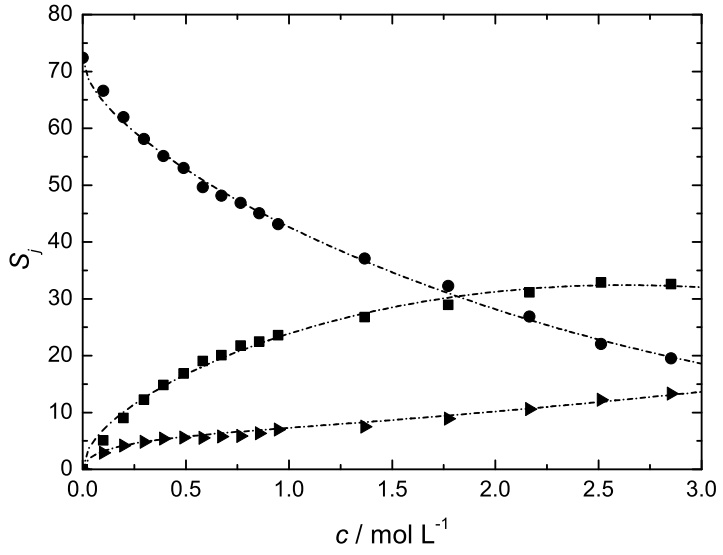

Figure 5.13: Amplitudes of the three Debye relaxation modes for $(NH_4)_2HPO_4$(aq) as a function of solute concentration at 25 °C: ion-pair + ion-cloud relaxation (S_1,▶), slow water + anion (S_2,■) and bulk water (S_3,●). Lines are visual guides only.

5.3.2 Hydration

The solvent related amplitudes are S_2 and S_3, with the later being the bulk water amplitude and the former a composite mode of slow water and the anion. For both aqueous salt solutions S_3 shows a monotonic decrease with increasing salt concentration, whereas S_2 exhibits a monotonic increase. The respective slopes are greatest at low concentration ($c \leq 0.5\,\mathrm{mol\,L^{-1}}$), and are leveling off at higher c. For $(NH_4)_2HPO_4$(aq) there is even a decrease in S_2 at the highest solute concentration. This hints at solvation shell overlap, especially as all involved ions exhibit significant hydration (mainly slow water).

The composite mode S_2 of $(NH_4)_2HPO_4$(aq) contains contributions of the two present anions, hydrogen phosphate and dihydrogen phosphate, and slow water around them. In order to calculate the amplitude solely due to HPO_4^{2-} and associated slow water, the relaxation strength of the present $H_2PO_4^-$ and corresponding slow water was evaluated from the results of $(NH_4)H_2PO_4$(aq). First, the amplitude $S_2((NH_4)H_2PO_4(aq))$ was fitted for $c \leq 1.383\,\mathrm{mol\,L^{-1}}$ with an third order polynomial, $S_2 = 36.21c - 11.18c^2 - 0.5928c^3$. Then the amplitudes due to $H_2PO_4^-$(aq) in the $(NH_4)_2HPOP_4$(aq) system were calculated with this empirical function and subtracted from the experimental $S_2((NH_4)_2HPO_4(aq))$.

The amplitude S_3 and a non-resolvable fast water mode were combined to a single bulk water mode $S_b = S_3 + (\varepsilon_\infty - \varepsilon_\infty(0))$, where $\varepsilon_\infty(0) = 3.52$ is the low frequency limit of bulk water. For the calculation of the slow water amplitude, S_{sw}, the amplitude of the intermediate process, S_2, had to be corrected for the free anion contribution, S_-. The later was obtained from the free anion concentration, $c_- = c - c_{\mathrm{IP}}$ (see Section 5.3.3) with the help of Eq. 1.47, assuming anion dipole moments of 4.409 D for HPO_4^{2-}(aq) and 5.905 D for $H_2PO_4^-$(aq).[93,96] Hydration numbers Z_{ib} and Z_{slow} were then calculated according to Eqs. 3.2 & 4.1. As $H_2PO_4^-$ and NH_4^+ are not able to strongly bind water, the ib water in $(NH_4)_2HPO_4$(aq) can solely be attributed to HPO_4^{2-}. Error bars, $\Delta Z_{\mathrm{ib}} = \Delta Z_{\mathrm{slow}}$ were estimated from the standard deviation, σ_{fit}, of the fit of the combined water related amplitudes, S_{w}, according to $S_{\mathrm{w}} = 74.848 + a_1 \cdot c + a_2 \cdot c^{3/2} + a_3 \cdot c^2$.

Figures 5.14 & 5.15 show the results for $(NH_4)H_2PO_4$(aq) and $(NH_4)_2HPO_4$(aq) respectively. Interestingly, Z_{ib} for both salts (Figures 5.14a & 5.15a) are essentially identical and have physically meaningless negative values if the usual treatment of kinetic depolarization under *slip* boundary conditions is chosen. Calculation of Z_{ib} neglecting kinetic depolarization yields higher values (filled circles in Figures 5.14a & 5.15a). For $(NH_4)H_2PO_4$(aq) the experimental values obtained for the two boundary conditions are both non-realistic, as *slip* boundary conditions results in physically meaningless negative values, whereas those obtained neglecting kinetic depolarization are tentatively too high. A previous DRS study on NH_4Cl(aq) showed that NH_4^+ is not able to irrotationally bind water molecules,[164] though no actual Z_{ib} were presented. Also, as shown in this work, the dihydrogen phosphate anion is not able to freeze water rotation. Assuming sub-*slip* conditions would result in reasonable Z_{ib} values around 0. The same treatment for the results of $(NH_4)_2HPO_4$(aq) again shows, that the expected values (from K_2HPO_4(aq)) are in between the results for *slip* boundary conditions and neglect of kinetic depolarization. As in both salts only HPO_4^{2-} is able to irrotationally bind water molecules, the Z_{ib} values should be similar and converge at the infinite dilution limit.

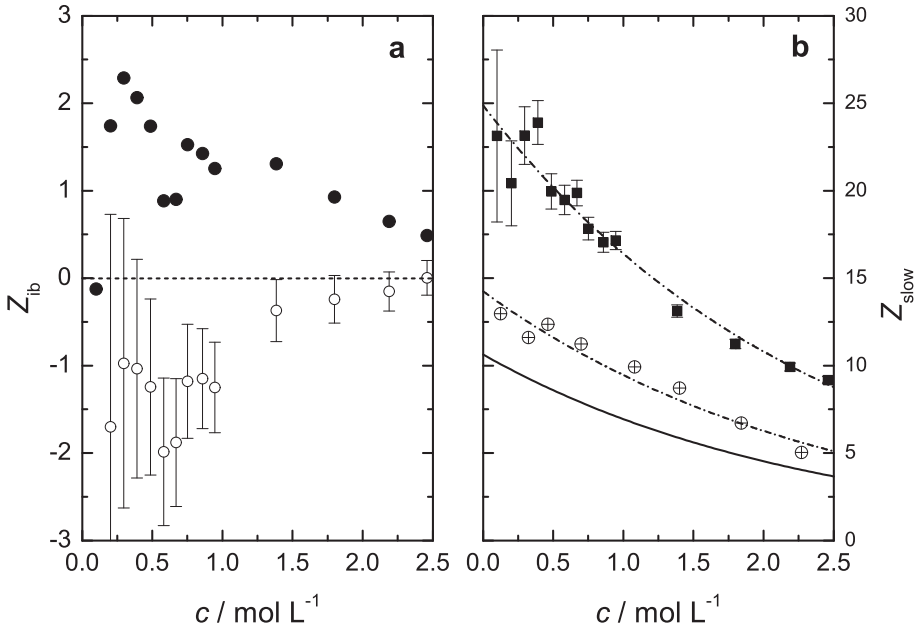

Figure 5.14: (a) Number of irrotationally bound, Z_{ib}, water molecules per unit of salt for $(NH_4)H_2PO_4$(aq) as calculated for *slip* (○) boundary conditions and negligible kinetic depolarization (●). The broken line just marks $Z_{\mathrm{ib}} = 0$, error bars have only been included for *slip* boundary conditions for visual clarity. (b) Number of slow water molecules, Z_{slow}, per unit of solute. Symbols represent experimental values for $(NH_4)H_2PO_4$(aq) (■) and NH_4Cl(aq)[164] (⊕), broken lines empirical fits thereof; solid line represents the c dependence of $Z_{\mathrm{slow}}(H_2PO_4^-)$.

The present results indicate, that for a correct assignment of Z_{ib} values of NH_4^+ salts sub-*slip* boundary conditions have to be chosen. A similar behavior has been observed for Cs^+(aq).[141] Also, a recent DRS study on LiI(aq) and CsI(aq) gave reasonable hydration numbers for LiI(aq) assuming slip boundary conditions, yet for CsI(aq) neither *slip* boundary conditions nor neglect of kinetic depolarization yielded satisfactory results.[180] Both ions, Cs^+ and NH_4^+ seem to be best described under sub-*slip* conditions. It appears like *slip* boundary conditions apply well to small, non-polarizable cations, whereas big and highly polarizable cations need sub-*slip* conditions for a correct assignment of Z_{ib} values.

The obtained Z_{slow} show a strong decrease with increasing solute concentration for both salts, with $(NH_4)_2HPO_4$(aq) exhibiting a more expressed decrease at low c. Both sets of Z_{slow} values were best described by a simple exponential function, $Z_{\mathrm{slow}} = A \cdot \exp(-c/B)$, with $A = 24.9 \pm 0.7, B = 2.4 \pm 0.2$ for $(NH_4)H_2PO_4$(aq) and $A = 37.0 \pm 0.8, B = 0.53 \pm 0.02$ for $(NH_4)_2HPO_4$(aq). The infinite dilution values (the A parameter) of the salts are in reasonable agreement with the sum of the respective single ion hydration numbers, though in the case of $(NH_4)_2HPO_4$(aq) $Z^{\circ}_{\mathrm{slow}}$ is tentatively too low. Here the position of the fixed slow water + anion mode has a crucial influence on the obtained Z_{slow}.

Fitting the concentration dependence of $Z_{\mathrm{slow}}((NH4)^+(aq))$ as determined by Shaukat,[164] with the same simple exponential function ($A = 14.2 \pm 0.6, B = 2.4 \pm 0.2$) allows the

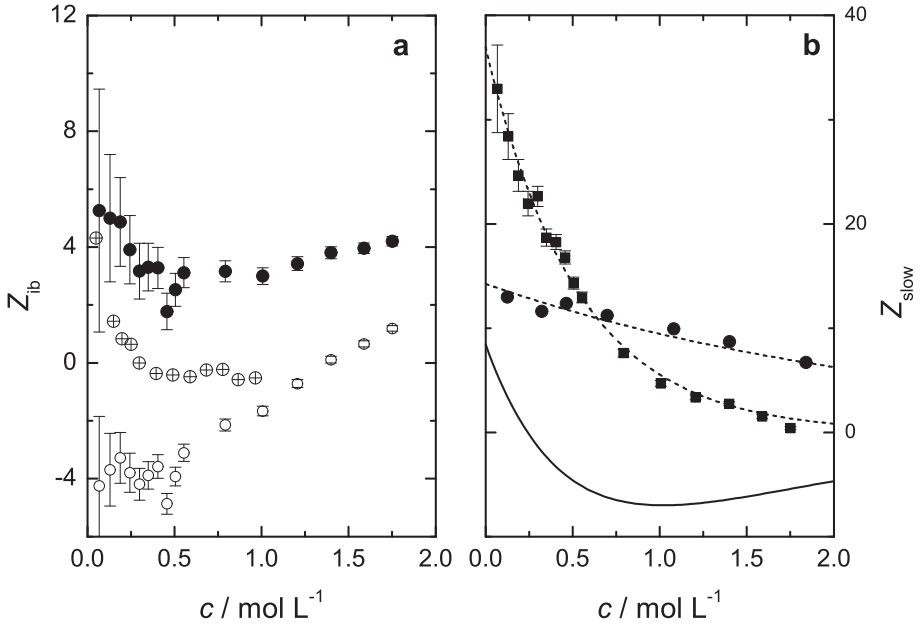

Figure 5.15: (a) Number of irrotationally bound, Z_{ib}, water molecules per unit of salt for $(NH_4)_2HPO_4$(aq) as calculated for no kinetic depolarization (●) and *slip* boundary conditions (○). Symbols (⊕) represent the respective values for K_2HPO_4(aq). (b) Number of slow water molecules, Z_{slow}, per unit of solute. Symbols represent experimental values for $(NH_4)_2HPO_4$(aq) (■) and NH_4Cl(aq)[164] (●), broken lines empirical fits thereof using a simple exponential . Solid line represents the c dependence of $Z_{\mathrm{slow}}(HPO_4{}^{2-})$.

extraction of $Z_{\mathrm{slow}}(c(\mathrm{anion}))$, which are given as solid lines in Figures 5.14b & 5.15b. For $H_2PO_4{}^-$ the usual monotonous decrease with increasing c is obtained, with $Z^\circ_{\mathrm{slow}} = 10.6 \pm 1.3$, whereas for $HPO_4{}^{2-}$ a non-monotonous behavior is observed with $Z^\circ_{\mathrm{slow}} = 8 \pm 2$. For concentrations $c > 0.25\,\mathrm{mol\,L^{-1}}$, even physically meaningless negative values for Z_{slow} are reached. This hints that the additivity of single ion Z_{slow} is strictly only true at infinite dilution but not for finite concentrations especially for solutions of highly hydrated ions. However, difficulties in the subtraction of contributions due to $H_2PO_4{}^-$ are probably the main reason for the negative Z_{slow} values.

5.3.3 Ion association

As the fit model and behavior of the single relaxation modes of both salts are broadly similar, ion-pairing results are discussed together. The low frequency relaxation of both salts is solute related with the respective relaxation times, $\tau_1((NH_4)H_2PO_4(\mathrm{aq})) \approx 100\,\mathrm{ps}$ and $\tau_1((NH_4)_2HPO_4(\mathrm{aq})) \approx 140\,\mathrm{ps}$, hinting at ion-pair relaxation. This is also indicated by comparing experimental τ_1 with rotation correlation times (Tables 5.10 & 5.11) for different types of ion pairs as obtained via Eq. 1.56. Both processes exhibit an initial drop of τ_1 to ∼90 ps and ∼110 ps for $(NH_4)H_2PO_4$(aq) and $(NH_4)_2HPO_4$(aq) respectively at $c \approx 0.5\,\mathrm{mol\,L^{-1}}$, with a subsequent increase at higher c. This behavior is in line with a contribution of ion-cloud relaxation to τ_1 at low concentrations, as well as a general

increase of relaxation time with c due to the increasing viscosity (Eq. 1.56). The amplitude, $S_1((NH_4)H_2PO_4(aq))$, shows linear behavior over the entire concentration range, whereas $S_1((NH_4)_2HPO_4(aq))$ exhibits a steep increase at $c < 0.2\,\mathrm{mol\,L^{-1}}$ followed by a linear increase at higher c. Standard state association constants, K_A°, were determined in the same way as for potassium phosphates (Chapter 4) and sodium phosphates (Chapter 5.2.3). As $(NH_4)_2HPO_4(aq)$ is a mixture of hydrogenphosphate and dihydrogenphosphate (Table 5.7), ion-pairing was evaluated in an analogous way as for $K_3PO_4(aq)$, using the results of $(NH_4)H_2PO_4(aq)$.
For the calculation of bare (gas phase) dipole moments of the respective ion pairs, a radius of $r(NH_4^+) = 148\,\mathrm{pm}$ was assumed, effective dipole moments were calculated using a polarizability $\alpha(NH_4^+) = 1.86\,\mathrm{Å}^3$.[107] Analogously to $KH_2PO_4(aq)$, extrapolation of K_A values to infinite dilution via Eq. 1.74 for $(NH_4)H_2PO_4(aq)$ was restricted to $c \geq 0.3917\,\mathrm{mol\,L^{-1}}$, to reduce the influence of ion-cloud relaxation on K_A°. For $(NH_4)_2HPO_4(aq)$, ion-cloud relaxation is expected to have only minor influence, as argued for $K_2HPO_4(aq)$ and $Na_2HPO_4(aq)$. Extrapolated K_A° values for both salts and all possible types of ion pairs are summarized in Tables 5.10 & 5.11.

Table 5.10: Relaxation Times, τ, of Different Ion Pair Species, Estimated via Eqs. (1.56) and (1.60) Assuming Stick or Slip Boundary Conditions, Together with Their Effective Dipole Moments, μ_{eff}, and Associated Standard-State Association Constants, K_A° for $(NH_4)H_2PO_4(aq)$.[a]

	τ_{stick}	τ_{slip}	μ_{eff}	K_A°
CIP	51	9	7.29	∞
SIP	99	33	21.7	$\underline{4.5 \pm 0.6}$
2SIP	172	79	34.0	1.7 ± 0.2

[a]Units: τ in ps, μ_{eff} in Debye (1D = $3.3356 \times 10^{-30} C \cdot m$), K_A° in $\mathrm{L\,mol^{-1}}$. Preferred K_A° values are underlined.

Unfortunately, there are no literature values for K_A° of both salts and also no independent information on which type of ion pair is predominantly formed. The only inference on the ion-pair type can thus be gained by a comparison of experimental τ_1 and calculated rotation correlation times (Eq. 1.56). As the ionic radii of $H_2PO_4^-$ and HPO_4^{2-} are assumed to be equal,[107] rotation correlation times for ion pairs of both salts are also equal. The experimental values, however, reveal a decisive difference between the two salts: $\tau_1((NH_4)H_2PO_4(aq))$ is on average $\sim$30 ps smaller than $\tau_1((NH_4)_2HPO_4(aq))$. This hints at the formation of an ion-pair species with more intervening water molecules in $((NH_4)_2HPO_4(aq))$. Very instructive is a comparison with the corresponding potassium salts, as K^+ and NH_4^+ have similar ionic radii (138 and 148 pm respectively). For $KH_2PO_4(aq)$ SIPs were identified as the most reasonable type of ion pair. As the observed $\tau_1(KH_2PO_4(aq))$ are very similar to $\tau_1((NH_4)H_2PO_4(aq))$, it is most likely, that SIPs are

Table 5.11: Relaxation Times, τ, of All Possible Ion Pair Species in $(NH_4)_2HPO_4$(aq), Estimated via Eq. (1.56) Assuming Stick or Slip Boundary Conditions, Together with The Effective Dipole Moments, μ_{eff} and Standard State Association Constants for Center of Mass (CM) and Center of Hydrodynamic Stress (CHS) Boundary Conditions.[a]

	τ_{stick}	τ_{slip}	$\mu_{\text{eff}}(CM)$	K_{A}°(CM)	$\mu_{\text{eff}}(CHS)$	K_{A}°(CHS)
CIP	51	9	15.8	1040 ± 350	19.3	167 ± 28
SIP	99	33	34.01	37 ± 5	40.2	22 ± 3
2SIP	172	79	50.8	15 ± 1	58.9	$\underline{10 \pm 1}$

[a]Units: K_{A}° in L mol^{-1}.

also the dominating ion-pair species in $(NH_4)H_2PO_4$(aq). Therefore, a standard state association constant of $K_{\text{A}}^{\circ} = (4.5 \pm 0.6)\,\text{L mol}^{-1}$ is obtained. Therefore, 2SIPs are the most reasonable attribution for the observed ion-pair relaxation in $(NH_4)_2HPO_4$(aq). Validation of this assignment is provided by the relaxation time $\tau_1((NH_4)_2HPO_4(\text{aq}))$, which is significantly higher than the one observed in $(NH_4)H_2PO_4$(aq), but at the same time also higher than the corresponding relaxation time in K_2HPO_4(aq). In the latter salt, two ion-pair relaxations (2SIP & SIP) could be differentiated: at low concentrations 2SIPs were the dominant ion-pair species, with SIPs becoming the only type of ion pair at higher concentrations ($c \geq 1\,\text{mol L}^{-1}$). A marked difference, between K_2HPO_4(aq) and $(NH_4)H_2PO_4$(aq) is that for the latter only one type of ion pair is observable. As $\tau_1((NH_4)_2HPO_4(\text{aq})) > \tau_1(K_2HPO_4(\text{aq}))$ over the entire probed concentration range, 2SIPs seem to be the overall dominating ion-pair species. The converging relaxation times at $c > 3\,\text{mol L}^{-1}$ indicate that for high concentrations also in $(NH_4)H_2PO_4$(aq) SIPs are dominating. A shift towards ion pairs with less intervening solvent molecules is commonly observed for increasing c in aqueous electrolyte solutions.[163] As both, NH_4^+ and HPO_4^{2-} are highly hydrated, CHS boundary conditions are preferred for the extrapolation of K_{A}°, yielding $K_{\text{A}}^{\circ} = 10 \pm 1\,\text{L mol}^{-1}$.

5.4 Conclusion

The results on hydration of ammonium phospahtes are in broad consistence with the results of the respective potassium salts (Chapter 4) and Shaukat.[164] However, the determination of exact Z°_{ib} values is difficult, as the correct boundary conditions for calculation of kinetic depolarization of $NH_4{}^+$ are not known. Thus, $Z^{\circ}_{\mathrm{ib}}((NH_4)_2HPO_4) \approx 0$, is different from the expected value of $\sim$4.
For NaH_2PO_4(aq), the determined hydration numbers are very similar to expected values: Z°_{ib} is about one unit smaller and $Z^{\circ}_{\mathrm{slow}}$ about one unit bigger than expected. For Na_2HPO_4(aq) a by $\sim$4 decreased Z°_{ib} is observed, whereas $Z^{\circ}_{\mathrm{slow}}$ is increased by $\sim$3.
Those observations show, that the total hydration number of the whole salt, $Z_{\mathrm{t}}(\mathrm{salt}) = Z_{\mathrm{ib}}(\mathrm{salt}) + Z_{\mathrm{slow}}(\mathrm{salt})$, is consistent with previous results, however a division into the single ions may result in deviating results. Also, shifts of water molecules from ib to slow seem to be rather common (see also A.2).

Regarding ion-pairing, NaH_2PO_4(aq) shows two separable ion pair modes: one attributed to 2SIPs, the other one to SIPs. Aqueous solutions of Na_2HPO_4 mainly containe SIPs, as does $(NH_4)H_2PO_4$(aq). On the other hand, the ion-pair mode in $(NH_4)_2HPO_4$ could mainly be attributed to 2SIPs.
Stronger ion-pairing has been detected for the sodium salts than for the ammonium salts at the same concentration.

Summary and conclusion

The present work represents the first detailed DRS study of inorganic phosphate hydration and ion-pairing. However, first aqueous NaCl solutions were investigated to gain more insight into the physical origin of a low-amplitude low-frequency mode frequently present in electrolyte solutions. Then the complete series of potassium phosphates was investigated in order to extract detailed information on the hydration of phosphate anions, especially the distribution of strongly bound and slowed water molecules over the first and second hydration shell. Also the change in ion-pairing behavior was examined. The same categories, hydration and ion-pairing, were examined for sodium and ammonium phosphates (dihydrogenphosphate and hydrogenphosphate). In the following, the results on those DRS studies at 25°C in the frequency range $0.2 \leq \nu/\mathrm{GHz} \leq 89$ will be summarized.

Ion-cloud relaxation

The study on NaCl(aq) for $c \leq 2.112\,\mathrm{mol\,L^{-1}}$ revealed that the low-frequency, low amplitude mode present in all recent DRS studies of weakly associating electrolytes in our group, is not an artefact. It is possible to resolve this mode now due to the increased sensitivity of the instrumentation, especially the new VNA. Detailed analysis showed, that neither ion-pair rotation, nor ion-cloud relaxation alone were able to fully explain the observed features of the amplitude S_1 and the relaxation time τ_1. The observed amplitude, however, was surprisingly similar to the one predicted by Yamaguchi *et al.*,[32] attributing it to combined ion-cloud and SIP relaxation. Thus it is most reasonable to assume, that the observed experimental mode is a composite of ion-cloud and ion-pair relaxation. Unfortunately, it is at present not possible to divide both contributions, neither experimentally nor with simulations. Therefore, it is only possible to extract association constants that represent upper limits.

The insights from this study could successfully be applied to the investigated aqueous potassium phosphate solutions. By comparing the amplitudes of assumed ion-pair processes with the one from NaCl(aq), it was possible to estimate the contribution of ion-cloud relaxation to the respective modes. Of course, this is just a very crude approximation, and should moreover only be valid for 1:1 electrolytes. Nevertheless, the prediction of strong ion-cloud contribution for KH_2PO_4(aq) and negligible one for K_2HPO_4(aq) and K_3PO_4(aq) was mirrored in the deviation of the extrapolated $K_A^\circ(KH_2PO_4)$ from the one from dilute

conductivity measurements,[155] while there was good agreement for K_2HPO_4(aq). This result has to be taken with a grain of salt though, as also dilute conductivity has its limitations for the determination of association constants $K_A^\circ \leq 10$.

Hydration of inorganic phosphate ions

Despite their importance in biological processes and technical applications, surprisingly little is known about the hydration of inorganic phosphate ions. The existing literature is scarce and even partly contradicting.[33–37] The results on the hydration of potassium phosphates showed, that with increasing charge of the phosphate the total hydration number, Z_t°, increased. Only one solvation shell was detected for H_2PO_4(aq), that contained 11-12 slow water molecules. For HPO_4^{2-} the first solvation shell contained 4-5 strongly bound and 7-8 slowed water molecules. Additionally, HPO_4^{2-} has a weak second hydration shell, which contains ∼3 slow water molecules. For PO_4^{3-} ∼15 ib water molecules were found, out of which 12 should reside in the first and 3 in the second hydration shell. Additional ∼7 slow water molecules are located in the pronounced second hydration shell.

A change of the cation has, within experimental errors, negligible effects on the $H_2PO_4^-$ hydration numbers. Yet, it has to be kept in mind that the Z_{slow} values of NH_4^+ and especially of K^+ are not very well known. For the hydrogen phosphates differences in the Z_{ib} and Z_{slow} values were detected. Surprisingly indifferent towards the respective cation seems to be the total hydration number, Z_t, which is ∼11 for $H_2PO_4^-$, ∼14 for HPO_4^{2-} and ∼22 for PO_4^{3-}. Thus, Z_t° might be the best variable to characterize the hydration of inorganic phosphate anions.

Ion specific effects: ion pairing and water dynamics

This final section is dedicated to extrapolate possible ion specific effects regarding phosphate ion pairing and water dynamics. Basis of this synopsis is the cation series Na^+, K^+ and NH_4^+ for the two phosphate anions $H_2PO_4^-$ and HPO_4^{2-}. In principle, Li^+ would have also been an interesting cation to study. However, due to the very low solubility of Li_3PO_4 in water, the synthesis of Li_2HPO_4 in aqueous solution is a non-trivial task. This is probably the reason why Li_2HPO_4 is not available commercially. It was therefore refrained from studying the lithium phosphates. Before the DR results are discussed regarding ion specific effects, it is worthwhile to give an introduction into the topic of ion specific effects and briefly summarize the existing knowledge of the investigated ions.

Inspired by the pioneering work of Franz Hofmeister on the effect of salts on protein denaturation,[171,181] also many other properties have been observed to be related in a systematic way on the nature of cations and anions.[166,182] Different to the work of Hofmeister, who draw conclusions for whole salts, today cations and anions are ordered separately. The typical ordering for the so called “Hofmeister series” is for cations[166]

$$N(CH_3)_4^+ > NH_4^+ > Cs^+ > Rb^+ > K^+ > Na^+ > Li^+ > Mg^{2+} > Ca^{2+}$$

and for anions[165]

$$CO_3^{2-} > SO_4^{2-} > H_2PO_4^- > F^- > Cl^- > Br^- \sim NO_3^- > I^- > ClO_4^- > SCN^-$$

Both series show a transition from salting out (protein stabilizing) to salting in (protein denaturating) ions. For cations this leads to a ordering of large, highly polarizable ions of low charge density to small, weakly polarizable ions of high charge density. For anions the ordering is just opposite to the one observed for cations.

The long range influence of ions on the structure of water[6] was traditionally regarded as one of the major reasons for the ordering of ions in the Hofmeister series.[183] Accordingly, ions are classified as structure makers or structure breaker - a concept that was introduced by Gurney in 1953.[184] However, as pointed out by Marcus,[6] both concepts seem to pertain to different regions of the solution: while structuring is a bulk property, Hofmeister effects apply to ions close to a surface. Furthermore, there is currently no consensus whether there is an effect of ions on the structure of water beyond the first hydration shell(s)[114,185–187] or not.[14,188–191] Overall, the scientific community is increasingly refraining from the use of the concept of structure-making and breaking: very recently Philip Ball even suggested to "retire [it] gracefully".[177]

More instructive seems to be the classification of ions as kosmotropes and chaotropes,[176] which makes a statement on the hydration of an ion, rather than the influence on the long-range order of liquid water. Kosmotropic ions are usually small with a high charge density and are able to bind water molecules strongly. The term chaotrope was introduced by Collins and denotes big ions of low charge density, that are only able to bind water molecules weakly. Regarding the studied cations, K^+ and NH_4^+ are classified as chaotropes and Na^+ is on the borderline between chaotropic and kosmotropic behavior.[192] The dihydrogen phosphate anion, $H_2PO_4^-$, is a borderline ion, whereas HPO_4^{2-} and PO_4^{3-} are kosmotropes. Based on the classification of ions as kosmotropes and chaotropes is the Collins' concept, or concept of "matching water affinities",[193–195] which allows the prediction of the predominantly formed type of ion pair. According to Collins, the decisive parameter for classification of an ion as chaotrope or kosmotrope is the strength of ion-water interactions as compared to water-water interactions: for kosmotropes, ion-water interactions are stronger than water-water interactions, whereas for chaotropes ion-water interactions are weaker. Collins now predicts, that two kosmotropic ions and two chaotropic ions preferentially form CIPs, whereas the combination of a chaotropic with a kosmotropic ion leads to the preferential formation of SIPs and 2SIPs. Though this model gives a very simplified picture and should only be taken as a rule of thumb,[166] it is able to explain many phenomena like heats of solution, solubilities and viscosity B-coefficients.

For the tested row of hydrogen phosphate salts the following trend for the observed types of ion pairs has been detected (Table 5.12): the kosmotropic HPO_4^{2-} predominantly forms 2SIPs with the chaotropic NH_4^+, whereas the borderline Na^+ leads to the formation of SIPs. This agrees very well with the predictions from the law of matching water affinities. Here a combination of chaotropic cation with kosmotropic anion results in the formation

Table 5.12: Summary of Predominantly Detected Types of Ion Pairs in NaH_2PO_4(aq), KH_2PO_4(aq), $(NH_4)H_2PO_4$(aq), Na_2HPO_4(aq), K_2HPO_4(aq), $(NH_4)_2HPO_4$(aq) and K_3PO_4(aq) Together with the Respective Overall Standard State Association Constants K_A°.[a]

	PO_4^{3-}	HPO_4^{2-}	$H_2PO_4^-$
Na^+		SIP 42 ± 2	SIP & 2SIP 11 ± 3
K^+	2SIP 49 ± 18	2SIP & SIP 21 ± 2	SIP 5.4 ± 0.6
NH_4^+		2SIP 10 ± 1	SIP 4.5 ± 0.6

[a]Units: τ in ps, μ_{eff} in Debye ($1\text{D} = 3.3356 \times 10^{-30} C \cdot m$), K_A° in L mol^{-1}. Preferred K_A° values are underlined.

of solvent separated ion pairs, whereas Na^+, with hydration properties more similar to the anion, predominantly forms solvent-shared ion pairs. For the borderline anion $H_2PO_4^-$,[192] SIPs are formed with the chaotropic cations K^+ and NH_4^+, but a small fraction of 2SIPs along with the dominant formation of SIPs is observed with the borderline Na^+. Based on this observation, the borderline anion $H_2PO_4^-$ has to be classified as rather chaotropic and Na^+ as rather kosmotropic. The also in Table 5.12 included combination of the chaotropic K^+ and the strongly kosmotropic PO_4^{3-} leads to the formation of 2SIPs. The agreement between the experimentally detected types of ion pairs and predictions by the concept of matching water affinity is surprisingly good, if the concept is extended in the way, that with increasing differences in the hydration properties of the ions, ion pairs with more intervening water molecules are formed. Thus, it looks like the Collins' concept may serve as an additional tool for the determination of the predominantly formed type of ion pair in aqueous electrolyte solutions.

It is important to note, however, that though the concept of matching water affinities seems to produce right predictions of the formed type of ion pair, it does not give any information on the degree of ion pairing. Table 5.12 also lists overall K_A° values for all examined electrolyte solutions. The presented data suggest, that the amount of formed ion pairs is principally governed by electrostatics: for a fixed anion more ion pairs are formed with the cation of higher charge density. The same trend is observed when the cation is fixed with varying anion: the higher charge density HPO_4^{2-} has a higher propensity to form ion pairs as $H_2PO_4^-$ for all studied cations.

Table 5.13 gives an overview of hydration numbers for cations and anions detected so far with DRS, which are ordered according to the Hofmeister series. The higher the Z_{ib} value, the more kosmotropic the ion. Different the situation for the amount of detected slow water: the higher the detected Z_{slow}, the more chaotropic the ion, at least for those ions

Table 5.13: Effective Solvation Numbers, Z_{ib} and Z_{slow} of Different Cations and Anions as Obtained with DRS.

Cation	Z_{ib}	Z_{slow}	Anion	Z_{ib}	Z_{slow}
Mg^{2+}	∼14	0 [126]	PO_4^{3-}	∼15	∼7
Li^+	8-12	0 [103]	CO_3^{2-}	13	0 [152]
Na^+	5.2	0	SO_4^{2-}	10 [151]	0
K^+	0 [27]	∼9 [142]	HPO_4^{2-}	∼4	∼10
Cs^+	0	0 [27]	$H_2PO_4^-$	0	∼12
NH_4^+	0	∼14 [a]	Cl^-	0	0

[a] Values as reported by Shaukat [164] have been fitted by a simple exponential function as described in Chapter 5.3.2.

which do not show ib water. This leads to the apparently paradox situation, that NH_4^+ is able to slow more water molecules than K^+, yet it is at the "lower hydration end" of the Hofmeister series. This apparent controversy is also expressed in the fact that the position of NH_4^+ and K^+ is reversed in the reported Hofmeister series of different authors.[6]

The question of ion effects on the water relaxation time(s) was addressed in Chapter 4.5. While, for potassium phosphates, the anions seem to have no notable effect on τ_{bw}, it appears as if there is a subtle dependence on the cation. This trend is in principal also observable for the sodium and ammonium phosphates, however, with mayor constraints. For most of the sodium salt samples τ_{bw} was fixed during the fitting procedure, and the $(NH_4)_2HPO_4$ samples follow the above mentioned trend only for $c < 0.6\,\mathrm{mol\,L^{-1}}$. Nevertheless, for sodium and potassium phosphates over the entire probed concentration range and for ammonium phosphates at $c < 0.6\,\mathrm{mol\,L^{-1}}$ there is a subtle trend of faster bulk water dynamics with increasing size and polarizability of the cation. At higher concentrations, though, clear deviations from this trend become evident for $(NH_4)_2HPO_4$(aq). At ammonium concentrations $> 3\,\mathrm{mol\,L^{-1}}$, this salt even shows the same τ_{bw} behavior as the respective sodium salt.

Regarding slow water relaxation time, τ_{slow}, the observable trends are less subtle. It must be noted at this point, that the stated τ_{slow} actually also contain a contribution from anion reorientation, which can be neglected as a first approximation. Table 5.14 gives an overview of the average slow water relaxation time for the probed dihydrogen phosphates and hydrogen phosphates.
For each row of phosphates, the respective sodium salts show the highest τ_{slow}, potassium salts a medium and ammonium salts the lowest τ_{slow}. For fixed cations, the dihydrogen phosphate salts have higher average τ_{slow} as compared to the hydrogen phosphates. The latter can be well explained with the differences in the anion hydration and was discussed in Chapter 4.5. The probed potassium and ammonium phosphates exhibit slow water due to both, anions **and** cations. Thus, the difference in τ_{slow} for a fixed anion hints at the

Table 5.14: Average Slow Water Relaxation Times, τ_{slow}, as Observed for Different Combinations of Inorganic Phosphate Anions and Cations at 25 °C.

	$H_2PO_4^-$	HPO_4^{2-}
Na^+	25 ps	23 ps
K^+	23 ps	21 ps
NH_4^+	20 ps	19 ps

degree of slowdown around the different cations. As Na^+ is not able to slow water rotation, the τ_{slow} values of the sodium salts may serve as a benchmark for the relaxation time of water molecules around the phosphate anions. The values of Table 5.14 suggest, that the water molecules around K^+ are more slowed down as compared to NH_4^+. This is in line with the lower charge density of NH_4^+. Consequently, K^+ shows stronger interaction with water than NH_4^+, and should thus also be the more kosmotropic ion. Apparently the absolute number of affected water molecules is of minor influence for the classification of ions as kosmotropes or chaotropes as compared to the water interaction strength.

Though the effect of ions on τ_{slow} is well explainable and thus seems to be real, it is strikingly paralleled by the effect on τ_{bw}: higher τ_{slow} are accompanied by tentatively higher τ_{bw}. This hints that the effect on τ_{bw} is actually an artefact of the fitting procedure and as such to some extend has to be regarded as an "echo" of τ_{slow}. Therefore, the observed dependence of τ_{bw} on the cation concentration for potassium phosphates and the apparent similarity of $\tau_{bw}(NaCl)$ and $\tau_{bw}(NaH_2PO_4)$ has to be regarded as fortuitous. The in electrolyte solutions commonly observed speedup of τ_{bw} might well be solely explained by an increased fraction of fast water with increasing solute concentration.

In summary, till now a conclusive explanation for the observed τ_{bw} remains elusive. Also this work is only able to add some tesserae, which in fact render the picture of solute effect on bulk water dynamics even more blurred. As already stated, an extended frequency range is necessary to reliably disentangle fast, bulk and slow water contributions to the DR spectrum. For the time being, we have to live with the unsatisfactory knowledge, that the extracted τ_{bw} are only of limited value for the judgement of solute and especially ion effects on water dynamics.

Appendix

A.1 Conductivities, Densities and Viscosities of Aqueous Phosphate Solutions at 25°C

Table A.1: Concentration, c, Conductivity, κ, Density, ρ, and Dynamic Viscosity, η, of Aqueous KH_2PO_4 Solutions at 25°C. Errors are Within the Limits Described in Chapter 2.3.[a]

c	κ	ρ	η
0.05008	0.4588	1001.87	0.9209
0.09990	0.8601	1006.57	0.9269
0.1492	1.231	1011.19	0.9350
0.1980	1.586	1015.73	0.9582
0.2965	2.240	1024.81	0.9765
0.3933	2.852[b]	1033.73	1.007
0.4900	3.440	1042.52	1.049
0.5842	3.935	1051.02	1.054
0.6791	4.413	1059.53	1.097
0.7721	4.892[b]	1067.82	1.125
0.8649	5.360	1076.05	1.165
0.9564	5.728[b]	1084.13	1.193
1.048	6.097	1092.08	1.228
1.137	6.438	1099.84	1.266
1.206	7.016	1105.82	1.289
1.332	7.189	1116.71	1.341

[a] Units: c in $\mathrm{mol\,L^{-1}}$, κ in $\mathrm{S\,m^{-1}}$, ρ in $\mathrm{g\,L^{-1}}$ and η in mPa s. [b] Interpolated values.

Table A.2: Concentration, c, Conductivity, κ, Density, ρ, and Dynamic Viscosity, η, of Aqueous K_2HPO_4 Solutions at 25°C. Errors are Within the Limits Described in Chapter 2.3.[a]

c	κ	ρ	η
0.02983	0.6071	1001.55	0.9160
0.04975	0.9615	1004.51	0.9207
0.1500	2.512	1019.04	0.9613
0.1989	3.209	1026.03	0.9756
0.2504	3.882	1033.36	1.004
0.2975	4.493	1039.99	1.013
0.3943	5.780	1053.50	1.069
0.4904	6.820	1066.76	1.100
0.5893	7.713	1080.26	1.141
0.6830	8.620	1092.87	1.172
0.7771	9.506	1105.54	1.233
0.8667	10.26	1117.38	1.289
0.9643	11.07[b]	1130.27	1.330
1.4150	14.05	1188.25	1.643
1.8480	16.01	1242.22	2.019
2.644	17.52	1337.89	3.060
3.349	16.83	1419.04	4.752
3.987	14.95	1490.04	7.110

[a] Units: c in $\mathrm{mol\,L^{-1}}$, κ in $\mathrm{S\,m^{-1}}$, ρ in $\mathrm{g\,L^{-1}}$ and η in mPa s. [b] Interpolated values.

Table A.3: Concentration, c, Conductivity, κ, and Density, ρ, of Aqueous K_3PO_4 Solutions at 25°C. Errors are Within the Limits Described in Chapter 2.3.[a]

c	κ	ρ
0.0250	0.8457	1002.01
0.0500	1.5330	1007.10
0.0749	2.094	1012.01
0.0999	2.695[b]	1017.19[b]
0.1497	3.691[b]	1026.46
0.1988	4.642[b]	1036.01
0.2489	5.584	1045.61
0.2985	6.488[b]	1055.30[b]
0.3476	7.258	1063.89
0.3985	8.087	1073.58
0.5920	10.97[b]	1108.70
0.7826	13.43[b]	1143.88
0.9730	15.53[b]	1175.72
0.9727	15.54[b]	1176.33[b]
1.4291	19.03[b]	1252.55
1.8623	20.41[b]	1322.65
2.2681	20.14[b]	1385.75
2.6507	18.75	1443.79
3.0119	16.86	1497.53

[a] Units: c in $\mathrm{mol\,L^{-1}}$, κ in $\mathrm{S\,m^{-1}}$ and ρ in $\mathrm{g\,L^{-1}}$. [b] Interpolated values.

Table A.4: Concentration, c, Conductivity, κ, and Density, ρ, of Aqueous Na_2HPO_4 Solutions at 25°C. Errors are Within the Limits Described in Chapter 2.3.[a]

c	κ	ρ
0.0520	0.3517	1001.84
0.0993	0.6460	1006.02
0.1484	0.9179	1010.35
0.2005	1.164	1014.88
0.2469	1.414	1018.92
0.2960	1.640	1023.17
0.3966	2.055	1031.82
0.4932	2.442	1040.05
0.5882	2.773	1048.06
0.6834	3.119	1056.08
0.7765	3.583	1063.82
0.8734	3.694	1071.83
0.9632	3.860	1079.23
1.860	5.536	1151.17
2.682	6.080	1214.40
3.438	6.192	1270.92
4.153	6.154	1326.11
4.794	6.002	1372.00

[a] Units: c in $\mathrm{mol\,L^{-1}}$, κ in $\mathrm{S\,m^{-1}}$ and ρ in $\mathrm{g\,L^{-1}}$.

Table A.5: Concentration, c, Conductivity, κ, Density, ρ, and Dynamic Viscosity, η, of Aqueous Na_2HPO_4 Solutions at 25°C. Errors are Within the Limits Described in Chapter 2.3.[a]

c	κ	ρ	η
0.0498	0.7434	1004.03	0.9268
0.0999	1.316	1010.77	0.9474
0.1499	1.845	1017.45	0.9840
0.1996	2.281	1023.98	1.012
0.2496	2.726	1030.46	1.036
0.2992	3.081	1036.84	1.059
0.3488	3.476	1043.21	1.103
0.3988	3.769	1049.56	1.145
0.4965	4.329	1061.83	1.208
0.6184	4.942	1076.97	1.324

[a] Units: c in $\mathrm{mol\,L^{-1}}$, κ in $\mathrm{S\,m^{-1}}$, ρ in $\mathrm{g\,L^{-1}}$ and η in mPa s.

Table A.6: Concentration, c, Conductivity, κ, and Density, ρ, of Aqueous $(NH_4)H_2PO_4$ Solutions at 25°C. Errors are Within the Limits Described in Chapter 2.3.[a]

c	κ	ρ
0.09976	0.8511	1003.52
0.2018	1.565[b]	1010.01
0.2964	2.179	1015.93
0.3917	2.735	1021.83
0.4865	3.267	1027.73
0.5810	3.758	1033.35
0.6695	4.195[b]	1038.63
0.7520	4.583	1044.60
0.8575	4.975	1049.77
0.9465	5.341	1055.10
1.383	6.895	1080.19
1.798	8.073	1103.64
2.188	8.944	1124.92
2.459	9.349	1139.61

[a] Units: c in $\mathrm{mol\,L^{-1}}$, κ in $\mathrm{S\,m^{-1}}$ and ρ in $\mathrm{g\,L^{-1}}$.[b] Interpolated values.

Table A.7: Concentration, c, Conductivity, κ, and Density, ρ, of Aqueous $(NH_4)_2HPO_4$ Solutions at 25°C. Errors are Within the Limits Described in Chapter 2.3.[a]

c	κ	ρ
0.09905	1.467	1005.39
0.1976	2.557	1013.34
0.2962	3.450	1021.11
0.3914	4.238	1028.45
0.4886	4.967	1035.79
0.5813	5.673[b]	1042.68
0.6719	6.254	1049.32
0.7647	6.824	1056.03
0.8558	7.350	1062.54
0.9468	7.770[b]	1068.95
1.366	9.466[b]	1097.64
1.771	10.57[b]	1124.03
2.165	11.26	1148.69
2.512	11.64[b]	1170.20
2.851	11.82[b]	1190.44
3.173	11.86[b]	1209.62

[a] Units: c in $\mathrm{mol\,L^{-1}}$, κ in $\mathrm{S\,m^{-1}}$ and ρ in $\mathrm{g\,L^{-1}}$. [b] Interpolated values.

A.2 Solvation of the osmolyte ectoine in water and aqueous NaCl

During the time period of this thesis, aqueous solutions of ectoine and ectoine+NaCl were investigated by Andreas Nazet for the preparation of his bachelor thesis. Initial studies on ectoine(aq) have been done by Thomas Rück and Alexander Stoppa. I was supervising and guiding the experimental part and the initial analysis. Also, I did the final analysis and interpretation of all available data. The following pages contain a manuscript draft, originally prepared for Angewandte Chemie.

Andreas Eiberweiser, Andreas Nazet, Alexander Stoppa, Thomas Rück and Richard Buchner

Institut für Physikalische und Theoretische Chemie, Universität Regensburg, D-93040 Regensburg, Germany.

Introduction Osmolytes are small molecules found in extremophilic microorganisms living under severe osmotic stress. They aid maintaining the cell volume and fluid balance, and thus enable organisms to survive even harsh environments like extreme saline waters. Examples are betaine, trimethylamine N-oxide (TMAO), glycine and ectoine. Those are also known as compatible solutes, as these natural products do not negatively affect the cell metabolism. In addition, compatible solutes also stabilize biomolecules against negative effects due to heat, dryness and UV-radiation.[196]

Ectoine, (S)-2-methyl-3,4,5,6-tetrahydropyrimidine-4-carboxylic acid (Figure A.1), which was first characterized by Galinski,[197,198] is widely found in halophilic bacteria. It is commercially used in cosmetics, as a cell and tissue protectant, and is a potential therapeutic agent for certain diseases.[199]

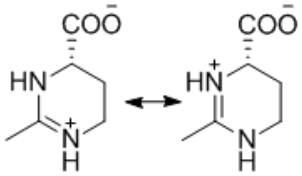

Figure A.1: Zwitterionic representation of ectoine, as it is found in aqueous solution. The molecule consists of hydrophilic (carboxylate group, ammonium groups) and hydrophobic (e.g. methyl group) parts.

The ability of ectoine to stabilize the native conformation of proteins is attributed to the water binding nature of this molecule and rationalized by the so called preferential exclusion model.[200] According to this approach, osmolytes are excluded from the surface of proteins, though being highly hydrated themselves. Thus the hydration of the protein is promoted, the diffusion of water molecules slowed down, and the natural conformation

of the protein is preserved.[201] The protective nature of ectoine is well known and could be applied to human skin.[202,203] However, with the exception of MD simulations,[201,204,205] little is known about the hydration structure of ectoine.

In this communication we report on the solvation of ectoine in aqueous solution and the influence of ectoine on water dynamics. We also shed light on the effect of NaCl, as a model electrolyte, on the hydration of ectoine. The main experimental technique used to gain this information was dielectric relaxation spectroscopy in the frequency range 50 MHz $\leq \nu \leq$ 89 GHz. This technique is sensitive to fluctuations of the macroscopic polarization of a sample in an external electric field, mainly occurring through the reorientation of dipolar species, and yields the complex relative permittivity $\hat{\varepsilon}(\nu) = \varepsilon'(\nu) - \mathrm{i}\varepsilon''(\nu)$.[18]

Experimental Section Ectoine samples were provided by bitop AG (Witten, Germany) in two different purity scales and used as received. Most samples of aqueous ectoine were prepared from a batch of ≥96% purity, the samples for the ectoine+NaCl(aq) study, as well as a series of additional ectoine(aq) solutions were prepared from a batch of ≥99.5% purity. As the spectra, and corresponding fit parameters, obtained for the NaCl-free ectoine solutions from the batches with 96% and 99.5% purity were consistent, the dielectric data of all samples were included in this study. NaCl (pro analysi, Merck, Germany) was dried for 48 h at 200 °C under reduced pressure ($p = 2 \cdot 10^{-6}$ bar), using P_2O_5 (Sicapent, Merck, Germany) as a desiccant. The dried salt was stored in a glove box under nitrogen atmosphere prior to use. Samples were prepared gravimetrically without buoyancy correction, using degassed water (Millipore, specific resistance ≥ 18 MΩ·cm).

Sample densities, ρ, were determined at (25 ± 0.01) °C with a vibrating tube densimeter (DMA 5000M, Anton Paar, Austria). Taking into account all sources of error, especially the different purities of both ectoine batches, we estimate the uncertainty of ρ to be within $\pm 2 \cdot 10^{-4}$ kg L^{-1}.

Electrical conductivities, κ, were determined at (25 ± 0.01) °C with a computer controlled setup as described previously.[91] The used set of five two-elecrode capillary cells with cell constants ranging from (24.9 to 359) cm^{-1} was calibrated with KCl(aq).[92] The cell resistance, R, was determined in the frequency range $200 \leq \nu/\mathrm{Hz} \leq 2000$ and extrapolated to infinite frequency, R_∞, using the empirical function $R(\nu) = R_\infty + A/\nu^a$. A is specific to the cell and the exponent a shows values of $0.5 < a < 1$. Data acquisition, temperature control and extrapolation of R_∞ values was done automatically by a home-built software package. The relative uncertainty of κ is ≤ 0.5%.

Dynamic viscosities, η, were measured with an automated rolling ball viscometer (AMVn, Anton Paar, Austria) at (25 ± 0.01) °C using a calibrated glass capillary with 1.6 mm diameter and corresponding steel balls. The relative uncertainty of η is ∼0.5%. Viscosities were only determined for ectoine(aq) samples made from the ectoine batch with purity ≥ 99.5%. The data for ρ, κ and η are summarized in Table A.8.

Broadband dielectric spectra of relative permittivity, $\varepsilon'(\nu)$, and total loss, $\eta''(\nu)$, were measured at (25 ± 0.05) °C in the frequency range $0.05 \leq \nu/\mathrm{GHz} \leq 89$. In the lower frequency range ($0.05 \leq \nu/\mathrm{GHz} \leq 50$) data were determined by reflectometry using an Agilent

Table A.8: Experimental values for density, ρ, viscosity, η, and conductivity, κ, for all studied samples.[a]

c(ectoine)	c(NaCl)	ρ	η	κ
0.0496	0	0.9990		
0.0987	0	1.0009		
0.0993	0	1.0010	0.941	
0.1951	0	1.0048		
0.3759	0	1.0118		
0.4739	0	1.0156	1.124	
0.6441	0	1.0223		
0.9035	0	1.0324	1.342	
1.2732	0	1.0469		
1.5124	0	1.0561	1.816	
1.6207	0	1.0605		
2.1668	0	1.0816	2.646	
2.2819	0	1.0862		
2.7921	0	1.1060		
0.8929	0.2233	1.0408	1.342	1.70
0.8959	0.4485	1.0495	1.388	3.22
0.8917	0.6691	1.0578	1.402	4.58
0.8878	0.8873	1.0660	1.446	5.84
0.8710	1.7442	1.0974	1.609	8.78

[a] Units: c in $\mathrm{mol\,L^{-1}}$, ρ in $\mathrm{kg\,L^{-1}}$, η in $\mathrm{mPa\,s}$ and κ in $\mathrm{S\,m^{-1}}$.

E8364B vector network analyzer (VNA) with corresponding E-Cal module. Coaxial-line cut-off cells[206] were used for $\nu \leq 0.5\,\mathrm{GHz}$ whereas two open-ended coaxial-line probes covered $0.2 \leq \nu/\mathrm{GHz} \leq 20$ and $1 \leq \nu/\mathrm{GHz} \leq 50$. Calibration of this instrument followed the procedure described in Chapter 2.2.2 for the two cell types. At mm-wave frequencies, $60 \leq \nu/\mathrm{GHz} \leq 89$, a waveguide interferometer with a variable-pathlength transmission cell was used.[207] This instrument does not require calibration.
From $\eta''(\nu)$ and the dc conductivity, κ, the corresponding dielectric loss $\varepsilon''(\nu) = \eta''(\nu) - \kappa/(2\pi\nu\varepsilon_0)$ was obtained (ε_0 is the permittivity of vacuum). The probable uncertainties of $\varepsilon'(\nu)$ and $\eta''(\nu)$ are 1-2% of the static permittivity, ε , of the sample. The obtained loss spectra, $\varepsilon''(\nu)$, for ectoine(aq) are shown in Figure A.2a. Figure A.3a shows the corresponding spectra of the ectoine+NaCl(aq) samples.

Data Analysis Real, $\varepsilon'(\nu)$, and imaginary, $\varepsilon''(\nu)$, part of the dielectric spectrum were fitted simultaneously by a sum of n independent relaxation modes j according to Eq. 1.19. All reasonable relaxation models for $n \leq 5$ were tested using a home-built software package based on a non-linear fitting routine. The quality of the fit model was assessed by the value of the reduced error function, χ^2_{r},[87] and the additional criteria discussed

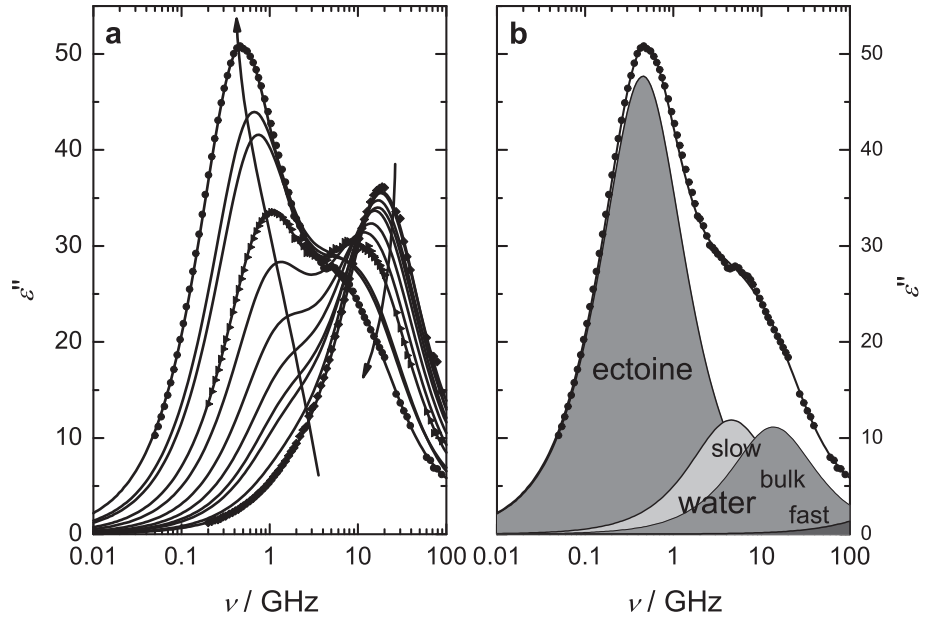

Figure A.2: (a) Dielectric loss spectra, $\varepsilon''(\nu)$, of aqueous ectoine solutions. Arrows indicate increasing ectoine concentration, $0.10 \leq c\,/\,\mathrm{mol\,L^{-1}} \leq 2.79$; symbols represent experimental data, lines fits thereof. (b) Resolved modes of the dielectric loss spectrum for $c = 2.79\,\mathrm{mol\,L^{-1}}$.

by Rahman *et al.*[30] It turned out that for all investigated samples the superposition of four Debye equations (the 4D model, $n = 4$) provided the best fit (Figures A.2b & A.3b), yielding sets of parameters for ectoine(aq) (Table A.9) and ectoine+NaCl(aq) (Table A.10) that smoothly varied with concentration.

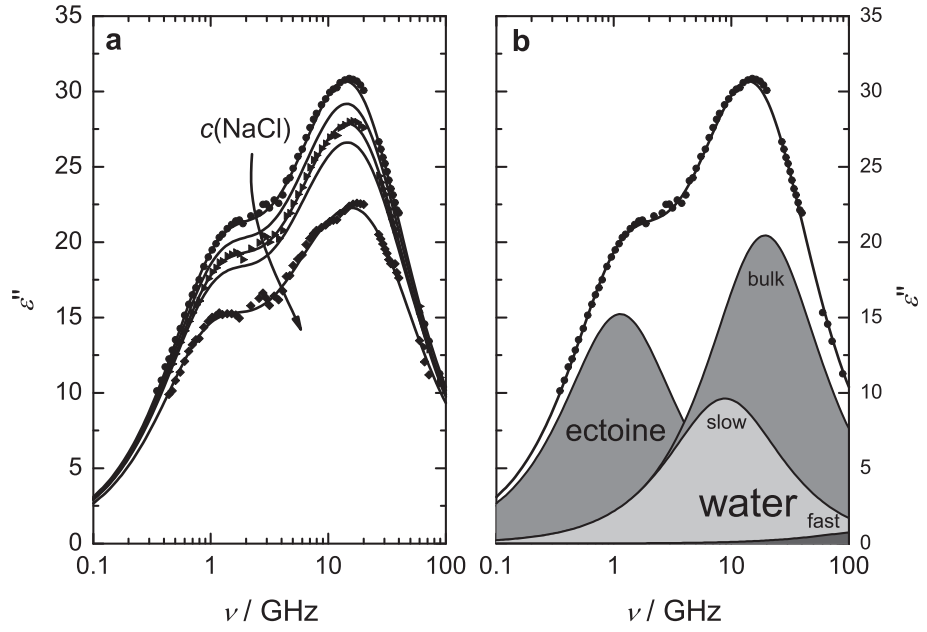

Figure A.3: (a) Spectra of dielectric loss, $\varepsilon''(\nu)$, for NaCl@ectoine(aq) at c(NaCl) = 0.22, 0.45, 0.67, 0.89 and 1.74 mol L^{-1}. Dots represent experimental data, lines fits thereof with Eq. 1.19. (b) Deconvolution of $\varepsilon''(\nu)$ into single relaxation modes of Debye type, corresponding to ectoine, slow, bulk and fast water.

Table A.9: Parameters of the 4D fit for the observed DR spectra of aqueous solutions of ectoine at 25 °C: limiting permittivities, ε_j ($j = 1-4$) & ε_∞, relaxation times, τ_j, and the value of the reduced error function, χ^2_r.[a]

c / mol L^{-1}	ε_1	τ_1 / ps	ε_2	τ_2 / ps	ε_3	τ_3 / ps	ε_4	τ_4 / ps	ε_∞	χ^2_r
0.0496	79.63	95.0	77.79		77.79	8.50	6.32	1.0F	3.83	0.0964
0.0987	80.95	91.0	77.14		77.14	8.57	6.40	1.0F	4.28	0.0915
0.0993	80.51	94.7	76.78		76.78	8.46	6.34	1.0F	5.66	0.0511
0.1951	83.45	95.1	76.07	15F	72.74	8.53	6.67	1.0F	3.36	0.0346
0.3759	88.19	103	74.05	15.5F	67.79	8.72	6.93	1.0F	3.46	0.0454
0.4739	90.11	106	72.31	15.4	64.33	8.55F	6.54	0.85	5.10	0.0358
0.6441	95.13	117	71.31	17F	60.27	8.76	6.44	0.5F	3.66	0.0682
0.9035	101.5	132	68.41	18F	52.93	8.72	6.46	0.33	3.64	0.0393
1.2732	111.5	157	65.62	21F	47.77	9.16	6.20	0.5F	4.54	0.0889
1.5124	116.9	173	62.69	21.9	44.13	9.5F	6.78	0.52	5.13	0.0639
1.6207	120.1	183	62.49	23.5	42.93	9.6F	6.55	0.5F	3.74	0.0598
2.1668	132.4	238	56.86	27F	35.93	10.5	6.94	0.5F	5.12	0.0921
2.2819	137.4	263	57.18	29.8	34.93	10.8F	6.88	0.5F	2.71	0.1124
2.7921	148.4	351	53.07	35F	29.30	11.6	7.00	0.5F	2.34	0.2075

[a] Parameter values followed by the letter F were not adjusted in the fitting procedure.

Table A.10: Parameters of the 4D fit for the observed DR spectra of ectoine+NaCl(aq) at 25 °C: limiting permittivities, ε_j ($j = 1 - 4$) & ε_∞, relaxation times, τ_j, together with the value of the reduced error function, χ^2_r.[a]

c(NaCl) / mol L^{-1}	c(ectoine) / mol L^{-1}	ε_1	τ_1 / ps	ε_2	τ_2 / ps	ε_3	τ_3 / ps	ε_4	τ_4 / ps	ε_∞	χ^2_r
0.2233	0.8929	97.24	140	66.80	18.0	47.57	8.2F	6.70	1.0F	5.08	0.0545
0.4485	0.8959	93.50	142	64.38	18.2	45.69	7.9F	6.44	1.15	5.64	0.0654
0.6691	0.8917	90.17	145	62.30	18.3	44.19	7.76	6.59	0.5F	4.98	0.0733
0.8873	0.8878	87.27	151	60.64	18.7	42.12	7.63	7.27	1.0F	4.26	0.0610
1.7442	0.8710	76.52	165	54.04	20.3	37.34	6.93	7.41	1.0F	4.57	0.1047

[a] Parameter values followed by the letter F were not adjusted in the fitting procedure.

Results and Discussion The lowest frequency mode at 0.6 GHz is attributed to ectoine. With the help of Eq. 1.47 the effective dipole moment of ectoine was calculated as a function of solute concentration, c, from the amplitude of the lowest-frequency mode, S_1. As can be seen from Figure A.4a, μ_{eff}(ectoine) exhibits only a weak linear decrease (intercept 20.39 ± 0.03 D; slope -0.47 ± 0.02) with increasing c. The effective dipole moment of 20.4 D for ectoine at $c \to 0$ is in excellent agreement with semiempirical calculations for the zwitterionic form (20.3 D).[93,96] Significant ectoine-ectoine interactions can be ruled out as the effective dipole moment only weakly decreases with increasing concentration.

The relaxation time determined by dielectric spectroscopy is a collective property incorporating static and dynamic dipole-dipole correlations. For ectoine, exhibiting the slowest relaxation in a series of four superimposed Debye modes, the corresponding rotational correlation time (molecular relaxation time), τ_1', can be calculated via Eq. 1.60. Provided strong ectoine-ectoine correlations are negligible, and molecular reorientation occurs through small-angle rotational diffusion, the thus obtained rotational correlation time should follow the generalized Stokes-Einstein-Debye (SED) equation (Eq. 1.56).

According to Figure A.4b, τ_1' is proportional to viscosity over the entire concentration range studied. This is clear evidence that ectoine-ectoine interactions are weak. From the slope, an empirical friction coefficient of $C = 0.63$ can be deduced with the help of the Van der Waals volume.[208] This value is in between the *stick* and *slip* limits, indicating that ectoine is well hydrated and carries at least part of its solvation shell when rotating.

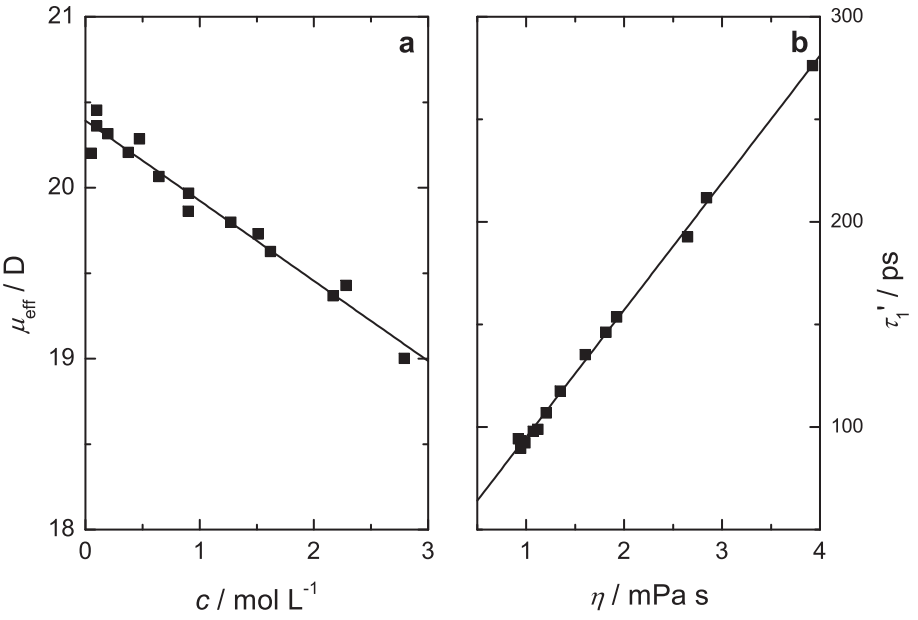

Figure A.4: (a) Effective dipole moment, $\mu_{\text{eff}}(c)$, of ectoine as determined by direct evaluation of the relaxation amplitude S_1 with Eq. 1.47. (b) Microscopic relaxation time, τ_1', of the ectoine molecule (■) as a function of solution viscosity, η. The solid line corresponds to a linear fit. The proportional increase of both quantities hints at rotational diffusion as the relaxation mechanism.

Both, for aqueous ectoine (Figure A.2b) as for NaCl solutions in 0.89 M ectoine(aq) (Figure A.3b), it was possible to discriminate three different water relaxations, namely slow, bulk and fast water.[18] While bulk water, at ∼18 GHz, and fast water (∼300 GHz) show comparable relaxation behavior as neat water,[62] slow water (∼7 GHz) can only be detected for the solutions and is typical for moderately bound hydration water.[18,30]

From the amplitude of the slow-water mode, the corresponding concentration $c(H_2O,$ slow) of retarded H_2O can be immediately calculated, whereas the sum of the amplitudes of slow, bulk and fast water yields the total amount of water, $c(H_2O,$ DRS), detected by DRS for that sample.[18] Together with the solute concentration, c(solute) [solute = ectoine or NaCl], and the analytical solvent concentration, $c(H_2O)$, this allows distinction of two hydration numbers: $Z_{\mathrm{slow}} = c(H_2O, \mathrm{slow})/c(\mathrm{solute})$ gives the number of moderately bound/slowed down H_2O molecules per equivalent of solute, whereas $Z_{\mathrm{ib}} = [c(H_2O) - c(H_2O, \mathrm{DRS})]/c(\mathrm{solute})$ gives the number of irrotationally bound solvent molecules, which are so strongly bound by the solute that they appear to be "frozen" on the DRS time scale, i.e. cannot be detected anymore.[24]

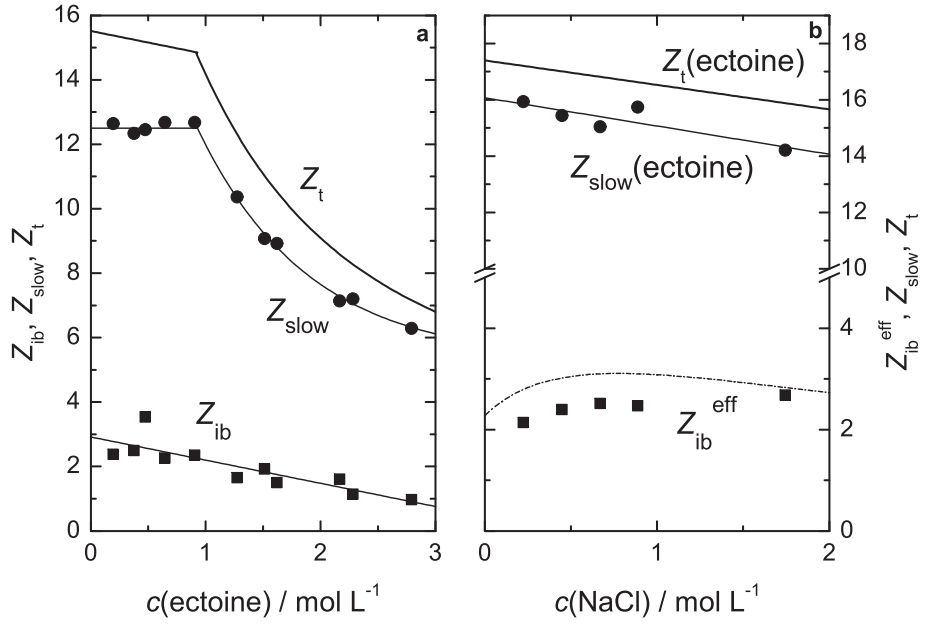

Figure A.5: Hydration numbers of strongly bound, Z_{ib} (■), and moderately bound, Z_{slow} (●), H_2O molecules, as well as the total hydration number, Z_{t} (fit only) for (a) aqueous ectoine solutions and (b) 0.89 M ectoine+NaCl(aq). Solid lines are a guide to the eye only; dashed line in (b): predicted $Z_{\mathrm{ib}}^{\mathrm{eff}}$ assuming additivity of ectoine and NaCl contributions.

Figure A.5 summarizes Z_{ib}, Z_{slow} and the total hydration number, $Z_{\mathrm{t}} = Z_{\mathrm{ib}} + Z_{\mathrm{slow}}$, of aqueous ectoine solutions. Clearly, ectoine is well hydrated up to the highest concentration, but the large majority of the bound water molecules is only retarded by a factor of ∼2 compared to bulk water. The amount of strongly bound water is rather small, with $Z_{\mathrm{ib}} = 2.9 \pm 0.2$ at infinite dilution and a subsequent linear decrease to ∼2 at the highest ectoine concentration. In contrast, $Z_{\mathrm{slow}} = 12.6 \pm 0.2$ up to ∼0.9 M and then decays sharply to

$\sim$6, indicating increasing hydration-shell overlap above this threshold concentration. It appears reasonable to associate the strongly bound water to the charged moieties of the zwitterionic ectoine (Figure A.1). From studies of aqueous sodium carboxylates,[30,179] it is known that the -COO^- moiety is able to "freeze" 1-2 and additionally to slow down 4-5 H_2O molecules by hydrogen bonding, keeping the total hydration number at $\sim$5-6 up to the saturation limit. This leaves $Z_{ib} \approx 1$ for the two equivalent ammonium groups, in line with computer simulations of Smiatek *et al.*, who found 5.59 H-bonds between water and -COO^- and 0.68, respectively 0.75, H-bonds for the two nitrogen atoms.[205] Thus, the remaining $\sim$8 slow water molecules must be due to interactions with the ammonium group and hydrophobic hydration. The total hydration number $Z_t = Z_{ib} + Z_{slow} = 15.5 \pm 0.4$ reveals that in sufficiently dilute solutions ectoine is indeed highly hydrated, corroborating thus the inference from the relaxation time of ectoine. However, most hydrating water molecules are just moderately bound.

To understand the functioning of ectoine in the presence of salt, knowledge on osmolyte-ion interactions and their effect on ectoine hydration and ion-ion interactions is indispensable and thus NaCl solutions in 0.89 M aqueous ectoine were studied. Interestingly, for all samples the spectra are again best fitted by a sum of four Debye equations, with the same assignment of the resolved modes as for the salt free solutions (Table A.10). There is no evidence for Na^+Cl^- ion pairs nor - more importantly - for any association between ectoine and Na^+(aq) or Cl^-(aq). This is corroborated by the data for density, conductivity and viscosity (Figure A.6a-c). The values determined for the aqueous ectoine+NaCl mixtures are fully explained by simply adding the contributions of both two-component systems. There are no excess contributions typical for direct solute-solute interactions. It is thus possible to conclude, that the hydration of Na^+(aq) and Cl^-(aq) in the mixture is not different from that in aqueous NaCl.[137]

For the NaCl-ectoine mixture, we have to deduce an effective Z_{ib}, as both, Na^+ and ectoine, are able to "freeze" surrounding water molecules. The dashed line in Figure A.5b shows the expected concentration dependence of $Z_{ib}^{eff} = (c(H_2O) - c(H_2O, DRS))/(c(\text{ectoine}) + c(\text{NaCl}))$ calculated from the data for NaCl-free ectoine(aq) (Figure A.5a) and NaCl(aq).[137] The experimental values are slightly below the expected Z_{ib}^{eff}, whereas Z_{slow} is substantially higher than the value of $\sim$12.6 for 0.89 M ectoine(aq). For the lowest NaCl concentration, it appears that each ectoine molecule freezes one water molecule less than in the NaCl-free solution, but 3 additional water molecules are slowed down. Apparently, the screening effect of the added electrolyte causes a shift from strongly bound to moderately bound water, which is accompanied by a significant increase of the total hydration number of ectoine, i.e. Z_t(0.22 M NaCl@ectoine(aq)) = 17.4 as compared to Z_t(ectoine) = 14.9 for the salt free solution. Moreover, this increased hydration shows only little dependence on NaCl concentration (Figure A.5b). These findings demonstrate impressively, that ectoine is not just able to further increase its hydration in electrolyte solutions, but also to maintain the hydration shell even in highly concentrated NaCl(aq). Its strong hydration despite the presence of hydrophilic ions makes ectoine the perfect candidate for an osmosis-regulating substance.

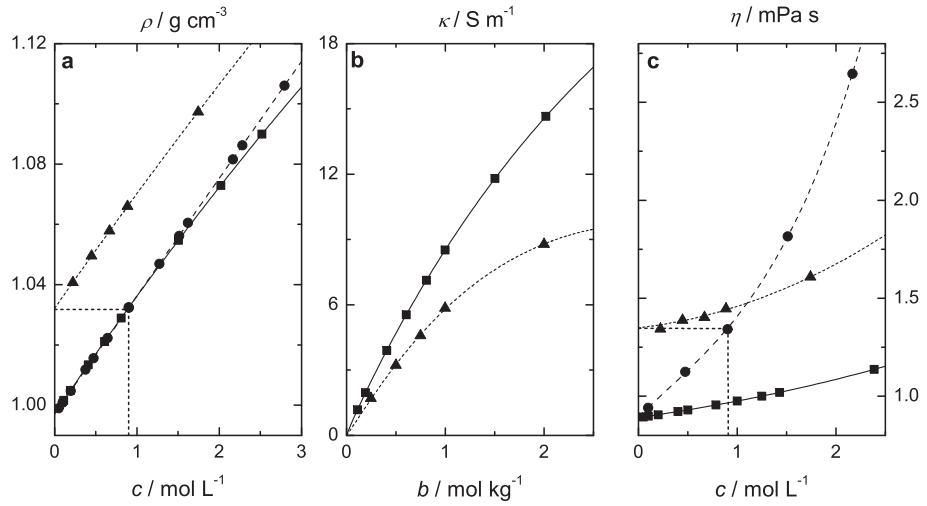

Figure A.6: Concentration dependence of (a) density, ρ, (b) conductivity, κ, and (c) viscosity, η, for aqueous solutions of NaCl (■), ectoine (●) and the ectoine/NaCl mixture (▲). Lines represent empirical fits. For density and viscosity the values for NaCl+ectoine show the same concentration behavior as NaCl and an infinite dilution limit (relative to NaCl) that corresponds to the density/viscosity of 0.89 M ectoine(aq). Regarding the conductivity, within measurement errors, the proportion between both sets of conductances, κ(NaCl)/κ(NaCl+ectoine), stays roughly constant at ≈ 1.5, and is in excellent agreement with the corresponding inverse value for viscosities, η(NaCl+ectoine)/η(NaCl).

The effect of the solutes on solvent structure is judged by the change in bulk water relaxation time (Figure A.7). Although we have to keep in mind, that this quantity is almost certainly a weighted average over states ranging from essentially unperturbed H_2O molecules far away from the solute to the transition zone between there and the solute's primary hydration shell (with its distinct water dynamics leading to Z_{slow} and Z_{ib}), it informs on the impact of solutes on the cooperative hydrogen bond dynamics.[62] Roughly speaking, faster bulk water dynamics indicates weaker/less H-bonding, slower dynamics consequently stronger/more H-bonding. Ectoine clearly is slowing down the bulk water dynamics, whereas NaCl has the opposite effect. Thus, in the notion of the structure maker, structure breaker concept, ectoine has to be classified as a structure maker (kosmotrope), NaCl as a structure breaker (chaotrope).[6] Interestingly, the bulk water relaxation time of ectoine+NaCl mixtures closely resembles that of pure NaCl(aq) even at high ectoine to NaCl ratio. In other words: although ectoine alone has a significant retarding effect on bulk water dynamics, this is not the case anymore as soon as ions are present. This clearly non-additive behavior is remarkable and might be the reason why ectoine does not show a negative effect on cell metabolism.

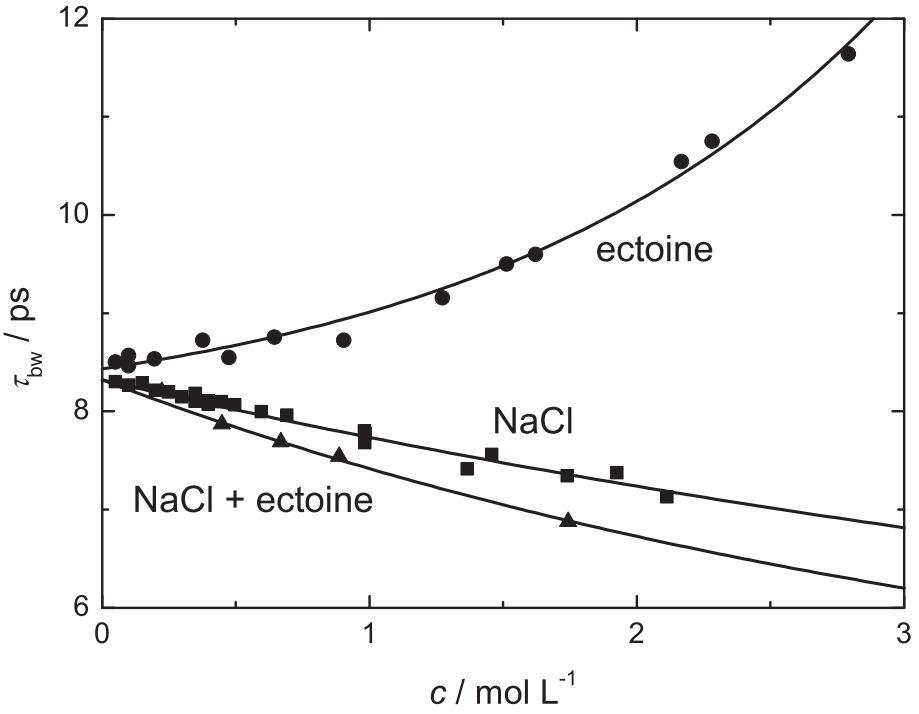

Figure A.7: Bulk water relaxation times, τ_{bw}, of aqueous solutions of ectoine, NaCl and 0.89 M ectoine+NaCl.

Conclusion The extensive hydration of the osmolyte in ectoine+NaCl solutions, mainly in the form of moderately bound water, stays constant even at high electrolyte concentrations. This allows microorganisms to regulate their water content in environments of high osmotic stress simply by uptake/production or release/degradation of ectoine. The finding that compatible solutes do not interfere in a cells metabolism can be explained by the fact that ectoine does not interact directly with ions, i.e. form associates, in addition to its exclusion from the surface of proteins via its stable hydration shell.[200] Also the striking finding that the influence of ectoine on bulk water dynamics vanishes as soon as ions are present in the system, works in this direction. It suggests, that the presence of the osmolyte does not interfere with processes where water molecules with dynamical properties pertaining to physiological salt solutions are relevant. This is in line with increasing evidence that water is not just a mere solvent, but instead takes part as an active player in biological processes.[7]

Bibliography

[1] Nelson, D. L.; Cox, M. M. *Lehninger Principles of Biochemistry*, 5th ed.; Freeman: New York, 2008.

[2] Corbridge, D. *Phosphorus 2000: Chemistry, Biochemistry & Technology*; Elsevier: Amsterdam, 2000.

[3] Berg, J.; Tymoczko, J.; Stryer, L. *Biochemistry*; Freeman: New York, 2008.

[4] Currey, J. *Bones: Structure and Mechanics*; Princeton University Press: Princeton, 2002.

[5] Brown, T. J.; Walters, A. S.; Idoine, N. E.; Shaw, R. A.; Wrighton, C. E.; Bide, T. *World Mineral Production 2006-10*; British Geological Survey: Keyworth, United Kingdom, 2012.

[6] Marcus, Y. *Chem. Rev.* **2009**, *109*, 1346.

[7] Ball, P. *ChemPhysChem* **2008**, *9*, 2677.

[8] Ball, P. *Chem. Rev.* **2008**, *108*, 74.

[9] Vrbka, L.; Vondrášek, J.; Jagoda-Cwiklik, B.; Vácha, R.; Jungwirth, P. *Proc. Natl. Acad. Sci. USA* **2006**, *103*, 15440.

[10] Jagoda-Cwiklik, B.; Vácha, R.; Lund, M.; Srebro, M.; Jungwirth, P. *J. Phys. Chem. B* **2007**, *111*, 14077.

[11] Aziz, E. F.; Ottosson, N.; Eisebitt, S.; Eberhardt, W.; Jagoda-Cwiklik, B.; Vácha, R.; Jungwirth, P.; Winter, B. *J. Phys. Chem. B* **2008**, *112*, 12567.

[12] Hess, B.; van der Vegt, N. F. A. *Proc. Natl. Acad. Sci. USA* **2009**, *106*, 13296.

[13] Bennion, B. J.; Daggett, V. *Proc. Natl. Acad. Sci. USA* **2004**, *101*, 6433.

[14] Bakker, H. J. *Chem. Rev.* **2008**, *108*, 1456.

[15] Hunger, J.; Tielrooij, K.-J.; Buchner, R.; Bonn, M.; Bakker, H. J. *J. Phys. Chem. B* **2012**, *116*, 4783.

[16] Rahman, H. M. A. Ph.D. thesis, University of Regensburg, 2012.

[17] Fennell, C. J.; Bizjak, A.; Vlachy, V.; Dill, K. A. *J. Phys. Chem. B* **2009**, *113*, 6782.

[18] Buchner, R.; Hefter, G. *Phys. Chem. Chem. Phys.* **2009**, *11*, 8984.

[19] Collins, K. D. *Biophys. Chem.* **2006**, *119*, 271.

[20] Ganguly, P.; Schravendijk, P.; Hess, B.; van der Vegt, N. F. A. *J. Phys. Chem. B* **2011**, *115*, 3734.

[21] Marcus, Y.; Hefter, G. *Chem. Rev.* **2006**, *106*, 4585.

[22] Powell, K.; Brown, P.; Byrne, R.; Gajda, T.; Hefter, G.; Leuz, A.-K.; S. Sjöberg, H. W. *Pure Appl. Chem.* **2011**, *83*, 1163.

[23] Hefter, G. *Pure Appl. Chem.* **2006**, *78*, 1571.

[24] Buchner, R. *Pure Appl. Chem.* **2008**, *80*, 1239.

[25] Kremer, F.; Schönhals, A. *Broadband Dielectric Spectroscopy*; Springer: Berlin, 2003.

[26] Böttcher, C.; van Belle, O.; Bordewijk, P.; Rip, A. *Theory of Electric Polarization*; Elsevier: Amsterdam, 1978; Vol. 1+2.

[27] Chen, T.; Hefter, G.; Buchner, R. *J. Phys. Chem. A* **2003**, *107*, 4025.

[28] Wachter, W.; Kunz, W.; Buchner, R.; Hefter, G. *J. Phys. Chem. A* **2005**, *109*, 8675.

[29] Fedotova, M. V.; Kruchinin, S. E.; Rahman, H. M. A.; Buchner, R. *J. Mol. Liq.* **2011**, *159*, 9.

[30] Rahman, H. M. A.; Hefter, G.; Buchner, R. *J. Phys. Chem. B* **2012**, *116*, 314.

[31] Buchner, R.; Hefter, G. T.; May, P. M. *J. Phys. Chem. A* **1999**, *103*, 1.

[32] Yamaguchi, T.; Matsuoka, T.; Koda, S. *J. Chem. Phys.* **2009**, *130*, 094506.

[33] Mason, P. E.; Cruickshank, J. M.; Neilson, G. W.; Buchanan, P. *Phys. Chem. Chem. Phys.* **2003**, *5*, 4686.

[34] Ebner, C.; Onthong, U.; Probst, M. *J. Mol. Liq.* **2005**, *118*, 15.

[35] Brandán, S.; Díaz, S.; Picot, R. C.; Disalvo, E.; Altabef, A. B. *Spectrochim. Acta A* **2007**, *66*, 1152.

[36] Rudolph, W. W.; Irmer, G. *Appl. Spectrosc.* **2007**, *61*, 1312.

[37] Tang, E.; Tommaso, D. D.; de Leeuw, N. H. *J. Chem. Phys.* **2009**, *130*, 234502.

[38] Buchner, R. *Encyclopedia of Applied Electrochemistry*; Springer: Berlin, 2012; Chapter Static Relative Permittivity (Dielectric Constant).

[39] Czeslik, C.; Seemann, H.; Winter, R. *Basiswissen Pysikalische Chemie*; Teubner: Wiesbaden, Germany, 2007.

[40] Barthel, J.; Buchner, R.; Steger, H. *Wiss. Zeitschr. THLM* **1989**, *31*, 409.

[41] Barthel, J.; Buchner, R. In *Encyclopedia of Physical Science and Technology*; Meyers, R. A., Ed.; Academic Press: Orlando, 2002; Chapter Permittivity of Liquids, pp 697–706.

[42] Hunger, J. Ph.D. thesis, Universität Regensburg, 2009.

[43] Barthel, J.; Buchner, R. *Chem. Soc. Rev.* **1992**, *21*, 263.

[44] Maxwell, J. C. *Treatise in Electricity and Magnetism*; Claredon Press: Oxford, 1881.

[45] Wagner, K. W. *Arch. Electrotechn.* **1914**, *2*, 371.

[46] http://www.microwaves101.com/encyclopedia/propagation.cfm.

[47] Debye, P.; Falkenhagen, H. *Phys. Z.* **1928**, *29*, 121.

[48] Onsager, L. *J. Am. Chem. Soc.* **1936**, *58*, 1486.

[49] Kirkwood, J. G. *J. Chem. Phys.* **1939**, *7*, 911.

[50] Fröhlich, H. *Theory of Dielectrics*; Oxford University Press: Oxford, 1965.

[51] Cavell, E. A. S.; Knight, P. C.; Sheikh, M. A. *Trans. Faraday Soc.* **1971**, *67*, 2225.

[52] Scholte, T. G. *Physica* **1949**, *15*, 437.

[53] Barthel, J.; Hetzenauer, H.; Buchner, R. *Ber. Bunsenges. Phys. Chem.* **1992**, *96*, 1424.

[54] Debye, P. *Polar Molecules*; Dover: New York, 1930.

[55] Dote, J. L.; Kivelson, D.; Schwartz, R. N. *J. Phys. Chem.* **1981**, *85*, 2169.

[56] Perrin, F. *J. Phys. Radium* **1934**, *5*, 497.

[57] Dote, J. C.; Kivelson, D. *J. Phys. Chem.* **1983**, *87*, 3889.

[58] Powles, J. G. *J. Chem. Phys.* **1953**, *21*, 633.

[59] Glarum, S. H. *J. Chem. Phys.* **1960**, *33*, 1371.

[60] Madden, P.; Kivelson, D. *Adv. Chem. Phys.* **1984**, *56*, 467.

[61] Hölzl, Ph.D. thesis, Universität Regensburg, 1998.

[62] Fukasawa, T.; Sato, T.; Watanabe, J.; Hama, Y.; Kunz, W.; Buchner, R. *Phys. Rev. Lett.* **2005**, *95*, 197802.

[63] Zelsmann, H. R. *J. Mol. Struct.* **1995**, *350*, 95.

[64] Laage, D.; Hynes, J. T. *Science* **2006**, *311*, 832.

[65] Laage, D.; Hynes, J. T. *J. Phys. Chem. B* **2008**, *112*, 7697.

[66] Laage, D.; Stirnemann, G.; Sterpone, F.; Rey, R.; Hynes, J. T. *Annu. Rev. Phys. Chem.* **2011**, *62*, 395.

[67] Debye, P.; Hückel, E. *Phys. Z.* **1923**, *24*, 185.

[68] Eigen, M.; Tamm, K. *Z. Elektrochem.* **1962**, *66*, 93.

[69] Eigen, M.; Tamm, K. *Z. Elektrochem.* **1962**, *66*, 107.

[70] Płaczek, A.; Hefter, G.; Rahman, H. M. A.; Buchner, R. *J. Phys. Chem. B* **2011**, *115*, 2234.

[71] Rittner, E. S. *J. Chem. Phys.* **1951**, *19*, 1030.

[72] Zemaitis, J.; Clark, D. M.; Rafal, M.; Scrivner, N. C. *Handbook of Aqueous Electrolyte Thermodynamics: Theory & Application*; DIPPR Publication: New York, 1986.

[73] Robinson, R. A.; Stokes, R. H. *Electrolyte Solutions*, 2nd ed.; Butterworths: London, 1970.

[74] Moldover, M. R.; Marsh, K. N.; Barthel, J.; Buchner, R. In *Experimental Thermodynamics, Vol. IV: Measurement of the Thermodynamic Properties of Single Phases*; Goodwin, A. R. H., Marsh, K. N., Wakeham, W. A., Eds.; Elsevier: Amsterdam, 2003; Chapter 9: Relative Permittivity and Refractive Index, pp 434–473.

[75] Barthel, J.; Bachhuber, K.; Buchner, R.; Hetzenauer, H.; Kleebauer, M. *Ber. Bunsenges. Phys. Chem.* **1991**, *95*, 853.

[76] Blackham, D. V. *IEEE Trans. Instr. Meas.* **1997**, *46*, 1093.

[77] Agilent Reference Guide N4693-90001, Electroninc Calibration Modules, August 9, 2012.

[78] Schrödle, S. Ph.D. thesis, Universität Regensburg, 2005.

[79] Levine, H.; Papas, C. H. *J. Appl. Phys.* **1951**, *22*, 29.

[80] Misra, D. K. *IEEE Trans. Microwave Theory Tech.* **1987**, *35*, 925.

[81] Ellison, W.; Lamkaouchi, K.; Moreau, J.-M. *J. Mol. Liq.* **1996**, *68*, 171.

[82] Schrödle, S.; Hefter, G.; Kunz, W.; Buchner, R. *Langmuir* **2006**, *22*, 924.

[83] Barthel, J.; Bachhuber, K.; Buchner, R.; Gill, J.; Kleebauer, M. *Chem. Phys. Lett.* **1990**, *167*, 62.

[84] Barthel, J.; Buchner, R.; Hölzl, C.; Münsterer, M. *Z. Phys. Chem.* **2000**, *214*, 1213.

[85] Barthel, J.; Buchner, R.; Wurm, B. *J. Mol. Liq.* **2002**, *98 - 99*, 51.

[86] Gregory, A. P.; Clarke, R. N. *Meas. Sci. Technol.* **2007**, *18*, 1372.

[87] Bevington, P. *Data reduction and error analysis for the physical sciences*; McGraw-Hill Higher Education; McGraw-Hill: New York, 1969.

[88] Zasetsky, A. Y.; Buchner, R. *J. Phys.: Condens. Matter* **2011**, *23*, 025903.

[89] Tikhonov, A. *Dokl. Akad. Nauk SSSR* **1963**, *151*, 501.

[90] Kratky, O.; Leopold, H.; Stabinger, H. *Z. Angew. Phys.* **1969**, *27*, 273.

[91] Shaukat, S.; Buchner, R. *J. Chem. Eng. Data* **2011**, *56*, 4944.

[92] Barthel, J.; Feuerlein, F.; Neueder, R.; Wachter, R. *J. Solution Chem.* **1980**, *9*, 209.

[93] MOPAC2009, J. J. P. Stewart, Stewart Computational Chemistry, Version 9.097W web: http://OpenMOPAC.net.

[94] Stewart, J. J. P. *J. Mol. Modeling* **2007**, *13*, 1173.

[95] Klamt, A.; Schüürmann, G. *J. Chem. Soc., Perkin Trans. 2* **1993**, 199.

[96] Senda, N. Winmostar, version 3.806o. http://winmostar.com.

[97] Cole, R. H. *Annu. Rev. Phys. Chem.* **1989**, *40*, 1.

[98] Carrique, F.; Ruiz-Reina, E.; Arroyo, F.; Delgado, A. *J. Phys. Chem. B* **2010**, *114*, 6134.

[99] Bordi, F.; Cametti, C.; Colby, R. *J. Phys.: Condens. Matter* **2004**, *16*, R1423.

[100] Buchner, R.; Baar, C.; Fernandez, P.; Schrödle, S.; Kunz, W. *J. Mol. Liq.* **2005**, *118*, 179.

[101] Anderson, J. E. *J. Non-Cryst. Solids* **1994**, *172-174*, 1190.

[102] Wachter, W.; Buchner, R.; Hefter, G. *J. Phys. Chem. B* **2006**, *110*, 5147.

[103] Wachter, W.; Fernandez, S.; Buchner, R.; Hefter, G. *J. Phys. Chem. B* **2007**, *111*, 9010.

[104] Kaatze, U. *Chem. Phys. Lett.* **1993**, *203*, 1.

[105] Yamaguchi, T. personal communication.

[106] Gibbs, J. H.; Cohen, C.; III, P. F.; Porosoff, H. *The Pysical Chemistry of Aqueous Systems*; Plenum: New York, 1973.

[107] Marcus, Y. *Ion Properties*; Marcel Dekker: New York, 1997.

[108] Korson, L.; Drost-Hansen, W.; Millero, F. *J. Phys. Chem.* **1969**, *73*, 34.

[109] Hasted, J. B. In *Water, a Comprehensive Treatise*; Franks, F., Ed.; Plenum: New York, 1972; Vol. 1.

[110] Fuoss, R. M. *Proc. Natl. Acad. Sci. USA* **1980**, *77*, 34.

[111] Bešter-Rogač, M.; Neueder, R.; Barthel, J. *J. Solution Chem.* **1999**, *28*, 1071.

[112] Laage, D.; Hynes, J. T. *Proc. Natl. Acad. Sci. USA* **2007**, *104*, 11167.

[113] Yui, K.; Sakuma, M.; Funazukuri, T. *Fluid Phase Equilib.* **2010**, *297*, 227.

[114] Mancinelli, R.; Botti, A.; Bruni, F.; Ricci, M. A.; Soper, A. K. *J. Phys. Chem. B* **2007**, *111*, 13570.

[115] Hunger, J.; Stoppa, A.; Buchner, R.; Hefter, G. *J. Phys. Chem. B* **2008**, *112*, 12913.

[116] Sangoro, J.; Iacob, C.; Serghei, A.; Naumov, S.; Galvosas, P.; Kärger, J.; Wespe, C.; Bordusa, F.; Stoppa, A.; Hunger, J.; Buchner, R.; Kremer, F. *J. Chem. Phys.* **2008**, *128*, 214509.

[117] Falkenhagen, H.; Ebeling, W. *Theorie der Elektrolyte*; S. Hirzel, 1971.

[118] Yamaguchi, T.; Matsuoka, T.; Koda, S. *J. Chem. Phys.* **2007**, *127*, 234501.

[119] Leonard, R. *Technical Report 1, Office of Naval Research Contract N6-onr-27507*; 1950.

[120] Breitschwerdt, K.; Kistenmacher, H. *J. Chem. Phys.* **1972**, *56*, 4800.

[121] Heisler, I. A.; Mazur, K.; Meech, S. R. *J. Phys. Chem. B* **2011**, *115*, 1863.

[122] Hubbard, J.; Onsager, L. *J. Chem. Phys.* **1977**, *67*, 4850.

[123] Hubbard, J. B. *J. Chem. Phys.* **1978**, *68*, 1649.

[124] Hubbard, J. B.; Colonomos, P.; Wolynes, P. G. *J. Chem. Phys.* **1979**, *71*, 2652.

[125] Hunger, J.; Niedermayer, S.; Buchner, R.; Hefter, G. *J. Phys. Chem. B* **2010**, *114*, 13617.

[126] Buchner, R.; Chen, T.; Hefter, G. *J. Phys. Chem. B.* **2004**, *108*, 2365.

[127] Tongraar, A.; Rode, B. *Chem. Phys. Lett.* **2004**, *385*, 378.

[128] White, J.; Schwegler, E.; Galli, G.; Gygi, F. *J. Chem. Phys.* **2000**, *113*, 4668.

[129] Tongraar, A.; Liedl, K.; Rode, B. *J. Phys. Chem. A* **1998**, *102*, 10340.

[130] Epstein, E. *Mineral Nutrition of Plants: Principles and Perspectives*; Wiley: New York, 1972.

[131] Chizhik, V.; Egorov, A.; Komolkin, A.; Vorontsova, A. *J. Mol. Liq.* **2002**, *98-99*, 173.

[132] Śmiechowski, M.; Gojło, E.; Stangret, J. *J. Phys. Chem. B* **2009**, *113*, 7650.

[133] Rouff, A. A.; Rabe, S.; Nachtegaal, M.; Vogel, F. *J. Phys. Chem. A* **2009**, *113*, 6895.

[134] Pluhářová, E.; Ončák, M.; Seidel, R.; Schroeder, C.; Schroeder, W.; Winter, B.; Bradforth, S. E.; Jungwirth, P.; Slavíček, P. *J. Phys. Chem. B* **2012**, *116*, 13254.

[135] Childs, C. W. *J. Phys. Chem.* **1969**, *73*, 2956.

[136] Buchner, R.; Hölzl, C.; Stauber, J.; Barthel, J. *Phys. Chem. Chem. Phys.* **2002**, *4*, 2169.

[137] Eiberweiser, A.; Buchner, R. *J. Mol. Liq.* **2012**, *176*, 52.

[138] Marcus, Y. *Ion solvation*; Wiley: New York, 1985.

[139] Ohtaki, H.; Radnai, T. *Chem. Rev.* **1993**, *93*, 1157.

[140] Hunger, J.; Liu, L.; Tielrooij, K.-J.; Bonn, M.; Bakker, H. *J. Chem. Phys.* **2011**, *135*, 124517.

[141] Takisawa, N.; Osugi, J.; Nakahara, M. *J. Chem. Phys.* **1983**, *78*, 2591.

[142] Hefter, G.; Buchner, R. unpublished results.

[143] Rahman, H. M. A.; Buchner, R. *J. Mol. Liq.* **2012**, *176*, 93.

[144] Lide, D., Ed. *CRC-Handbook of Chemistry and Physics*, 85th ed.; CRC Press: Boca Raton, Florida, 2004.

[145] White, A. personal communication.

[146] Rasmussen, S. E.; Jørgensen, J.-E.; Lundtoft, B. *Powder Diffr.* **1993**, *8*, 164.

[147] Sowa, H. *Z. Kristallogr.* **1994**, *209*, 954.

[148] Ni, Y.-X.; Hughes, J. M.; Mariano, A. *Am. Mineral.* **1995**, *80*, 21.

[149] Bridgeman, A. J.; Cavigliasso, G. *Polyhedron* **2001**, *20*, 2269.

[150] Pribil, A. B.; Hofer, T. S.; Randolf, B. R.; Rode, B. M. *J. Comput. Chem.* **2008**, *29*, 2330.

[151] Buchner, R.; Capewell, S. G.; Hefter, G.; May, P. M. *J. Phys. Chem. B.* **1999**, *103*, 1185.

[152] Capewell, S. G.; Buchner, R.; Hefter, G.; May, P. M. *Phys. Chem. Chem. Phys.* **1999**, *1*, 1933.

[153] Akilan, C.; Hefter, G.; Rohman, N.; Buchner, R. *J. Phys. Chem. B* **2006**, *110*, 14961.

[154] Franks, F. *Water, a Comprehensive Treatise: The physics and physical chemistry of water*; Plenum: New York, 1972.

[155] Pethybridge, A.; Talbot, J.; House, W. *J. Solution Chem.* **2006**, *35*, 381.

[156] Eiberweiser, A.; Buchner, R. unpublished results.

[157] Veintemillas, V. S.; Rull, F. *Z. Phys. Chem.* **1994**, *187*, 93.

[158] Adams, W. A.; Preston, C. M.; Chew, H. A. M. *J. Chem. Phys.* **1979**, *70*, 2074.

[159] Preston, C. M.; Adams, W. A. *J. Phys. Chem.* **1979**, *83*, 814.

[160] Rull, F.; Del Valle, A.; Sobron, F.; Veintemillas, S. *J. Raman Spectrosc.* **1989**, *20*, 625.

[161] Syed, K. A.; Pang, S.-F.; Zhang, Y.; Zeng, G.; Zhang, Y.-H. *J. Phys. Chem. A* **2012**, *116*, 1558.

[162] Kerker, M.; Espenscheid, W. F. *J. Am. Chem. Soc.* **1958**, *80*, 776.

[163] Rudolph, W. W. *J. Solution Chem.* **2012**, *41*, 630.

[164] Shaukat, S. Ph.D. thesis, Universität Regensburg, 2012.

[165] Zhang, Y.; Cremer, P. *Annu. Rev. Phys. Chem.* **2010**, *61*, 658.

[166] Kunz, W., Ed. *Specific Ion Effects*; World Scientific: Singapore, 2010.

[167] Parsons, D. F.; Boström, M.; Lo Nostro, P.; Ninham, B. W. *Phys. Chem. Chem. Phys.* **2011**, *13*, 12352.

[168] Lo Nostro, P.; Ninham, B. W. *Chem. Rev.* **2012**, *112*, 2286.

[169] Lewith, S. *Arch. Exp. Pathol. Pharmakol.* **1887**, *24*, 1.

[170] Hofmeister, F. *Arch. Exp. Pathol. Pharmakol.* **1887**, *24*, 247.

[171] Hofmeister, F. *Arch. Exp. Pathol. Pharmakol.* **1888**, *25*, 1.

[172] Limbeck, R. *Arch. Exp. Pathol. Pharmakol.* **1888**, *25*, 69.

[173] Hofmeister, F. *Arch. Exp. Pathol. Pharmakol.* **1890**, *27*, 395.

[174] Hofmeister, F. *Arch. Exp. Pathol. Pharmakol.* **1891**, *28*, 210.

[175] Münzer, E. *Arch. Exp. Pathol. Pharmakol.* **1898**, *41*, 74.

[176] Collins, K. D.; Washabaugh, M. W. *Q. Rev. Biophys.* **1985**, *18*, 323.

[177] Ball, P. *Faraday Discuss.* **2013**, *160*, 405.

[178] *World Population Prospects: The 2010 Revision, Highlights and Advance Tables*; United Nations: New York, 2011.

[179] Rahman, H. M. A.; Hefter, G.; Buchner, R. *J. Phys. Chem. B* **2013**, *117*, 2142.

[180] Rieder, J.; Eiberweiser, A.; Buchner, R. unpublished results.

[181] Kunz, W.; Henle, J.; Ninham, B. W. *Curr. Op. Coll. Interf. Sci.* **2004**, *9*, 19.

[182] Kunz, W. *Curr. Op. Coll. Interf. Sci.* **2010**, *15*, 34.

[183] Tobias, D. J.; Hemminger, J. C. *Science* **2008**, *319*, 1197.

[184] Gurney, R. W. *Ionic Processes in Solution*; McGraw-Hill: New York, 1953.

[185] O'Brien, J. T.; Prell, J. S.; Bush, M. F.; Williams, E. R. *J. Am. Chem. Soc.* **2010**, *132*, 8248.

[186] Tielrooij, K. J.; Garcia-Araez, N.; Bonn, M.; Bakker, H. J. *Science* **2010**, *328*, 1006.

[187] Paschek, D.; Ludwig, R. *Angew. Chem. Int. Ed.* **2011**, *50*, 352.

[188] Omta, A. W.; Kropman, M. F.; Woutersen, S.; Bakker, H. J. *Science* **2003**, *301*, 347.

[189] Smith, J. D.; Saykally, R. J.; Geissler, P. L. *J. Am. Chem. Soc.* **2007**, *129*, 13847.

[190] Lin, Y.-S.; Auer, B. M.; Skinner, J. L. *J. Chem. Phys.* **2009**, *131*, 144511.

[191] Fayer, M. D.; Moilanen, D. E.; Wong, D.; Rosenfeld, D. E.; Fenn, E. E.; Park, S. *Acc. Chem. Res.* **2009**, *42*, 1210.

[192] Marcus, Y. *J. Solution Chem.* **1994**, *23*, 831.

[193] Collins, K. D. *Biophys. J.* **1997**, *72*, 65.

[194] Collins, K. D. *Methods* **2004**, *34*, 300.

[195] Collins, K. D.; Neilson, G. W.; Enderby, J. E. *Biophys. Chem.* **2007**, *128*, 95.

[196] Yancey, P. H. *Amer. Zool.* **2001**, *41*, 699.

[197] Galinski, E. A.; Pfeiffer, H.-P.; Trüper, H. G. *Eur. J. Biochem.* **1985**, *149*, 135.

[198] Pastor, J. M.; Salvador, M.; Argandoña, M.; Bernal, V.; Reina-Bueno, M.; Csonka, L. N.; Iborra, J. L.; Vargas, C.; Nieto, J. J.; Cánovas, M. *Biotech. Adv.* **2010**, *28*, 782.

[199] Lippert, K.; Galinski, E. A. *Appl. Microbiol. Biotechnol.* **1992**, *37*, 61.

[200] Arakawa, T.; Timasheff, S. N. *Biophys. J.* **1985**, *47*, 411.

[201] Yu, I.; Nagaoka, M. *Chem. Phys. Lett.* **2004**, *388*, 316.

[202] Oren, A. *Environ. Technol.* **2010**, *31*, 825.

[203] Beyer, N.; Driller, H.; Bünger, J. *Seifen Öle Fette Wachse* **2000**, *126*, 26.

[204] Yu, I.; Jindo, Y.; Nagaoka, *J. Phys. Chem. B* **2007**, *111*, 10231.

[205] Smiatek, J.; Harishchandra, R. K.; Rubner, O.; Galla, H.; Heuer, A. *Biophys. Chem.* **2012**, *160*, 62.

[206] Buchner, R.; Barthel, J. *Ber. Bunsenges. Phys. Chem.* **1997**, *101*, 1509.

[207] Barthel, J.; Buchner, R.; Eberspächer, P.-N.; Münsterer, M.; Stauber, J.; Wurm, B. *J. Mol. Liq.* **1998**, *78*, 83.

[208] Zhao, Y. H.; Abraham, M. H.; Zissimos, A. M. *J. Org. Chem.* **2003**, *68*, 7368.

Regensburg, den 15. März 2013

Andreas Eiberweiser